TOWARDS VERIFIABLE ADAPTIVE CONTROL OF GAS TURBINE ENGINES

A Dissertation
Presented to
The Academic Faculty

by

Mehrdad Pakmehr

In Partial Fulfillment
of the Requirements for the Degree
Doctor of Philosophy in the
School of Aerospace Engineering

Georgia Institute of Technology
August 2013

TOWARDS VERIFIABLE ADAPTIVE CONTROL OF GAS TURBINE ENGINES

Approved by:

Professor Eric Feron,
Committee Chair
School of Aerospace Engineering
Georgia Institute of Technology

Professor Vigor Yang
School of Aerospace Engineering
Georgia Institute of Technology

Professor Eric Johnson
School of Aerospace Engineering
Georgia Institute of Technology

Professor Marilyn Wolf
School of Electrical and Computer Engineering
Georgia Institute of Technology

Dr. James Paduano
Lead Engineer for Autonomy, Controls, and Estimation
Aurora Flight Sciences

Professor Jeff Shamma
School of Electrical and Computer Engineering
Georgia Institute of Technology

Date Approved: 17 May 2013

To my parents.

The knowledge of anything, since all things have causes, is not acquired or complete unless it is known by its causes.

Pur Sina (also known as Avicenna or Ibn Sina), 980-1037 A.D.
Persian philosopher, mathematician, and physician

ACKNOWLEDGEMENTS

I am eternally grateful for the guidance from my advisor, Dr. Eric Feron. His support, advice, and suggestions over the years have helped me grow as a researcher and an engineer. Without his direction, this dissertation would not have been possible.

I would also like to thank the people at Aurora Flight Sciences, whom I worked with on the gas turbine engine control project, including Dr. James Paduano, Nathan Fitzgerald and George Kiwada. Especially, I am thankful to Dr. James Paduano, who provided me with precious comments and pieces of advice during this research, and Nathan Fitzgerald who managed to develop a very good physics-based model of the turboshaft engine and conducted experiments to verify the model.

I am also thankful to Dr. Alireza Behbahani of the Air Force Research Lab (AFRL) for his support during the course of this research project. I am also indebted to Dr. Jeff Shamma who helped me to understand and develop gain scheduled systems. I would like also to thank my other committee members including Dr. Yang, Dr. Johnson, and Dr. Wolf for their support. I would like to thank AFOSR and NSF for sponsoring my research.

I sincerely thank my parents for everything they have done for me, especially for their support, love, and sacrifices over the years. I am also thankful for all of the enlightening discussions with all of my lab mates and co-workers at Georgia Tech. I would like to thank all of my fellow colleagues in the School of Aerospace Engineering, including Dr. Tansel Yucelen, Dr. Alireza Esna-Ashari, Gi Yun Chung, Romain Jobredeaux, Emmanuel Boidot, Aude Marzuoli, Sang Hyun Kim, and Timothy Wang.

TABLE OF CONTENTS

LIST OF TABLES

LIST OF FIGURES

LIST OF SYMBOLS AND ABBREVIATIONS

Nomenclature

$\mathcal{T}$	=	torque
$\mathcal{P}$	=	power
I	=	overall rotational inertia of spool
ω	=	rotational speed of the spool
T	=	stagnation temperature at a given thermodynamic station
P	=	pressure
m	=	air mass
f	=	fuel fraction
c_p	=	specific heat
γ	=	specific heat ratio
$h(.)$	=	enthalpy
$s(.)$	=	entropy
h_{fuel}	=	lower heating value of the fuel
τ	=	temperature ratio across the component
π	=	pressure ratio across the component
η	=	component efficiency
FP	=	flow parameter function
$TSFC$	=	thrust specific fuel consumption
N_1	=	low pressure spool speed (RPM)
N_2	=	high pressure spool speed (RPM)
W_f	=	fuel flow input (kg/s)
F_N	=	thrust (N)
W_c	=	corrected air flow (kg/s)
N_c	=	corrected spool speed

ρ_0	=	air density (kg/m^3)
R_p	=	propeller radius (m)
J_p	=	propeller advance ratio
β	=	propeller pitch angle input (deg)
C_T	=	propeller thrust coefficient
C_P	=	propeller power coefficient
α	=	scheduling parameter
λ	=	eigenvalue
x^p	=	plant state vector
x^c	=	controller state vector
u	=	plant input vector
y	=	plant output vector
v	=	augmented system input vector
r	=	reference signal vector
Co	=	convex hull of a set

Subscripts

des	=	design
amb	=	ambient
std	=	standard
comp	=	compressor
comb	=	combustor
noz	=	nozzle
turb	=	turbine
prop	=	propeller
burn	=	burner
hpc	=	high pressure compressor

hpt	=	high pressure turbine
lpt	=	low pressure turbine
hps	=	high pressure spool
lps	=	low pressure spool
$poly$	=	polytropic
e	=	equilibrium
nom	=	nominal engine
ag	=	aged engine
Co	=	core subsystem
Pr	=	prop subsystem
k	=	kth subsystem
q	=	qth subsystem

Abbreviations

SISO	=	Single Input Single Output
MIMO	=	Multi Input Multi Output
LTI	=	Linear Time Invariant
LTV	=	Linear Time Varying
LPV	=	Linear Parameter Varying
PWL	=	Piecewise Linear
LMI	=	Linear Matrix Inequality
GS	=	Gain Scheduled
GS-MRAC	=	Gain Scheduled Model Reference Adaptive Control
D-GS-MRAC	=	Decentralized Gain Scheduled Model Reference Adaptive Control
FADEC	=	Full Authority Digital Engine Controller
HIL	=	Hardware in the Loop
FAA	=	Federal Aviation Administration

RTCA	=	Radio Technical Commission for Aeronautics
UAV	=	Unmanned Aerial Vehicle
GTE	=	Gas Turbine Engine
VTOL	=	Vertical Take-Off and Landing
HP	=	High Pressure
LP	=	Low Pressure
HPC	=	High Pressure Compressor
HPT	=	High Pressure Turbine
LPT	=	Low Pressure Turbine
PnP	=	Plug and Play
SW	=	Software

SUMMARY

This dissertation investigates the problem of developing verifiable stable control architectures for gas turbine engines. First, a nonlinear physics-based dynamic model of a twin spool turboshaft engine which drives a variable pitch propeller is developed. In this model, the dynamics of the engine are defined to be the two spool speeds, and the two control inputs to the system are fuel flow rate and prop pitch angle. Experimental results are used to verify the dynamic model of JetCat SPT5 turboshaft engine. Based on the experimental data, performance maps of the engine components including propeller, high pressure compressor, high pressure, and low pressure turbines are constructed. The engine numerical model is implemented using Matlab.

Second, a stable gain scheduled controller is described and developed for a gas turbine engine that drives a variable pitch propeller. A stability proof is developed for a gain scheduled closed-loop system using global linearization and linear matrix inequality (LMI) techniques. Using convex optimization tools, a single quadratic Lyapunov function is computed for multiple linearizations near equilibrium and non-equilibrium points of the nonlinear closed-loop system. This approach guarantees stability of the closed-loop gas turbine engine system. To verify the stability of the closed-loop system on-line, an optimization problem is proposed which is solvable using convex optimization tools. Through simulations, we show the developed gain scheduled controller is capable to regulate a turboshaft engine for large thrust commands in a stable fashion with proper tracking performance.

Third, a gain scheduled model reference adaptive control (GS-MRAC) concept for multi-input multi-output (MIMO) nonlinear plants with constraints on the control

inputs is developed and described. Specifically, adaptive state feedback for the output tracking control problem of MIMO nonlinear systems is studied. Gain scheduled reference model system is used for generating desired state trajectories, and the stability of this reference model is also analyzed using convex optimization tools. This approach guarantees stability of the closed-loop gain scheduled gas turbine engine system, which is used as a gain scheduled reference model. An adaptive state feedback control scheme is developed and its stability is proven, in addition to transient and steady-state performance guarantees. The resulting closed-loop system is shown to have ultimately bounded solutions with a priori adjustable bounded tracking error. The results are then extended to GS-MRAC with constraints on the magnitudes of multiple control inputs. Sufficient conditions for uniform boundedness of the closed-loop system is derived. A semi-global stability result is proven with respect to the level of saturation for open-loop unstable plants, while the stability result is shown to be global for open-loop stable plants. Simulations are performed for three different models of the turboshaft engine, including the nominal engine model and two models where the engine is degraded. Through simulations, we show the developed GS-MRAC architecture can be used for the tracking problem of degraded turboshaft engine for large thrust commands with guaranteed stability.

Finally, a decentralized linear parameter dependent representation of the engine model is developed, suitable for decentralized control of the engine with core and fan/prop subsystems. Control theoretic concepts for decentralized gain scheduled model reference adaptive control (D-GS-MRAC) systems is developed. For each subsystem, a linear parameter dependent model is available and a common Lyapunov matrix can be computed using convex optimization tools. With this control architecture, the two subsystems of the engine (i.e., engine core and engine prop/fan) can be controlled with independent controllers for large throttle commands in a decentralized

manner. Based on this D-GS-MRAC architecture, a "plug and play" (PnP) technology concept for gas turbine engine control systems is investigated, which allows us to match different engine cores with different engine fans/propellers. With this plug and play engine control architecture, engine cores and fans/props could be used with their on-board subordinate controllers ready for integration into a functional propulsion system. Simulation results for three different models of the engine, including the nominal engine model, the model with a new prop, and the model with a new engine core, illustrate the possibility of PnP technology development for gas turbine engine control systems.

CHAPTER I

INTRODUCTION

1.1 Gas Turbine Engine

The contents of this subsection are mainly adopted from [35, 157], to present a brief review of gas turbine engines.

The gas turbine can be used in several different modes in critical industries such as power generation, oil and gas, process plants, aviation, as well as domestic and smaller related industries. A gas turbine essentially brings together fuel and air that it compresses in its compressor module, which are then ignited. Resulting gases are expanded through a turbine. That turbine's shaft continues to rotate and drive the compressor which is on the same shaft, and operation continues. A separate starter unit is used to provide initial rotor motion, until the turbine's rotation is up to design speed and can keep the entire unit running. The compressor, combustor, and turbine modules connected by one or more shafts are collectively called the gas generator [157].

The gas turbine itself operates essentially in the same manner, regardless of whether it is on land, in the air, or at sea. However, the operating environment and criticality of the application in question, may make design and system modifications necessary. Essentially the same machine can be used to generate power. It can also be used as a power plant on an aircraft. However the layout, the other turbomachinery supplied with the gas turbine, and optional systems varies in each case [157].

In aircraft engine applications, if the turbine is driving a rotor (helicopter) or a propeller (turboprop aircraft), then its power is usually measured in horsepower.

This means that the torque transmission from the gas turbine shaft is, in principle, a variation of mechanical drive application. If an aircraft gas turbine engine (GTE) operates in turbothrust or ramjet mode (i.e. the gas turbine expels its exhaust gases and the thrust of that expulsion propels the aircraft forward), its power is usually measured in pounds of thrust [157].

One way to subdivide aeroengines is by whether they have a centrifugal compressor or an axial compressor. In very general terms, the former type offers more in terms of simplicity and ruggedness. The axial compressor however, is used in most high performance, more complex designs. Another subdivision that can be made is whether the aeroengine drives a propeller (via the gas generator shaft or a free power turbine) and just basically pushes its exhaust gases out its exhaust section and thus pushes the plane forward (jet propulsion). This operational mode (turboshaft or turbojet) is independent of what type of compressor the gas turbine has. A turboshaft which also has a large fan at the front (air intake) end is called a turbofan engine [157].

Here we briefly explain some of the more commonly used gas turbine engines in aerospace industry, including turbofan, turboshaft, and turboprop engines.

Turbofan with Fan Exhausted: Turbofans are always multi spool engines. In the front of the engine, the air is first diffused. The air enters the fan, which compresses the air and increases the pressure somewhat. The air is then split at the splitter, and a portion of it enters the low-pressure compressor and continues down the core of the engine. Eventually this core air exhausts through the primary exhaust nozzle and produces thrust. The second stream of air is called the bypass air. In this engine type, the bypass air is accelerated in the fan nozzle, producing a second or additional thrust. The fan and usually the first few stages of the low pressure compressor are driven by the low-pressure turbine. The high pressure compressor extracts its energy from the high-pressure turbine. In a few cases, three shafts are used [35].

Turbofan with Fan Mixed: It is similar in comparison to the previous type, but the bypass air is not directly exhausted. The secondary air is bypassed around the low and high pressure compressors, combustor, and the low and high pressure turbines through a duct. The secondary air is then mixed with the turbine exhaust in a mixer. The mixed air is then accelerated through the nozzle to produce the thrust [35].

In both of the turbofan types, the secondary air is used as a source of low pressure, low-temperature air. This air is bled off the fan and used as a driver for controllers, as cooling air for the turbine, and for other applications. These engine types produce thrust with better fuel economy than does a turbojet. As a result, almost all modern commercial transport and military aircraft use one of the two types of turbofans. Typically, commercial aircraft use high bypass ratios (much more air flow in the fan than in the core), and military aircraft use low bypass ratios (approximately equivalent air flow rates). Finally, a hybrid form of the two fundamental types of turbofan is sometimes used. For this type of turbofan, a portion of the air that enters the fan is exhausted through the fan exhaust, and the remainder of the air is exhausted through the primary exhaust [35].

Turboprop: For this type, the core of the engine consists of a diffuser, combustor, compressor, and turbine. The core airflow is accelerated through the exhaust nozzle, which produces one component of thrust. A second component of thrust, and usually the largest, is obtained from the propeller. The power for the propeller is extracted from the turboshaft in the core -that is a part of the turbine work drives the propeller. A gearbox reduces the speed so that the propeller spins at a lower speed than the compressor [35].

Turboshaft: The last gas turbine engine type we are describing here is the turboshaft engine. It is basically the same as the turboprop except that thrust is not

derived from the exhaust. The gas from the core exhausts at a low velocity, and consequently additional thrust is not obtained. In low-speed flight vehicles, or when very high propulsive efficiency is desired, turboshaft engines are used. These engines are used largely for helicopter applications, although it is noteworthy that turboshaft engines are used to drive tanks and other ground vehicles with a transmission attached to the shaft in lieu of the rotating blades [35].

Some of the good references to read more about gas turbine engine theory, performance, and applications are [19, 25, 29, 35, 69, 93, 94, 109, 110, 157, 172]. In this dissertation we are working on a turboshaft/turboprop engine driving a variable pitch propeller as a testbed for gas turbine engine adaptive control development. The developed controllers can be implemented on any MIMO gas turbine model.

1.2 Gas Turbine Engine Modeling

Over the years considerable effort has been expended in gaining a greater understanding of the nonlinear gas turbine engine dynamics and in representing these increasingly complex engine models. With the increasing costs of engine programs with high investment and high commercial risks, modeling is being used more frequently. High fidelity models that accurately represent the engine are essential in development to analyze and predict engine performance. They are also crucial in control law development to optimize important parameters such as specific fuel consumption (SFC) and to meet increasingly rigorous engine handling requirements driven by customers, certification organizations, and environmental legislation [73].

The level of complexity of an aero gas turbine engine model depends on its intended application such as research, analysis, or synthesis of control systems. Using a nonlinear model has the advantage of being more precise, and hence it involves fewer modeling errors; however, this is at the expense of computation which can increase significantly compared to linear analysis. Using simpler linear models enables more

rapid control development cycles, but the estimation of errors represents an additional problem [73].

Here, a brief review of the literature dedicated to the aero gas turbine engine modeling and simulation, is presented. There have been efforts on aero gas turbine engine modeling with applications for control [59, 73, 160], gas path analysis [75, 170], Hardware-in-the-Loop (HIL) research [26, 27, 96], and real time simulation [83]. Common engine model types for real-time simulation are aerothermodynamic, piecewise linear state-space, and transfer function [144].

A comprehensive review of modeling methodologies for real-time simulation of gas-turbine engine performance has been done by the Society of Automotive Engineers [159]. Hurt [53] presented one of the possible ways to develop a real-time simulation model by (1) linearizing the nonlinear model about the selected operating points; (2) relating the coefficients of the linear model to the engine state and the inputs; and (3) implementing the resulting piecewise linear model as a set of transfer function models. The advantages of dynamic simulation in control system development have been described in [62]. Case studies pertaining to the RM12 turbofan engine also have been discussed to illustrate the importance of simulation as a development tool. The author further discusses various simulation-related aspects like the various types of mathematical models (such as continuous and discrete, distributed and lumped parameter, and linear and nonlinear), engineering applications of simulation, model representations, simulation tools and software, numerical solution of ordinary differential equations, real-time, non-real-time, and HIL simulations.

High fidelity engine simulations have been developed by engine manufacturers for engine and control system designs. Recently graphical modeling tools such as Simulink have been used to build high fidelity engine simulations. These graphical modeling tools provide efficient design means for building models as well as for analyzing engine control system performance [59]. Two of these graphical model based

simulations are the U.S. Air Force Research Laboratory's (AFRL) generic engine simulation for a two spool, low bypass turbofan engine [97], and NASA's generic, two spool high bypass turbofan engine [31, 36, 95, 121, 122]. The AFRL generic engine model is used in the Propulsion Directorate's Intelligent Controls Facility (ICF), where it forms the foundation for interchangeability of simulated and actual controllers, actuators, mechanical and electrical devices in a Hardware-in-the-Loop setup [97]. NASA's Modular Aero-Propulsion System Simulation (MAPSS) [121, 122] is a flexible turbofan engine simulation environment that provides easy access to health, control, and engine parameters through a graphical user interface. Both military and commercial turbofan engine versions of MAPSS exist. The military-engine version, referred to simply as MAPSS; and the commercial-engine version, referred to as C-MAPSS [36].

In this dissertation, a physics-based model of a turboshaft engine driving a variable pitch propeller is developed and used for gas turbine engine control research.

1.3 Gain Scheduled Control

A wide variety of control methods are often described as gain scheduling approaches. They are usually linked by a design procedure whereby the nonlinear control design task is decomposed into a number of linear sub-problems. This is the source of much of the popularity of gain scheduling methods since it allows well established linear design methods to be applied to non-linear problems. However, it is also emphasized that the benefits of continuity with linear methods often extend beyond purely technical considerations. One of the important considerations is in the aerospace industry, where safety certification requirements are often based on linear control criteria and the development of new certification procedures using nonlinear approaches may well be prohibitive. This question remains be answered as to whether a wide class of nonlinear design tasks can genuinely be decomposed into linear sub-problems. Although

it is well known that certain classes of problems present greater difficulty than others for gain scheduling methods, the general usefulness of such methods is well established both in practice and from a theoretical viewpoint [81, 136]. Here, we use gain scheduling in the sense of continuously varying the controller coefficients according to the current value of scheduling signals, also called scheduling variables, that may be either exogenous signals or endogenous signals with respect to the plant [136, 151].

To facilitate the stability analysis of nonlinear systems, such as gas turbine engines, an efficient technique is to approximate the nonlinear model by a linear time-varying (LTV) system. To design a controller for gas turbine engine system, gain scheduling (GS) technique can be used; gain scheduling is one of the most popular nonlinear control design approaches and has been widely and successfully applied in fields ranging from aerospace to process control [81, 136]. One good example of the gain scheduling application to high performance aircraft can be reviewed in [98, 99, 100]. Research on gain scheduled control of gas turbine engines is presented in [10, 16, 21, 39, 41, 65, 176, 179]. A simplified scheme for scheduling multivariable controllers for robust performance over a wide range of turbofan engine operating points is presented in [39].

In this dissertation, a gain scheduled control architecture for gas turbine engine systems is developed with stability guarantees, which can also be used easily for gas turbine engine control software verification.

1.4 Model Reference Adaptive Control

Adaptive control development is mainly invoked by the fact that the models employed in control system design may not properly represent the actual system dynamics due to idealized assumptions, linearization, model order reduction, external disturbances, and degraded modes of operation. Since such parameter uncertainties, variations, or imperfections occur in many practical problems, adaptive control is useful in many

industrial contexts. Robust control can also be used to deal with parameter uncertainty. In principle, adaptive control is superior to robust control in dealing with uncertainties in constant or slowly-varying parameters. The basic reason lies in the learning behavior of adaptive control systems: an adaptive controller improves its performance as adaptation goes on, while a robust controller simply attempts to keep consistent performance. On the other hand, adaptive controllers are capable to deal with uncertainty without necessarily sacrificing performance. Another reason is that an adaptive controller requires little or no a priori information about the unknown parameters, while a robust controller usually requires reasonable a priori estimates of the parameter bounds [156].

An adaptive controller differs from an ordinary controller in that the adaptive controller gains are time varying, and there is a mechanism for adjusting these gains online based on signals in the system. There are two main approaches for constructing adaptive controllers. One is the so-called model reference adaptive control (MRAC) method, and the other is the so-called self-tuning method.

A Model Reference Adaptive Control (MRAC) system is composed of four major parts: a plant containing unknown parameters and/or uncertainties, a reference model for compactly specifying the desired output of the control system, a feedback control law containing adjustable gains, and an adaptation mechanism for updating the adjustable gains. The output (or state) of the uncertain system is compared to the output (or state) of the reference model. This comparison results in an error signal used in the gain update law. The controller employs the gain information from the gain update law to form the adaptive control signal.

In the early 1950s there was extensive research on adaptive control in connection with the design of autopilots for high performance aircraft; in the late 1950s MRAC was developed by Whitaker and his colleagues [12]. This new idea based on a gradient method has been developed in [112]. In this work, the gain update law

is constructed as the negative gradient of a cost function chosen as the square of the error signal norm. This approach drives the trajectories of the uncertain system to the trajectories of the reference model asymptotically. Butchart and Shackcloth [22] and Parks [123] analyzed the stability of this gradient method for the first time using Lyapunov stability theory [91, 92]. Some of the well known works on MRAC can be found in [12, 42, 49, 54, 56, 67, 72, 103, 145, 156, 161, 165]. Some of the well known work on the decentralized adaptive control research can also be found in [24, 40, 50, 52, 55, 101, 111, 155, 154, 153, 175, 162, 106, 107].

Some of the works dedicated to the adaptive control of systems with multiple equilibrium points and with time varying reference systems are [9, 49, 57, 58, 139, 140, 141, 142, 143, 173]. Other MRAC architectures which are involving some form of LTV plant or multiple LTI reference models can be found in [46, 104, 105, 108, 166, 167, 168].

Table 1 presents a brief comparison of different MRAC architectures for characteristics like plant type, reference model type, switching in the structure, and applicability of the method for large thrust commands.

Table 1: Comparison of different MRAC architectures

Case	**References**	**Plant**	**Ref Model**	**Switching**	**Large Comm**
Basic MRAC	[12]	LTI	LTI	No	No
Ioannou *et. al.*	[166, 167, 168]	LTV	LTI	No	No
Narendra *et. al.*	[104, 105]	LTI	Multiple LTI	Yes	No
Narendra *et. al.*	[46, 108]	LTI	Multiple LTV	Yes	No
Tao *et. al.*	[140, 142, 143]	Multiple LTI (PWL)	PWL	Yes	Yes
Annaswamy *et. al.*	[9, 58, 57]	LTV	LTV	No	Yes
Hovakimyan *et. al.*	[173, 49]	LTV	LTV	No	Yes
GS-MRAC	Chapter 4	GS (LPV)	GS (LPV)	No	Yes

In this dissertation, a new approach is developed to extend the standard MRAC design for the systems with gain scheduled reference models and constrained control inputs; moreover, the decentralized version of this architecture is also developed. Some of the advantages of the adaptive control development for gas turbine engine systems can be categorized as follows:

- Appropriate for controlling a deteriorated gas turbine engine as a result of aging;
- Appropriate for controlling a damaged but still operable gas turbine engine due to exterior objects or accidents;
- Could enable plug and play (PnP) technology development for gas turbine engines, for the cases where there is a need to match different engine cores with different engine fans/props.

1.5 Plug and Play Technology for Engine Control

The plug and play (PnP) engine development scenario envisioned here has gas turbine engine cores being utilized in a more modular manner similar to the current use of internal combustion (IC) engines. As an illustrative example, consider a simple IC engine helicopter. The IC engine is purchased with its own governor or Engine Control Unit (ECU) and connected via a transmission to the rotor, a variable load. The operator has control over the engine RPM as well as the engine load (via the rotor). Applying this analogy to a gas turbine instead of a helicopter, the IC engine represents a gas generator core (High Pressure Compressor (HPC), combustor, High Pressure Turbine (HPT)), the rotor load represents either a shaft driven device or even a new spool (Fan/Prop, Low Pressure Turbine (LPT)), and the operator is a supervisory controller. Creating a separate engine controller for the gas generator has commercial applications, both in large scale commercial gas turbine design and small scale UAV development.

Adaptive control integrated in a distributed architecture [17, 28] could enable plug and play development of entire families of propulsion systems. In the distributed engine control vision [17, 28], engine cores and props/fans could be purchased with their onboard subordinate controllers ready for integration into a functional propulsion system, whereas the FADEC was developed independently for the integrated

engine. Structuring engine control in such a distributed fashion would increase compatibility between different engine manufacturers and reduce development time and cost for new engines.

Some of the potential examples of propulsion systems for PnP technology application are presented here. Aurora Flight Sciences Inc. [2] has a few different systems in which they have had to integrate commercial power systems into the overall propulsor, either using one fan or several fans. One potential application is the Excalibur platform [14]. It uses a hybrid electric propulsion system where a turbine engine powers three electric fans during VTOL flight, but then the turbine alone produces thrust for high speed flight. Another potential application is with Aurora's Golden Eye series of UAV's [15]. It has an engine attached to a lift fan. Currently, that fan is fixed pitch and the motor is internal combustion, but a turbine application would require the incorporation of a variable pitch fan system. Another potential example could be the Pratt & Whitney (P&W) PurePower geared turbofan engines which have been developed recently [129]. The current version of the engines utilize fixed pitch fans, but using PnP technology, variable pitch fans potentially can be used in P&W geared turbofan engines.

In this dissertation, a new decentralized MRAC architecture is developed with gain scheduled reference models for each subsystem, which enables the PnP technology development for gas turbine engine control systems.

1.6 Control Software Verification and Certification

When the operation of a control system is highly critical due to human safety factors or the high cost of failure in damaged capital or products, the software designers have to expend more effort to validate and verify their software before it can be released. In flight-critical operations, validation and verification are part of the flight certification process [48]. Software system certification involves many challenges, including the

necessity to certify the system at the level of functional requirements, code and binary levels, the need to detect run-time errors, and the need for proving timing properties of the eventual, compiled system [34, 134].

Provable closed-loop stability constitutes an essential attribute of control systems, especially when human safety is involved, as in many aeronautical systems like gas turbine engines. Motivated by such applications, there exist many theorems to support system stability and performance under various assumptions [33]. Stability criteria apply to a class of dynamical systems for which a stability proof is established; and Lyapunov's stability theory plays a critical role in this regard. Control-system domain knowledge, in particular, Lyapunov-theoretic proofs of stability and performance, can be migrated toward computer-readable and verifiable certificates [33, 61]. Some of the recent research results on the control software verification can be reviewed in [33, 60, 61, 131, 132, 174].

Software verification process for aerospace systems is explained in "RTCA/DO-178B: Software Considerations in Airborne Systems and Equipment Certification" [133]. Currently there is no detailed theoretical process for software verification; and the verification is mainly performed by running the software long enough to make sure that it works properly for the system at hand. Since the publication of DO-178B [133], experience and scientific advances have been gained in the formal methods, their application, and tools. Formal methods are mathematically based techniques for specification, development, and verification of software aspects of digital systems [135]. "RTCA/DO-333: Formal Methods Supplement to DO-178C and DO-278A" [135] provides guidance for applicants to facilitate the use of formal methods in aerospace systems.

In this dissertation, we aim at taking the first steps towards a more rigorous software verification process for gas turbine engine control systems, by developing stability proofs for the entire engine control architecture using the Lyapunov stability

theory. This approach later helps us in constructing an ellipsoid invariant set [20, 74] to be used as an efficient tool for control code stability analysis. The complete detailed engine control software verification process is beyond the scope of this dissertation and it remains a research topic for future.

Table 2 provides a brief comparison of various control algorithms from the control software verification point of view. The first five items are the algorithms that are presented in this dissertation, and the rest are other approaches available in the adaptive control literature, which are closer to the developed adaptive controllers in this dissertation.

Table 2: Comparison of control algorithms from the control software verification point of view

Case	References	Lyap Proof	No Switch	Single P	Disc Lyap Proof	Verif SW
GS	Chapter 3	✓	✓	✓	✓	✓
GS with Sat	Chapter 3	✓	✓	✓	✓	✓
GS-MRAC	Chapter 4	✓	✓	✓	N/A	N/A
GS-MRAC with Sat	Chapter 4	✓	✓	✓	N/A	N/A
D-GS-MRAC	Chapter 5	✓	✓	✓	N/A	N/A
Hovakimyan *et. al.*	[173, 49]	✓	✓	✗	N/A	N/A
Annaswamy *et. al.*	[9, 58, 57]	✓	✓	✗	N/A	N/A
Tao *et. al.*	[140, 142, 143]	✓	✗	✓	N/A	N/A

Currently the only control algorithm from the above items, that can be verified using the formal methods is the GS control approach, due to the availability of the Lyapunov stability proof for discrete-time GS system. For continuous-time MRAC algorithm, there exists Lyapunov stability analysis; however, complete Lyapunov stability analysis for general discrete-time MRAC system is still an active area of research [6, 7, 8, 45, 47, 64, 169]. As a Result, right now there is no complete software verification process based on the formal methods for MRAC and GS-MRAC algorithms.

1.7 Motivations

The research in this dissertation is mainly motivated by the challenging process of developing theoretical control architectures for gas turbine engines without sacrificing

performance and having in mind engine performance limits. Designing a controller which can be used for large thrust commands for gas turbine engines with acceptable tracking performance is a challenging problem itself [59, 130]. On the other hand, while developing new control architectures, there is a need to handle engine performance/structural limits such as constraints on the turbine temperature, spool speeds, spool accelerations, and also fuel control input, which introduce new challenges in the engine control design process [59, 130]. On the top of all of these issues control software verification for a gas turbine engine, which is a safety-critical aerospace system, is always of concern, especially for official aerospace certification entities like the FAA. All of these challenges together, triggered the process of developing new verifiable control architectures for gas turbine engines capable of handling the engine performance limits.

This dissertation tries to answer the following questions:

- **Research Question 1**: How can we develop fully stable control architectures for the entire operational envelope of gas turbine engines without sacrificing performance?

- **Research Question 2**: How can we develop fully stable adaptive controllers with some features to handle the gas turbine engine performance limits for the entire operational envelope without sacrificing performance?

- **Research Question 3**: How can we develop fully stable decentralized control algorithms for the entire operational envelope of gas turbine engines without sacrificing performance?

- **Research Question 4**: How can we develop some form of plug and play technology concept for gas turbine engine control systems, which enables us to integrate various gas turbine engine cores with various fans/props without too much effort to match these subsystems?

1.8 Contributions

The main contribution of this dissertation is to develop new verifiable stable control architectures for the entire operational envelope of gas turbine engines without sacrificing performance. This study of the new verifiable controllers was achieved by the following contributions:

- A verifiable gain scheduled (GS) control architecture for gas turbine engines is developed.
- A verifiable gain scheduled model reference adaptive control (GS-MRAC) architecture for gas turbine engines is developed, and then using these results a verifiable GS-MRAC architecture with constrained control inputs is developed.
- A verifiable decentralized gain scheduled model reference adaptive control (D-GS-MRAC) architecture for gas turbine engines is developed.
- A plug and play (PnP) technology concept for gas turbine engine control systems is investigated, based on the D-GS-MRAC architecture.

1.9 Dissertation Outline

This dissertation is organized in 6 chapters. Chapter 1 provides the introduction. Chapter 2 presents the physics-based modeling of a turboshaft engine driving a variable pitch propeller, which has been used for engine control development research. Chapter 3 addresses Research Question 1, and presents the detailed process of design and stability analysis of a verifiable gain scheduled control architecture for gas turbine engines. Chapter 4 addresses Research Question 2, and presents the design and stability analysis of GS-MRAC for gas turbine engines and GS-MRAC with constrained control inputs, which uses the results from Chapter 3. Chapter 5 addresses Research Questions 3 and 4, whereas the results of Chapters 3 and 4 are used for developing

a decentralized version of GS-MRAC; PnP technology concept for gas turbine engine control systems is also developed in Chapter 5. Finally, Chapter 6 concludes the dissertation.

CHAPTER II

PHYSICS-BASED MODELING OF A GAS TURBINE ENGINE

2.1 Introduction

Performance-based engine models give great accuracy and are used extensively in the design process. With increasing processing capability, it is possible to use performance models for control law development and execution. In this chapter, a nonlinear physics-based model for a twin spool JetCat SPT5 turboshaft engine [3] driving a variable pitch propeller is developed. The dynamic model is implemented using Matlab. In this model, the two spool speeds are the two main states of the state-space, and fuel flow and propeller pitch angle are the two control inputs. Mockups of the JetCat SPT5 turboshaft engine have been developed with CAD software, and using the mockups, a testbed for gas turbine engine static tests is developed. At the end, the model is verified, with experimental data obtained from static tests of the engine. Performance maps of the engine components including the compressor, the propeller, and the turbines are also constructed based on the experimental data. This physics-based engine model has been developed by Nathan Fitzgerald [114, 118], and presented here as an example for aero gas turbine engine control development.

2.2 Engine Test Apparatus

A testbed has been developed for conducting experiments on the JetCat SPT5 turboshaft engine [3] driving a variable pitch propeller. The engine tests were conducted at the Massachusetts Institute of Technology (MIT) Gas Turbine Lab (GTL) [4] by Aurora Flight Sciences [2]. In this section, test stand characteristics for experimental

purposes are presented briefly.

2.2.1 Testbed Engine

To construct a testbed in Aurora's existing facilities, an important limitation was that the engine be in a small enough thrust class; the constraints limited the engine's thrust to be approximately 100 *lbs* of thrust or less. The small size of the engine is appropriate for the scope of this research as it allows fast development with lower programmatic risk. The engine is affordable enough to be easily replaced if needed, and can be instrumented with a similarly affordable test rig. Engines in this size class typically have a service life measured in tens of hours due to the lubrication systems used at this size. Therefore a secondary driver on engine selection was service cost and demonstrated reliability of the engine. With these characteristics in mind, a small turboshaft engine, the JetCat SPT5 [3], depicted in Figure 1, with specifications shown in Table 3, was selected.

Figure 1: JetCat SPT5 turboshaft engine [3].

2.2.2 Test Stand and Instrumentation

A test stand was built to couple the core engine to a variable pitch propeller system. Diagrams and pictures of the test stand appear in Figures 2 to 8. The core and fan components sit on a translating platform. The propeller is cantilevered off the end of the table, producing horizontal thrust forces. A load cell attached to the side

Table 3: JetCat SPT5 turboshaft engine specifications [1, 3]

Characteristic	**Value**
Weight (including starter)	4.9 (lb)
Shaft Power	11 (hp)
Thrust (with 27" prop at 70000 RPM)	55 (lbs)
Service Life	25 (hrs)
Low Pressure Spool Speed Range	1500-7000 (RPM)
High Pressure Spool Speed Range	50-170000 (RPM)
Core Pressure Ratio	2:1
Outer Diameter and Length	83 × 365 (mm)
Exhaust Gas Temperature	580-710°C
Fuel Consumption at Full Power	8 (oz/min)
Fuel	Jet A1, 1-K kerosene

of the platform, measures the thrust; and a torque sensor, installed on the power shaft, measures the shaft moment provided to the fan. Figure 2 shows the engine and its mount. A ring holder secures the turbine to sheet metal flanges with 6xM3 screws, this supports the weight of the turbine. The turbine secures to the front of the holder with 3xM5 screws, this supports the thrust of the turbine. Figure 3 shows the engine exhaust gas path. Exhaust gases reaching 710°C vented from chamber through ductwork not shown in these figures.

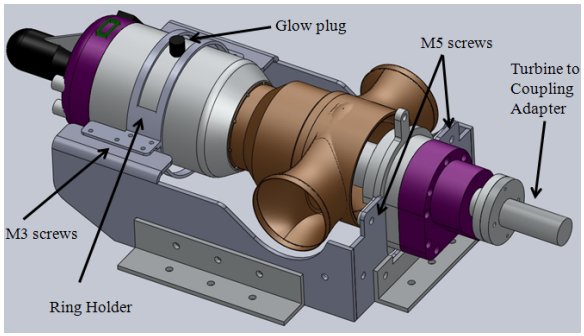

Figure 2: CAD drawing of the engine and its mount.

Figure 4 shows the CAD drawing of the variable pitch propeller. A high torque servo attaches to the swash plate with linear bearings and it controls the pitch of the blades without creating unwanted cyclic movements. Figure 5 shows the variable pitch propeller installed on the JetCat SPT5 engine setting.

Figure 6 shows the CAD drawing of the test setup with the JetCat engine, a

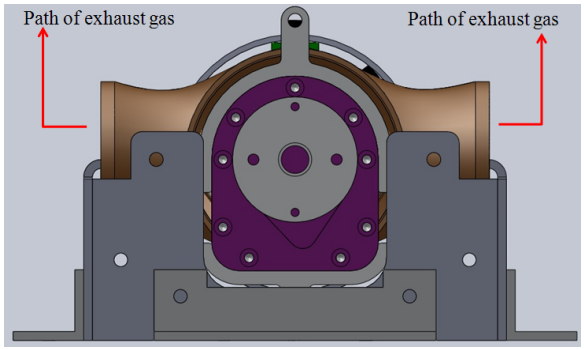

Figure 3: CAD drawing of the engine exhaust gas path.

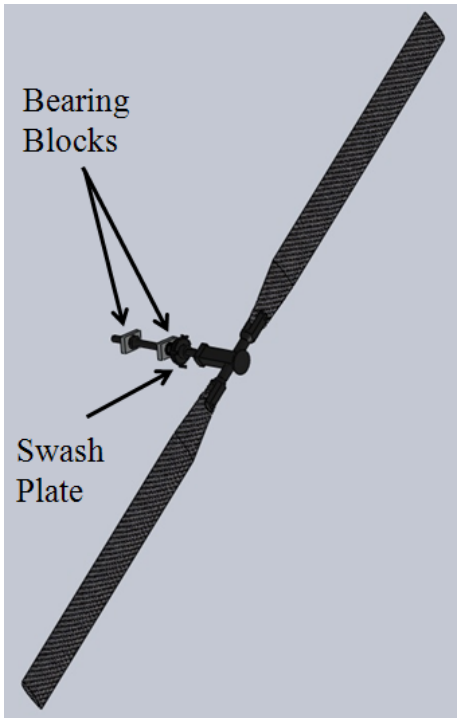

Figure 4: CAD drawing of the variable pitch propeller with its swash plate and bearing blocks.

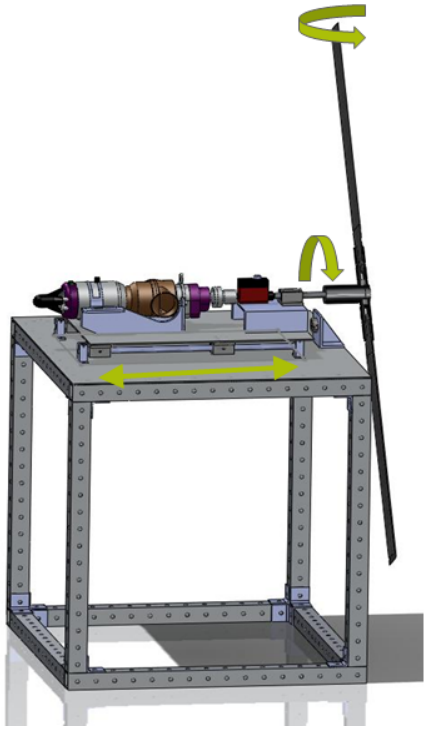

Figure 5: CAD drawing of the variable pitch propeller installed on the JetCat SPT5 engine.

variable rotor head, a load cell, a torque sensor, and shaft adapters. Figure 7 shows the pictures of the engine test stand configuration. Figure 7(a), shows an aluminum framing with precision linear bearings which can be fastened to the floor to avoid imbalance from the engine thrust. Lock-nuts are used wherever possible to prevent looseness caused by any vibrations. With this setup, the engine can be put on a cart

for rolling transport. Figure 7(b), shows the engine test aluminum frame with its sled removed and the engine holder mounted directly to a base plate with clearance for the propeller. Figure 7(c), shows the propeller shaft mounted to the stand with bearing blocks to prevent motion in Z and Y directions.

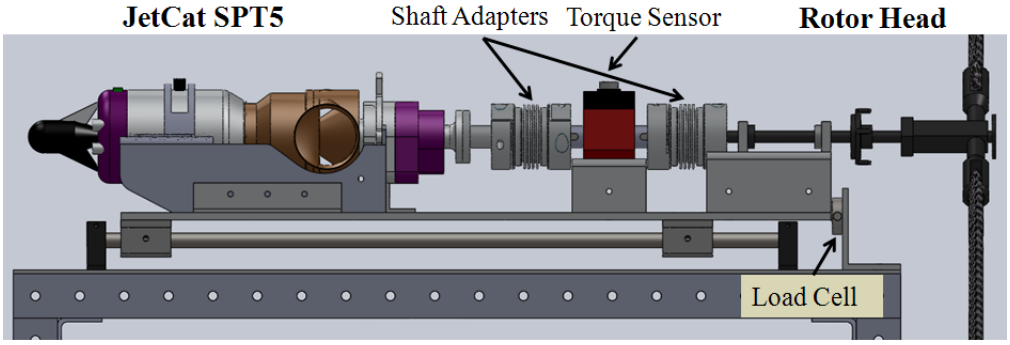

Figure 6: CAD drawing of the engine test setup with its load cell, torque sensor, and shaft adapters.

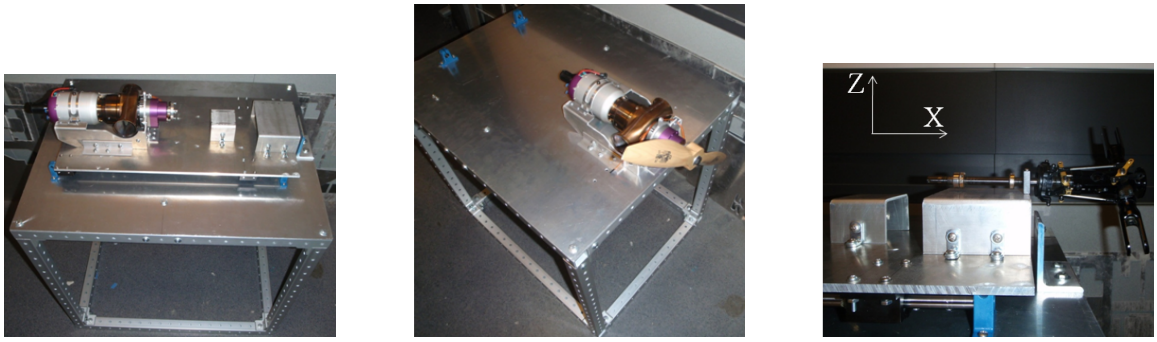

(a) (b) (c)

Figure 7: Engine test stand configuration.

The stock JetCat SPT5 contains instrumentation for high and low pressure spool rotational speed measurements, as well as for exhaust gas temperature measurements. Larger gas turbine engines typically use a much more extensive sensor suite. Furthermore, characterization of the engine for computational model calibration requires additional instrumentation for calculation of the engine performance and dynamic characteristics. Therefore, custom modifications on the the SPT5 engine have been performed to install pressure and temperature ports in the cases at the combustor,

the high pressure turbine-low pressure turbine (HPT-LPT) interface, and the exhaust. Pictures of the complete test stand installation for engine performance characterization is shown in Figure 8, with front and rear views.

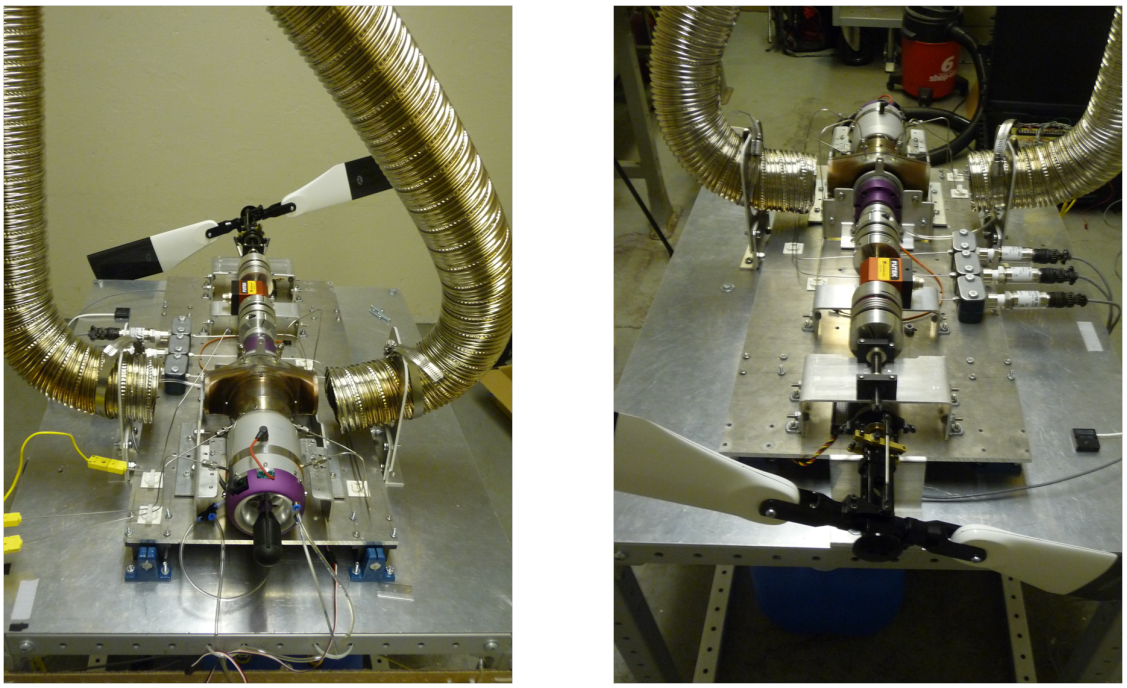

(a) Front View

(b) Rear View

Figure 8: JetCat SPT5 engine with variable pitch propeller installed in test stand.

2.3 Twin Spool Turboshaft Engine Model

This section was mainly written by Nathan Fitzgerald, and it is included here for the completeness of the dissertation.

The engine is modeled using three types of variables which are states, inputs, and outputs. States represent the spool speeds. Inputs are variables that perturb or control the system, such as fuel flow and propeller pitch angle. Outputs are additional parameters of interest other than the state and input variables, such as engine air flows, thrust, specific fuel consumption, etc. The dynamics of the engine are characterized by differential equations relating the time rate of change of state variables to the state variables themselves and the input parameters. States are obtained

transiently by calculating the derivatives and numerically integrating them in time.

2.3.1 Overview

A physics-based numerical engine model is constructed here, which can be used for engine control research purposes. A schematic of the engine is shown in Figure 9. Fuel is provided to the core of the engine, which is comprised of a compressor, a combustor, and a high speed turbine. Exhaust gases from the core engine power a low pressure turbine that transmits power to the variable pitch propeller through a reduction gearbox. For simplicity, both the low and high speed turbines are modeled as uncooled; no airflow is diverted around the combustor to provide cooling as is typical for larger aircraft gas turbines.

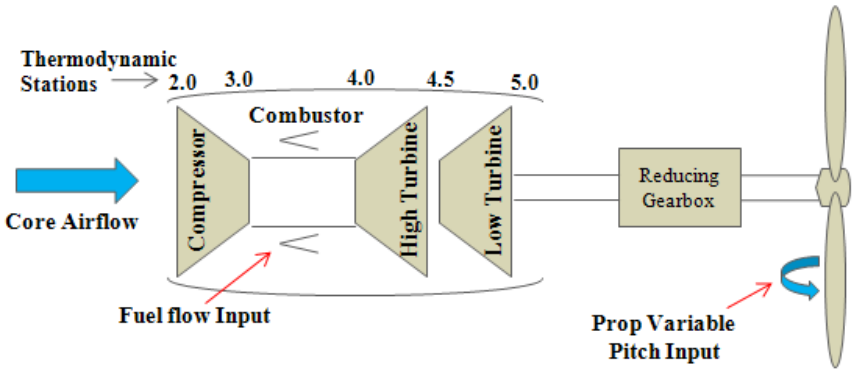

Figure 9: Schematic turboshaft engine diagram.

The dynamics of the engine are modeled using a lumped-parameter, first-principles approach that is commonly presented in standard gas turbine textbooks [69, 25]. The current model is an approximation of the JetCat SPT5 based on the limited cycle information available from the manufacturer. This model was updated to reflect the performance observed during the initial performance testing of the engine.

The model is broken up into three sections with separate dynamic models for the actuators, engine, and sensors. For the engine itself, the thermodynamic matching

between the propeller, compressor, and turbine components are calculated to determine the net torques on the two rotating spools. The inertial effects of the two spools are the only dynamic aspects of the engine model. Other low speed dynamics, like heat transfer from the gas path to metal, or higher speed dynamics, such as acoustics, volume dynamics, and combustor heat release dynamics, are currently ignored.

The model of the engine system includes the following assumptions and simplifications:

- Non-ideal efficiencies are assumed for the propeller, compressor, combustor, and turbine, but all other components are assumed to operate ideally. In particular, duct losses are not explicitly modeled. All engine losses are assumed to be included in the turbomachinary efficiencies.

- The core engine is assumed to be adiabatic. Effects of heat transfer to the environment, other than through the engine exhaust, are neglected.

- Fuel flow input is modeled using a "lower heating value". In other words, the temperature of the fuel is ignored in the combustion calculations.

- The working fluid is assumed to be standard atmospheric air throughout the flow path. The effects of changing gas composition through the combustor are not included.

- Gas path thermodynamic properties are assumed to be temperature dependent.

2.3.2 Detailed Description

Within the assumptions described in the previous section, the dynamics of the spool can be described from Newton's second law by the sum of the torques, $\mathcal{T}$, produced by the turbomachinery components, as well as the overall rotational inertias, I, of each of the two spools.

$$I_{hps}\dot{\omega}_2 = \mathcal{T}_{hpt} - \mathcal{T}_{hpc}, \tag{1}$$

$$I_{lps}\dot{\omega}_1 = \mathcal{T}_{lpt} - \mathcal{T}_{lpc}. \tag{2}$$

Noting that the power output of each of those components is defined by $\mathcal{P} = \mathcal{T}\omega$ and expressing the key parameters as fractions of the design value, (1) and (2) can be re-written as

$$\frac{\dot{N}_2}{N_{2,des}} = \left(\frac{\mathcal{P}_{hpt}}{\mathcal{P}_{hpt,des}} - \frac{\mathcal{P}_{hpc}}{\mathcal{P}_{hpc,des}}\right) / \left(\frac{N_2}{N_{2,des}}\right) / \left(\frac{\frac{1}{2}I_{high}\omega_{2,des}^2}{\mathcal{P}_{hpt,des}}\right) /2, \tag{3}$$

$$\frac{\dot{N}_1}{N_{1,des}} = \left(\frac{\mathcal{P}_{lpt}}{\mathcal{P}_{lpt,des}} - \frac{\mathcal{P}_{prop}}{\mathcal{P}_{prop,des}}\right) / \left(\frac{N_1}{N_{1,des}}\right) / \left(\frac{\frac{1}{2}I_{low}\omega_{1,des}^2}{\mathcal{P}_{lpt,des}}\right) /2, \tag{4}$$

noting that the high pressure compressor (HPC) and HPT powers are equal at design, as are the LPT and propeller power. The derivatives of the spool speeds are functions of the difference in power between the power input from the turbines, the power extraction from the propeller and compressor, and the spool inertias. In (3) and (4), the $I\omega_{des}^2/2/\mathcal{P}_{des}$ terms represent the spool inertias in terms of the stored energy when operating at design speed.

The following discussion of the power requirements uses the nomenclature for the thermodynamic stations shown in Figure 9. For each of the turbomachinery components, the power produced or absorbed is a function of the mass flow of air passing through it as well as the difference in stagnation enthalpy. For the compressor, assuming that the enthalpy is a function of temperature only, this can be written as

$$\frac{\mathcal{P}_{hpc}}{\mathcal{P}_{hpc,des}} = \frac{\dot{m}\left(h\left(T_3, 0\right) - h\left(T_2, 0\right)\right)}{\dot{m}_{des}\left(h\left(T_{3,des}, 0\right) - h\left(T_{2,des}, 0\right)\right)}. \tag{5}$$

Here, $\dot{m}$ represents the mass flow at the inlet to the compressor and $h(T, f)$ is the enthalpy of the gas path as a function of temperature and fuel/air ratio, $f = \dot{m}_{fuel}/\dot{m}_{air}$. For compressors, the fuel/air ratio is zero, as presented in (5).

For turbines, there is an increase in the mass flow an a non-zero fuel/air ratio due to the addition of fuel in the combustor. The power provided by the high pressure turbine can be written as

$$\frac{\mathcal{P}_{hpt}}{\mathcal{P}_{hpt,des}} = \frac{\left(1+f\right)\dot{m}\left(h\left(T_4, f\right) - h\left(T_{4.5}, f\right)\right)}{\left(1+f_{des}\right)\dot{m}_{des}\left(h\left(T_{4,des}, f_{des}\right) - h\left(T_{4.5,des}, f_{des}\right)\right)}, \tag{6}$$

and the low pressure turbine power can be written as

$$\frac{\mathcal{P}_{lpt}}{\mathcal{P}_{lpt,des}} = \frac{(1+f)\,\dot{m}\,(h\,(T_{4.5},f) - h\,(T_5,f))}{(1+f_{des})\,\dot{m}_{des}\,(h\,(T_{4.5,des},f_{des}) - h\,(T_{5,des},f_{des}))}. \tag{7}$$

A simpler approach to the modeling of the off-design power requirements is taken for the propeller. Here, it is assumed that the propeller power is proportional to the cube of the spool speed for a given setting of the variable pitch blades.

$$\frac{\mathcal{P}_{prop}}{\mathcal{P}_{prop,des}} = \frac{C_P\,(J_p,\beta)}{C_P\,(J_{p,des},\beta_{des})}\left(\frac{N_1}{N_{1,des}}\right)^3. \tag{8}$$

For a turbine or compressor, the adiabatic efficiency describes the actual power input or extracted from the turbomachine in relation to the ideal power at the same pressure ratio. For a compressor,

$$\eta_{comp} = \frac{h\,(T_{ideal,out},0) - h\,(T_{in},0)}{h\,(T_{out},0) - h\,(T_{in},0)}, \tag{9}$$

where the ideal output temperature is defined for an ideal gas as

$$s\,(T_{ideal,out},0) - s\,(T_{in},0) = R(0)\log\frac{P_{out}}{P_{in}}, \tag{10}$$

where $s(T,f)$ is the standard entropy as a function of temperature and fuel air ratio, and $R(f)$ is the ideal gas constant, from $P = \rho RT$, which has a small dependence on fuel/air ratio. For the turbine

$$\eta_{turb} = \frac{h\,(T_{out},f) - h\,(T_{in},f)}{h\,(T_{out,ideal},f) - h\,(T_{in},f)}, \tag{11}$$

where the ideal output temperature is again defined using Equation (10).

The combustor exit temperature is determined from the lower heating value of the fuel, h_{fuel}, the compressor exit temperature, and the fuel air mass flow ratio through an enthalpy balance

$$(1+f)\,h\,(T_4,f) = h\,(T_3,0) + f h_{fuel}\eta_{comb}, \tag{12}$$

where η_{comb} is the combustion efficiency.

Equations (5) through (12) define the power balances required to satisfy the first and second laws of thermodynamics. For off-design operation, the engine must also satisfy the conservation of mass flow, set by the physical cross-sectional areas throughout the flow path. The high pressure turbine, low pressure turbine, and exit nozzle act as restricting orifices where the corrected mass flow through the component is a function of the pressure drop across them. For the high pressure turbine, low pressure turbine, and the core nozzle, these continuity conditions can be expressed as

$$\frac{FP\left(P_4/P_{4.5}, Nc_2\right)}{FP\left(P_{4,des}/P_{4.5,des}, Nc_{2,des}\right)} = \frac{\left(1+f\right)\dot{m}\sqrt{h\left(T_4, f\right)/P_4}}{\left(1+f_{des}\right)\dot{m}_{des}\sqrt{h\left(T_{4,des}, f_{des}\right)/P_{4,des}}}, \tag{13}$$

$$\frac{FP\left(P_{4.5}/P_5, Nc_1\right)}{FP\left(P_{4.5,des}/P_{5,des}, Nc_{1,des}\right)} = \frac{\left(1+f\right)\dot{m}\sqrt{h\left(T_{4.5}, f\right)/P_{4.5}}}{\left(1+f_{des}\right)\dot{m}_{des}\sqrt{h\left(T_{4.5,des}, f_{des}\right)/P_{4.5,des}}}, \tag{14}$$

and

$$\frac{FP\left(P_5/P_{amb}\right)}{FP\left(P_{5,des}/P_{amb}\right)} = \frac{\left(1+f\right)\dot{m}\sqrt{h\left(T_5, f\right)/P_5}}{\left(1+f_{des}\right)\dot{m}_{des}\sqrt{h\left(T_{5,des}, f_{des}\right)/P_{5,des}}}. \tag{15}$$

Here, the FP combustor equation represents the flow parameter function, which is a function of pressure ratio and speed in the case of the turbomachinery, and a function of pressure ratio for the nozzle. For the nozzle, the flow parameter can be determined from the ideal expansion to ambient pressure. For the turbines, the model uses values from the turbine maps, tuned to match data from the engine test.

The final important pieces of the core model are the maps of compressor and turbines, which express the component pressure ratio and efficiency as functions of the component corrected speed and corrected mass flow. These maps are represented in (16), (17), and (18). The engine compressor map is described by

$$\left[\pi_{hpc}, \eta_{hpc}\right] = \text{HPCompressorMap}\left(W_{c,hpc}, N_{c,hpc}\right), \tag{16}$$

where $W_{c,hpc} = \dfrac{\dot{m}\sqrt{h_2(T_2)}/P_2}{\dot{m}_{des}\sqrt{h_2(T_{2,des})}/P_{2,des}}$, and $N_{c,hpc} = \dfrac{N_2}{N_{2,des}}/\sqrt{\dfrac{h_2(T_2)}{h_2(T_{2,des})}}$. The engine high pressure turbine map is described by

$$\left[\pi_{hpt}, \eta_{hpt}\right] = \text{HPTurbineMap}\left(W_{c,hpt}, N_{c,hpt}\right), \tag{17}$$

where $W_{c,hpt} = \dfrac{\dot{m}\sqrt{h_4(T_4)}/P_4}{\dot{m}_{des}\sqrt{h_4(T_{4,des})}/P_{4,des}}$, and $N_{c,hpt} = \dfrac{N_2}{N_{2,des}}/\sqrt{\dfrac{h_4(T_4)}{h_4(T_{4,des})}}$. The engine low pressure turbine map is described by

$$[\pi_{lpt}, \eta_{lpt}] = \text{LPTurbineMap}\left(W_{c,lpt}, N_{c,lpt}\right), \tag{18}$$

where $W_{c,lpt} = \dfrac{\dot{m}\sqrt{h_{4.5}(T_{4.5})}/P_{4.5}}{\dot{m}_{des}\sqrt{h_{4.5}(T_{4.5,des})}/P_{4.5,des}}$, and $N_{c,lpt} = \dfrac{N_1}{N_{1,des}}/\sqrt{\dfrac{h_{4.5}(T_{4.5})}{h_{4.5}(T_{4.5,des})}}$.

The turboshaft engine drives a variable pitch propeller. Some of the advantages of variable pitch propellers are: (a) getting more thrust at a constant shaft speed (engine power), or less power/fuel consumption for a given thrust level; (b) having more efficient thrust control (more rapid changes in thrust, etc); (c) decreasing the drag or maximizing the (L/D) ratio; (d) improving range, endurance, and cruising speed of the aircraft; (e) and decreasing the noise and pollution for a given thrust level, by the proper application in the control system. In our model, the variable pitch propeller thrust, F_N, and power, $\mathcal{P}_{prop}$, can be computed using

$$F_N = C_T(J_p, \beta)\rho_0 \left(\frac{N_1}{60}\right)^2 (2R_p)^4, \tag{19}$$

$$\mathcal{P}_{prop} = C_P(J_p, \beta)\rho_0 \left(\frac{N_1}{60}\right)^3 (2R_p)^5, \tag{20}$$

where ρ_0 is the air density, R_p is the propeller radius, J_P is the propeller advance ratio, β is the pitch angle, C_T is the propeller thrust coefficient, and C_P is the propeller power coefficient. To compute propeller thrust and power, there is a need to construct a map, described by equation (21), which takes propeller advance ratio and pitch angle as the inputs, and generates propeller thrust coefficient and power coefficient as the outputs.

$$[C_T, C_P] = \text{PropMap}\left(J_p,\ \beta\right). \tag{21}$$

All the performance maps of the engine components, including compressor, propeller, and turbines, are constructed based on the engine experimental data, which are presented in the next section. The engine dynamic model computation is as follows. For

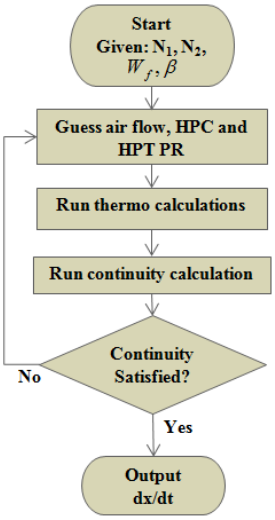

Figure 10: Numerical process of gas turbine engine modeling.

given spool speeds, fuel flow, and propeller variable pitch angle setting, the power output of the turbomachinary is calculated by assuming values of compressor mass flow, high pressure turbine pressure ratio, and low pressure turbine pressure ratio. The results are checked against (13), (14), and (15) to see if mass flow continuity is satisfied. If not, mass flow and turbine pressure ratio guesses are updated by Newton iteration, forming residual expressions from the continuity equations and iterating until the residuals are driven to zero. The results of that computation are input to (3) and (4), giving the change in engine spool speed as a function of its current state and input conditions. Figure 10 schematically shows the numerical process of engine modeling.

2.4 Engine Characterization Testing

2.4.1 Experiments

A numerical model of the engine system capable of simulating large throttle transients was constructed using Matlab. A series of performance characterization tests was conducted and the data collected was used to adjust the propeller, compressor, and turbine performance maps to match the physical engine apparatus as closely as

possible. No closed-loop tests were conducted.

The engine was operated at stabilized steady state setting from idle to full power, approximately 50,000 RPM to 170,000 RPM core spool speed, over the full range of pitch settings for the propeller system, approximately 0 deg to 35 degrees of pitch. These experiments were performed using the digital engine controller provided by the engine manufacturer. For a given blade pitch angle setting, the engine was slowly accelerated to the desired power setting. After a 20-second stabilization period, a Labview-based data system collected transient data at approximately 20 Hz for 20 seconds. The transient pressures, temperatures, core and propeller rotational speeds, thrust, and torque measurements were averaged over that time period to construct the steady state data used for performance matching. This process repeated over increasing power settings until either the engine reached full power, or (for lower propeller pitch angles) the propeller rotational speed limit was reached.

For each pitch setting tested, large throttle transients were performed from idle to the maximum power setting, and they were achieved without exceeding propeller speed limits. Whereas the the steady state data allowed the power balance between the engine components to be adjusted through the model performance maps, the transient data was used to adjust the values of moment of inertia for the two rotating spools in the system.

2.4.2 Performance Maps of Engine Components

The performance map of a compressor is presented using the following performance parameters: total pressure ratio, corrected mass flow rate, corrected spool speed, and adiabatic efficiency. Variations in the axial flow velocity in response to changes in pressure cause the multistage compressor to have quite different mass flow vs pressure ratio characteristics than one of its stages [93]. The high pressure compressor map, described in (16) is generated based on the JetCat SPT5 turboshaft engine

experimental data, shown in Figure 11. The parameters that are used to express

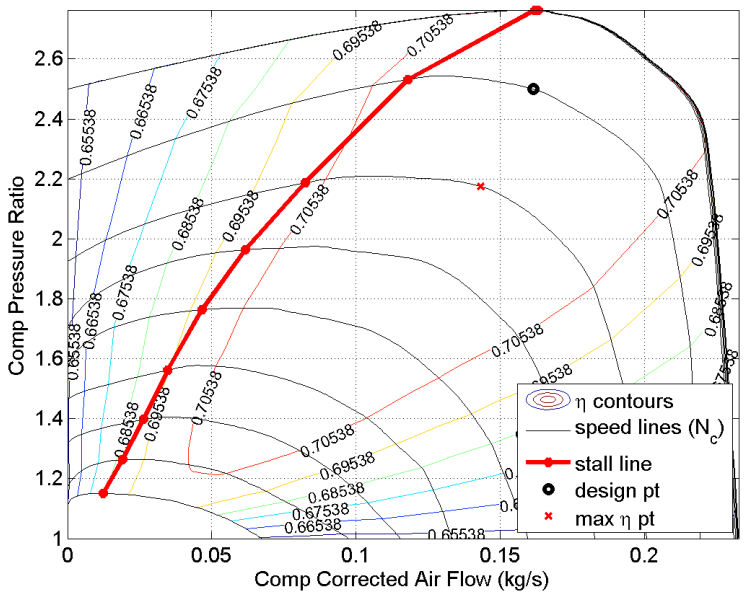

Figure 11: Compressor map of JetCat SPT5 engine.

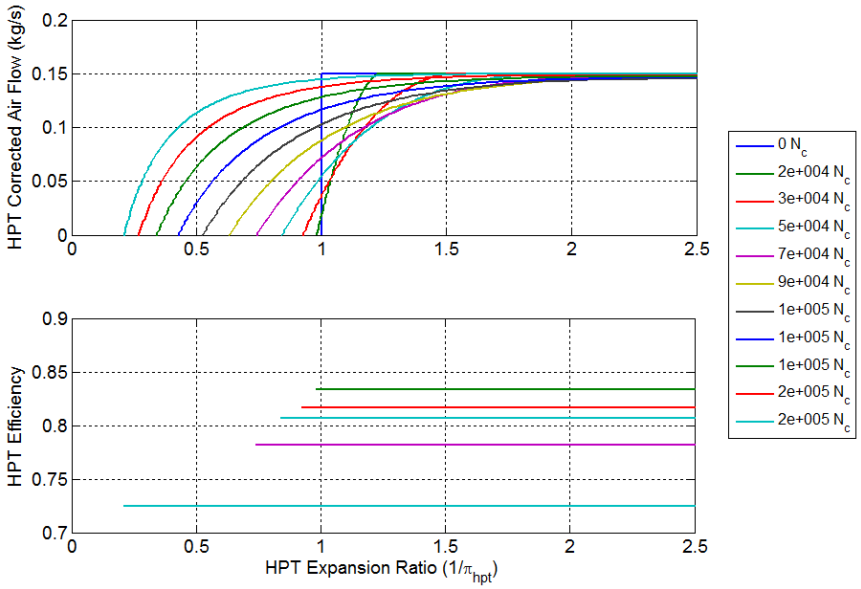

Figure 12: High pressure turbine map of JetCat SPT5 engine.

the performance of a turbine are the inverse of total pressure ratio (i.e. the turbine expansion ratio $(1/\pi_t)$), corrected mass flow rate, corrected spool speed, and adiabatic efficiency. For this engine the high pressure turbine is not like a choked nozzle. The

maps of the high pressure and low pressure turbines, described in (17) and (18), are generated based on the JetCat SPT5 turboshaft engine experimental data, shown in Figures 12 and 13. These plots show the expansion ratio, plotted as a function of the corrected mass flow rate and corrected mechanical speed. The maximum flow of gas that can be accommodated by the nozzles when when it is clearly evident that the nozzles are choked. Figure 14 shows the variable pitch propeller map, described by

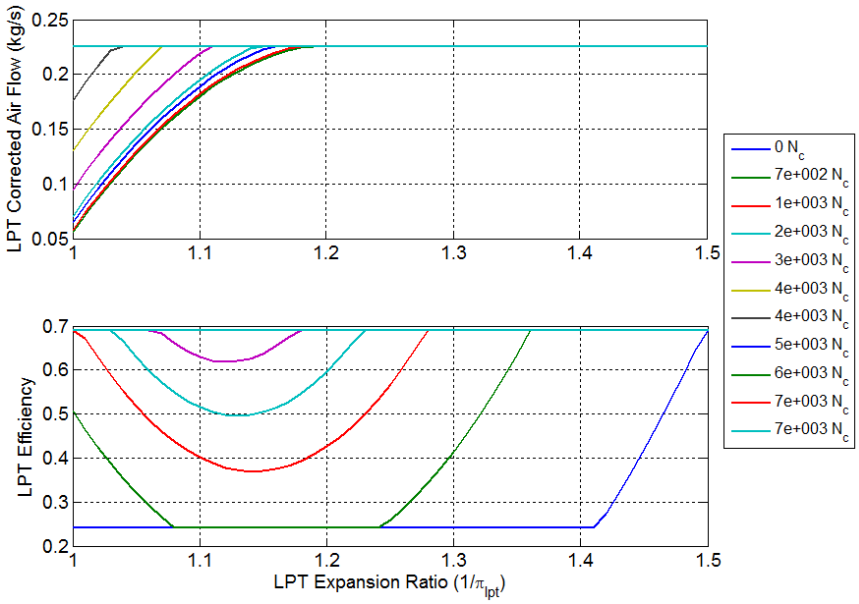

Figure 13: Low pressure turbine map of JetCat SPT5 engine.

(21). The propeller map is generated based on the JetCat SPT5 turboshaft engine experimental data. On the propeller map, the points on the various curves C_P vs. J_P that correspond to the same value of C_T are joined by the dashed curves. The map thus consists of two families of curves plotted in a coordinate system with J_p as abscissa and C_P as ordinate. The curves of the first family correspond each to a certain blade setting and show C_P vs. J_P. Along the curves of the second family, the blade angle varies, and C_T has a constant value [171]. The optimal steady state value of the propeller pitch angle, which has been shown by the red line in the map, was found to be 16 degrees by experiment.

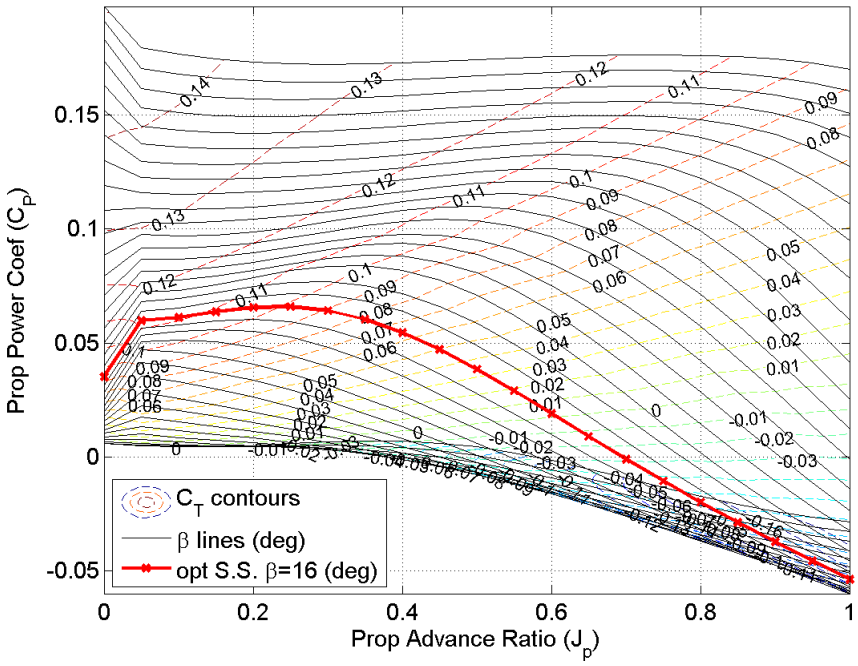

Figure 14: Propeller map.

2.4.3 Data Matching Results

This subsection was written by Nathan Fitzgerald, and it is included here for the completeness of the dissertation.

Figures 15 though 21 compare simulations of the data-matched engine model with the data from the JetCat SPT5 engine tests. The simulations were run at the same propeller pitch angles as the tests. As fuel flow was not measured during the tests, the fuel flow in the simulations was adjusted until the compressor pressure ratio from the model matched that of the data. The figures show a comparison of the propeller and core spools speeds, as well as the output engine thrust from the model with the corresponding engine test.

In all of the figures, the agreement in core spool speed is excellent. Initial versions of the model used a scaled version of a generic turbocharger map to model the centrifugal compressor. The scaled map required only minor adjustments to match

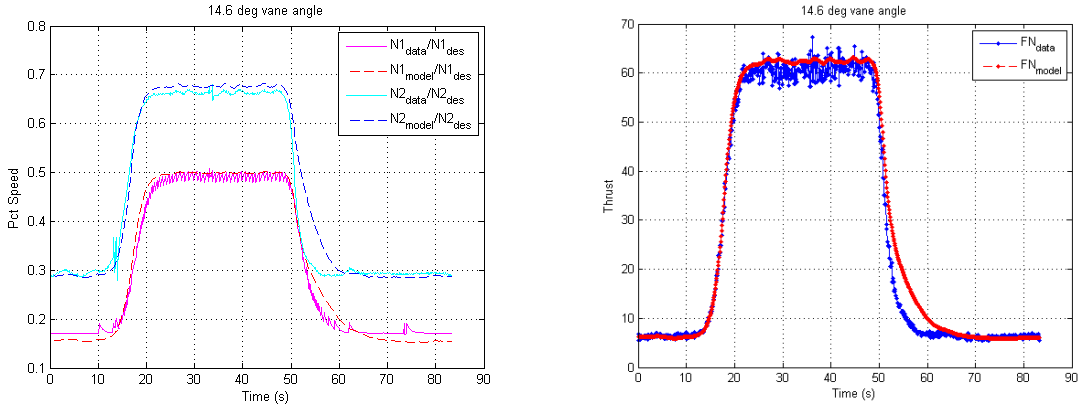

Figure 15: Comparison of model results to JetCat SPT5 data at 14.6 degree propeller pitch angle.

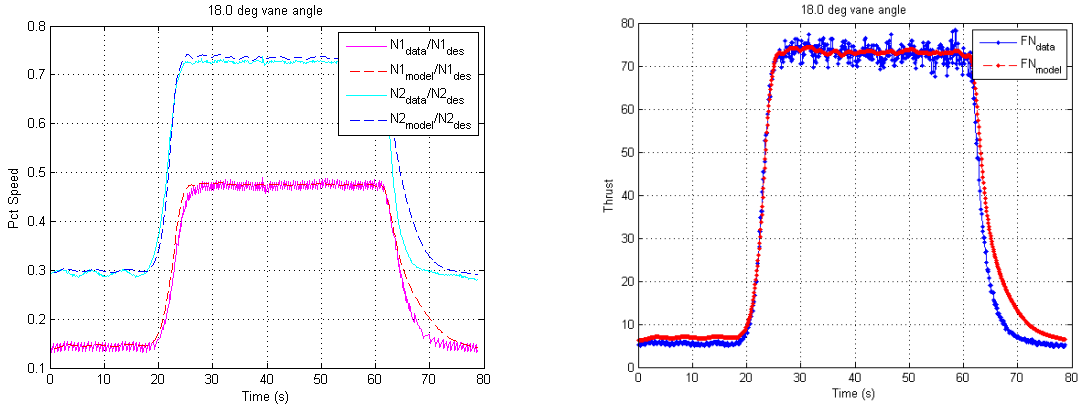

Figure 16: Comparison of model results to JetCat SPT5 data at 18 degree propeller pitch angle.

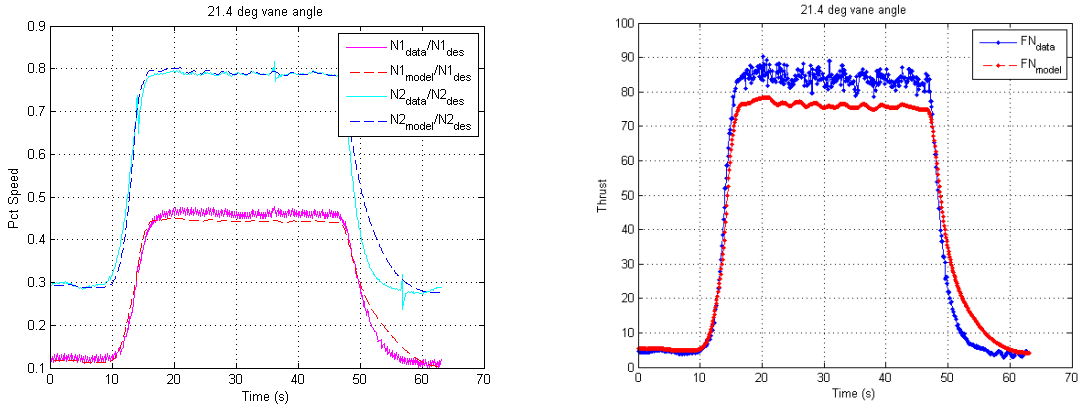

Figure 17: Comparison of model results to JetCat SPT5 data at 21.4 degree propeller pitch angle.

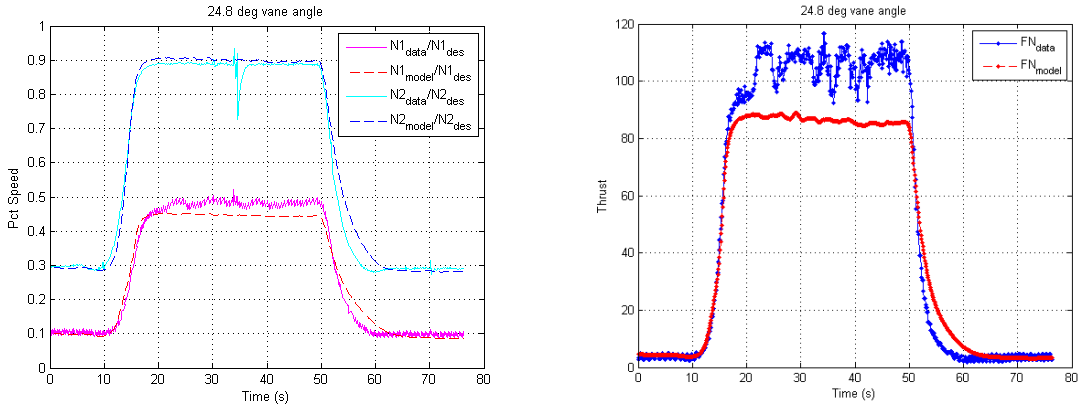

Figure 18: Comparison of model results to JetCat SPT5 data at 24.8 degree propeller pitch angle.

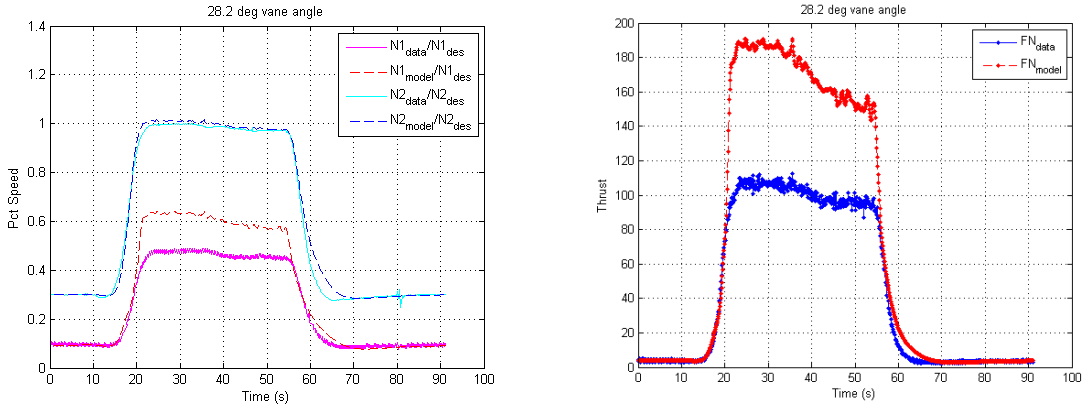

Figure 19: Comparison of model results to JetCat SPT5 data at 28.2 degree propeller pitch angle.

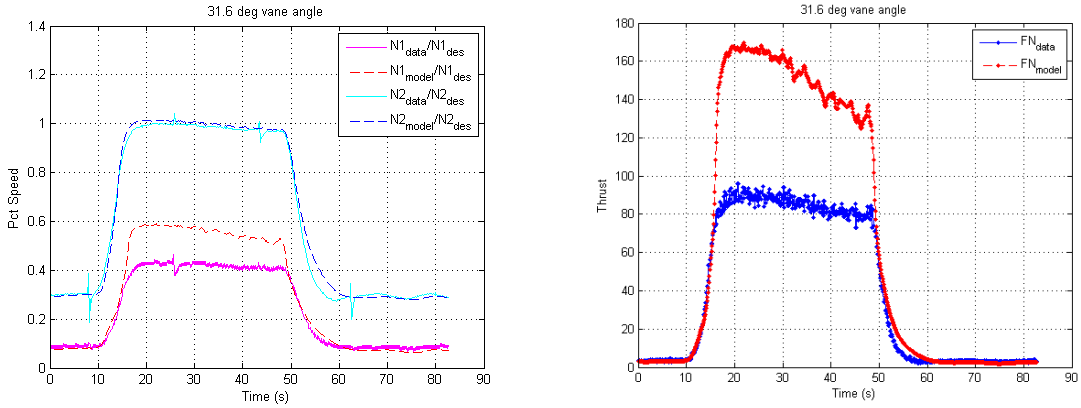

Figure 20: Comparison of model results to JetCat SPT5 data at 31.6 degree propeller pitch angle.

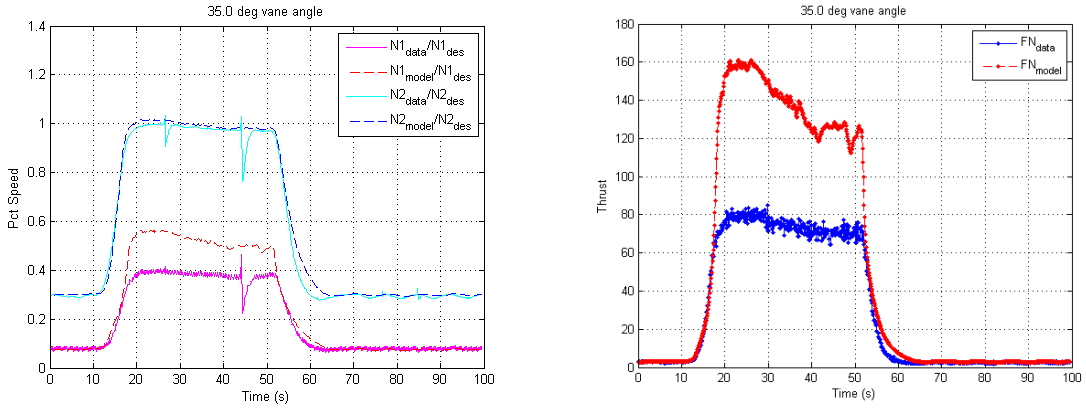

Figure 21: Comparison of model results to JetCat SPT5 data at 35 degree propeller pitch angle.

the pressure ratio to speed relationship seen in the data. The agreement in propeller speed and thrust are much more varied. At propeller pitch angles below 20 degrees, the agreement is reasonable at the higher power settings, within 5%. Between 20 and 25 degrees, the model begins to underpredict the propeller speed and thrust by more than 10%. At higher pitch angles up to 35 degrees, the model grossly overpredicts the propeller speed and thrust produced by the engine, in some cases by more than 100%. The variation in the model-data agreement in the low pressure spool was due to difficulties matching the low pressure turbine map with the steady state data. As propeller speed decreases with increasing propeller pitch angle, the engine data showes a substantial decrease in the lower pressure turbine power output for similar turbine expansion ratios. The efficiency of the LPT is very sensitive to speed, making it difficult to find a single map that could simultaneously match all power settings. The large over-estimation of thrust at the higher pitch angle can be attributed to an underestimation of the efficiency lapse with spool speed in the model.

Fortunately, the model agrees well in the region of most efficient operation for the engine. The pitch angle corresponding to the highest propeller efficiency is 16 degrees. This is the setting where most simulations of the engine were run during the program, giving confidence that the simulations used to develop the engine control

laws are valid.

2.5 Open-Loop Simulation Results

Open-loop simulation of the engine is performed in this section to illustrate the functionality of the developed physics-based dynamic model of the JetCat SPT5 turboshaft engine which drives a variable pitch propeller. The numerical values of the parameters which have been used for this simulation, and also the important engine operating points (including idle, cruise, and full thrust conditions), are also given in this section.

The gas turbine engine can be described as a nonlinear dynamical system

$$\begin{aligned} \dot{x}(t) &= f(x(t), u(t)), \\ y(t) &= g(x(t), u(t)), \end{aligned} \tag{22}$$

where $x(t) \in \Re^2$ is the state vector, $u(t) \in \Re^2$ is the control input vector, $y(t) \in \Re$ is the output vector, $f(.)$ is a 2-dimensional differentiable nonlinear vector function that represents the plant dynamics, and $g(.)$ is a 1-dimensional differentiable nonlinear vector function that generates the plant outputs. In this simulation, $x_1(t)$ is nondimensional HP spool speed, $x_2(t)$ is nondimensional LP spool speed, $u_1(t)$ is nondimensional fuel flow control input, $u_2(t)$ is propeller pitch angle control input, and $y(t)$ is the thrust of the engine.

For a standard day at sea level condition, steady state values of the states, the inputs and the output (thrust) of the system were found for three important operating points of the engine, which are idle, cruise and full thrust operating conditions. The steady state values are:

- Operating Point 1 (Full Thrust):

  $u_1^* = 1.0,\ u_2^* = 16$ (deg), $x_1^* = 1.0,\ x_2^* = 0.9524,\ y^* = 255.8685\ (N)$.

- Operating Point 2 (Cruise):

  $u_1^* = 0.4685,\ u_2^* = 16$ (deg), $x_1^* = 0.7264,\ x_2^* = 0.5,\ y^* = 70.5125\ (N)$.

- Operating Point 3 (Idle):

  $u_1^* = 0.145,\ u_2^* = 16$ (deg), $x_1^* = 0.295,\ x_2^* = 0.161,\ y^* = 7.317\ (N)$.

The numerical values of the engine parameters and other constants in the physics-based model are presented in Table 4.

Table 4: Numerical values of the parameters for JetCat SPT5 turboshaft engine simulation

Parameter	Value	Parameter	Value	Parameter	Value
T_0	288.15 (°K)	K_{burn}	0.049867	$W_{f,des}$	0.0035323 (kg/s)
P_0	101325 (Pa)	A_{noz}	0.002009 (m^2)	$r_{hpc,des}$	0.555600
T_{amb}	288.15 (°K)	R_p	0.335 (m)	$r_{hpt,des}$	0.720360
P_{amb}	101325 (Pa)	I_{hps}	4×10^{-5} ($kg.m^2$)	$r_{lpt,des}$	0.273120
T_{std}	288.15 (°K)	I_{lps}	0.0216 ($kg.m^2$)	$M_{exit,des}$	0.374345
P_{std}	101325 (Pa)	η_{comb}	0.9	$W_{c3,des}$	0.076884 (kg/s)
h_{fuel}	43286000 (J/kg)	V_{flight}	0	$W_{c4,des}$	0.138315 (kg/s)
f_{stoic}	0.062	$N_{1,des}$	7000 (RPM)	$W_{c4.5,des}$	0.225094 (kg/s)
π_{burn}	0.95	$N_{2,des}$	170000 (RPM)	$W_{c5,des}$	0.280924 (kg/s)

h_{fuel} is fuel lower heating value, f_{stoic} is stoichiometric fuel air ratio, r_{hpc} is compressor map r-line, r_{hpt} is HPT expansion ratio, r_{lpt} is LPT expansion ratio, R_p is propeller radius, A_{noz} is nozzle area, M_{exit} is nozzle exit Mach number guess, I_{hps} is high pressure spool inertia, and I_{lps} is low pressure spool inertia. For more convenience in the simulations, pressure and temperature outputs are normalized by standard day conditions, 101325 Pa and 288.15°K respectively. Some of the plant states and inputs also have been nondimensionalized by their design values; fuel flow input, W_f, is divided by 0.0035323 (kg/s), HP spool speed, N_2, is divided by 170000 RPM, and LP spool speed, N_1, is divided by 7000 RPM.

The results of the open-loop simulation of SPT5 engine dynamics are presented, using the developed physics-based model in Matlab. The simulation scenario is to increase the thrust from idle to cruise condition and again back to the idle condition for a standard day at sea level condition. Figures 22 to 28 show the results of this open-loop simulation.

Figure 22 shows high and low pressure spool speeds. Figure 23 shows the fuel and angle control inputs histories. Figure 24 shows the time history for high and

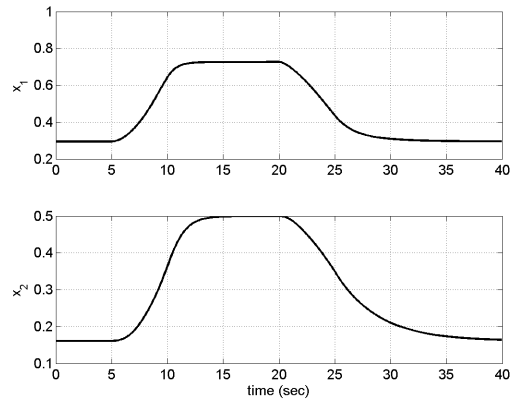

Figure 22: HP and LP spool speeds.

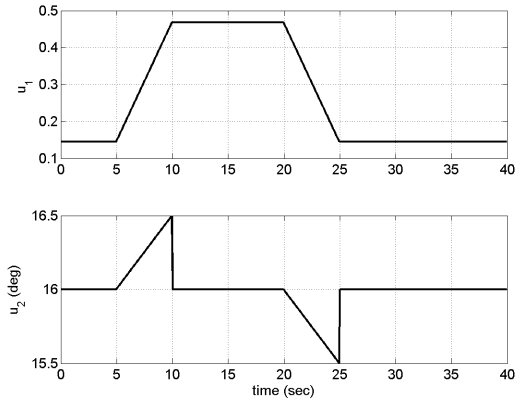

Figure 23: Fuel and angle control inputs.

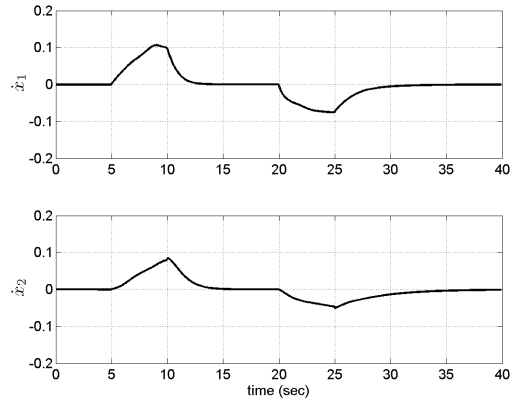

Figure 24: HP and LP spool accelerations.

low pressure spool accelerations. Figure 25 shows the thrust time history. Figure 26 shows the time history of the engine parameters such as turbine temperature,

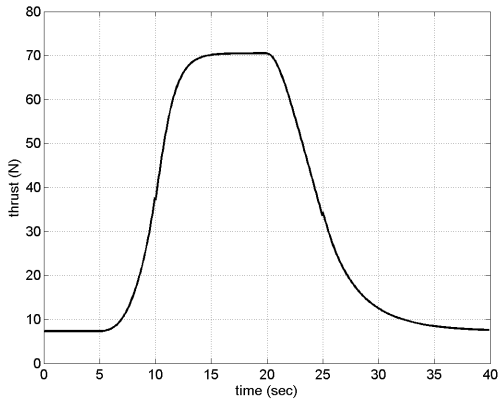

Figure 25: Engine thrust.

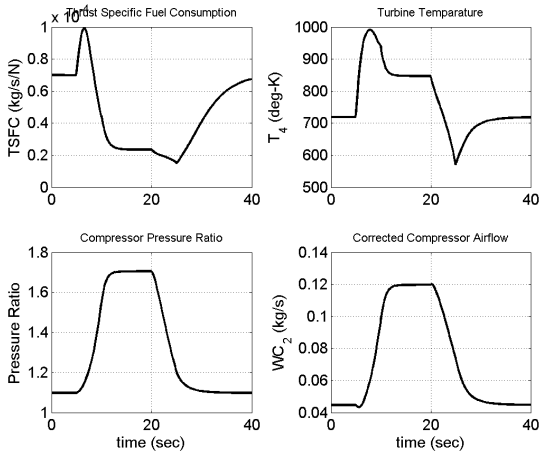

Figure 26: Turbine temperature, TSFC, compressor pressure ratio, and compressor mass flow rate.

TSFC, compressor mass flow rate, and compressor pressure ratio. Figure 27 shows the compressor map. The operating line of this simulation is shown on the compressor map. After five seconds of simulation, engine accelerates due to a jump in fuel control input, so the operating line is above the steady state operating line of the engine. After twenty seconds, engine decelerates due to a sudden decrease in the fuel flow, so the operating line goes below the steady state operating line shown on the compressor map. Figure 28 show the time histories of the four pressure, four temperature, and two spool speed sensor outputs.

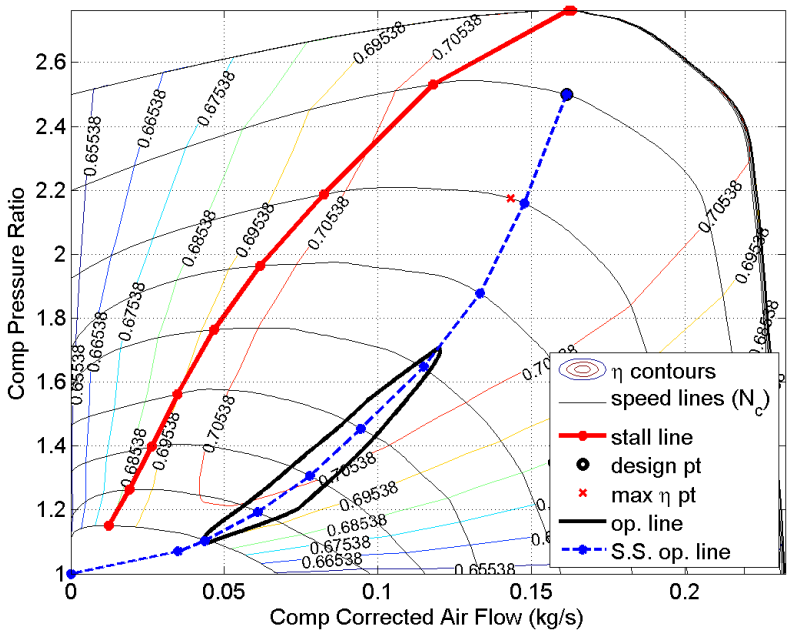

Figure 27: Compressor map showing the engine operating line for the simulation.

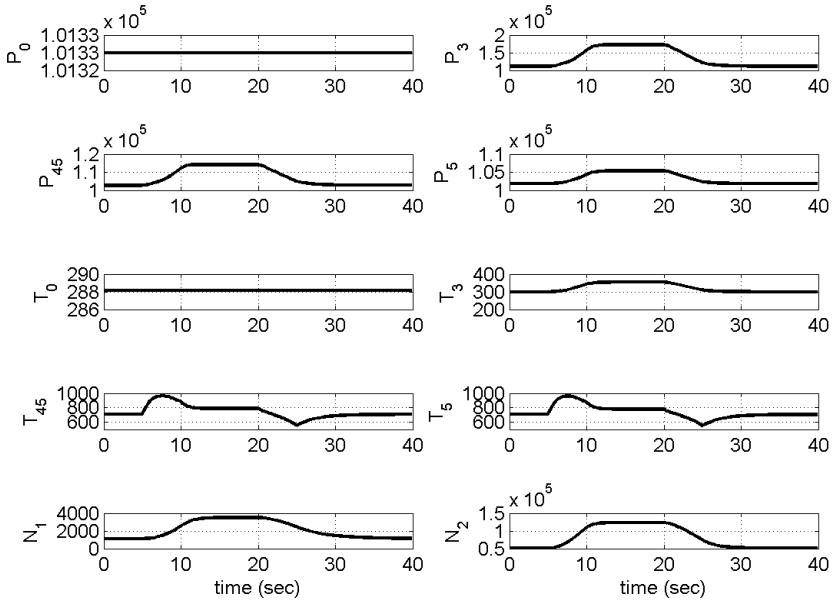

Figure 28: Pressure, temperature, and spool speed sensor outputs.

2.6 Summary

A nonlinear physics-based model was developed for a twin spool JetCat SPT5 turboshaft engine which drives a variable pitch propeller. The dynamic model was then

implemented using Matlab. Two spool speeds were used as the two main states, and fuel flow rate and propeller pitch angle were used as two control inputs of the state-space model. The model was verified with experimental data, obtained from static tests of the engine. Performance maps for the propeller, compressor, and high and low pressure turbines were also constructed based on the gathered experimental data. As a result of the experimental tests, the propeller pitch angle of 16 degree was found to be the optimal steady state angle setting (i.e., the pitch angle corresponding to the highest propeller efficiency) at steady-state engine operating points ranging from idle to full thrust condition. Open-loop simulation results of the engine model were also presented. The developed physics-based model of the JetCat SPT5 turboshaft engine is used as an example gas turbine engine model for nonlinear control research which is presented in the next chapters of the dissertation.

CHAPTER III

GAIN SCHEDULED CONTROL: STABILITY AND VERIFICATION

3.1 Introduction

Stability and control of gas turbine engines have been of interest to researchers and engineers from a variety of perspectives. An introduction to the analysis and design of engine control systems can be found in [158]. The basics of controlling a gas turbine engine while satisfying numerous constraints have been reviewed in [160]. The design of engine control and monitoring systems with a dual interest in both turbofan and turboshaft engines has been covered in [59]. An application of robust stability analysis tools for uncertain turbine engine systems is presented in [11]. An application of the Linear-Quadratic-Gaussian with Loop-Transfer-Recovery methodology to design a control system for a simplified turbofan engine model and the F-100 turbofan engine model is presented in [13, 38]. A unified robust multivariable approach to propulsion control design has been developed in [37]. The development of other control techniques, such as sliding mode, for gas turbine engine application can be found in [130]. Adaptive controllers for single and twin spool turboshaft systems for small throttle commands are described in [117, 119].

To facilitate the stability analysis of nonlinear systems, such as gas turbine engines, an efficient technique is to approximate them by a linear time-varying (LTV) system. This concept, which we have used for our stability analysis, is known as global linearization and can be found in [84, 85]. More recent work on global linearization and the use of Linear Matrix Inequalities (LMIs) for the analysis of dynamical systems can be found in [20]. Some Soviet literature on the absolute stability problem,

like Lur'e and Postnikov [90, 89] and Popov [126, 127, 128], also implicitly use the idea of global linearization. Recent literature that demonstrates the practical power of global linearization techniques include [88, 87]. The idea of global linearization along with the notion of incremental stability has been used in [44].

An example of engine control architecture using multiple sensors and actuators for a gas turbine engine is schematically represented in Figure 29. In this control architecture, three different sets of sensors are used for pressure, temperature, and speed measurements; and three types of actuators are used for fuel flow, fan/prop blade angle, and fan exit area actuation.

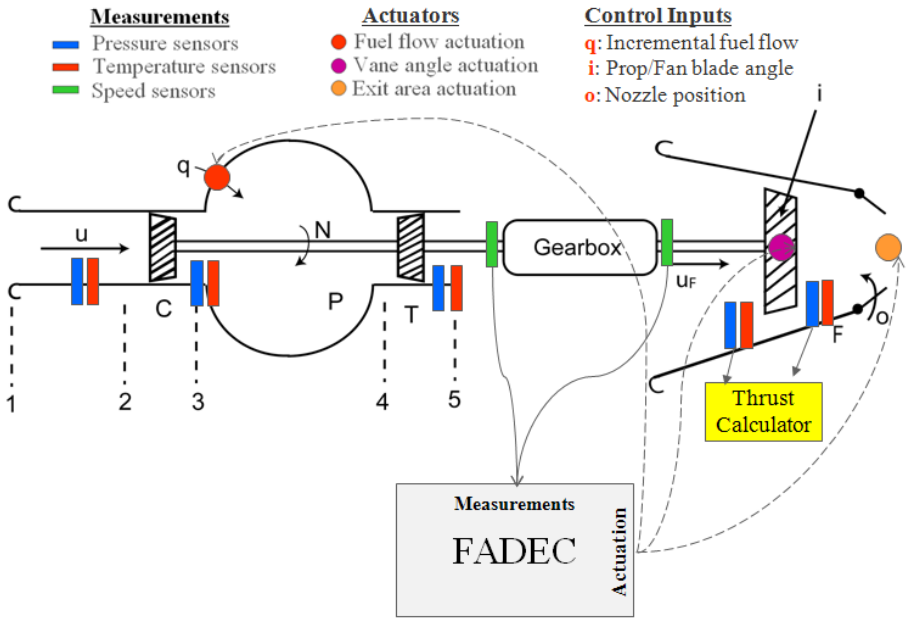

Figure 29: Example of gas turbine engine control architecture.

To design a controller for our turboshaft engine we use gain scheduling (GS), which perhaps is one of the most popular nonlinear control design approaches and has been widely and successfully applied in fields ranging from aerospace to process control [81, 136]. Gas turbine engines are no exception, and research on gain scheduled control of gas turbine engines is presented in [10, 16, 21, 39, 41, 65, 176, 179]. A simplified scheme for scheduling multivariable controllers for robust performance over

a wide range of turbofan engine operating points is presented in [39]. In a recent work presented in [41], results on polynomial fixed-order controller design are extended to SISO gain scheduling with guaranteed stability and H_∞ performance for a turbofan engine over the whole scheduling parameter range. In [41], the engine Linear Parameter Varying (LPV) representation depends on an exogenous variable parameter which is the combustion chamber pressure. In this chapter we develop an output dependent gain scheduled control structure for a MIMO linear parameter dependent model of the JetCat SPT5 turboshaft engine developed in Chapter 2 using the method presented in [136, 149, 150, 152]. This controller is designed to be used for the entire flight envelope of the twin spool turboshaft engine with stability guarantees. The scheduling variable in our design process is an *endogenous* parameter, which is a function of the gas turbine engine spool speeds. This endogenous scheduling variable captures the plant nonlinearities as explained in [149, 152], since the spool speeds are the main states of the turboshaft engine state-space model, and also the outputs of the system.

The stability analysis for the closed-loop system with gain scheduled control inputs is presented in this chapter. The essential part of the stability analysis is to find a single quadratic Lyapunov function for multiple linearizations near equilibrium and non-equilibrium points, which are distributed over the entire operational envelope of the plant. Hence, computing a single Lyapunov matrix P using convex optimization tools not only guarantees the stability of the closed-loop system over the entire flight envelope of the engine, but also facilitates the engine control software verification using formal methods [33, 34, 134]. An optimization problem, which is solvable using convex optimization tools, is also proposed to verify that the linearized plant always lives in the convex hull of the linearization matrix samples, and hence to verify the stability of the closed-loop system numerically.

This chapter is organized as follows. First, a linear parameter dependent representation of the plant is presented. Second, concepts for output dependent gain scheduled

control of this model are developed. Third, the stability analysis of the closed-loop system and also a numerical approach to verify the stability of the closed-loop system in an on-line fashion are presented; the extension of this stability analysis for the systems with constrained control inputs is also presented. Finally, simulation results for gain scheduled control of a MIMO physics-based model of a JetCat SPT5 turboshaft engine are presented. Simulation results show the efficiency of the proposed controller for the entire flight envelope of the turboshaft engine with guaranteed stability and proper tracking performance.

3.2 Gain Scheduled Control Design

Consider the nonlinear dynamical system

$$\begin{aligned} \dot{x}^p(t) &= f^p(x^p(t), u(t)), \\ y(t) &= g^p(x^p(t), u(t)), \end{aligned} \tag{23}$$

where $x^p(t) \in \Re^n$ is the state vector, $u(t) \in \Re^m$ is the control input vector, $y(t) \in \Re^m$ is the output vector, $f^p(.)$ is an n-dimensional differentiable nonlinear vector function which represents the plant dynamics, and $g^p(.)$ is an m-dimensional differentiable nonlinear vector function which generates the plant outputs. We intend to design a feedback control such that $y(t)$ properly tracks a reference signal $r(t)$ as time goes to infinity, where $r(t) \in D_r \subset \Re^m$, and D_r is a compact set.

Assume that for each $r \in D_r$, there is a unique pair (x_e^p, u_e) that depends continuously on r and satisfies the equations

$$\begin{aligned} 0 &= f^p(x_e^p, u_e), \\ r &= g^p(x_e^p, u_e), \end{aligned} \tag{24}$$

where x_e^p is the desired equilibrium point and u_e is the steady-state control that is needed to maintain equilibrium at x_e^p. It is often useful to parameterize the family of system equilibria as follows:

Definition 1. *The functions $x_e^p(\alpha(t)), u_e(\alpha(t))$, and $r_e(\alpha(t))$ define an equilibrium family for the plant (23) on the set Ω if*

$$\begin{aligned} &f^p(x_e^p(\alpha(t)), u_e(\alpha(t))) = 0, \\ &g^p(x_e^p(\alpha(t)), u_e(\alpha(t))) = r_e(\alpha(t)), \quad \forall \alpha \in \Omega. \end{aligned} \tag{25}$$

Let $O \subset \Re^{m+n}$ be the region of interest for all possible system state and control vector (x^p, u) during the system operation, and denote x_{ei}^p and u_{ei}, $i \in I = 1, 2, ..., q$, as a set of constant operating points located at some representative and properly separated points inside O. Introduce a set of q regions $O_i, i \in I$ centered at the chosen operating points (x_{ei}^p, u_{ei}), and denote their interiors as O_{i0}, such that $O_{j0} \bigcap O_{k0} = \oslash$ for all $j \neq k$, and $\bigcup_{i=1}^{l} O_i = O$. The linearization of the plant at each equilibrium point is

$$\begin{aligned} \dot{x}^p(t) &= A_i^p(x^p(t) - x_{ei}^p) + B_i^p(u(t) - u_{ei}), \\ y(t) &= C_i^p(x^p(t) - x_{ei}^p) + D_i^p(u(t) - u_{ei}) + y_{ei}, \end{aligned} \tag{26}$$

where the matrices are obtained as follows

$$\begin{aligned} A_i^p &= \frac{\partial f^p(.)}{\partial x^p(t)}|_{(x_{ei}^p, u_{ei})}, \quad \forall (x^p(t), u(t)) \in O_i, \\ B_i^p &= \frac{\partial f^p(.)}{\partial u(t)}|_{(x_{ei}^p, u_{ei})}, \quad \forall (x^p(t), u(t)) \in O_i, \\ C_i^p &= \frac{\partial g^p(.)}{\partial x^p(t)}|_{(x_{ei}^p, u_{ei})}, \quad \forall (x^p(t), u(t)) \in O_i, \\ D_i^p &= \frac{\partial g^p(.)}{\partial u(t)}|_{(x_{ei}^p, u_{ei})}, \quad \forall (x^p(t), u(t)) \in O_i. \end{aligned} \tag{27}$$

Note that $(x^p(t), u(t))$ belongs to only one O_i at each time. Corresponding to each linearization at ith equilibrium point, there exists an $\alpha_i \in \Omega$, which is a function of equilibrium values of the system outputs, i.e. y_{ei}.

The family of plant linear models (26) can be written as

$$\begin{aligned} \delta\dot{x}^p(t) &= A^p(\alpha(t))\delta x^p(t) + B^p(\alpha(t))\delta u(t), \\ \delta y(t) &= C^p(\alpha(t))\delta x^p(t) + D^p(\alpha(t))\delta u(t), \quad \forall \alpha \in \Omega, \end{aligned} \tag{28}$$

where

$$\begin{aligned} \delta x^p(t) &= x^p(t) - x_e^p(\alpha(t)), \\ \delta y(t) &= y(t) - y_e(\alpha(t)), \\ \delta u(t) &= u(t) - u_e(\alpha(t)). \end{aligned} \tag{29}$$

$A^p(\alpha(t))$, $B^p(\alpha(t))$, $C^p(\alpha(t))$, and $D^p(\alpha(t))$ are the parameterized plant linearization family matrices and $x_e^p(\alpha(t))$, $u_e(\alpha(t))$, and $y_e(\alpha(t))$ are the parameterized steady-state variables for the states, inputs, and outputs of the plant, which form the equilibrium manifold of plant (23). The subscript "e" stands for "steady-state" throughout this dissertation.

Based on the results from [149, 152, 136, 150], an output dependent gain scheduled controller for plant (28) is designed as follows. First, a set of parameter values α_i is selected, which represent the range of the plant's dynamics, and a linear time-invariant controller is designed for each corresponding linear model. Then, in between operating points, the controller gains are linearly interpolated such that for all frozen values of the parameters, the closed-loop system has satisfactory properties, such as nominal stability and robust performance. To guarantee that the closed-loop system retains the dynamic properties of the frozen-parameter designs, the scheduling variables should vary slowly with respect to the system dynamics [149].

The parameter $\alpha(t)$ is called the scheduling variable and should be measurable in real time; $\alpha(t)$ can be a function of endogenous variables (i.e., depending on the plant states) and/or exogenous variables (i.e., independent of the plant states). In LPV systems, this parameter is an exogenous parameter [151]. Some of the examples of exogenous parameter selection in LPV control of turbine engines are presented in [21, 16, 41]. In [21], the scheduling parameter is defined as a function of the exogenous signals describing the surroundings, like altitude, intake Mach number, and a health parameter describing the state of the compressor. In [16], the scheduling parameter is defined as a function of lagged measurement of engine thrust and altitude, which are

exogenous variables. In [41], the scheduling parameter is defined to be the combustion chamber pressure, which is an exogenous variable. In gain-scheduling, this parameter is a function of the output and hence it is an endogenous parameter [151]. Some of the examples of endogenous parameter selection for gain-scheduled control of turbine engines can be found in [65, 179, 176]. In [65], the scheduling parameter is defined to be the engine low pressure spool speed, which is one of the outputs of the system. In [179, 176], the scheduling parameter is defined to be the engine high pressure spool speed. In the turboshaft engine control example described later in this chapter, $\alpha(t)$ is defined to be the Euclidean norm of the engine spool speeds, which can be measured in real-time. Since the spool speeds are the only plant states in the model and also due to the fact that we need the plant nonlinearities to be captured by the output vector, as explained in [149, 152], we defined the scheduling parameter to be a function of both spool speeds ($\alpha(t) = ||x^p(t)||$), which is a scalar, so a simpler interpolation process can be used in the simulations. In general, the linear parameter dependent model should reselect the static and dynamic characteristics of the engine in the $\pm 20\%$ neighbourhood of the equilibrium manifold (or operating line) of the engine with the error being less than 4% [73].

The design of a linearization gain scheduled controller requires designing a linear controller family corresponding to the plant linearization family (28). Let the parameterized linear controller family be

$$\begin{aligned} \delta\dot{x}^c(t) &= A^c(\alpha(t))\delta x^c(t) + B^c(\alpha(t))[\delta y(t) - \delta r(t)], \\ \delta u(t) &= C^c(\alpha(t))\delta x^c(t) + D^c(\alpha(t))[\delta y(t) - \delta r(t)], \quad \forall \alpha \in \Omega, \end{aligned} \tag{30}$$

where

$$\begin{aligned} \delta x^c(t) &= x^c(t) - x_e^c(\alpha(t)), \\ \delta r(t) &= r(t) - r_e(\alpha(t)), \quad \forall \alpha \in \Omega. \end{aligned} \tag{31}$$

$x_e^c(\alpha)$ and $r_e(\alpha)$ are the parameterized steady-state variables for the controller states and reference signals. A standard realization of the parameterized controller can be

written with the reference signal explicitly displayed as

$$\begin{bmatrix} \delta\dot{x}^c(t) \\ \delta u(t) \end{bmatrix} = \begin{bmatrix} A^c(\alpha(t)) & B^c(\alpha(t)) & -B^c(\alpha(t)) \\ C^c(\alpha(t)) & D^c(\alpha(t)) & -D^c(\alpha(t)) \end{bmatrix} \begin{bmatrix} \delta x^c(t) \\ \delta y(t) \\ \delta r(t) \end{bmatrix}, \quad \forall\alpha \in \Omega. \tag{32}$$

We have to obtain, based on the linear controller family (32), a controller that has the general form

$$\begin{aligned} \dot{x}^c(t) &= f^c(x^c(t), y(t), r(t)), \\ u(t) &= g^c(x^c(t), y(t), r(t)), \end{aligned} \tag{33}$$

with the input and output signals corresponding to the nonlinear plant (23). $f^c(.)$ is an m-dimensional differentiable nonlinear vector function which represents the controller dynamics, and $g^c(.)$ is an m-dimensional differentiable nonlinear vector function which generates the controller outputs.

The objective in linearization scheduling is that the equilibrium family of the controller (33) match the plant equilibrium family, so that the closed-loop system maintains suitable trim values, and the linearization family of the controller obtained from linearizing (33) is the same as the designed family of linear controllers shown in (30) [136]. For the equilibrium conditions of plant (23) and controller (33) to match, there must exist a function $x_e^c(\alpha(t))$ such that

$$\begin{aligned} 0 &= f^c(x_e^c(\alpha(t)), y_e(\alpha(t)), r_e(\alpha(t))), \\ u_e(\alpha(t)) &= g^c(x_e^c(\alpha(t)), y_e(\alpha(t)), r_e(\alpha(t))), \quad \forall\alpha \in \Omega, \end{aligned} \tag{34}$$

where

$$\begin{aligned} A^c(\alpha(t)) &= \frac{\partial f^c(.)}{\partial x^c(t)}|_{(x_e^c(\alpha(t)), y_e(\alpha(t)), r_e(\alpha(t)))}, \\ B^c(\alpha(t)) &= \frac{\partial f^c(.)}{\partial y(t)}|_{(x_e^c(\alpha(t)), y_e(\alpha(t)), r_e(\alpha(t)))}, \\ C^c(\alpha(t)) &= \frac{\partial g^c(.)}{\partial x^c(t)}|_{(x_e^c(\alpha(t)), y_e(\alpha(t)), r_e(\alpha(t)))}, \\ D^c(\alpha(t)) &= \frac{\partial g^c(.)}{\partial y(t)}|_{(x_e^c(\alpha(t)), y_e(\alpha(t)), r_e(\alpha(t)))}, \quad \forall\alpha \in \Omega. \end{aligned} \tag{35}$$

So the controller family for all $\alpha \in \Omega$ has the form

$$\begin{aligned} \dot{x}^c(t) &= A^c(\alpha(t))[x^c(t) - x_e^c(\alpha(t))] + B^c(\alpha(t))[y(t) - r(t)], \\ u(t) &= C^c(\alpha(t))[x^c(t) - x_e^c(\alpha(t))] + D^c(\alpha(t))[y(t) - r(t)] + u_e(\alpha(t)). \end{aligned} \tag{36}$$

Note that $r_e(\alpha(t)) = y_e(\alpha(t))$, as a result $\delta y(t) - \delta r(t) = y(t) - r(t)$. The scheduling parameter $\alpha(t)$ is treated as a parameter throughout the design process, and then it becomes a time-varying input signal to the gain-scheduled controller implementation through the dependence $\alpha(t) = p(y(t))$. The parameter $\alpha(t)$ is an endogenous variable, since it is a function of the plant outputs. Replacing $\alpha(t)$ with $p(y(t))$, the gain-scheduled controller becomes

$$\begin{aligned} \dot{x}^c(t) &= A^c(p(y(t)))[x^c(t) - x_e^c(p(y(t)))] + B^c(p(y(t)))[y(t) - r(t)], \\ u(t) &= C^c(p(y(t)))[x^c(t) - x_e^c(p(y(t)))] + D^c(p(y(t)))[y(t) - r(t)] + u_e(p(y(t))). \end{aligned} \tag{37}$$

Linearization of (37) about an equilibrium specified by $\alpha(t)$ yields

$$\begin{aligned} \delta\dot{x}^c(t) &= A^c(\alpha(t))\delta x^c(t) + B^c(\alpha(t))[y(t) - r(t)] \\ &\quad - [A^c(\alpha(t))\tfrac{\partial x_e^c(\alpha(t))}{\partial \alpha(t)}] \times [\tfrac{\partial p(.)}{\partial y(t)}(y_e(\alpha(t)))\delta y(t)], \\ \delta u(t) &= C^c(\alpha(t))\delta x^c(t) + D^c(\alpha(t))[y(t) - r(t)] \\ &\quad + [\tfrac{\partial u_e(\alpha(t))}{\partial \alpha(t)} - C^c(\alpha(t))\tfrac{\partial x_e^c(\alpha(t))}{\partial \alpha(t)}] \times [\frac{\partial p(.)}{\partial y(t)}(y_e(\alpha(t)))\delta y(t)]. \end{aligned} \tag{38}$$

Comparing (38) with (32), we see there are additional terms, and we refer to them as hidden coupling terms following the notation of [136]. In order to get rid of these hidden coupling terms, the following condition must be satisfied

$$\begin{aligned} &[A^c(\alpha(t))\frac{\partial x_e^c(\alpha(t))}{\partial \alpha(t)}] \times [\frac{\partial p(.)}{\partial y(t)}(y_e(\alpha(t)))\delta y(t)] = 0, \\ &[\frac{\partial u_e(\alpha(t))}{\partial \alpha(t)} - C^c(\alpha(t))\frac{\partial x_e^c(\alpha(t))}{\partial \alpha(t)}] \times [\frac{\partial p(.)}{\partial y(t)}(y_e(\alpha(t)))\delta y(t)] = 0. \end{aligned} \tag{39}$$

It is not always easy to come up with solutions to satisfy condition (39). In order to make the design process easier, we control the system via filtered inputs, rather than

the input themselves, so there is no need for equilibrium control value other than zero (i.e. $x_e^c(\alpha) = 0, v_e(\alpha) = 0, \forall\alpha$, where $v_e(\alpha)$ is the parameterized steady-state variables for the new inputs).

The plant (23) with the filtered inputs, becomes

$$\begin{aligned} \begin{bmatrix} \dot{x}^p(t) \\ \dot{u}(t) \end{bmatrix} &= \begin{bmatrix} f^p(x^p(t), u(t)) \\ -\eta_c u(t) \end{bmatrix} + \begin{bmatrix} 0 \\ \eta_c \times I \end{bmatrix} v(t), \\ y(t) &= g^p(x^p(t), u(t)). \end{aligned} \tag{40}$$

The controller has the general form

$$\begin{aligned} \dot{x}^c(t) &= f^c(x^c(t), y(t), r(t)), \\ v(t) &= g^c(x^c(t), y(t), r(t)), \end{aligned} \tag{41}$$

with the input and output signals corresponding to those of the nonlinear plant (40). Now, combining (40) and (41) leads to

$$\begin{aligned} \underbrace{\begin{bmatrix} \dot{x}^p(t) \\ \dot{u}(t) \\ \dot{x}^c(t) \end{bmatrix}}_{\dot{x}(t)} &= \underbrace{\begin{bmatrix} f^p(x^p(t), u(t)) \\ -\eta_c u(t) \\ f^c(x^c(t), g^p(x^p(t), u(t)), r(t)) \end{bmatrix}}_{f(x(t), r(t))} + \underbrace{\begin{bmatrix} 0 \\ \eta_c \times I \\ 0 \end{bmatrix}}_{B} v(t), \\ v(t) &= \underbrace{g^c(x^c(t), g^p(x^p(t), u(t)), r(t))}_{g(x(t), r(t))}, \end{aligned} \tag{42}$$

and the closed-loop nonlinear system is

$$\begin{aligned} \dot{x}(t) &= f(x(t), r(t)) + Bg(x(t), r(t)), \\ &= F(x(t), r(t)), \end{aligned} \tag{43}$$

where $x(t) \in D_x \subset \Re^l$, $l = n + 2m$, and $r(t) \in D_r \subset \Re^m$. The augmented linear

family of systems for the augmented plant (40) becomes

$$\begin{aligned}
\underbrace{\begin{bmatrix} \delta\dot{x}^p(t) \\ \delta\dot{u}(t) \end{bmatrix}}_{\delta\dot{x}_{\text{aug}}(t)} &= \underbrace{\begin{bmatrix} A^p(\alpha(t)) & B^p(\alpha(t)) \\ 0 & -\eta_c \times I \end{bmatrix}}_{A_{\text{aug}}(\alpha(t))} \underbrace{\begin{bmatrix} \delta x^p(t) \\ \delta u(t) \end{bmatrix}}_{\delta x_{\text{aug}}(t)} + \underbrace{\begin{bmatrix} 0 \\ \eta_c \times I \end{bmatrix}}_{B_{\text{aug}}} \delta v(t), \\
\delta y(t) &= \underbrace{[C^p(\alpha(t)), D^p(\alpha(t))]}_{C_{\text{aug}}(\alpha(t))} \underbrace{\begin{bmatrix} \delta x^p(t) \\ \delta u(t) \end{bmatrix}}_{\delta x_{\text{aug}}(t)},
\end{aligned} \tag{44}$$

and the controller has the similar structure as (30)

$$\begin{aligned}
\delta\dot{x}^c(t) &= A_v^c(\alpha(t))\delta x^c(t) + B_v^c(\alpha(t))[\delta y(t) - \delta r(t)], \\
\delta v(t) &= C_v^c(\alpha(t))\delta x^c(t) + D_v^c(\alpha(t))[\delta y(t) - \delta r(t)], \quad \forall \alpha \in \Omega,
\end{aligned} \tag{45}$$

where

$$\delta v(t) = v(t) - v_e(\alpha(t)), \quad \forall \alpha \in \Omega. \tag{46}$$

Now, since $x_e^c(\alpha(t)) = 0,\ v_e(\alpha(t)) = 0,\ \forall \alpha \in \Omega$, the controller is

$$\begin{aligned}
\dot{x}^c(t) &= A_v^c(\alpha(t))x^c(t) + B_v^c(\alpha(t))[\delta y(t) - \delta r(t)], \\
v(t) &= C_v^c(\alpha(t))x^c(t) + D_v^c(\alpha(t))[\delta y(t) - \delta r(t)], \quad \forall \alpha \in \Omega,
\end{aligned} \tag{47}$$

rewriting controller (47) with $\alpha(t) = p(y(t))$, we obtain

$$\begin{aligned}
\dot{x}^c(t) &= A_v^c(p(y(t)))x^c(t) + B_v^c(p(y(t)))[y(t) - r(t)], \\
v(t) &= C_v^c(p(y(t)))x^c(t) + D_v^c(p(y(t)))[y(t) - r(t)].
\end{aligned} \tag{48}$$

Linearization of (48) about an equilibrium specified by α gives (47), so there are no hidden coupling terms similar to the ones we saw in (38), and the condition (39) is satisfied. One of the options for control design is to set the controller matrices as follows

$$\begin{aligned}
A_v^c(\alpha(t)) &= A_v^c = -\epsilon_c I, \quad & B_v^c(\alpha(t)) &= B^c = I, \\
C_v^c(\alpha(t)) &= K_i(\alpha(t)), & D_v^c(\alpha(t)) &= K_p(\alpha(t)),
\end{aligned} \tag{49}$$

which is a kind of proportional-plus-integral (PI) control, where $K_i(\alpha(t))$ is the integral control gain matrix, and $K_p(\alpha(t))$ is the proportional control gain matrix. Hence the controller for the augmented plant linearization family (44) has the final form

$$\begin{bmatrix} \dot{x}^c(t) \\ v(t) \end{bmatrix} = \begin{bmatrix} -\epsilon_c I & I & -I \\ K_i(\alpha(t)) & K_p(\alpha(t)) & -K_p(\alpha(t)) \end{bmatrix} \begin{bmatrix} x^c(t) \\ \delta y(t) \\ \delta r(t) \end{bmatrix}, \quad \forall \alpha \in \Omega. \tag{50}$$

Combining linearized augmented system (44) with controller (47) yields

$$\begin{aligned} \underbrace{\begin{bmatrix} \delta\dot{x}^p(t) \\ \delta\dot{u}(t) \\ \dot{x}^c(t) \end{bmatrix}}_{\delta\dot{x}(t)} &= \underbrace{\begin{bmatrix} A^p(\alpha(t)) & B^p(\alpha(t)) & 0 \\ 0 & -\eta_c I & 0 \\ B_v^c(\alpha(t))C^p(\alpha(t)) & B_v^c(\alpha(t))D^p(\alpha(t)) & A_v^c(\alpha(t)) \end{bmatrix}}_{A_{ol}(\alpha(t))} \\ &\quad \underbrace{\begin{bmatrix} \delta x^p(t) \\ \delta u(t) \\ x^c(t) \end{bmatrix}}_{\delta x(t)} + \underbrace{\begin{bmatrix} 0 \\ \eta_c I \\ 0 \end{bmatrix}}_{B} v(t) + \underbrace{\begin{bmatrix} 0 \\ 0 \\ -B_v^c(\alpha(t)) \end{bmatrix}}_{B_r(\alpha(t))} \delta r(t), \quad \forall \alpha \in \Omega, \end{aligned} \tag{51}$$

$$\begin{aligned} v(t) &= \underbrace{\left[D_v^c(\alpha(t))C^p(\alpha(t)),\ D_v^c(\alpha(t))D^p(\alpha(t)),\ C_v^c(\alpha(t))\right]}_{K^{\mathsf{T}}(\alpha(t))} \delta x(t) \\ &\quad + \underbrace{\left[-D_v^c(\alpha(t))\right]}_{K_r^{\mathsf{T}}(\alpha(t))} \delta r(t). \end{aligned}$$

For the case where we have plant states as the outputs $\delta y(t) = \delta x^p(t)$, (i.e. $C^p(\alpha(t)) =$

$I, D^p(\alpha(t)) = 0$) the combination of the linearized augmented system (44) with controller (50) yields

$$\begin{aligned}\underbrace{\begin{bmatrix}\delta\dot{x}^p(t)\\ \delta\dot{u}(t)\\ \dot{x}^c(t)\end{bmatrix}}_{\delta\dot{x}(t)} &= \underbrace{\begin{bmatrix}A^p(\alpha(t)) & B^p(\alpha(t)) & 0\\ 0 & -\eta_c I & 0\\ I & 0 & -\epsilon_c I\end{bmatrix}}_{A_{ol}(\alpha(t))}\underbrace{\begin{bmatrix}\delta x^p(t)\\ \delta u(t)\\ x^c(t)\end{bmatrix}}_{\delta x(t)}\\ &+ \underbrace{\begin{bmatrix}0\\ \eta_c I\\ 0\end{bmatrix}}_{B} v(t) + \underbrace{\begin{bmatrix}0\\ 0\\ -I\end{bmatrix}}_{B_r}\delta r(t), \quad \forall\alpha\in\Omega,\\ v(t) &= \underbrace{[K_p(\alpha(t)),\ \ 0,\ \ K_i(\alpha(t))]}_{K^{\mathsf{T}}(\alpha(t))}\delta x(t) + \underbrace{[-K_p(\alpha(t))]}_{K_r^{\mathsf{T}}(\alpha(t))}\delta r(t).\end{aligned} \tag{52}$$

The closed-loop linearized augmented system (44) with controller (47) becomes

$$\begin{aligned}\delta\dot{x}(t) = &\underbrace{\begin{bmatrix}A^p(\alpha(t)) & B^p(\alpha(t)) & 0\\ \eta_c D_v^c(\alpha(t))C^p(\alpha(t)) & -\eta_c I + D_v^c(\alpha(t))D^p(\alpha(t)) & \eta_c C_v^c(\alpha(t))\\ B_v^c(\alpha(t))C^p(\alpha(t)) & B_v^c(\alpha(t))D^p(\alpha(t)) & A_v^c(\alpha(t))\end{bmatrix}}_{A_{cl}(\alpha(t))}\delta x(t)\\ &+\underbrace{\begin{bmatrix}0\\ -\eta_c D_v^c(\alpha(t))\\ -B_v^c(\alpha(t))\end{bmatrix}}_{B_{cl}(\alpha(t))}\delta r(t), \quad \forall\alpha\in\Omega,\end{aligned} \tag{53}$$

where $A_{cl}(\alpha(t)) = [A_{ol}(\alpha(t)) + BK^{\mathsf{T}}(\alpha(t))] \in \Re^{l\times l}$, and $B_{cl}(\alpha(t)) = [B_r(\alpha(t)) + BK_r^{\mathsf{T}}(\alpha(t))] \in \Re^{l\times m}$. For the case where we have plant states as the outputs $\delta y(t) = \delta x^p(t)$, (i.e. $C^p(\alpha(t)) = I, D^p(\alpha(t)) = 0$) the closed-loop linearized augmented system

(44) with controller (50) becomes

$$\delta\dot{x}(t) = \underbrace{\begin{bmatrix} A^p(\alpha(t)) & B^p(\alpha(t)) & 0 \\ \eta_c K_p(\alpha(t)) & -\eta_c I & \eta_c K_i(\alpha(t)) \\ I & 0 & -\epsilon_c I \end{bmatrix}}_{A_{cl}(\alpha(t))} \delta x(t) + \underbrace{\begin{bmatrix} 0 \\ -\eta_c K_p(\alpha(t)) \\ -I \end{bmatrix}}_{B_{cl}(\alpha(t))} \delta r(t), \quad \forall \alpha \in \Omega. \tag{54}$$

Figure 30, shows a visualization of the developed output dependent gain scheduled controller.

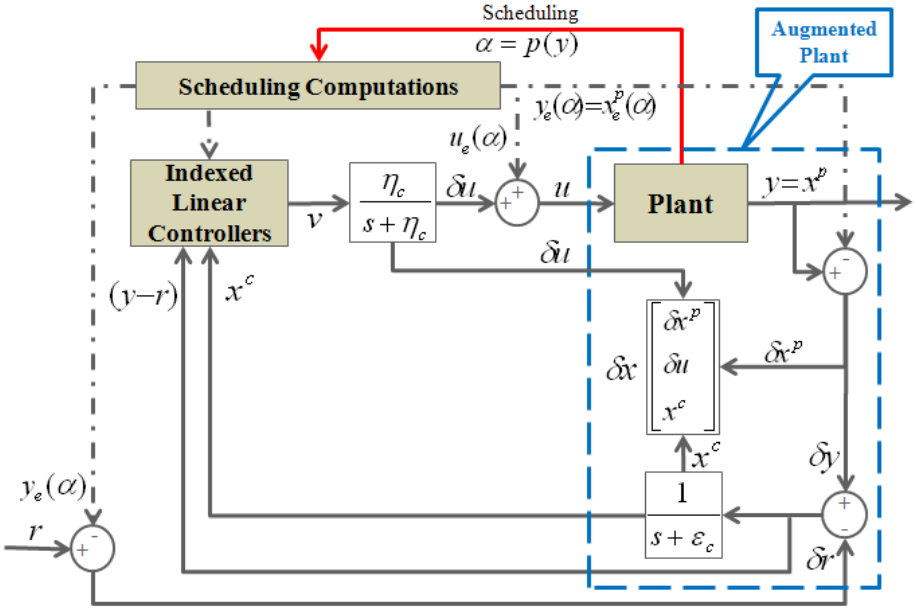

Figure 30: Output dependent gain scheduled controller diagram.

3.2.1 System with Constrained Control Inputs

The plant (51) with saturated control inputs can be written as

$$\begin{aligned} \delta\dot{x}(t) &= A_{ol}(\alpha(t))\delta x(t) + B\ \mathrm{sat}(v(t)) + B_r(\alpha(t))\delta r(t), \\ v(t) &= K^{\mathsf{T}}(\alpha(t))\delta x + K_r^{\mathsf{T}}(\alpha(t))\delta r, \quad \forall \alpha \in \Omega, \end{aligned} \tag{55}$$

where $v(t)$ is the gain scheduled control input. Definition of multiple-dimensional saturation functions is given in Subsection 4.2.2. The closed-loop system (55) with saturated control inputs can be written as

$$\delta\dot{x}(t) = \bar{A}_{cl}(\alpha(t))\delta x(t) + \bar{B} + \bar{B}_r(\alpha(t))\delta r(t), \quad \forall\alpha \in \Omega. \tag{56}$$

Depending on which control inputs are saturated and which ones are not, we can expect the following three cases for system (56):

- *Case i*: None of control inputs are saturated and $|v_i| \leq v_{i,max}$ for all $i = 1, ..., m$, where $v_{i,max}$ is the saturation limit for the $i$the control input. In this case the system is similar to system (53) and

$$\bar{A}_{cl}(\alpha(t)) = A_{cl}(\alpha(t)), \quad \bar{B} = 0, \quad \bar{B}_r(\alpha(t)) = B_r(\alpha(t)), \quad \forall\alpha \in \Omega. \tag{57}$$

- *Case ii*: All of the control inputs are saturated and $|v_i| > v_{i,max}$ for all $i = 1, ..., m$. In this case system matrices are

$$\bar{A}_{cl}(\alpha(t)) = A_{ol}(\alpha(t)), \quad \bar{B} = B\bar{v}, \quad \bar{B}_r(\alpha(t)) = B_r(\alpha(t)), \quad \forall\alpha \in \Omega, \tag{58}$$

  where $\bar{v} = [v_{1,max}\text{sgn}(v_1), ..., v_{m,max}\text{sgn}(v_m)]^\mathsf{T}$.

- *Case iii*: Some of the control inputs are saturated and some of them are not. For a case where $m = 2$, ith control input is saturated and $j$the control input is not saturated, the matrices are

$$\begin{aligned} &\bar{A}_{cl}(\alpha(t)) = A_{ol}(\alpha(t)) + b_j k_j^\mathsf{T}(\alpha(t)), \\ &\bar{B} = b_i\bar{v}_i, \quad \bar{B}_r(\alpha(t)) = b_{rj}(\alpha(t)) + b_j k_{rj}^\mathsf{T}(\alpha(t)), \quad \forall\alpha \in \Omega, \end{aligned} \tag{59}$$

  where $b_j, b_{rj}(\alpha(t)), k_j(\alpha(t))$, and $k_{rj}(\alpha(t))$ are the $j$the columns of $B, B_r(\alpha(t)), K(\alpha(t))$, and $K_r(\alpha(t))$ matrices.

3.2.2 Controller Interpolation

A linear controller is designed for each corresponding plant linearization and selected equilibrium α_i. The equilibria $\alpha_1, \alpha_2, ..., \alpha_q$ belong to the equilibrium family $\alpha \in \Omega$. This results in an indexed collection of controllers Λ_i

$$\Lambda_i := \left[\begin{array}{c|c} A_i^c & B_i^c \\ \hline C_i^c & D_i^c \end{array}\right], \quad i = 1, 2, ...q, \tag{60}$$

each one corresponding to one indexed plant linearization Σ_i

$$\Sigma_i := \Sigma(\alpha_i) := \left[\begin{array}{c|c} A_{\text{aug}_\text{i}} & B_{\text{aug}_\text{i}} \\ \hline C_{\text{aug}_\text{i}} & 0 \end{array}\right], \quad i = 1, 2, ...q. \tag{61}$$

Then the indexed controllers are interpolated with respect to the scheduling parameter α in a smooth, continuous way. An approach by which the interpolated controller stabilizes the linearized plant for all $\alpha \in \Omega$ has been developed in [163]. Here we use this approach for our problem.

Since Λ_i stabilizes $\Sigma(\alpha_i)$ by design, there exists an open neighborhood U_i containing α_i such that Λ_i stabilizes $\Sigma(\alpha(t))$ for all $\alpha \in U_i,\ i = 1, 2, ..., q$. If $\Omega \subset \cup_{i=1}^{q} U_i$, then, as defined in [163], the controllers cover the scheduling space. In other words, for each $\alpha \in \Omega$ there exists at least one linear controller Λ_i that stabilizes $\Sigma(\alpha(t))$.

Given the plant $\Sigma(\alpha(t))$ with $\alpha \in \Omega \subset \Re$, suppose $\Lambda_1, \Lambda_2, ..., \Lambda_q$ have been designed, corresponding to $\alpha_1 < \alpha_2 < ... < \alpha_q$ with open sets U_i such that the controllers cover the scheduling space. Then there exist intervals $[a_i,\ b_i] \subset U_i \cap U_{i+1}$, $i = 1, 2, ..., q$, such that both Λ_i and Λ_{i+1} stabilize $\Sigma(\alpha(t))$ for all $\alpha \in [a_i,\ b_i]$. The stability preserving interpolation method [163] generates controllers $\hat{\Lambda}_i(\alpha(t)),\ i = 1, 2, ..., q-1$, that stabilize $\Sigma(\alpha(t))$ for all $\alpha \in [a_i,\ b_i]$. Hence the stability preserving controller for the entire interval Ω is

$$\Lambda(\alpha(t)) := \begin{cases} \Lambda_i, & \alpha \in U_i, \alpha \notin \cup_{j=1}^{q-1}[a_j,\ b_j],\ i = 1, 2, ..., q, \\ \hat{\Lambda}_j(\alpha(t)), & \alpha \in [a_j,\ b_j],\ j = 1, 2, ..., q-1. \end{cases} \tag{62}$$

Theoretical results on the stability preserving interpolation approach can be found in [163]. Later in this chapter, we use *piecewise linear* interpolation method, which linearly interpolates controllers between each pair of controllers from the indexed collection of controllers $\Lambda_1, \Lambda_2, ..., \Lambda_q$. The linearly interpolated controller $\hat{\Lambda}_i(\alpha(t))$, $i = 1, 2, ..., q-1$, is

$$\hat{\Lambda}_i(\alpha(t)) = \Lambda_i + \frac{\alpha(t) - \alpha_i}{\alpha_{i+1} - \alpha_i}(\Lambda_{i+1} - \Lambda_i), \quad \forall \alpha \in [a_i,\ b_i]. \tag{63}$$

Figure 31, schematically shows this approach of controller interpolation.

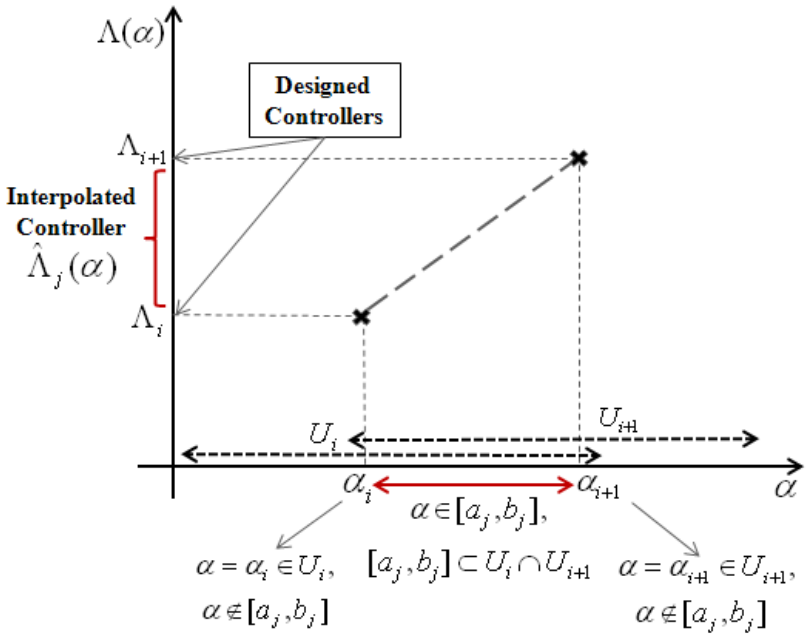

Figure 31: Controller interpolation schematic.

3.3 Stability and Verification

In this section we show the stability of the closed-loop nonlinear system by using "global linearization" technique. The stability is due to the existence of a single quadratic Lyapunov function for all $\alpha \in \Omega$, by computing a single Lyapunov matrix P using convex optimization tools. We also verify the stability by proposing a numerical optimization process.

3.3.1 Stability Analysis

Assumption 1. *The matrices $A_{cl}(\alpha(t))$ and $B_{cl}(\alpha(t))$ are bounded*

$$||A_{cl}(\alpha(t))|| \leq k_A, \quad ||B_{cl}(\alpha(t))|| \leq k_B, \quad \forall t > 0, \tag{64}$$

where k_A and k_B are constants.

To analyze the stability of the nonlinear closed-loop system, we use a technique known as "global linearization" developed in [20, 85, 84].

Theorem 1. *Consider the closed-loop system (43), and assume there is a family of equilibrium points (x_e, r_e) such that $F(x_e, r_e) = 0$. Define $A_{cl}^{nl} = \frac{\partial F(.)}{\partial x(t)} \in \overline{S}$, $\forall x(t) \in D_x$, where $\overline{S}$ is the set of linearizations of system (43)*

$$\overline{S} := \{A_{cl}^{nl}, \forall x(t) \in D_x\}. \tag{65}$$

Assume there exist symmetric positive definite matrices P and Q, such that

$$PA_{cl}^{nl} + A_{cl}^{nl\mathsf{T}}P \leq -Q, \quad \forall A_{cl}^{nl} \in \overline{S}, \tag{66}$$

then the system (43) is stable. In other words, assuming the initial state is sufficiently close to some equilibrium, then the closed-loop system remains in a neighborhood of the equilibrium manifold for all $t \geq 0$.

Remark 1. *In practice we can not obtain $\overline{S}$, instead, we can linearize system (43) for a large number of states x_i, $i = 1, \ldots, L$, which we claim is sufficient to cover the set of actual operating conditions, to show the stability of the closed-loop system. Define S as a matrix polytope described by its vertices*

$$S := \text{Co}\{A_{cl_1}^{nl}, ..., A_{cl_L}^{nl}\}, \tag{67}$$

where $A_{cl_i}^{nl} = \left.\frac{\partial F(.)}{\partial x(t)}\right|_{x(t)=x_i} \in S$, for all $i \in \{1, 2, ..., L\}$. Note that $A_{cl_i}^{nl}$ can be obtained by linearizing the nonlinear system (43) at non-equilibrium points (transient condition),

and also at equilibrium points (steady state condition), which in this dissertation, are represented by $A_{cl}(\alpha_i)$. Then using convex optimization tools [86, 164], for a $Q = Q^{\mathsf{T}} > 0$, we compute a common symmetric positive definite matrix P, such that

$$PA_{cl_i}^{nl} + A_{cl_i}^{nl\mathsf{T}}P \leq -Q, \quad \forall i \in \{1, 2, ..., L\}. \tag{68}$$

In the next section, we will show how to verify the above claim.

Lemma 1. *Let Assumption 1 hold. If a single symmetric positive definite P exists such that LMI (68) is satisfied, and $A_{cl}(\alpha) \in S$, for all $\alpha \in \Omega$, then system (53) is stable.*

Proof. Since $PA_{cl_i}^{nl} + A_{cl_i}^{nl\mathsf{T}}P \leq -Q$, and assuming $\beta_i \in [0,\ 1]$, for all $i \in \{1, 2, ..., L\}$, we have

$$\begin{aligned} P(\beta_1 A_{cl_1}^{nl}) + (A_{cl_1}^{nl\mathsf{T}}\beta_1)P &\leq -\beta_1 Q, \\ &\vdots \\ P(\beta_L A_{cl_L}^{nl}) + (A_{cl_L}^{nl\mathsf{T}}\beta_L)P &\leq -\beta_L Q, \end{aligned} \tag{69}$$

adding all the above inequalities we obtain

$$P\left(\sum_{i=1}^{L}\beta_i A_{cl_i}^{nl}\right) + \left(\sum_{i=1}^{L}\beta_i A_{cl_i}^{nl}\right)^{\mathsf{T}} P \leq -\left(\sum_{i=1}^{L}\beta_i\right) Q, \tag{70}$$

since $A_{cl}(\alpha(t)) \in S$ for all $\alpha \in \Omega$, in other words, $A_{cl}(\alpha(t)) = \sum_{i=1}^{L}\beta_i A_{cl_i}^{nl}$, and $\sum_{i=1}^{L}\beta_i = 1$ for all $\alpha \in \Omega$, then

$$PA_{cl}(\alpha(t)) + A_{cl}^{\mathsf{T}}(\alpha(t))P \leq -Q, \quad \forall \alpha \in \Omega. \tag{71}$$

Hence the closed-loop system (53) is stable. □

Figure 32, shows a schematic of the equilibrium manifold and the stability region for the closed-loop nonlinear plant (43).

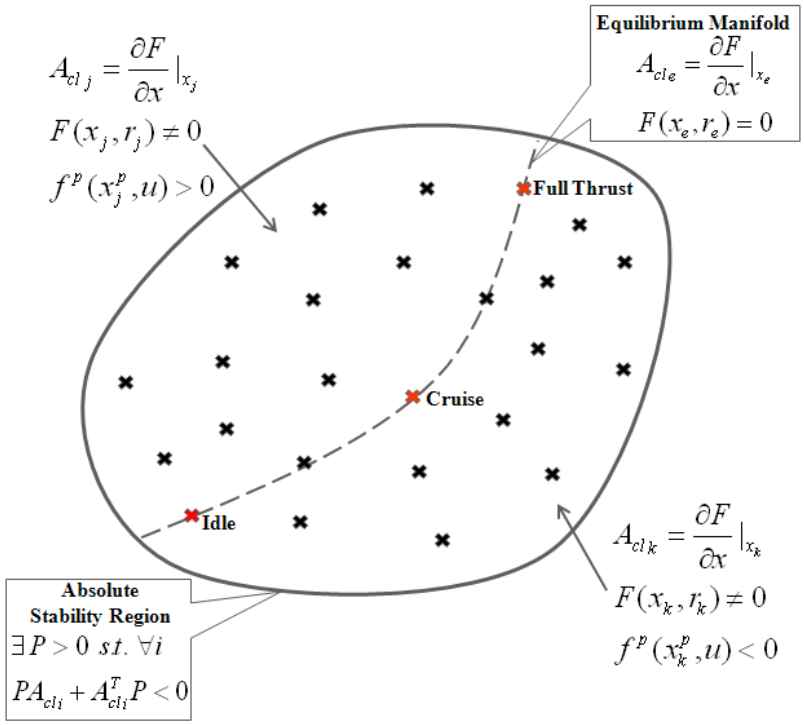

Figure 32: Stability region.

Remark 2. *An alternative approach to show the stability of the closed-loop system can be found in [136], which has been developed based on the results from [68, 80, 71]. If there are no hidden coupling terms involving $\delta y(t)$, then the design of a stabilizing linear controller family can be assumed to guarantee the stability of the linearized closed-loop system in a neighborhood of every $\alpha \in \Omega$. The closed-loop system is not restricted to remain in a neighborhood of any single equilibrium, but it is assumed to be slowly varying and to have initial state sufficiently close to some equilibrium in Ω. Then the conclusion is that the closed-loop system remains in a neighborhood of the equilibrium manifold [136].*

The next Lemma deals with the stability of system (56) with saturated control inputs; and it is an extended version of Lemma 1.

Lemma 2. *Let Assumption 1 hold. Define S_{sat} as a matrix polytope described by its*

vertices

$$S_{sat} := \text{Co}\{A_{cl_1}^{nl}, ..., A_{cl_L}^{nl}, A_{ol_1}^{nl}, ..., A_{ol_L}^{nl}\}, \tag{72}$$

where $A_{cl_i}^{nl}$ *is defined as before, and* $A_{ol_i}^{nl} = \frac{\partial f(.)}{\partial x(t)}\Big|_{x(t)=x_i} \in S_{sat}$*, for all* $i \in \{1, 2, ..., L\}$*. If a single symmetric positive definite* P_s *exists such that*

$$P_s A_i^{nl} + A_i^{nl\mathsf{T}} P_s \leq -Q_s, \quad \forall i \in \{1, 2, ..., 2L\}, \tag{73}$$

where $A_i^{nl} = \{A_{ol_i}^{nl}, A_{cl_i}^{nl}, i = 1, ..., L\}$*,* $Q_s = Q_s^{\mathsf{T}} > 0$*,* $A_{cl}(\alpha(t)) \in S_{sat}$*, and* $A_{ol}(\alpha(t)) \in S_{sat}$ *for all* $\alpha \in \Omega$*, then* $\bar{A}_{cl}(\alpha(t)) \in S_{sat}$ *and system (56) is stable.*

Remark 3. *Note that in the presence of saturation, the closed-loop system behaves like an open-loop system, then computing sufficient number of open-loop linearizations of the system should be enough to draw stability conclusions. Note also that* $A_{ol_i}^{nl}$ *can be obtained by linearizing the term* $f(.)$ *in the nonlinear system (43) at non-equilibrium points (transient condition), and also at equilibrium points (steady state condition), which in this dissertation are represented by* $A_{ol}(\alpha_i)$*. Using convex optimization tools [86, 164], we can try to compute a single symmetric positive definite matrix* P_s*, which its existence guarantees the stability of the closed-loop system with saturated inputs.*

3.3.2 Stability Verification

Since stability verification in aerospace systems is of great importance, we would like to be able to verify that the stability hypotheses we proposed in remark 1 hold true. In other words, we have to verify that $A_{cl}(\alpha(t)) \in S$ for all $\alpha \in \Omega$. In order to achieve that, for each $\alpha \in \Omega$ we have to be able to find a vector $\beta = [\beta_1, ..., \beta_L]$, such that

$$\begin{aligned} &A_{cl}(\alpha(t)) = \sum_{i=1}^{L} \beta_i A_{cl_i}^{nl}, \quad \forall \alpha \in \Omega, \\ &\sum_{i=1}^{L} \beta_i = 1, \\ &0 \leq \beta_i \leq 1. \end{aligned} \tag{74}$$

To solve this problem numerically, we propose a simple optimization problem which helps us to verify the stability of the engine operation in an on-line fashion. The convex optimization problem which we solve for stability verification of the closed-loop system (43) is

$$\begin{aligned} \underset{\beta_i}{\text{minimize}} \quad & \underbrace{\left\| A_{cl}(\alpha(t)) - \sum_{i=1}^{L} \beta_i A_{cl_i}^{nl} \right\|_2}_{e_{opt}(t)}, \quad \forall \alpha \in \Omega, \\ \text{subject to} \quad & \sum_{i=1}^{L} \beta_i = 1, \\ & 0 \leq \beta_i \leq 1. \end{aligned} \tag{75}$$

3.3.3 Towards GS Control Software Verification

For the engine GS control architecture, the stability of system (53) is investigated using a single quadratic Lyapunov function $V(x(t)) = x^{\mathsf{T}}(t)Px(t)$, where P satisfies (71). The stability can also be interpreted in terms of the following invariant ellipsoid [20] centered at origin

$$\mathcal{E} = \left\{ x \in \Re^{l} | x^{\mathsf{T}} P x \leq 1 \right\}, \tag{76}$$

the ellipsoid $\mathcal{E}$ is said to be invariant for system (53), if for every trajectory x of system (53), $x(0) \in \mathcal{E}$ implies $x(t) \in \mathcal{E}$ for all $t \geq 0$. This is another mathematical interpretation of (71) for all $\alpha \in \Omega$.

This invariant set can be used to develop control software stability analysis. In this vision there is a dynamical system interpretation and modeling of computer programs [33, 131, 132], which is based on the existence of an invariant set. In most of the cases this invariant set is developed based on the existence of a quadratic Lyapunov function, and it can be constructed similar to (76). In the engine GS control problem, this whole process depends on the existence of a single constant matrix P, which satisfies (71).

By presenting a detailed Lyapunov stability analysis for closed-loop gas turbine

engines with gain scheduled controllers, we fulfilled the first step towards a verifiable control system for gas turbine propulsion systems. Hopefully this is a meaningful step for gas turbine engine control software verification problem. The complete theoretical engine control software verification is beyond the scope of this dissertation, and it is a topic for future research.

3.4 Turboshaft Engine Example

We apply the proposed output dependent gain scheduled controller to a physics-based model of the JetCat SPT5 turboshaft engine driving a variable pitch propeller developed in Chapter 2. Note that some of the plant states and inputs have been non-dimensionalized by their design values: fuel flow input, $u_1(t)$, is divided by 0.0035323 (kg/s), core spool speed, $N_2(t)$, which is the first plant state ($x_1^p(t)$), and is divided by 170000 RPM, and fan spool speed, $N_1(t)$, which is the second plant state ($x_2^p(t)$), and is divided by 7000 RPM.

3.4.1 Equilibrium Manifold

For a standard day at sea level condition we chose five properly separated equilibrium points on the plant equilibrium manifold for linearizing the plant model at those points. The linearization matrices for these five equilibrium points and steady state values of the engine variables, the control parameters, and the scheduling parameter are given as follows:

- Equilibrium Point 1 (Full Thrust):

  $u_{1e1} = 1.0$, $u_{2e1} = 16$ (deg), $x_{1e1} = 1.0$, $x_{2e1} = 0.9524$, $T_{e1} = 255.8685$ (N), $\alpha_1 =$

1.3810, and

$$A_1^p = \begin{bmatrix} -5 & 0 \\ 3.5 & -2.3 \end{bmatrix},\ B_1^p = \begin{bmatrix} 1.5 & 0 \\ 0.63 & -0.085 \end{bmatrix},\ C_1^p = I,$$
$$Ki_1 = \begin{bmatrix} -0.5 & -0.5 \\ -0.5 & -0.5 \end{bmatrix},\ Kp_1 = \begin{bmatrix} -0.5 & -0.5 \\ -0.5 & -0.5 \end{bmatrix}. \tag{77}$$

- Equilibrium Point 2:

  $u_{1e2} = 0.7,\ u_{2e2} = 16\,(\text{deg}),\ x_{1e2} = 0.9041,\ x_{2e2} = 0.6557,\ T_{e2} = 121.2905\,(\text{N}),\ \alpha_2 = 1.1168$, and

$$A_2^p = \begin{bmatrix} -2.8 & 0.2 \\ 2 & -1.7 \end{bmatrix},\ B_2^p = \begin{bmatrix} 1.42 & 0 \\ 0.3768 & -0.05 \end{bmatrix},\ C_2^p = I,$$
$$Ki_2 = \begin{bmatrix} -0.4 & -0.4 \\ -0.4 & -0.4 \end{bmatrix},\ Kp_2 = \begin{bmatrix} -0.4 & -0.4 \\ -0.4 & -0.4 \end{bmatrix}. \tag{78}$$

- Equilibrium Point 3 (Cruise):

  $u_{1e3} = 0.4685,\ u_{2e3} = 16\,(\text{deg}),\ x_{1e3} = 0.7264,\ x_{2e3} = 0.5,\ T_{e3} = 70.5125\,(\text{N}),\ \alpha_3 = 0.8818$, and

$$A_3^p = \begin{bmatrix} -1.7 & 0.1 \\ 0.6 & -1.1 \end{bmatrix},\ B_3^p = \begin{bmatrix} 1.2 & 0 \\ 0.3 & -0.023 \end{bmatrix},\ C_3^p = I,$$
$$Ki_3 = \begin{bmatrix} -0.3 & -0.3 \\ -0.3 & -0.3 \end{bmatrix},\ Kp_3 = \begin{bmatrix} -0.3 & -0.3 \\ -0.3 & -0.3 \end{bmatrix}. \tag{79}$$

- Equilibrium Point 4:

  $u_{1e4} = 0.3,\ u_{2e4} = 16\,(\text{deg}),\ x_{1e4} = 0.5327,\ x_{2e4} = 0.3678,\ T_{e4} = 38.155\,(\text{N}),\ \alpha_4 = 0.6473$, and

$$A_4^p = \begin{bmatrix} -0.85 & 0.032 \\ 0.32 & -0.64 \end{bmatrix},\ B_4^p = \begin{bmatrix} 1.0 & 0 \\ 0.17 & -0.011 \end{bmatrix},\ C_4^p = I,$$
$$Ki_4 = \begin{bmatrix} -0.2 & -0.2 \\ -0.2 & -0.2 \end{bmatrix},\ Kp_4 = \begin{bmatrix} -0.2 & -0.2 \\ -0.2 & -0.2 \end{bmatrix}. \tag{80}$$

- Equilibrium Point 5 (Idle):

  $u_{1e5} = 0.145,\ u_{2e5} = 16\ (\text{deg}),\ x_{1e5} = 0.295,\ x_{2e5} = 0.161,\ T_{e5} = 7.317\ (\text{N}),\ \alpha_5 = 0.3361$, and

$$A_5^p = \begin{bmatrix} -0.38 & -0.0008 \\ 0.26 & -0.34 \end{bmatrix},\ B_5^p = \begin{bmatrix} 0.7 & 0 \\ 0.1 & -0.0024 \end{bmatrix},\ C_5^p = I,$$
$$Ki_5 = \begin{bmatrix} -0.1 & -0.1 \\ -0.1 & -0.1 \end{bmatrix},\ Kp_5 = \begin{bmatrix} -0.1 & -0.1 \\ -0.1 & -0.1 \end{bmatrix}. \tag{81}$$

Other controller parameters are $\epsilon_c = 1,\ \eta_c = 3$. The elements of $A^p(\alpha(t))$ and $B^p(\alpha(t))$ matrices have been shown as functions of the scheduling parameter $\alpha(t)$ in figures 33 and 34. In this simulation, the scheduling parameter $\alpha(t)$ is defined to be the Euclidean norm of the gas turbine engine spool speeds, which are the plant outputs and capture the engine nonlinearities. Piecewise linear interpolation has been used to compute matrices in between the available linearization matrices of each pair of adjacent equilibrium points.

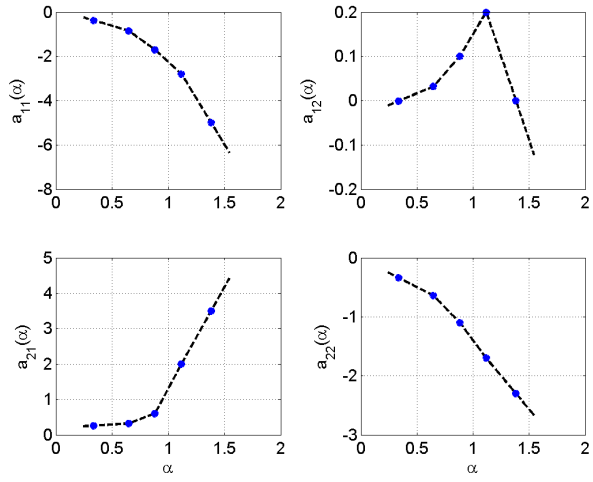

Figure 33: $A^p(\alpha(t))$ components as functions of scheduling parameter $\alpha(t)$.

The equilibrium values of the plant states and control inputs are shown in figure 35 as functions of the scheduling parameter $\alpha(t)$. Piecewise linear interpolation has

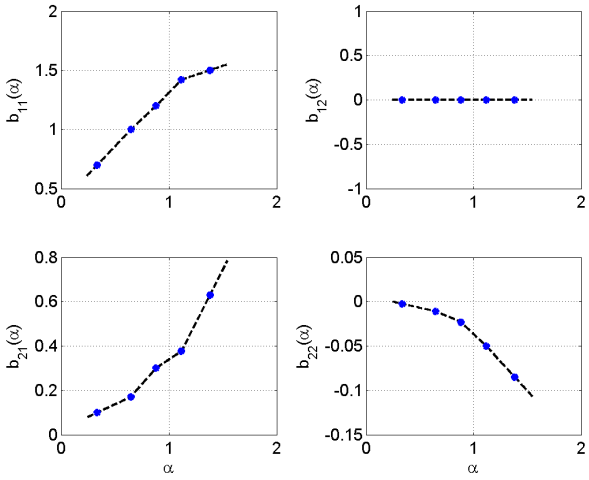

Figure 34: $B^p(\alpha(t))$ components as functions of scheduling parameter $\alpha(t)$.

been used to compute equilibrium values in between each pair of adjacent equilibrium points. The equilibrium manifold in a 3D space of two spool speeds and fuel flow control input is shown in figure 36.

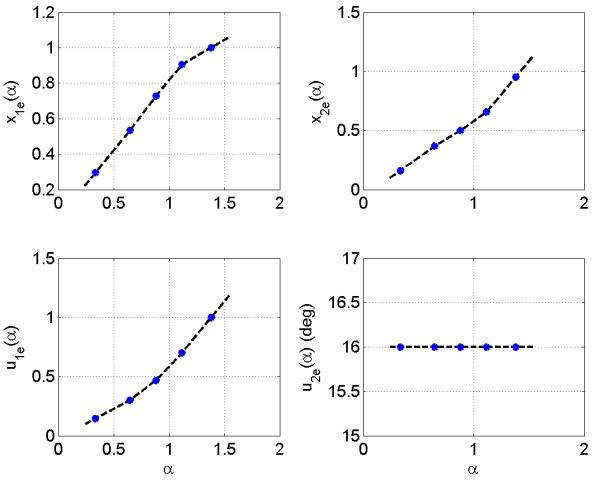

Figure 35: $x_e^p(\alpha(t))$ and $u_e(\alpha(t))$ as functions of scheduling parameter $\alpha(t)$.

The elements of control matrices $K_p(\alpha(t))$ and $K_i(\alpha(t))$ have been shown as functions of scheduling parameter $\alpha(t)$ in figures 37 and 38. Piecewise linear interpolation has been used to interpolate $K_p(\alpha(t))$ and $K_i(\alpha(t))$ using the predesigned indexed linear controllers, which are given in (77) to (81).

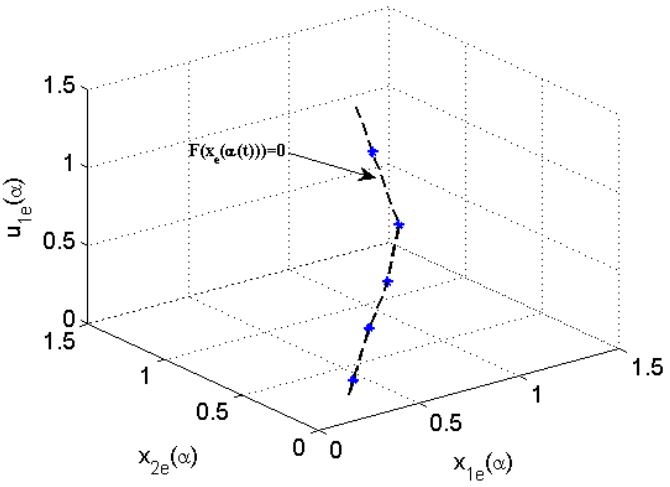

Figure 36: Engine equilibrium manifold in 3D space of spool speeds and fuel control input.

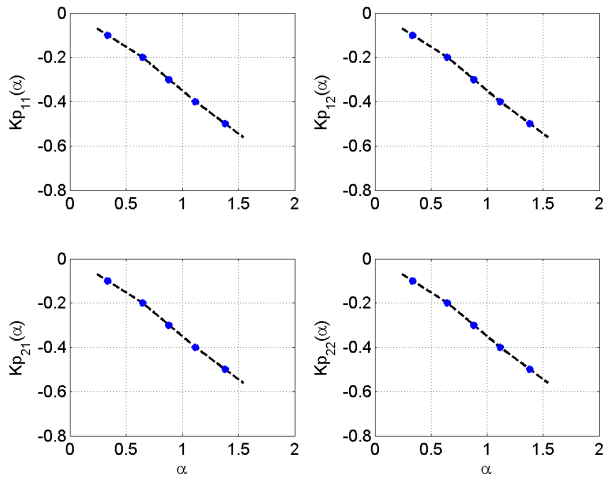

Figure 37: $K_p(\alpha(t))$ components as functions of scheduling parameter $\alpha(t)$.

3.4.2 Closed-Loop Stability Verification

To show the stability of the closed-loop system, 40 different (30 equilibrium, and 10 non-equilibrium) linearizations have been used to solve inequality (68) in Matlab with the aid of YALMIP [86] and SeDuMi [164] packages. The numerical value for

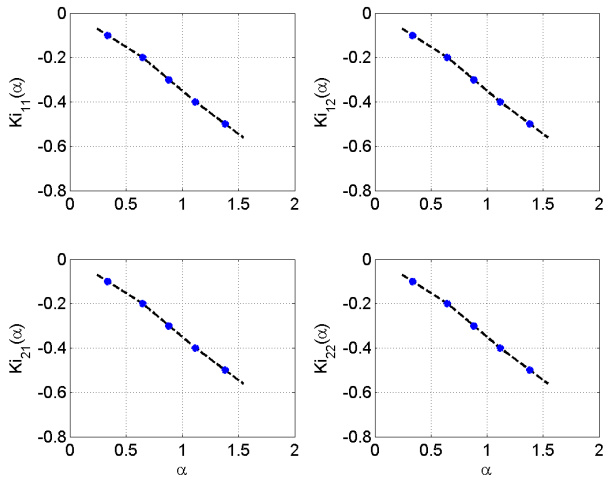

Figure 38: $K_i(\alpha(t))$ components as functions of scheduling parameter $\alpha(t)$.

the common matrix P is

$$P = \begin{bmatrix} 0.5232 & 0.0059 & 0.0913 & -0.0177 & -0.0293 & -0.0011 \\ 0.0059 & 0.3406 & 0.0132 & -0.0082 & -0.0862 & -0.0114 \\ 0.0913 & 0.0132 & 0.1721 & -0.0461 & 0.0044 & 0.0105 \\ -0.0177 & -0.0082 & -0.0461 & 0.1275 & 0.0388 & 0.0282 \\ -0.0293 & -0.0862 & 0.0044 & 0.0388 & 0.2684 & -0.0211 \\ -0.0011 & -0.0114 & 0.0105 & 0.0282 & -0.0211 & 0.2484 \end{bmatrix}, \qquad (82)$$

where its condition number is 6.8910. Figure 39, shows JetCat SPT5 turboshaft engine compressor map. In this map the approximate stall line and also the operating line for this simulation have been shown. The engine operates in a safe region with a big stall margin during its acceleration from idle to cruise, and during its deceleration back to the idle condition. The 40 points which are used for linearization and stability analysis of the closed-loop system also have been shown in this figure. 30 of these points are related to the equilibrium linearizations which are situated on the steady-state operating line of the engine, and the other 10 points are related to the non-equilibrium linearizations which are situated near the steady-state operating line of the engine.

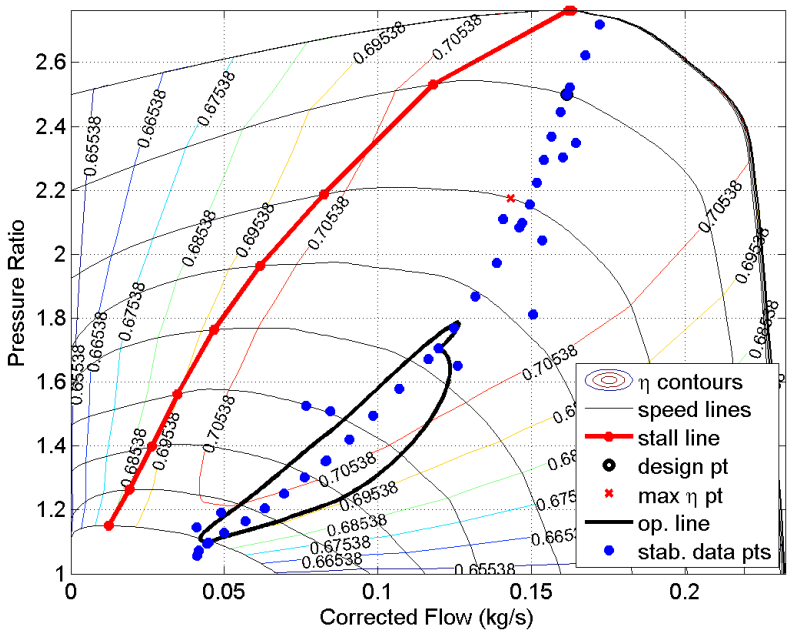

Figure 39: JetCat SPT5 engine compressor map with data points used to compute P.

To verify that the assumption of Lemma 1 is satisfied (that is the linearized plant lives in the convex hull of the linearization matrix samples), in other words $A_{cl}(\alpha(t)) \in S$ for all $\alpha \in \Omega$, we solve minimization problem (75) using CVX, a package for specifying and solving convex programs [30, 43]. Figure 40 shows the history of the optimization error, e_{opt}, proposed in (75), and figure 41 shows the history of the coefficients $\beta_i,\ i = 1, ..., 40$ in (75). These coefficients have been computed for the trajectory which has been shown as a closed curve with solid black line (i.e., the operating line) in figure 39.

As can be observed in these figures, the error is pretty small for this simulation and hence for all $\alpha \in \Omega$, $A_{cl}(\alpha(t))$ is a linear combination of $A_{cl_i}^{nl}, i = 1, ..., L$. Due to the fact that coefficients $\beta_i,\ i = 31, ..., 40$, which are corresponding to the non-equilibrium linearizations, are zero, and also because the non-zero coefficients β_i are the ones related to the equilibrium linearizations, we can infer that the closed-loop system remains in a neighborhood of the equilibrium manifold.

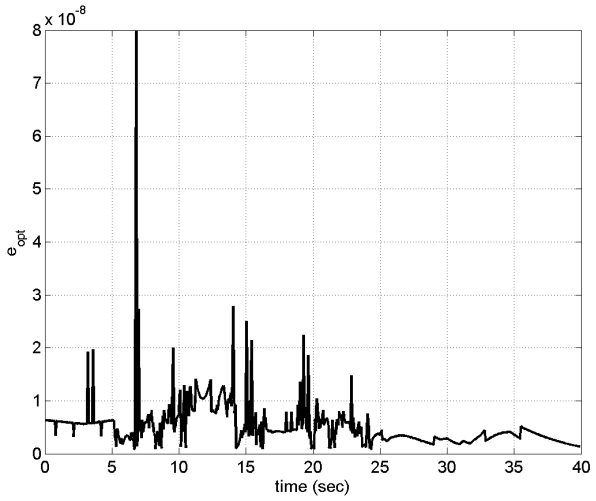

Figure 40: History of the optimization error ($e_{opt}(t)$).

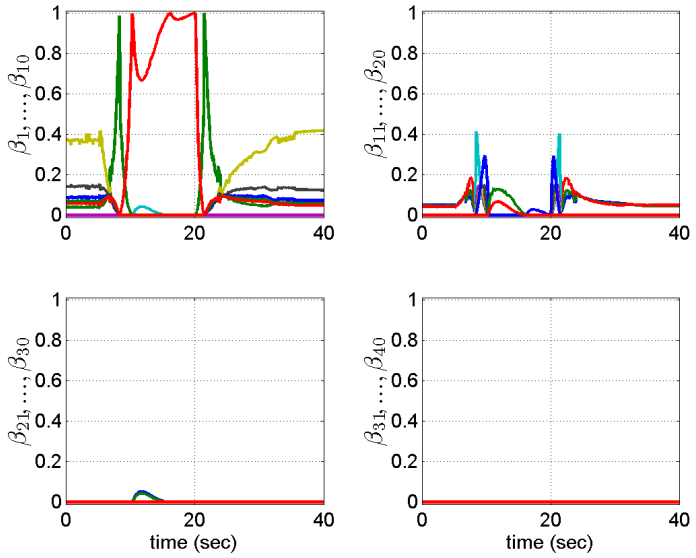

Figure 41: History of the coefficients $\beta_i,\ i = 1, ..., 40$.

3.4.3 Bode Plots

Frequency response of the compensated engine is obtained using the Bode approach. These Bode plots are generated using Matlab. Figure 42 shows the block diagram of the compensated engine plant for a constant α. In Figure 42, $H(s) = \dfrac{v(s)}{e(s)}$ is the PI controller transfer function, $G^p(s) = \dfrac{y(s)}{u(s)}$ is the plant transfer function, $G^{ap}(s) =$

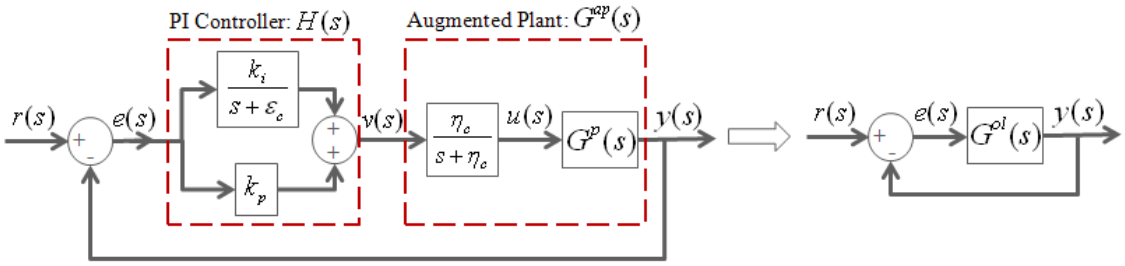

Figure 42: Block diagram of the compensated engine for a constant α.

$\frac{y(s)}{v(s)}$ is the augmented plant transfer function, $G^{ol}(s) = G^{ap}H(s) = \frac{y(s)}{e(s)}$ is the open-loop compensated plant transfer function, and the closed-loop system transfer function is $G^{cl}(s) = \frac{y(s)}{r(s)} = \frac{G^{ol}(s)}{1+G^{ol}(s)}$. In this system we have 2 control inputs (v_1 and v_2) and 2 outputs (N_2 and N_1). The elements of the transfer function matrices are $G^p_{ij}(s) = \frac{y_i(s)}{u_j(s)}$, $G^{ap}_{ij}(s) = \frac{y_i(s)}{v_j(s)}$, $G^{ol}_{ij} = \frac{y_i(s)}{e_j(s)}$, and $G^{cl}_{ij} = \frac{y_i(s)}{r_j(s)}$, where $i = \{1, 2\}$, and $j = \{1, 2\}$.

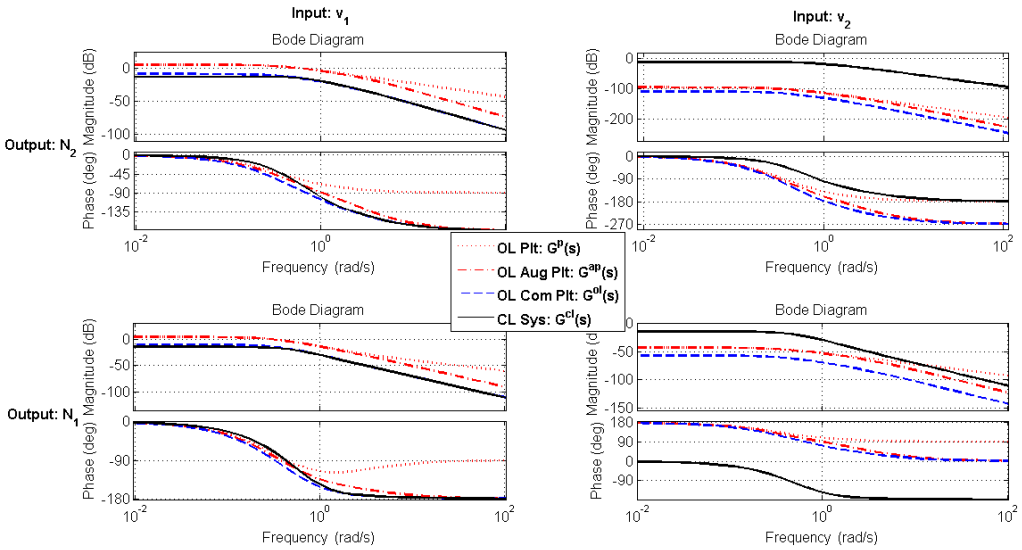

Figure 43: Bode plots of the open-loop plant ($G^p(s)$), open-loop augmented plant ($G^{ap}(s)$), open-loop compensated plant ($G^{ol}(s)$), and closed-loop compensated plant ($G^{cl}(s)$) at *idle* operating condition where $\alpha(t) = 0.3361$.

Figures 43 to 45 show the Bode plots of the open-loop plant ($G^p(s)$), open-loop augmented plant ($G^{ap}(s)$), open-loop compensated plant ($G^{ol}(s)$), and closed-loop compensated plant ($G^{cl}(s)$) for three operating conditions including idle, cruise, and

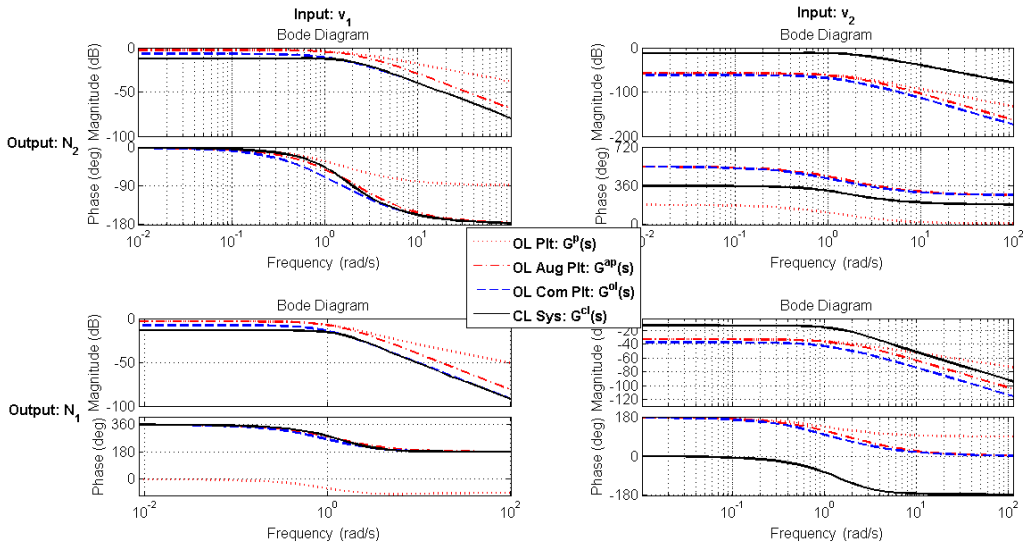

Figure 44: Bode plots of the open-loop plant ($G^p(s)$), open-loop augmented plant ($G^{ap}(s)$), open-loop compensated plant ($G^{ol}(s)$), and closed-loop compensated plant ($G^{cl}(s)$) at *cruise* operating condition where $\alpha(t) = 0.8818$.

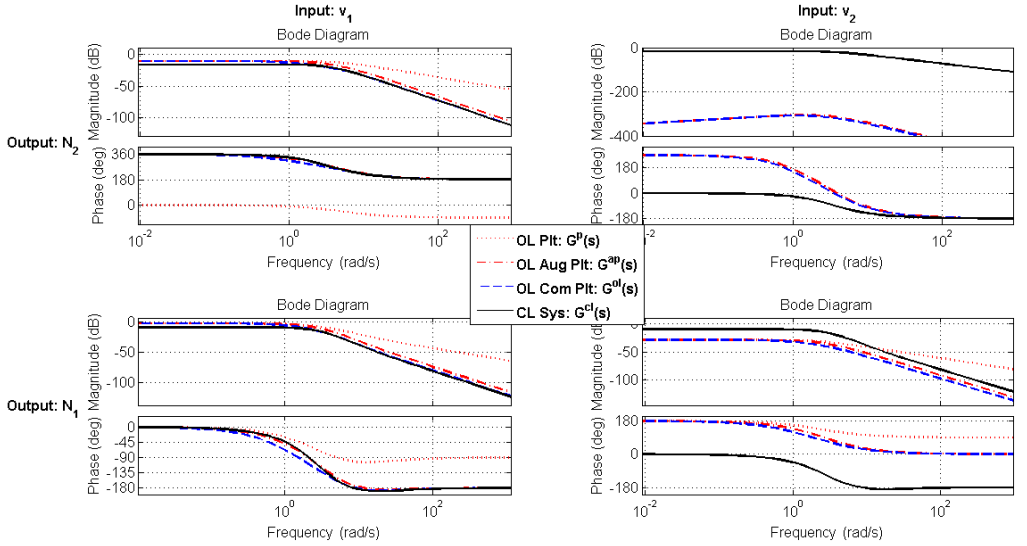

Figure 45: Bode plots of the open-loop plant ($G^p(s)$), open-loop augmented plant ($G^{ap}(s)$), open-loop compensated plant ($G^{ol}(s)$),, and closed-loop compensated plant ($G^{cl}(s)$) at *full thrust* operating condition where $\alpha(t) = 1.3810$.

full thrust points. Scheduling parameter α is constant at each one of these operating points. The Bode diagrams of the closed-loop systems show slight improvements in the gain margin (GM) and phase margin (PM) compared to the open-loop systems.

3.4.4 Simulation Results

Here, we implement the proposed parameter dependent gain scheduled controller to operate the JetCat SPT5 turboshaft engine. This case study simulates the engine acceleration from the idle thrust to the cruise condition and then its deceleration back to the idle condition in a stable manner, with proper tracking performance, for the standard day sea level condition. Simulation results are shown in figures 46 to 62.

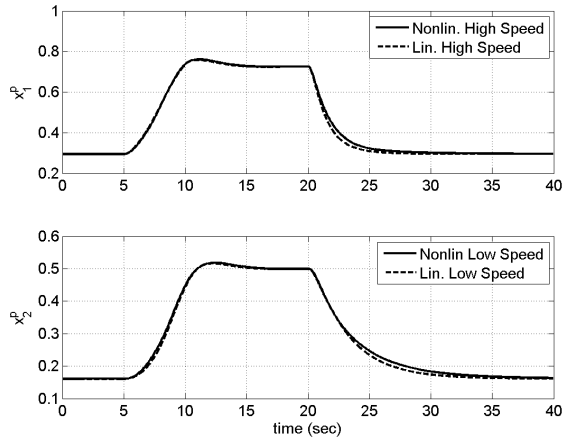

Figure 46: History of the states $(x^p(t))$ for the nonlinear system and the linear parameter dependent model.

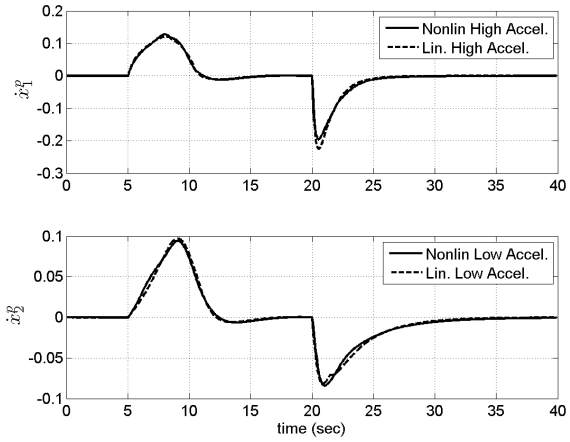

Figure 47: History of the rate of states $(\dot{x}^p(t))$ for the nonlinear system and the linear parameter dependent model.

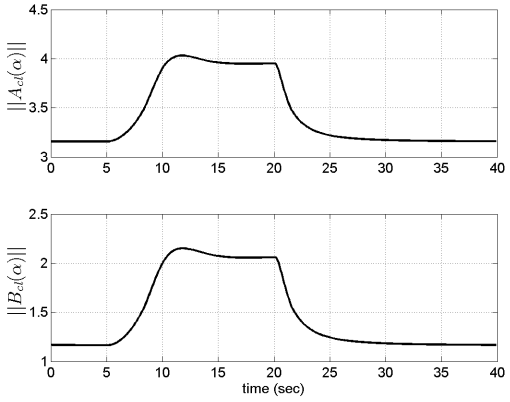

Figure 48: Norm of the closed-loop system matrices ($||A_{cl}(t)||$), and ($||B_{cl}(t)||$).

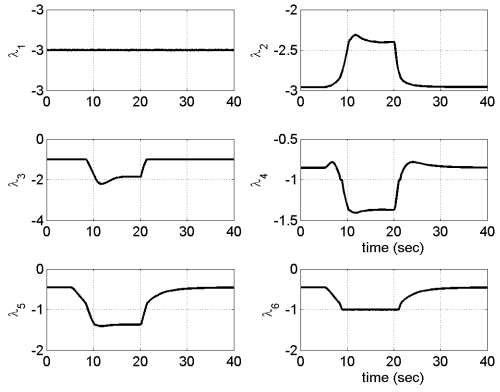

Figure 49: Closed-loop system eigenvalues ($\lambda[A_{cl}(\alpha(t))]$).

Figures 46 and 47 show the history of the nonlinear system and the linear parameter dependent model states, $x^p(t)$, and the rate of states, $\dot{x}^p(t)$. We can conclude that the linearized model is a very good approximation of the nonlinear model.

Figure 48, shows the history of the norm of the closed-loop system matrices $||A_{cl}(t)||$, and $||B_{cl}(t)||$. The figure shows the boundedness of these two matrices, in accordance with Assumption 1, where $k_A = 4.0327$, and $k_B = 2.1512$. Figure 49, shows the history of the closed-loop system matrix eigenvalues $\lambda[A_{cl}(\alpha(t))]$. All the eigenvalues remain negative with the time change of the scheduling parameter α.

Figure 50 shows the history of the scheduling parameter $\alpha(t) = p(y(t)) = ||y(t)|| =$

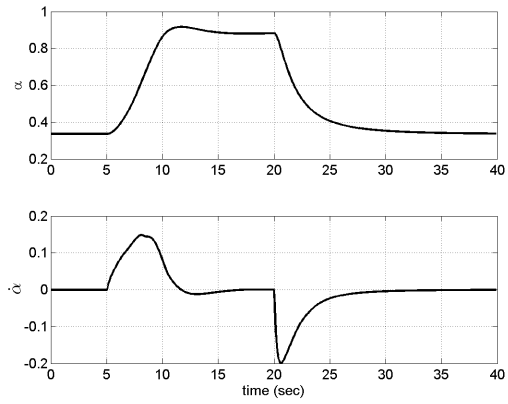

Figure 50: Scheduling Parameter ($\alpha(t) = ||x^p(t)||$) and its rate of change ($\dot{\alpha}(t)$).

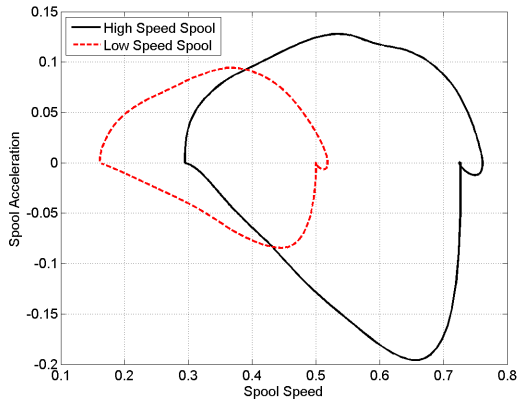

Figure 51: High and low spool speeds vs. high and low spool accelerations.

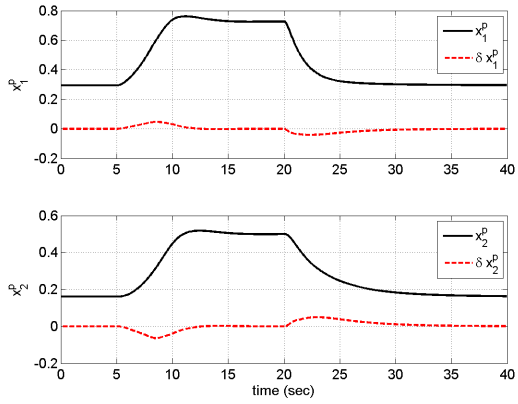

Figure 52: Plant states: high and low spool speeds ($x^p(t)$).

$||x^p(t)||$ (the Euclidean norm of the engine spool speeds), and the scheduling parameter rate $\dot{\alpha}(t) = \frac{x^p(t)^\mathsf{T}\dot{x}^p(t)}{||x^p(t)||}$. Both $\alpha(t)$ and $\dot{\alpha}(t)$ are bounded. Figure 51 shows the

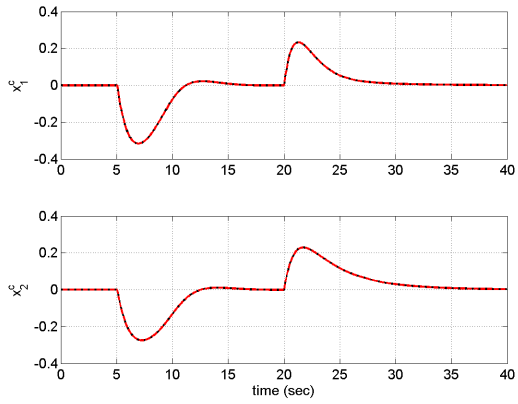

Figure 53: Controller states ($x^c(t)$).

phase plot for both spool dynamics.

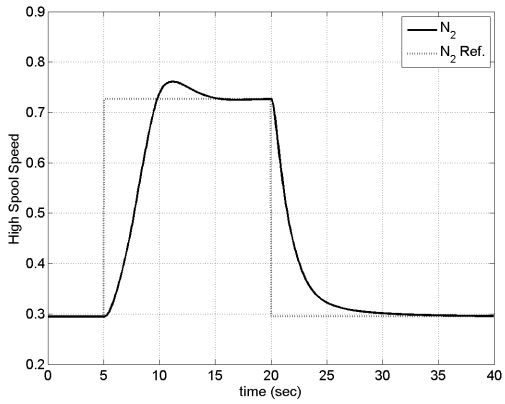

Figure 54: Output: high spool speed and its reference signal.

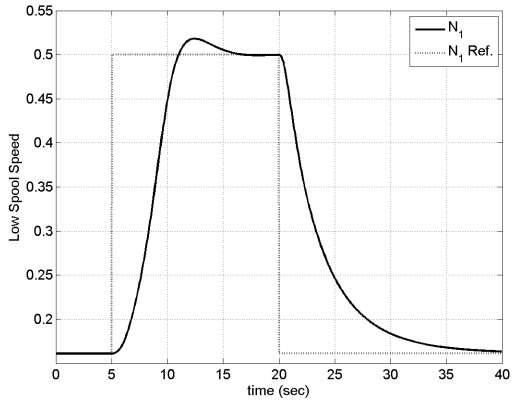

Figure 55: Output: low spool speed and its reference signal.

Figure 52 shows the evolution of the plant states which are high and low spool speeds. Figure 53 shows the time evolution of the controller states.

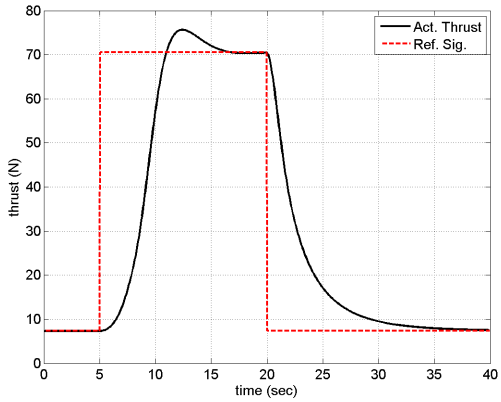

Figure 56: Thrust and its reference signal.

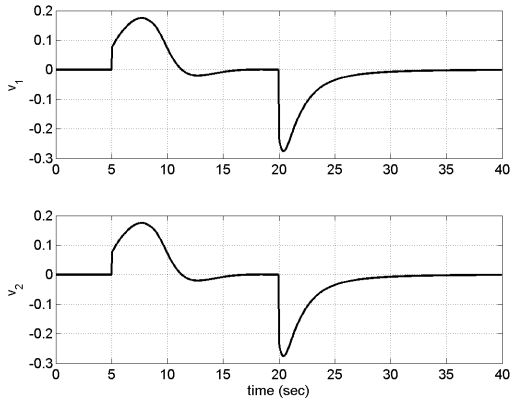

Figure 57: Control inputs to the augmented system ($v(t)$).

Figures 54 and 55 show the outputs (i.e., high and low spool speeds) tracking their reference signals properly. Figure 56 shows the history of the thrust and it is following its reference command from idle to cruise condition and then back to the idle for standard day, sea level conditions. Figure 57 shows the evolution of the control inputs $v(t) = [v_1(t), v_2(t)]^T$, which are inputs to the augmented system; each element is corresponding to one of the control inputs to the original system.

Figure 58 shows time rates of fuel and prop pitch angle inputs. Figure 59 shows fuel flow and propeller pitch angle histories as the control inputs to the plant. Figures

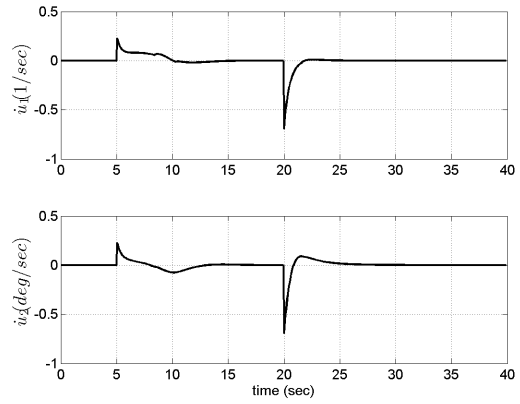

Figure 58: Rate of change for fuel and prop pitch angle control inputs ($\dot{u}(t)$).

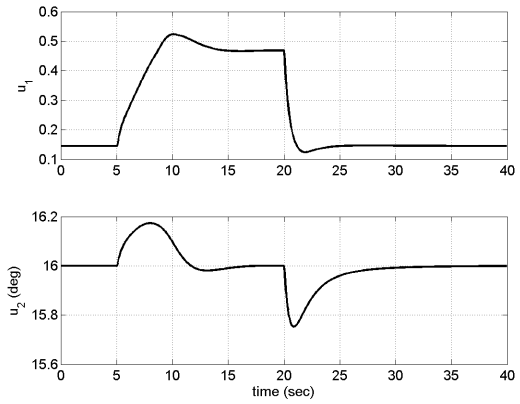

Figure 59: Fuel and prop pitch angle control inputs ($u(t)$).

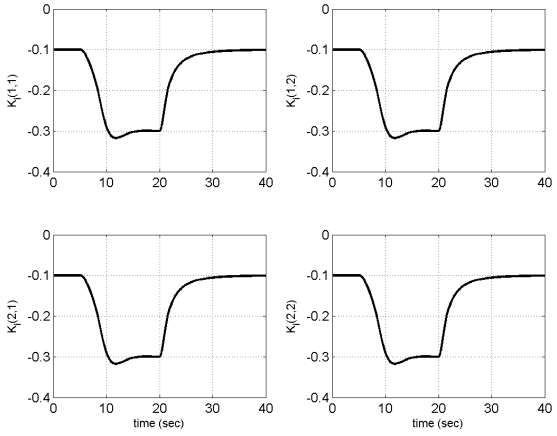

Figure 60: Controllers integral gain matrix ($K_i(\alpha(t))$) elements.

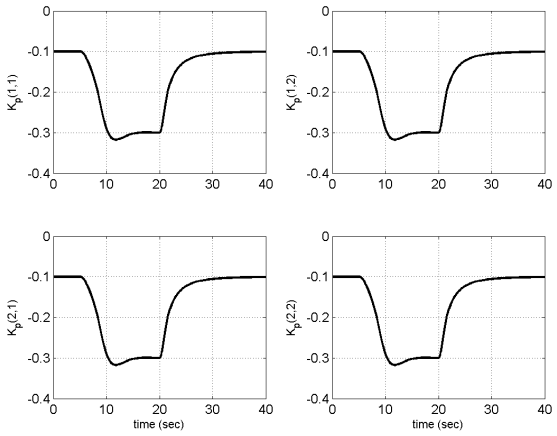

Figure 61: Controllers proportional gain matrix ($K_p(\alpha(t))$) elements.

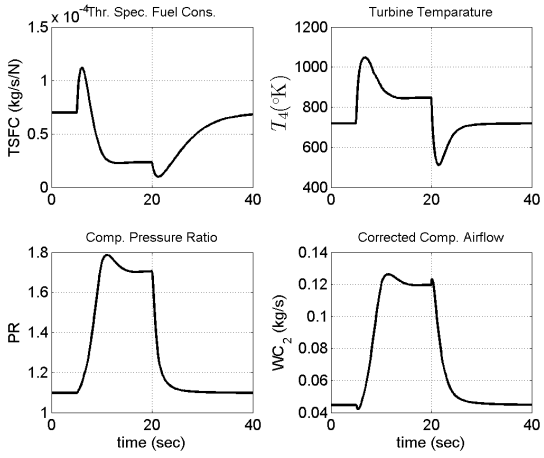

Figure 62: Turbine temperature, TSFC, compressor overall pressure ratio, and air flow rate.

60 and 61 show the evolution of the controllers integral ($K_i(\alpha)$) and proportional ($K_p(\alpha)$) gain matrices. These gains have been obtained by interpolation using the predesigned indexed family of fixed-gain controllers, and each controller corresponds to one equilibrium point of the engine. The numerical values of these gains are given in (79) to (81), which represents the controller gains for idle and cruise conditions and one more equilibrium point in between these two operating points. Figure 62 shows the histories of turbine temperature, thrust specific fuel consumption (TSFC), compressor pressure ratio, and corrected air flow rate.

3.4.5 Engine Limit Control Discussion

To handle the limits on the turbine engine system states and control inputs, the developed gain scheduled control system can be integrated with a reference governor. Reference governors have been developed previously; one of the good examples of this approach is presented in [18]. This method addresses the problem of satisfying input and/or state hard constraints in nonlinear control systems. The approach uses receding horizon strategy and consists of adding to the primal compensated nonlinear system a reference governor. The proposed reference governor is a discrete-time device which handles the reference to be tracked in an on-line fashion. The resulting hybrid system satisfies the constraints as well as stability and tracking requirements [18]. Detailed development of the GS system integrated with a reference governor is a topic for future research.

3.5 Summary

First, a MIMO linear parameter dependent model of the nonlinear gas turbine engine system was developed. Then, a gain scheduled controller with stability guarantees for this system was designed. Piecewise linear interpolation technique, which is a stability preserving interpolation approach, was used for interpolating the parameter varying gain scheduled controller in between the predesigned indexed family of fixed-gain controllers. The scheduling variable in the design process is an endogenous parameter (i.e., a function of the plant outputs) and it has been defined to be the Euclidean norm of the gas turbine engine spool speeds. Using the global linearization method, guaranteed stability of the closed-loop gas turbine engine system with a gain scheduled controller was shown. With the aid of convex optimization tools, a single quadratic Lyapunov function was computed, which guarantees the stability of the gain scheduled gas turbine engine systems. To verify the stability of the closed-loop system, an optimization problem was proposed, which was solved with sufficiently

small optimization error history, using convex optimization tools. Simulation results were presented to show the applicability of the proposed controller to the nonlinear physics-based JetCat SPT5 turboshaft engine model for large thrust commands from idle to cruise condition, and vice versa. Many other simulations were performed to fully verify system performance and stability.

CHAPTER IV

GAIN SCHEDULED MODEL REFERENCE ADAPTIVE CONTROL

4.1 Introduction

Previously developed control systems for gas turbine engines have not taken advantage of recent progress in adaptive control algorithms. A few of the recent works on the adaptive control of single and twin spool gas turbine engines for small throttle commands are described in [117, 119]. Another work on the adaptive control of twin spool gas turbine engines, which handles large throttle commands have been reported in [120]. However, in this work, complete stability analysis for the adaptive control of gas turbine engines for large throttle commands have not been done. Some of the works dedicated to the adaptive control of systems with multiple equilibrium points and with time varying reference systems are [9, 49, 57, 58, 139, 140, 141, 142, 143, 173]. Adaptive control of piecewise linear systems has been developed in [139, 140, 141, 142, 143]. In this kind of adaptive control system, multiple linear time invariant (LTI) systems are used and transitions between these models are modeled as switches. These switchings introduce discontinuities and jumps in the control inputs. $\mathcal{L}_1$ adaptive control for systems with gain scheduled reference systems is done in [49, 173]. The stability analysis for this system is done using a time varying quadratic Lyapunov function, with some conditions on the time varying Lyapunov matrix $P(t)$ and its rate $\dot{P}(t)$. Adaptive control of time varying systems with gain scheduling is done in [9, 57, 58]. The stability analysis for this system is also done using a time varying quadratic Lyapunov function, with some conditions on time varying Lyapunov matrix $P(t)$ and its rate $\dot{P}(t)$. Adaptive control of systems with

input saturation and actuator constraints for single input plants is done in [66, 76], and for multi input plants is done in [5, 57, 63, 77, 82, 102, 146, 147, 148]. The stability proofs in these works are presented for adaptive control systems with LTI reference models.

In this chapter, we use the gain scheduled model from Chapter 3, as a reference model for the model reference adaptive controller. This reference model helps the development of a MRAC algorithm, which can handle the engine control problem for large thrust commands; as the engine system can be controlled smoothly by commanding the thrust to move from one operation point (like idle) to another operating point (like cruise), and vice versa. Gain scheduled reference model design and stability analysis is done using the method presented in [136, 149, 150, 152]. The scheduling variable in our reference model design process is an *endogenous* parameter, which in the gas turbine engine case is a function of the gas turbine engine spool speeds. Note that designing this reference model does not include any switchings to shift between the equilibrium points. As we know from Chapter 3, in case of the gas turbine engine example, the stability of the GS reference model can be shown by finding a single Lyapunov function. Then rigorous stability analysis is done for a state feedback gain scheduled model reference adaptive control (GS-MRAC) system. Then the stability analysis is extended for a GS-MRAC system with constraints on magnitudes of multi control inputs using the results from [57, 66]. The constraints on the control inputs are implemented using a multi-dimensional rectangular saturation function. The Lyapunov stability analysis of GS-MRAC systems with constrained control inputs is done, due to the need for verifiable engine control systems which can handle the engine performance limits such as limits on the fuel control input, high and low pressure spool speeds, and spool accelerations. This controller then, is implemented on the physics-based JetCat SPT5 turboshaft engine model developed in Chapter 2.

This chapter is organized as follows. First, mathematical preliminaries for matrix

projection operators and multi-dimensional rectangular saturation functions are presented. Second, a model reference adaptive control with a gain scheduled reference model is designed with rigorous stability proof. The results then are extended for GS-MRAC systems with constraints on the magnitude of multiple control inputs. Finally, simulation results for a gain scheduled model reference adaptive control system of a MIMO physics-based nonlinear model of a JetCat SPT5 turboshaft engine with control input constraints are presented. The simulations are performed for three different cases including the nominal engine case, and two cases of degraded engine due to aging, which are the deteriorated versions of the nominal engine by changing some of the health parameters. Simulation results show that the developed GS-MRAC can be used for the entire flight envelope of the degraded turboshaft engine with guaranteed stability and proper tracking performance.

4.2 Mathematical Preliminaries

4.2.1 Projection Operator

The definitions and lemmas presented here are mainly adopted from [78, 79, 125].

Definition 2. *Consider a convex compact set with a smooth boundary*

$$\Omega_c = \{\theta \in R^n | f(\theta) \leq c\},\ 0 \leq c \leq 1, \tag{83}$$

where $f : \Re^n \to \Re$ *is a smooth convex function defined as*

$$f(\theta) = \frac{\theta^\mathsf{T}\theta - \theta_{max}^2}{\epsilon_\theta \theta_{max}^2}, \tag{84}$$

where θ_{max} *is the norm bound imposed on the parameter vector* θ*, and* ϵ_θ *denotes the convergence tolerance of our choice. Let the true value of the parameter* θ*, denoted by* θ^**, belong to* Ω_0*, i.e.* $\theta^* \in \Omega_0$*, the projection operator for two vectors* $\theta, y \in \Re^n$ *is defined as*

$$\text{Proj}(\theta, y) = \begin{cases} y - \frac{\nabla f}{||\nabla f||}\langle \frac{\nabla f^\mathsf{T}}{||\nabla f||}, y\rangle f(\theta), & \text{if } f(\theta) > 0 \wedge \nabla f^\mathsf{T} y > 0, \\ y, & \text{otherwise}, \end{cases} \tag{85}$$

where $\nabla f(\theta) = \left(\frac{\partial f(\theta)}{\partial \theta_1}, ..., \frac{\partial f(\theta)}{\partial \theta_n}\right) \in \Re^n$ *is the gradient vector of* f *evaluated at* θ *and it is computed as*

$$\nabla f(\theta) = \frac{2\theta^{\mathsf{T}}}{\epsilon_\theta \theta_{max}^2}, \tag{86}$$

Figure 63 illustrates the projection operator.

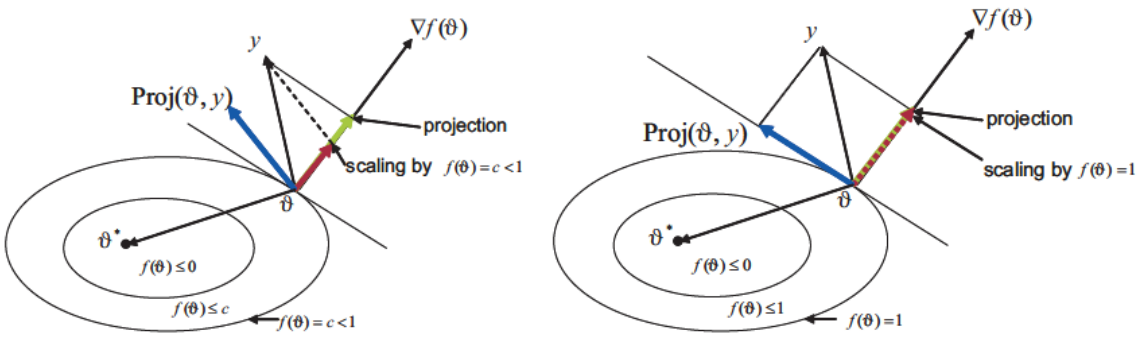

Figure 63: Illustration of the projection operator [51].

Lemma 3. *One important property of the projection operator follows. Given* $\theta^* \in \Omega_0$,

$$(\theta - \theta^*)^{\mathsf{T}}(\text{Proj}(\theta, y) - y) \leq 0. \tag{87}$$

Proof. Note that $(\theta - \theta^*)^{\mathsf{T}}(\text{Proj}(\theta, y) - y) = (\theta^* - \theta)^{\mathsf{T}}(y - \text{Proj}(\theta, y))$. For $f(\theta) > 0$ and $\nabla f^{\mathsf{T}} y > 0$, the left-hand side of inequality (87) is

$$(\theta^* - \theta)^{\mathsf{T}} \left(y - \left(y - \frac{\nabla f(\theta)(\nabla f(\theta))^{\mathsf{T}}}{||\nabla f(\theta)||^2}\right)\right), \tag{88}$$

Since $\theta^* \in \Omega_0$ and due to the convexity of $f(\theta)$, we have $(\theta^* - \theta)^{\mathsf{T}} \nabla f(\theta) \leq 0$. Hence

$$\frac{(\theta^* - \theta)^{\mathsf{T}} \nabla f(\theta)(\nabla f(\theta))^{\mathsf{T}} y}{||\nabla f(\theta)||^2} \leq 0, \tag{89}$$

otherwise $\text{Proj}(\theta, y) = y$. □

Definition 3. *The general form of the projection operator is the* $n \times m$ *matrix extension of the vector definition (2).*

$$\text{Proj}(\Theta, Y) = [\text{Proj}(\theta_1, y_1), ..., \text{Proj}(\theta_m, y_m)], \tag{90}$$

where $\Theta = [\theta_1 ... \theta_m] \in \mathbb{R}^{n\times m}, Y = [y_1 ... y_m] \in \mathbb{R}^{n\times m}$, *and* $F = [f_1(\theta_1) ... f_m(\theta_m)]^\mathsf{T} \in \mathbb{R}^{m\times 1}$, *then using definition (2) we have*

$$\text{Proj}(\theta_j, y_j) = \begin{cases} y_j - \frac{\nabla f_j}{||\nabla f_j||}\langle \frac{\nabla f_j^\mathsf{T}}{||\nabla f_j||}, y_j\rangle f_j(\theta_j), & \text{if } f_j(\theta_j) > 0 \wedge \nabla f_j^\mathsf{T} y_j > 0, \\ y_j, & \text{otherwise,} \end{cases} \tag{91}$$

for $j = 1$ *to* m.

Lemma 4. *Let* $F = [f_1(\theta_1) ... f_m(\theta_m)]^\mathsf{T} \in \mathbb{R}^{m\times 1}$ *be a convex vector function and* $\Theta = [\theta_1 ... \theta_m], \Theta^* = [\theta_1^* ... \theta_m^*], Y = [y_1 ... y_m]$, *where* $\Theta, \Theta^*, Y \in \mathbb{R}^{n\times m}$ *then,*

$$\text{trace}\left\{(\Theta - \Theta^*)^\mathsf{T}(\text{Proj}(\Theta, Y) - Y)\right\} \leq 0. \tag{92}$$

Proof. Using (87)

$$\begin{aligned} &\text{trace}\left\{(\Theta - \Theta^*)^\mathsf{T}(\text{Proj}(\Theta, Y) - Y)\right\} \\ &= \textstyle\sum_{j=1}^m (\theta_j - \theta_j^*)^\mathsf{T}(\text{Proj}(\theta_j, y_j) - y_j) \leq 0. \end{aligned} \tag{93}$$

□

Lemma 5. *If an initial value problem, such as adaptive control algorithm with adaptive law and initial conditions, is defined by*

1. $\dot{\theta} = \text{Proj}(\theta, y)$;
2. $\theta(t = 0) = \theta_0 \in \Omega_1$;
3. $f(\theta) : \mathbb{R}^m \to \mathbb{R}$ *is convex.*

Then $\theta(t) \in \Omega_1 \forall t \geq 0$.

Proof. Taking the derivative of the convex function

$$\dot{f}(\theta) = (\nabla f(\theta))^\mathsf{T}\dot{\theta} = (\nabla f(\theta))^\mathsf{T}\text{Proj}(\theta, y). \tag{94}$$

Substituting (94) into (85) leads to

$$\begin{aligned}\dot{f}(\theta) &= (\nabla f(\theta))^{\mathsf{T}}\text{Proj}(\theta, y) \\ &= \begin{cases} (\nabla f(\theta))^{\mathsf{T}} y(1 - f(\theta)), & \text{if } f(\theta) > 0 \wedge \nabla f^{\mathsf{T}} y > 0, \\ (\nabla f(\theta))^{\mathsf{T}} y, & \text{otherwise,} \end{cases}\end{aligned} \tag{95}$$

therefore

$$\begin{cases} \dot{f}(\theta) > 0, & \text{if } 0 < f(\theta) < 1 \wedge \nabla f^{\mathsf{T}} y > 0, \\ \dot{f}(\theta) = 0, & \text{if } f(\theta) = 1 \wedge \nabla f^{\mathsf{T}} y > 0, \\ \dot{f}(\theta) < 0, & \text{if } f(\theta) \leq 0 \vee \nabla f^{\mathsf{T}} y \leq 0. \end{cases} \tag{96}$$

Thus $f(\theta_0) \leq 1 \Rightarrow f(\theta(t)) \leq 1$ for all $t \geq 0$, hence $\theta(t) \in \Omega_1$ for all $t \geq 0$. □

Definition 4. *[56, 79] A variant of the projection algorithm, Γ-projection, updates the parameter along a symmetric positive definite gain Γ as defined below*

$$\text{Proj}_{\Gamma}(\theta, y) = \begin{cases} \Gamma y - \Gamma \frac{\nabla f(\theta)(\nabla f(\theta))^{\mathsf{T}}}{(\nabla f(\theta))^{\mathsf{T}} \Gamma \nabla f(\theta)} \Gamma y f(\theta), & \text{if } f(\theta) > 0 \wedge \nabla f^{\mathsf{T}} \Gamma y > 0, \\ \Gamma y, & \text{otherwise.} \end{cases} \tag{97}$$

Lemma 6. *Given $\theta^* \in \Omega_0$, then*

$$(\theta - \theta^*)^{\mathsf{T}}(\Gamma^{-1}\text{Proj}_{\Gamma}(\theta, y) - y) \leq 0. \tag{98}$$

Proof. Note that $(\theta - \theta^*)^{\mathsf{T}}(\Gamma^{-1}\text{Proj}_{\Gamma}(\theta, y) - y) = (\theta^* - \theta)^{\mathsf{T}}(y - \Gamma^{-1}\text{Proj}_{\Gamma}(\theta, y))$. For $f(\theta) > 0$ and $\nabla f^{\mathsf{T}} \Gamma y > 0$, the left-hand side of inequality (97) is

$$(\theta^* - \theta)^{\mathsf{T}} \left(y - \Gamma^{-1} \left(\Gamma y - \Gamma \frac{\nabla f(\theta)(\nabla f(\theta))^{\mathsf{T}}}{(\nabla f(\theta))^{\mathsf{T}} \Gamma \nabla f(\theta)} \Gamma y f(\theta) \right) \right). \tag{99}$$

Since $\theta^* \in \Omega_0$ and due to the convexity of $f(\theta)$, we have $(\theta^* - \theta)^{\mathsf{T}} \nabla f(\theta) \leq 0$. Hence

$$\frac{(\theta^* - \theta)^{\mathsf{T}} \nabla f(\theta)(\nabla f(\theta))^{\mathsf{T}} \Gamma y}{(\nabla f(\theta))^{\mathsf{T}} \Gamma \nabla f(\theta)} f(\theta) \leq 0, \tag{100}$$

otherwise $\text{Proj}(\theta, y) = \Gamma y$. □

Lemma 7. *Let $\text{Proj}_{\Gamma}(\Theta, Y)$ be defined similar to Definition 3, $F = [f_1(\theta_1)...f_m(\theta_m)]^{\mathsf{T}} \in \mathbb{R}^{m \times 1}$ be a convex vector function and $\Theta = [\theta_1...\theta_m], \Theta^* = [\theta_1^*...\theta_m^*], Y = [y_1...y_m]$, where $\Theta, \Theta^*, Y \in \mathbb{R}^{n \times m}$ then,*

$$\text{trace}\left\{(\Theta - \Theta^*)^{\mathsf{T}}(\Gamma^{-1}\text{Proj}_{\Gamma}(\Theta, Y) - Y)\right\} \leq 0. \tag{101}$$

Proof. The proof is similar to the proof of Lemma 4. □

4.2.2 Rectangular Saturation Function

The definitions in this section are adopted from [57, 146].

The constraints on the control inputs will be defined as a rectangular saturation function of v. The saturation function is given by $R_s(v)$, where the elements of R_s are defined by

$$R_{S_i} = \text{sat}(v_i) = \begin{cases} v_i, & \text{if } |v_i| \leq v_{i,\max},\ i = 1, ..., m, \\ v_{i,\max}\text{sgn}(v_i), & \text{if } |v_i| > v_{i,\max}. \end{cases} \tag{102}$$

This saturation function can be expressed as the sum of a direction preserving component and an error component, so that

$$R_S = \text{sat}(v) = \begin{cases} v, & \text{if } ||v|| \leq h(v), \\ \bar{v} = v_d + \tilde{v}, & \text{if } ||v|| > h(v), \end{cases} \tag{103}$$

where $v_d = \hat{e}h(v)$. $\hat{e} = v/||v||$ is the unit vector in the direction of v, and $h(v)$ returns the magnitude of the projection of v onto the hyper-rectangle. In this formulation v_d is in the same direction as v and $\tilde{v}$ is an error vector. Figure 64 illustrates the nature of R_s for the case where $m = 2$. It can be shown that $\tilde{v}$ is a bounded vector.

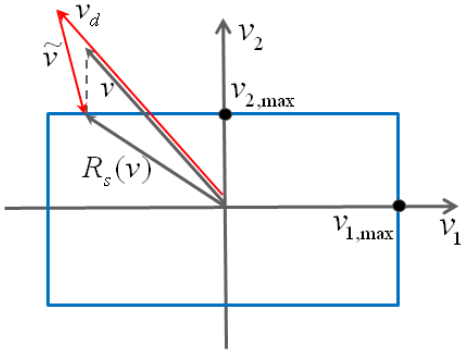

Figure 64: The control input $\bar{v}$, saturated by rectangular saturation can be decomposed into v_d and $\tilde{v}$ [57].

Definition 5. *The function $R_s(.)$, is a multi-dimensional rectangular saturation function defined by*

$$R_s(v) = \begin{bmatrix} v_{1,\max}\text{sat}\left(\frac{v_1}{v_{1,\max}}\right) \\ . \\ . \\ v_{m,\max}\text{sat}\left(\frac{v_m}{v_{m,\max}}\right) \end{bmatrix}, \tag{104}$$

where sat(.) *for all* $x \in \Re$ *is given by*

$$\text{sat}(x) = \begin{cases} x, & \text{if } |x| \leq 1, \\ \text{sgn}(x), & \text{if } |x| > 1. \end{cases} \tag{105}$$

Despite the advantages of $R_s(v)$, the direction of $R_s(v)$ is not necessarily consistent with that of v, which causes additional complexities in the stability analysis.

4.3 Model Reference Adaptive Control

In this section a gain scheduled model reference adaptive control architecture is developed. In this architecture a gain scheduled reference model is used for the system to track. Chapter 3 is dedicated to the gain scheduled reference model design and stability.

4.3.1 Problem Formulation

$A_{\text{aug}}(\alpha(t))$ and $C_{\text{aug}}(\alpha(t))$ in (44) are obtained by linear interpolation of A_i, B_i, C_i and D_i, for $i = 1, ..., s$, using scheduling parameter $\alpha(t) = ||x^p(t)||$, where A_i, B_i, C_i and D_i are unknown but constant matrices, representing the plant dynamics at s different equilibrium points.

Combining equations (44) and (47) we obtain

$$\underbrace{\begin{bmatrix} \dot{x}_{\text{aug}}(t) \\ \dot{x}^c(t) \end{bmatrix}}_{\delta\dot{x}(t)} = \underbrace{\begin{bmatrix} A_{\text{aug}}(\alpha(t)) & 0 \\ C_{\text{aug}}(\alpha(t)) & -\epsilon_c \times I \end{bmatrix}}_{A(\alpha(t))} \underbrace{\begin{bmatrix} \delta x_{\text{aug}}(t) \\ x^c(t) \end{bmatrix}}_{\delta x(t)} + \underbrace{\begin{bmatrix} B_{\text{aug}} \\ 0 \end{bmatrix}}_{B} v(t) + \underbrace{\begin{bmatrix} 0 \\ -I \end{bmatrix}}_{B_r} \delta r(t), \quad \forall \alpha \in \Omega. \tag{106}$$

Replacing $A_{\text{aug}}(\alpha(t)), B_{\text{aug}}$, and $C_{\text{aug}}(\alpha(t))$ with their values

$$\underbrace{\begin{bmatrix} \dot{x}^p(t) \\ \dot{u}(t) \\ \dot{x}^c(t) \end{bmatrix}}_{\delta\dot{x}(t)} = \underbrace{\begin{bmatrix} A^p(\alpha(t)) & B^p(\alpha(t)) & 0 \\ 0 & -\eta_c \times I & 0 \\ C^p(\alpha(t)) & D^p(\alpha(t)) & -\epsilon_c \times I \end{bmatrix}}_{A(\alpha(t))} \underbrace{\begin{bmatrix} \delta x^p(t) \\ \delta u(t) \\ x^c(t) \end{bmatrix}}_{\delta x(t)} + \underbrace{\begin{bmatrix} 0 \\ \eta_c \times I \\ 0 \end{bmatrix}}_{B} v(t) + \underbrace{\begin{bmatrix} 0 \\ 0 \\ -I \end{bmatrix}}_{B_r} \delta r(t), \quad \forall \alpha \in \Omega. \tag{107}$$

For the case where $\delta y(t) = \delta x^p(t)$, i.e. $C^p(\alpha(t)) = I, D^p(\alpha(t)) = 0$ we have

$$A(\alpha) = \begin{bmatrix} A^p(\alpha(t)) & B^p(\alpha(t)) & 0 \\ 0 & -\eta_c \times I & 0 \\ I & 0 & -\epsilon_c \times I \end{bmatrix}. \tag{108}$$

For simplicity, from now on we rename the variables $\delta x(t), \delta y(t)$ and $\delta r(t)$ as $\delta x(t) := x(t)$, $\delta y(t) := y(t)$ and $\delta r(t) := r(t)$. The plant (107) can be written as

$$\dot{x}(t) = A(\alpha(t))x(t) + Bv(t) + B_r r(t), \quad x(0) = x_0, \quad \forall \alpha \in \Omega. \tag{109}$$

The nominal control for this system is

$$v_{nom}(t) = K^{\mathsf{T}}(\alpha(t))x(t), \quad \forall \alpha \in \Omega, \tag{110}$$

where $K^{\mathsf{T}}(\alpha(t)) = [0,\ 0,\ K_i^{\mathsf{T}}(\alpha(t))] \in \Re^{l\times m}$, $l = n + 2m$.

The time-varying reference model is defined as

$$\dot{x}_m(t) = A_m(\alpha(t))x_m(t) + B_r r(t), \quad x_m(0) = x_0, \quad \forall\alpha \in \Omega. \tag{111}$$

In the previous section we showed the stability of this reference model. Note that $r(t) \in \Re^m$ is the command signal such that $||r(t)|| \leq r_{\max}$.

Assumption 2. *There exists an ideal gain matrix* $K^{*\mathsf{T}}(\alpha(t)) = [0, 0, K_i^{*\mathsf{T}}(\alpha(t))] \in \Re^{m\times(n+2m)}$*, that results in perfect matching between the reference model (111) and the plant (109) such that*

$$A_m(\alpha(t)) = A(\alpha(t)) + BK^{*\mathsf{T}}(\alpha(t)), \quad \forall\alpha \in \Omega, \tag{112}$$

where $A_m(\alpha(t)) \in \Re^{l\times l}$ *has the following form*

$$A_m(\alpha(t)) = \begin{bmatrix} A^p(\alpha(t)) & B^p(\alpha(t)) & 0 \\ 0 & -\eta_c \times I & \eta_c K_i^*(\alpha(t)) \\ I & 0 & -\epsilon_c \times I \end{bmatrix}. \tag{113}$$

Assumption 3. *Let* $K^*(t) \in \Theta_K$ *for all* $t \geq 0$*, where* Θ_K *is a known convex compact set. Note that* $\Theta_K = \left\{\Theta_{K_j}, j = 1, ..., m | \Theta_{K_j} = \{\theta_{k_{ij}}, i = 1, ..., l\}\right\}$*, and* $K^*(t) = [K_1^*(t), ..., K_m^*(t)]$*. We also assume that* $K^*(t)$ *is continuously differentiable, and the derivative is uniformly bounded,* $||\dot{K}^*(t)|| \leq d_k < \infty$*, and* $||\dot{K}_j^*(t)|| \leq d_{k_j} < \infty$ *for all* $t \geq 0$.

4.3.2 Adaptive Control Design

In order to improve the tracking performance, we design the adaptive controller to be

$$v(t) = v_{ad}(t) = \hat{K}^{\mathsf{T}}(t)x, \quad \forall\alpha \in \Omega. \tag{114}$$

Combining (106) and (114), we obtain the closed-loop system

$$\begin{aligned} &\dot{x}(t) = A_m(\alpha(t))x(t) + B\tilde{K}^{\mathsf{T}}(t)x(t) + B_r r(t), \quad \forall\alpha \in \Omega, \\ &x(0) = x_0 \end{aligned} \tag{115}$$

where $\tilde{K}(t) = \hat{K}(t) - K^*(t)$. Defining $e(t) = x(t) - x_m(t)$, the error dynamics are

$$\dot{e}(t) = A_m(\alpha(t))e(t) + B\tilde{K}^{\mathsf{T}}(t)x(t), \quad e(0) = 0, \quad \forall \alpha \in \Omega. \tag{116}$$

With the knowledge of lower and upper bounds of the parameters $K^*(t)$, the parameter projection adaptive law is

$$\dot{\hat{K}}(t) = \mathrm{Proj}_{\Gamma}\left(\hat{K}(t), -x(t)e^{\mathsf{T}}(t)PB\right), \quad \hat{K}(0) = \hat{K}_0, \tag{117}$$

where $\Gamma = \Gamma^{\mathsf{T}} > 0$, $P = P^{\mathsf{T}} > 0$ is a solution of LMI (71), and Proj(.,.) is the projection operator defined in Definition 3. Note that the error dynamics for the controller gain $\dot{\tilde{K}}(t)$, is given by

$$\dot{\tilde{K}}(t) = \dot{\hat{K}}(t) - \dot{K}^*(t), \quad \tilde{K}(0) = \tilde{K}_0, \tag{118}$$

Note that because the gain update law for $\hat{K}(t)$, $t \geq 0$, is updated using a projection operator, and because by Assumption 3, $K^*(t)$ belongs to a compact set for all $t \geq 0$, there exists a norm bound $\tilde{K}_{\max}$ such that $||\tilde{K}(t)||_F \leq \tilde{K}_{\max}$. Figure 65 shows a schematic diagram of the GS-MRAC system.

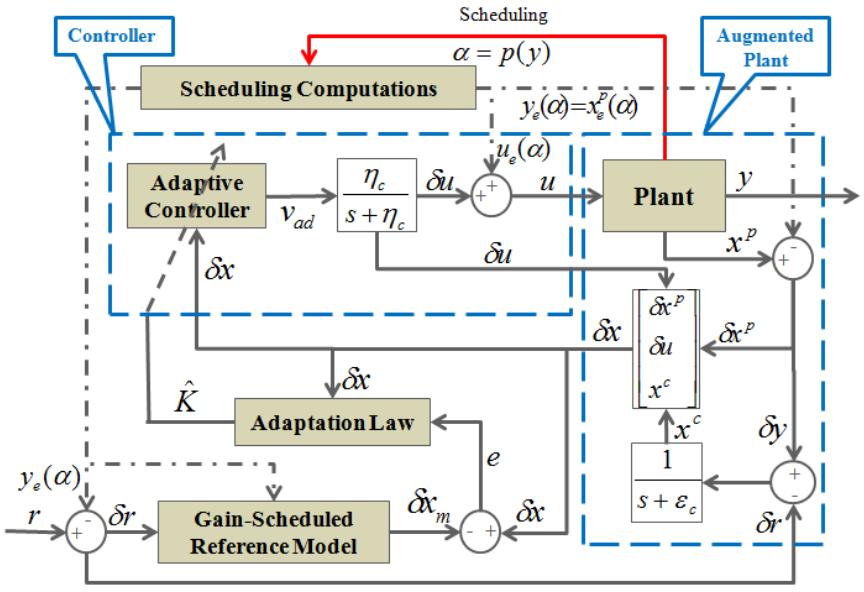

Figure 65: Gain scheduled model reference adaptive control (GS-MRAC).

Here we extended the results from [70, 177] to construct a stability proof for gain scheduled model reference adaptive control systems, in addition to transient and steady-state performance guarantees.

Theorem 2. *Consider the dynamical system given by (109) with the reference system given by (111), and assume that Assumptions 1, 2, and 3 hold. Furthermore, let the adaptive control law be given by (114) with the controller gain update law given by (117). Then, the closed-loop error signals given by (116) and (118) are uniformly bounded for all* $(e(0), \tilde{K}(0)) \in \mathcal{D}_\rho$*, where* $\mathcal{D}_\rho$ *is a compact positively invariant set, with ultimate bound* $||e(t)||_2 < \epsilon_e$*, for* $t \geq T$ *where*

$$\epsilon_e > \sqrt{\lambda_{\max}(P)\vartheta^2 + \lambda_{\max}(\Gamma^{-1})\tilde{K}_{\max}^2}, \tag{119}$$

$$\vartheta := \sqrt{\frac{2\lambda_{\max}(\Gamma^{-1})\tilde{K}_{\max} d_k}{\lambda_{\min}(Q)}}. \tag{120}$$

In addition, for $t \in [0,\ T)$*, the system error* $e(t)$*, and gain update error* $\tilde{K}(t)$ *satisfy*

$$||e(t)||_2 \leq ||\tilde{K}(0)||_F \sqrt{\frac{||\Gamma^{-1}||_F}{\lambda_{\min}(P)}}, \tag{121}$$

$$||\tilde{K}(t)||_F \leq ||\tilde{K}(0)||_F \sqrt{\frac{||\Gamma^{-1}||_F}{\lambda_{\min}(\Gamma^{-1})}}. \tag{122}$$

Proof. A Lyapunov candidate function chosen as

$$V(e(t), \tilde{K}(t)) = e^{\mathsf{T}}(t)Pe(t) + \text{trace}\left(\tilde{K}(t)^{\mathsf{T}}\Gamma^{-1}\tilde{K}(t)\right), \tag{123}$$

where $P > 0$ satisfies (71). Note that (123) satisfies $\gamma_1(||\zeta||_2) \leq V(\zeta) \leq \gamma_2(||\zeta||_2)$, where $\zeta := [e^{\mathsf{T}}, (\text{vec}\tilde{K})^{\mathsf{T}}]^{\mathsf{T}}$, $\gamma_1(||\zeta||_2) = \gamma_2(||\zeta||_2) = ||\zeta||_2^2$ with $||\zeta||_2^2 = e^{\mathsf{T}}Pe + \text{trace}\left(\tilde{K}^{\mathsf{T}}\Gamma^{-1}\tilde{K}\right)$. Furthermore, note that $\gamma_1(.)$ and $\gamma_2(.)$ are class $\mathcal{K}_\infty$ functions. Differentiating (123) along the closed-loop system trajectories (116) and (118) yields where its time-derivative is given by

$$\begin{aligned}
\dot{V}(.) &= \dot{e}^{\mathsf{T}}(t)Pe(t) + e^{\mathsf{T}}(t)P\dot{e}(t) + \text{trace}\left(\dot{\tilde{K}}^{\mathsf{T}}(t)\Gamma^{-1}\tilde{K}(t) + \tilde{K}^{\mathsf{T}}(t)\Gamma^{-1}\dot{\tilde{K}}(t)\right) \\
&= e^{\mathsf{T}}(t)\left(A_m^{\mathsf{T}}(\alpha(t))P + PA_m(\alpha(t))\right)e(t) + 2e^{\mathsf{T}}(t)PB\tilde{K}^{\mathsf{T}}(t)x(t) \\
&\quad + 2\text{trace}\left(\tilde{K}^{\mathsf{T}}(t)\Gamma^{-1}\dot{\tilde{K}}(t)\right), \quad \forall \alpha \in \Omega.
\end{aligned} \tag{124}$$

Using Lemma 1, applying trace identity (valid for any two co-dimensional vectors a and b: $a^{\mathsf{T}}b = \text{trace}\left(ba^{\mathsf{T}}\right)$), and letting $Y_K(t) = -x(t)e^{\mathsf{T}}(t)PB$ leads to

$$\begin{aligned}\dot{V}(.) &\leq -e^{\mathsf{T}}(t)Qe(t) + 2\text{trace}\left(\tilde{K}^{\mathsf{T}}(t)\left[\Gamma^{-1}\dot{\hat{K}}(t) - Y_K(t)\right]\right) \\ &\quad + 2\text{trace}\left(-\tilde{K}^{\mathsf{T}}(t)\Gamma^{-1}\dot{K}^*(t)\right) \\ &= -e^{\mathsf{T}}(t)Qe(t) + 2\text{trace}\left(\tilde{K}^{\mathsf{T}}(t)\left[\Gamma^{-1}\text{Proj}_{\Gamma}(\hat{K}(t), Y_K(t)) - Y_K(t)\right]\right) \\ &\quad - 2\text{trace}\left(\tilde{K}^{\mathsf{T}}(t)\Gamma^{-1}\dot{K}^*(t)\right).\end{aligned} \tag{125}$$

Using Lemma 7

$$\begin{aligned}\dot{V}(.) &\leq -e^{\mathsf{T}}(t)Qe(t) - 2\text{trace}\left(\tilde{K}^{\mathsf{T}}(t)\Gamma^{-1}\dot{K}^*(t)\right) \\ &\leq -\lambda_{\min}(Q)||e(t)||^2 + \left|2\text{trace}\left(\tilde{K}^{\mathsf{T}}(t)\Gamma^{-1}\dot{K}^*(t)\right)\right|.\end{aligned} \tag{126}$$

By Assumption 3, we have

$$\left|2\text{trace}\left(\tilde{K}^{\mathsf{T}}(t)\Gamma^{-1}\dot{K}^*(t)\right)\right| \leq 2\lambda_{\max}(\Gamma^{-1})\tilde{K}_{\max}d_k, \quad t \geq 0. \tag{127}$$

Substituting (127) into (126) yields

$$\dot{V}(.) \leq -\lambda_{\min}(Q)||e(t)||^2 + 2\lambda_{\max}(\Gamma^{-1})\tilde{K}_{\max}d_k, \quad t \geq 0. \tag{128}$$

Let ϑ be given by (120). Now for $||e(t)||_2 \geq \vartheta$, it follows that $\dot{V}(e(t), \tilde{K}(t)) \leq 0$ for all $(e(t), \tilde{K}(t)) \in \{\mathcal{D}_e - \mathcal{D}_r\}$ and $t \geq 0$, where

$$\mathcal{D}_e := \left\{(e(t), \tilde{K}(t)) \in \Re^l \times \Re^{l\times m} |\ x(t) \in \Re^l\right\}, \tag{129}$$

$$\mathcal{D}_r := \left\{(e(t), \tilde{K}(t)) \in \Re^l \times \Re^{l\times m} |\ ||e(t)||_2 \leq \vartheta\right\}, \tag{130}$$

where $l = n + 2m$. Finally, define

$$\mathcal{D}_\rho := \left\{(e(t), \tilde{K}(t)) \in \Re^l \times \Re^{l\times m} |\ V(e(t), \tilde{K}(t)) \leq \rho\right\}, \tag{131}$$

where ρ is the maximum value such that $\mathcal{D}_\rho \subseteq \mathcal{D}_e$, and define

$$\mathcal{D}_\eta := \left\{(e(t), \tilde{K}(t)) \in \Re^l \times \Re^{l\times m} |\ V(e(t), \tilde{K}(t)) \leq \eta\right\}, \tag{132}$$

where $\eta > \gamma_2(\mu) = \mu^2 = \lambda_{\max}(P)\vartheta^2 + \lambda_{\max}(\Gamma^{-1})\tilde{K}_{\max}^2$. The sets $\mathcal{D}_\eta$ and $\mathcal{D}_\rho$ have the property that a solution starting in either set can't leave it, because $\dot{V}(e(t), \tilde{K}(t))$ is negative on the boundary.

To show ultimate boundedness of the closed-loop system (116) and (118), note that $\mathcal{D}_\eta \subset \mathcal{D}_\rho$. Now, since $\dot{V}(e(t), \tilde{K}(t)) \leq 0$, $t \geq 0$, for all $(e(t), \tilde{K}(t)) \in \{\mathcal{D}_e - \mathcal{D}_r\}$ and $\mathcal{D}_r \subset \mathcal{D}_\rho$, it follows that $\mathcal{D}_\rho$ is positively invariant. Hence if $(e(0), \tilde{K}(0)) \in \mathcal{D}_\rho$, then it follows from Theorem 4.18 of [70] that the solution $(e(t), \tilde{K}(t))$, $t \geq 0$ to (116) and (118) is ultimately bounded with ultimate bound given by $\gamma_1^{-1}(\eta) = \sqrt{\eta}$, which yields (119).

Finally, over the interval $t \in [0, T)$, $\dot{V}(e(t), \tilde{K}(t)) \leq 0, t \geq 0$, because $(e(t), \tilde{K}(t)) \in \{\mathcal{D}_e - \mathcal{D}_r\}$. This implies that

$$V(e(t), \tilde{K}(t)) \leq V(e(0), \tilde{K}(0)), \quad t \in [0, T). \tag{133}$$

Using the inequalities

$$\begin{aligned} &\lambda_{\min}(P)||e(t)||_2^2 \leq V(e(t), \tilde{K}(t)), \\ &V(e(0), \tilde{K}(0)) = \text{trace}\left(\tilde{K}(0)^\intercal \Gamma^{-1} \tilde{K}(0)\right) \leq ||\Gamma^{-1}||_F ||\tilde{K}(0)||_F^2, \end{aligned} \tag{134}$$

in (133) gives (121). Similarly using the inequalities

$$\begin{aligned} &\lambda_{\min}(\Gamma^{-1})||\tilde{K}||_F^2 \leq V(e(t), \tilde{K}(t)), \\ &V(e(0), \tilde{K}(0)) \leq ||\Gamma^{-1}||_F ||\tilde{K}(0)||_F^2, \end{aligned} \tag{135}$$

in (133) gives (122). This completes the proof. □

Remark 4. *Theorem 2 shows that over a transient finite-time T, the closed-loop error signals (116) and (118) are bounded from above by (121) and (122), respectively. This implies along with uniform ultimate boundedness of the closed-loop error signals (116) and (118), that* $e(.) \in \mathcal{L}_\infty$ *and* $vec\tilde{K}(.) \in \mathcal{L}_\infty$*, and hence,* $x(.) \in \mathcal{L}_\infty$ *and* $v(.) \in \mathcal{L}_\infty$*. Furthermore, note that* $e(t)$*,* $t \in [0, T)$*, can be made sufficiently small (satisfying* ϑ *in (120)) by letting* $\lambda_{\min}(\Gamma) \to \infty$*.*

Remark 5. *Consider a system with a constant shift in its equilibrium manifold, which can be defined as* $d = x_{ag,e}(\alpha(t)) - x_e(\alpha(t))$*, where* $x_e(\alpha(t))$ *is the parameterized steady state variable for the nominal system, and* $x_{ag,e}(\alpha(t))$ *is the parameterized steady state variable for the new system. Let the reference model dynamics be defined as* $\delta\dot{x}_m(t) = A_m(\alpha(t))\delta x_m(t) + B_r\delta r(t)$*, where* $\delta x_m(t) = x_m(t) - x_e(\alpha(t))$*, and the linearized closed-loop form of the new system be defined as* $\delta\dot{x}_{ag}(t) = A_m(\alpha(t))\delta x_{ag}(t) + B\tilde{K}^{\mathsf{T}}(t)\delta x_{ag}(t) + B_r\delta r(t)$*, where* $\delta x_{ag}(t) = x_{ag}(t) - x_{ag,e}(\alpha(t))$*. Now define the error as* $e_{ag}(t) = \delta x_{ag}(t) - \delta x_m(t) = \bar{e}_{ag}(t) - d$*, where* $\bar{e}_{ag}(t) = x_{ag}(t) - x_m(t)$*. Then the error dynamic is* $\dot{e}_{ag}(t) = \dot{\bar{e}}_{ag}(t) = A_m(\alpha(t))\bar{e}_{ag}(t) - A_m(\alpha(t))d + B\tilde{K}^{\mathsf{T}}(t)\delta x_{ag}(t)$*. For the cases where* d *is not zero, there is a shift in the error due to the bounded* $A_m(\alpha(t))d$ *term in the error dynamics. For the steady state condition where* $A_m(\alpha(t)) = A_m(\alpha_{ss})$*, there is a constant shift in the error, since we can only have* $e_{ag,ss} = 0$*, and* $\bar{e}_{ag,ss} = d$ *or* $x_{ag,ss} \to x_{m,ss} + d$*.*

Based on this discussion, $A_m(\alpha(t))d$ *can be viewed as a resulted unmatched uncertainty due to an equilibrium shift, which does not exist for the original system. It is well known that unmatched uncertainties can lead to poor performance and under some circumstances that can result in system instabilities [49]. In order to verify the robustness of our proposed algorithm for the engine simulation, we consider the aforementioned equilibrium shift scenario. Our simulation studies indicate that the engine system achieves acceptable performance without causing instability. However, from a theoretical point of view, mathematical proofs that highlight this fact are beyond the scope of this dissertation, because the problem of adaptive control for systems with unmatched uncertainties is not an entirely solved problem in the adaptive control literature [49]. Therefore we are going to investigate this as future research.*

4.3.3 Model Reference Adaptive Control with Constrained Control Inputs

Since we are dealing with engine performance limits for gas turbine engine control problem, we need to have a mechanism to handle the issue. Limits on the fuel control input, high and low pressure spool speeds, and accelerations can be implemented by defining constraints on the control input to the augmented plant ($v(t)$). These constraints are defined in the form of a multi-dimensional saturation function for multiple control inputs of the augmented engine model.

Here we extend the results from the previous part to the systems with constraints on the magnitude of multiple control inputs. In order to avoid the adaptive controller parameters being adjusted improperly by the saturation error, we use the augmented error method in the adaptive control design developed in [66] for SISO systems and [57] for MIMO systems to provide the stability analysis rigorously for a gain scheduled model reference adaptive control system. The overall controller is shown to result in semi-global boundedness with respect to the entire space as the saturation level decreases. Theoretical results are validated with simulation studies through the JetCat SPT5 turboshaft engine model with control input magnitude constraints. Simulation results show that adaptive control stabilizes the closed-loop system and tracks the gain scheduled reference model properly. Compensation for magnitude saturation is proven to be useful to avoid high oscillation in the adaptive control inputs due to saturation errors.

The plant (109) with saturated control inputs can be written as

$$\dot{x} = A(\alpha(t))x(t) + BR_s(v(t)) + B_r r(t), \quad \forall \alpha \in \Omega, \tag{136}$$

where $v(t)$ is the adaptive control input which introduced in equation (114). the ultimate goal is to determine adaptive parameters such that all signals in the plant (136) are guaranteed to be bounded, and $y(t)$ tracks $r(t)$. The deficiency of $v(t)$ is

defined as

$$\Delta v(t) = v(t) - R_s(v(t)). \tag{137}$$

The plant (136) can be written as

$$\begin{aligned} \dot{x} &= A(\alpha(t))x(t) + Bv(t) - B\Delta v(t) + B_r r(t), \quad \forall \alpha \in \Omega, \\ x(0) &= x_0. \end{aligned} \tag{138}$$

Plant (138) with controller (114) can be written as

$$\begin{aligned} \dot{x} &= A(\alpha(t))x(t) + B\hat{K}^{\mathsf{T}}(t)x(t) - B\Delta v(t) + B_r r(t), \quad \forall \alpha \in \Omega, \\ x(0) &= x_0. \end{aligned} \tag{139}$$

Subtracting the reference model (111) and the plant (139), a closed-loop error dynamics equation is obtained as

$$\begin{aligned} \dot{e}(t) &= A_m(\alpha(t))e(t) + B\tilde{K}^{\mathsf{T}}(t)x(t) - B\Delta v(t), \quad \forall \alpha \in \Omega, \\ e(0) &= 0. \end{aligned} \tag{140}$$

In order to eliminate the adverse effect of the disturbance $\Delta v(t)$, we generate a signal $e_\Delta(t)$ as

$$\begin{aligned} \dot{e}_\Delta(t) &= A_m(\alpha(t))e_\Delta(t) - \hat{K}_\Delta(t)\Delta v(t), \quad \forall \alpha \in \Omega, \\ e_\Delta(0) &= 0, \end{aligned} \tag{141}$$

where $\hat{K}_\Delta(t) \in \Re^{l \times m}$. The undesirable effects due to control input saturation can be removed from the error dynamics in equation (140) by defining an augmented error $e_v(t) = e(t) - e_\Delta(t)$. Its dynamics can be determined as

$$\begin{aligned} \dot{e}_v(t) &= A_m(\alpha(t))e_v(t) + B\tilde{K}^{\mathsf{T}}(t)x(t) - \tilde{K}_\Delta(t)\Delta v(t), \quad \forall \alpha \in \Omega, \\ e_v(t) &= 0, \end{aligned} \tag{142}$$

where $\tilde{K}_\Delta(t) = B - \hat{K}_\Delta(t)$.

We now choose the following projection adaptive laws for adjusting the parameters

$$\begin{aligned} \dot{\hat{K}}(t) &= \mathrm{Proj}_\Gamma\left(\hat{K}(t), -x(t)e_v^{\mathsf{T}}(t)PB\right), \\ \dot{\hat{K}}_\Delta^{\mathsf{T}}(t) &= \mathrm{Proj}_\Gamma\left(\hat{K}_\Delta^{\mathsf{T}}(t), \Delta v(t)e_v^{\mathsf{T}}(t)P\right), \end{aligned} \tag{143}$$

where $P = P^{\mathsf{T}} > 0$ is a solution of LMI (71). The gains in adaptive laws $\Gamma \in \Re^{l \times l}$, $\Gamma_{\Delta} \in \Re^{m \times m}$ are positive definite matrices $\Gamma = \Gamma^{\mathsf{T}} > 0$ and $\Gamma_{\Delta} = \Gamma_{\Delta}^{\mathsf{T}} > 0$. Note that the error dynamics for the controller gain $\dot{\tilde{K}}(t)$, and the saturation compensation gain $\dot{\tilde{K}}_{\Delta}(t)$ are given by

$$\begin{aligned} \dot{\tilde{K}}(t) &= \dot{\hat{K}}(t) - \dot{K}^{*}(t), \quad \tilde{K}(0) = \tilde{K}_{0}, \\ \dot{\tilde{K}}_{\Delta}(t) &= -\dot{\hat{K}}_{\Delta}(t), \quad \tilde{K}_{\Delta}(0) = \tilde{K}_{\Delta_{0}}. \end{aligned} \tag{144}$$

Since we are using a projection operator to update parameters $\hat{K}_{\Delta}(t)$, then $\hat{K}_{\Delta}(t) \in \Theta_{\Delta}$, where Θ_{Δ} is a convex compact set. Because B is a constant matrix, then there exists a norm bound $\tilde{K}_{\Delta,\max}$ such that $||\tilde{K}_{\Delta}(t)||_{F} \leq \tilde{K}_{\Delta,\max}$.

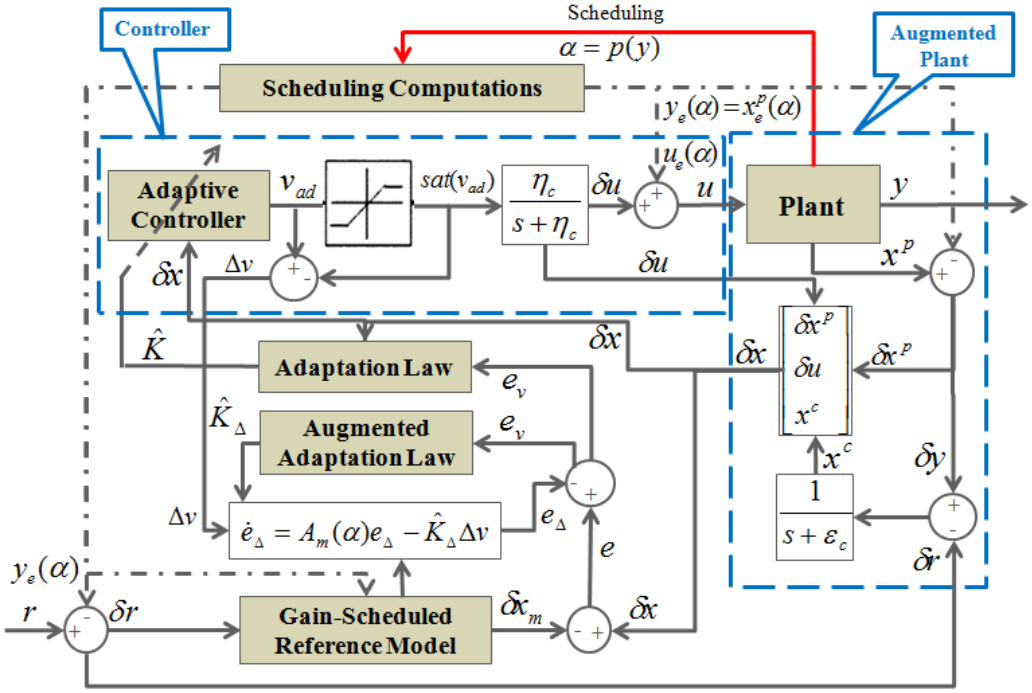

Figure 66: Gain scheduled model reference adaptive control (GS-MRAC) with constrained control inputs.

Figure 66 shows a schematic diagram of the GS-MRAC system with input magnitude saturation. In the next theorem, we extend the results from [70, 177] to construct a stability proof for the gain scheduled model reference adaptive control systems with multiple constrained control inputs, in addition to transient and steady-state performance guarantees.

Theorem 3. *Consider the error dynamical system given by (142), and assume that Assumptions 1, 2, and 3 hold. Furthermore, let the adaptive control law be given by (114), and the control deficiency be defined as (137) with the controller gain update law given by (143). Then, the error signals given by (142) and (144) are uniformly bounded for all* $(e_v(0), \tilde{K}(0), \tilde{K}_\Delta(0)) \in \mathcal{D}_\rho$*, where* $\mathcal{D}_\rho$ *is a compact positively invariant set, with ultimate bound* $||e_v(t)||_2 < \epsilon_e$*, for* $t \geq T$ *where*

$$\epsilon_e > \left[\lambda_{\max}(P)\vartheta^2 + \lambda_{\max}(\Gamma^{-1})\tilde{K}_{\max}^2 + \lambda_{\max}(\Gamma_\Delta^{-1})\tilde{K}_{\Delta,\max}^2\right]^{\frac{1}{2}}, \tag{145}$$

$$\vartheta := \sqrt{\frac{2\lambda_{\max}(\Gamma^{-1})\tilde{K}_{\max}d_k}{\lambda_{\min}(Q)}}. \tag{146}$$

In addition, for $t \in [0,\ T)$*, the system error* $e(t)$*, gain update error* $\tilde{K}(t)$*, and saturation compensation gain update error* $\tilde{K}_\Delta(t)$ *satisfy*

$$||e_v(t)||_2 \leq \tilde{K}_{0,\max}\left[\frac{\gamma_{\max}}{\lambda_{\min}(P)}\right]^{\frac{1}{2}}, \tag{147}$$

$$||\tilde{K}(t)||_F \leq \tilde{K}_{0,\max}\left[\frac{\gamma_{\max} - \lambda_{\min}\Theta_{\min}^2}{\lambda_{\min}(\Gamma^{-1})}\right]^{\frac{1}{2}}, \tag{148}$$

$$||\tilde{K}_\Delta(t)||_F \leq \tilde{K}_{0,\max}\left[\frac{\gamma_{\max} - \lambda_{\min}\Theta_{\min}^2}{\lambda_{\min}(\Gamma_\Delta^{-1})}\right]^{\frac{1}{2}}, \tag{149}$$

where $\tilde{K}_{0,\max} := \max\left[||\tilde{K}(0)||_F, ||\tilde{K}_\Delta(0)||_F\right]$, $\Theta_{\min} := \min\left[\inf||\tilde{K}(t)||_F, \inf||\tilde{K}_\Delta(t)||_F\right]$, $\gamma_{\max} := \max\left[||\Gamma^{-1}||_F, ||\Gamma_\Delta^{-1}||_F\right]$*, and* $\lambda_{\min} := \min\left[\lambda_{\min}(\Gamma^{-1}), \lambda_{\min}(\Gamma_\Delta^{-1})\right]$.

Proof. For the case where $\Delta v(t) = 0$ the proof is similar to the proof of Theorem 2. For the case which $\Delta v(t) \neq 0$, a Lyapunov candidate function is chosen as

$$\begin{aligned} V(e_v(t), \tilde{K}(t), \tilde{K}_\Delta(t)) = e_v^\mathsf{T}(t)Pe_v(t) + \text{trace}\left(\tilde{K}(t)^\mathsf{T}\Gamma^{-1}\tilde{K}(t)\right) \\ + \text{trace}\left(\tilde{K}_\Delta(t)\Gamma_\Delta^{-1}\tilde{K}_\Delta^\mathsf{T}(t)\right), \end{aligned} \tag{150}$$

where $P > 0$ satisfies (71). Note that (150) satisfies $\gamma_1(||\zeta||_2) \leq V(\zeta) \leq \gamma_2(||\zeta||_2)$, where $\zeta := [e^\mathsf{T},\ (\text{vec}\tilde{K})^\mathsf{T},\ (\text{vec}\tilde{K}_\Delta^\mathsf{T})^\mathsf{T}]^\mathsf{T}$, $\gamma_1(||\zeta||_2) = \gamma_2(||\zeta||_2) = ||\zeta||_2^2$ with $||\zeta||_2^2 = e^\mathsf{T}Pe + \text{trace}\left(\tilde{K}^\mathsf{T}\Gamma^{-1}\tilde{K}\right) + \text{trace}\left(\tilde{K}_\Delta\Gamma_\Delta^{-1}\tilde{K}_\Delta^\mathsf{T}\right)$. Furthermore, note that $\gamma_1(.)$ and $\gamma_2(.)$

are class $\mathcal{K}_\infty$ functions. Differentiating (150) along the closed-loop system trajectories (142) and (144) yields

$$\begin{aligned}\dot{V}(.) &= \dot{e}_v^{\mathsf{T}}(t)Pe_v(t) + e_v^{\mathsf{T}}(t)P\dot{e}_v(t) \\ &\quad + \text{trace}\left(\dot{\tilde{K}}^{\mathsf{T}}(t)\Gamma^{-1}\tilde{K}(t) + \tilde{K}^{\mathsf{T}}(t)\Gamma^{-1}\dot{\tilde{K}}(t)\right) \\ &\quad + \text{trace}\left(\dot{\tilde{K}}_\Delta(t)\Gamma_\Delta^{-1}\tilde{K}_\Delta^{\mathsf{T}}(t) + \tilde{K}_\Delta(t)\Gamma_\Delta^{-1}\dot{\tilde{K}}_\Delta^{\mathsf{T}}(t)\right) \\ &= e_v^{\mathsf{T}}(t)\left(A_m^{\mathsf{T}}(\alpha(t))P + PA_m(\alpha(t))\right)e_v(t) \\ &\quad + 2e_v^{\mathsf{T}}(t)PB\tilde{K}^{\mathsf{T}}(t)x(t) + 2\text{trace}\left(\tilde{K}^{\mathsf{T}}(t)\Gamma^{-1}\dot{\tilde{K}}(t)\right) \\ &\quad - 2e_v^{\mathsf{T}}(t)P\tilde{K}_\Delta(t)\Delta v(t) + 2\text{trace}\left(\tilde{K}_\Delta(t)\Gamma_\Delta^{-1}\dot{\tilde{K}}_\Delta^{\mathsf{T}}(t)\right), \quad \forall\alpha\in\Omega.\end{aligned} \tag{151}$$

Using Lemma 1, applying trace identity, and letting $Y_K(t) = -x(t)e_v^{\mathsf{T}}(t)PB$, and $Y_{K_\Delta}(t) = \Delta v(t)e_v^{\mathsf{T}}(t)P$ leads to

$$\begin{aligned}\dot{V}(.) &\le -e_v^{\mathsf{T}}(t)Qe_v(t) + 2\text{trace}\left(\tilde{K}^{\mathsf{T}}(t)\left[\Gamma^{-1}\dot{\hat{K}}(t) - Y_K(t)\right]\right) \\ &\quad + 2\text{trace}\left(-\tilde{K}^{\mathsf{T}}(t)\Gamma^{-1}\dot{K}^*(t)\right) \\ &\quad + 2\text{trace}\left(\tilde{K}_\Delta(t)\left[\Gamma_\Delta^{-1}\dot{\hat{K}}_\Delta^{\mathsf{T}}(t) - Y_{K_\Delta}(t)\right]\right) \\ &= -e_v^{\mathsf{T}}(t)Qe_v(t) + 2\text{trace}\left(\tilde{K}^{\mathsf{T}}(t)\left[\Gamma^{-1}\text{Proj}_\Gamma(\hat{K}(t), Y_K(t)) - Y_K(t)\right]\right) \\ &\quad - 2\text{trace}\left(\tilde{K}^{\mathsf{T}}(t)\Gamma^{-1}\dot{K}^*(t)\right) \\ &\quad + 2\text{trace}\left(\tilde{K}_\Delta(t)\left[\Gamma_\Delta^{-1}\text{Proj}_\Gamma(\hat{K}_\Delta^{\mathsf{T}}(t), Y_{K_\Delta}(t)) - Y_{K_\Delta}(t)\right]\right).\end{aligned} \tag{152}$$

Using Lemma 7

$$\begin{aligned}\dot{V}(.) &\le -e_v^{\mathsf{T}}(t)Qe_v(t) - 2\text{trace}\left(\tilde{K}^{\mathsf{T}}(t)\Gamma^{-1}\dot{K}^*(t)\right) \\ &\le -\lambda_{\min}(Q)||e_v(t)||^2 + \left|2\text{trace}\left(\tilde{K}^{\mathsf{T}}(t)\Gamma^{-1}\dot{K}^*(t)\right)\right|.\end{aligned} \tag{153}$$

By Assumption 3, we have

$$\left|2\text{trace}\left(\tilde{K}^{\mathsf{T}}(t)\Gamma^{-1}\dot{K}^*(t)\right)\right| \le 2\lambda_{\max}(\Gamma^{-1})\tilde{K}_{\max}d_k, \quad t\ge 0. \tag{154}$$

Substituting (154) into (153) yields

$$\dot{V}(.) \le -\lambda_{\min}(Q)||e_v(t)||^2 + 2\lambda_{\max}(\Gamma^{-1})\tilde{K}_{\max}d_k, \quad t\ge 0. \tag{155}$$

Let ϑ be given by (146). Now, for $||e_v(t)||_2 \geq \vartheta$, it follows that $\dot{V}(e_v(t), \tilde{K}(t), \tilde{K}_\Delta(t)) \leq 0$ for all $(e_v(t), \tilde{K}(t), \tilde{K}_\Delta(t)) \in \{\mathcal{D}_e - \mathcal{D}_r\}$ and $t \geq 0$, where

$$\mathcal{D}_e := \left\{(e_v(t), \tilde{K}(t), \tilde{K}_\Delta(t)) \in \Re^l \times \Re^{l\times m} \times \Re^{l\times m} |\ x(t) \in \Re^l\right\}, \tag{156}$$

$$\mathcal{D}_r := \left\{(e_v(t), \tilde{K}(t), \tilde{K}_\Delta(t)) \in \Re^l \times \Re^{l\times m} \times \Re^{l\times m} |\ ||e_v(t)||_2 \leq \vartheta\right\}, \tag{157}$$

where $l = n + 2m$. Finally, define

$$\mathcal{D}_\rho := \left\{(e_v(t), \tilde{K}(t), \tilde{K}_\Delta(t)) \in \Re^l \times \Re^{l\times m} \times \Re^{l\times m} |\ V(e_v(t), \tilde{K}(t)) \leq \rho\right\}, \tag{158}$$

where ρ is the maximum value such that $\mathcal{D}_\rho \subseteq \mathcal{D}_e$, and define

$$\mathcal{D}_\eta := \left\{(e_v(t), \tilde{K}(t), \tilde{K}_\Delta(t)) \in \Re^l \times \Re^{l\times m} \times \Re^{l\times m} |\ V(e_v(t), \tilde{K}(t)) \leq \eta\right\}, \tag{159}$$

where $\eta > \gamma_2(\mu) = \mu^2 = \lambda_{\max}(P)\vartheta^2 + \lambda_{\max}(\Gamma^{-1})\tilde{K}^2_{\max} + \lambda_{\max}(\Gamma_\Delta^{-1})\tilde{K}^2_{\Delta,\max}$. The sets $\mathcal{D}_\eta$ and $\mathcal{D}_\rho$ have the property that a solution starting in either set can't leave it, because $\dot{V}(e(t), \tilde{K}(t), \tilde{K}_\Delta(t))$ is negative on the boundary.

To show ultimate boundedness of the closed-loop system (142) and (144), note that $\mathcal{D}_\eta \subset \mathcal{D}_\rho$. Now, since $\dot{V}(e_v(t), \tilde{K}(t), \tilde{K}_\Delta(t)) \leq 0$, $t \geq 0$, for all $(e_v(t), \tilde{K}(t), \tilde{K}_\Delta(t)) \in \{\mathcal{D}_e - \mathcal{D}_r\}$ and $\mathcal{D}_r \subset \mathcal{D}_\rho$, it follows that $\mathcal{D}_\rho$ is positively invariant. Hence if we have $(e_v(0), \tilde{K}(0), \tilde{K}_\Delta(0)) \in \mathcal{D}_\rho$, then it follows from Theorem 4.18 of [70] that the solution $(e_v(t), \tilde{K}(t), \tilde{K}_\Delta(t))$, $t \geq 0$, to (142) and (144) is ultimately bounded with an ultimate bound given by $\gamma_1^{-1}(\eta) = \sqrt{\eta}$, which yields (145).

Finally, over the interval $t \in [0, T)$, $\dot{V}(e_v(t), \tilde{K}(t), \tilde{K}_\Delta(t)) \leq 0$, $t \geq 0$, because $(e(t), \tilde{K}(t)) \in \{\mathcal{D}_e - \mathcal{D}_r\}$. This implies that

$$V(e_v(t), \tilde{K}(t), \tilde{K}_\Delta(t)) \leq V(e_v(0), \tilde{K}(0), \tilde{K}_\Delta(0)), \quad t \in [0, T). \tag{160}$$

Using the inequalities

$$\begin{aligned}
&\lambda_{\min}(P)||e_v(t)||_2^2 \leq V(e_v(t), \tilde{K}(t)), \\
&V(e_v(0), \tilde{K}(0), \tilde{K}_\Delta(0)) = \text{trace}\left(\tilde{K}(0)^\intercal \Gamma^{-1} \tilde{K}(0)\right) \\
&\qquad\qquad \leq ||\Gamma^{-1}||_F ||\tilde{K}(0)||_F^2 + ||\Gamma_\Delta^{-1}||_F ||\tilde{K}_\Delta(0)||_F^2 \\
&\qquad\qquad \leq \gamma_{\max} \tilde{K}_{0,\max}^2,
\end{aligned} \tag{161}$$

in (160) gives (147). Using the inequalities

$$\begin{aligned}
&\lambda_{\min}(\Gamma^{-1})||\tilde{K}||_F^2 + \lambda_{\min}\Theta_{\min}^2 \leq V(e_v(t), \tilde{K}(t), \tilde{K}_\Delta(t)), \\
&V(e_v(0), \tilde{K}(0), \tilde{K}_\Delta(0)) \leq \gamma_{\max} \tilde{K}_{0,\max}^2,
\end{aligned} \tag{162}$$

in (160) gives (148). Similarly, using the inequalities

$$\begin{aligned}
&\lambda_{\min}(\Gamma_\Delta^{-1})||\tilde{K}_\Delta||_F^2 + \lambda_{\min}\Theta_{\min}^2 \leq V(e_v(t), \tilde{K}(t), \tilde{K}_\Delta(t)), \\
&V(e_v(0), \tilde{K}(0), \tilde{K}_\Delta(0)) \leq \gamma_{\max} \tilde{K}_{0,\max}^2,
\end{aligned} \tag{163}$$

in (160) gives (149). Note that proper selection of Γ and Γ_Δ gives $\gamma_{\max} - \lambda_{\min}\Theta_{\min}^2 \geq 0$. This completes the proof. □

Remark 6. *The proof of Theorem 3 showed the boundedness of $e_v(t)$, however it can not guarantee the boundedness of the tracking error $e(t)$. To prove the boundedness of $e(t)$, we must prove that $x(t)$ is bounded when the control inputs are constrained under rectangular saturation.*

We define $\Theta_{\max}^*$ and $\Theta_{\max}$ as

$$\begin{aligned}
&\Theta_{\max}^* := \sup||K^*(t)||_F, \\
&\Theta_{\max} := \max\left[\sup||\tilde{K}(t)||_F,\ \sup||\tilde{K}_\Delta(t)||_F\right].
\end{aligned} \tag{164}$$

Since we assumed the control gains belong to a known compact set, then $\Theta_{\max}^*$ and $\Theta_{\max}$ are positive and finite, hence there exists a smallest $n \in \mathbb{N}$ such that $\Theta_{\max}^* \leq n\Theta_{\max}$. Remember $\gamma_{\max} := \max\left[||\Gamma^{-1}||_F,\ ||\Gamma_\Delta^{-1}||_F\right]$, and note the following newly

defined constants

$$\rho := \sqrt{\frac{\lambda_{\max}(P)}{\lambda_{\min}(P)}}, \quad v_0 := \sqrt{\sum_{i=1}^{m} v_{i,\max}^2}, \\ v_{\min} := \min_i(v_{i,\max}), \quad v_{\max} := \max_i(v_{i,\max}), \tag{165}$$

where $v_{i,\max} > 0$ is the limit of the ith element of $v(t)$ and $Z_B \in \Re$ is defined using the induced norm by the vector 2-norm such that the property is described by

$$||x^{\mathsf{T}}(t)P[B,\ B_r]|| \leq Z_B||x(t)||. \tag{166}$$

We also define the following constants for simplicity

$$x_{\min} := \frac{Z_B(2v_0 + 2r_{\max})}{\lambda_{\min}(Q) - (3n+2)Z_B\Theta_{\max}}, \\ x_{\max} := \frac{Z_B v_{\min}}{|\lambda_{\min}(Q) - 2Z_B\Theta^*_{\max}|}, \\ Z_{\max} := \frac{\lambda_{\min}(Q) - Z_B\frac{\rho}{x_{\max}}(2v_0 + 2r_{\max})}{Z_B(3\frac{\rho}{x_{\max}} + 3n + 2)}. \tag{167}$$

In the next theorem, we extend the results from [66, 57] to prove the boundedness of the error signal $e(t)$ for gain scheduled model reference adaptive control systems with constrained control inputs.

Theorem 4. *Under Assumptions 2 and 3 for the system (136) with the controller (114) and the adaptive laws (143), $x(t)$ has a semi-globally bounded trajectory with respect to the control deficiency (137) for all $t > 0$ if*

$$\text{(i) } ||x(0)|| < \frac{x_{\max}}{\rho}, \\ \text{(ii) } \sqrt{V(0)} < \frac{Z_{\max}}{\sqrt{\gamma_{\max}}}. \tag{168}$$

Furthermore

$$||x(t)|| < x_{\max}, \quad \forall t > 0, \tag{169}$$

and error $e(t)$ is in the order of

$$||e(t)|| = \mathcal{O}[\sup_{\tau \leq t} ||\Delta v(\tau)||]. \tag{170}$$

Proof. We choose a positive definite function $W(x(t))$, as

$$W(x(t)) = x^{\mathsf{T}}(t)Px(t), \tag{171}$$

and define a level set $\mathcal{N}$ of $W(x(t))$ as

$$\mathcal{N} = \left\{x(t)|W(x(t)) = \lambda_{\min}(P)x_{\max}^2\right\}, \tag{172}$$

where $x_{\max}$ is defined in (165). We now define the region of attraction $\mathcal{M}$ as

$$\mathcal{M} = \left\{x_{\min} < ||x(t)|| < x_{\max}\right\}. \tag{173}$$

The following proceeds in two steps. First, we show that condition (ii) in (168) implies that $\mathcal{N} \subset \mathcal{M}$. Then we show that $\dot{W}(x(t)) < 0$ for all $x(t) \in \mathcal{M}$. Condition (i) in (168) implies that

$$W(x(0)) < W(\mathcal{N}). \tag{174}$$

Therefore the results of these two steps yield to

$$W(x(t)) < W(x(0)), \quad \forall t > 0, \tag{175}$$

and Theorem 4 follows directly. Figure 67 shows a schematic of the level set $\mathcal{N}$ and the region of attraction $\mathcal{M}$ in a 2-dimensional space.

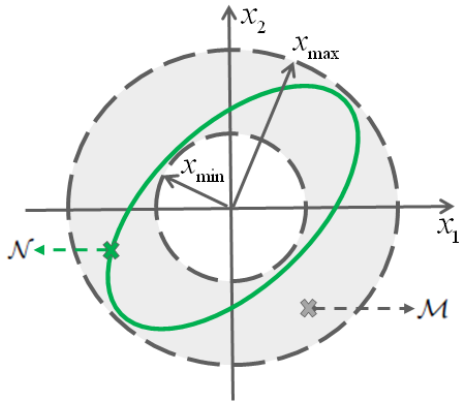

Figure 67: Depiction of level set $\mathcal{N}$ and region of attraction $\mathcal{M}$.

Here we show that $\mathcal{N} \subset \mathcal{M}$. From condition (ii), it follows that $\Theta_{\max} < Z_{\max}$. Substituting for $Z_{\max}$ yields

$$\frac{\rho}{x_{\max}} < \frac{\lambda_{\min}(Q) - (3n+2)Z_B\Theta_{\max}}{Z_B(2v_0 + 2r_{\max} + 3\Theta_{\max})}, \tag{176}$$

since by definition $x_{\max} > 0$ and also $\rho,\ v_0,\ r_{\max},\ \Theta_{\max}$, and $Z_{\max}$ are all positive, hence $(\lambda_{\min}(Q) - (2n+3)Z_B\Theta_{\max}) > 0$. Using the definition of $x_{\min}$ from equation (165) we obtain

$$x_{\min} < \frac{Z_B(2v_0 + 2r_{\max} + 3\Theta_{\max})}{\lambda_{\min}(Q) - (3n+2)Z_B\Theta_{\max}}, \tag{177}$$

Hence

$$\rho x_{\min} < x_{\max}. \tag{178}$$

In equation (171), $W(x)$ can be lower bounded by $\lambda_{\min}(P)||x(t)||^2 \leq W(x)$, which from equation (172) implies

$$||x(t)|| \leq x_{\max}, \quad \forall x(t) \in \mathcal{N}. \tag{179}$$

In a similar process from equation (173), $W(x(t))$ can be upper bounded by $W(x(t)) \leq \lambda_{\max}(P)||x(t)||^2$. From (172) and (178) we obtain

$$x_{\min} < \frac{1}{\rho}x_{\max} < ||x(t)||, \quad \forall t > 0. \tag{180}$$

From the definition of $\mathcal{N}$ and $\mathcal{M}$, we now have $\mathcal{N} \subset \mathcal{M}$.

Now we prove that $\dot{W}(.) < 0$ for all $x(t) \in \mathcal{M}$. The first case is when there is no saturation in the control inputs and the second case is when the control inputs are limited by a rectangular saturation function.

Case I: $\Delta v(t) = 0$

From Assumption 2, plant (139), and $\tilde{K}(t) = \hat{K}(t) - K^*(t)$, we obtain

$$\dot{x}(t) = A_m(\alpha(t))x(t) + B\tilde{K}^{\mathsf{T}}(t)x(t) - B_r r(t), \quad \forall \alpha \in \Omega, \tag{181}$$

which leads to

$$\dot{W}(.) = x^{\mathsf{T}}(t)(A_m^{\mathsf{T}}(\alpha(t))P + PA_m(\alpha(t)))x(t) + x^{\mathsf{T}}(t)(2PB\tilde{K}^{\mathsf{T}}(t))x(t) + 2x^{\mathsf{T}}(t)PB_r r(t). \tag{182}$$

By tacking bounds on the right hand side of (182), we obtain

$$\dot{W}(.) < (2Z_B\Theta_{\max} - \lambda_{\min}(Q))\,||x(t)||^2 + 2Z_B r_{\max}||x(t)||. \tag{183}$$

From condition (ii) and the definition of $\Theta_{\max}$, we obtain

$$\Theta_{\max} < Z_{\max} < \frac{\lambda_{\min}(Q)}{Z_B(3n+2)}. \tag{184}$$

Therefore

$$\dot{W}(.) < 0, \quad ||x(t)|| > \frac{2Z_B r_{\max}}{\lambda_{\min}(Q) - 2Z_B\Theta_{\max}}. \tag{185}$$

The choice of $x_{\min}$ in (165) leads to

$$x_{\min} > \frac{2Z_B r_{\max}}{\lambda_{\min}(Q) - 2Z_B\Theta_{\max}}. \tag{186}$$

Hence it is shown that in Case I

$$\dot{W}(.) < 0, \quad \forall x(t) \in \mathcal{M}. \tag{187}$$

Case II: $\Delta v(t) \neq 0$

For the case where $A(\alpha(t))$ is a Hurwitz for all $\alpha \in \Omega$, and consider the following Lyapunov function candidate for the system dynamics

$$W_A(x(t)) = x^{\mathsf{T}}(t)P_A x(t), \tag{188}$$

where $P_A = P_A^{\mathsf{T}} > 0$ solves the following inequality

$$A^{\mathsf{T}}(\alpha(t))P_A + P_A A(\alpha(t)) \leq -Q_A, \quad \forall \alpha \in \Omega, \tag{189}$$

for some positive definite $Q_A = Q_A^{\mathsf{T}} > 0$. Because $\Delta v(t) \neq 0$, then $R_s(v(t)) = \bar{v}(t)$ and the system dynamics in equation (136) becomes

$$\dot{x} = A(\alpha(t))x(t) + B\bar{v}(t) + B_r r(t), \quad \forall \alpha \in \Omega. \tag{190}$$

From the definition of v_0 in (165), we know $||\bar{v}(t)|| \leq v_0$. Consequently

$$\begin{aligned}\dot{W}_A(.) &= x^{\mathsf{T}}(A^{\mathsf{T}}(\alpha(t))P_A + P_A A(\alpha(t)))x(t) + 2x^{\mathsf{T}}(t)P_A B\bar{v}(t) + 2x^{\mathsf{T}}(t)P_A B_r r(t) \\ &\leq -\lambda_{\min}(Q_A)||x(t)||^2 + Z_B\,(2r_{\max} + 2v_0)\,||x(t)||.\end{aligned} \tag{191}$$

For open-loop stable systems, it immediately implies that

$$\dot{W}(.) < 0, \quad ||x(t)|| > \frac{Z_B \left(2r_{\max} + 2v_0\right)}{\lambda_{\min}(Q_A)}. \tag{192}$$

Therefore the system states remain bounded.

Next, for the case where $A(\alpha(t))$ is not Hurwitz, we write the dynamics in the following form

$$\begin{aligned} \dot{x}(t) &= A(\alpha(t))x(t) + BK^{*\mathsf{T}}(t)x(t) - BK^{*\mathsf{T}}(t)x(t) + B\bar{v}(t) + B_r r(t), \\ &= A_m(\alpha(t))x(t) - BK^{*\mathsf{T}}(t)x(t) + B\bar{v}(t) + B_r r(t), \quad \forall \alpha \in \Omega. \end{aligned} \tag{193}$$

Then

$$\dot{W}(.) \leq -x^{\mathsf{T}}(t)Qx(t) - 2x^{\mathsf{T}}(t)PBK^{*\mathsf{T}}(t)x(t) + 2x^{\mathsf{T}}(t)PB\bar{v}(t) + 2x^{\mathsf{T}}(t)PB_r r(t). \tag{194}$$

Now, the following two subcases are considered:

Case II.a: $2x^{\mathsf{T}}(t)PB\bar{v}(t) < -v_{\min}Z_B||x(t)||$

Using for this subcase and previously defined bounds, we can bound $\dot{W}(.)$ as

$$\dot{W}(.) < \left|\lambda_{\min}(Q) - 2Z_B\Theta^*_{\max}\right| ||x(t)||^2 + \left(2Z_B r_{\max} - Z_B v_{\min}\right)||x(t)||. \tag{195}$$

This implies that

$$\dot{W}(.) < 0, \quad ||x(t)|| \leq \frac{Z_B v_{\min} - 2Z_B r_{\max}}{\left|\lambda_{\min}(Q) - 2Z_B\Theta^*_{\max}\right|}. \tag{196}$$

From the definition of $x_{\max}$, we obtain

$$||x(t)|| \leq \frac{Z_B v_{\min} - 2Z_B r_{\max}}{\left|\lambda_{\min}(Q) - 2Z_B\Theta^*_{\max}\right|} < x_{\max}. \tag{197}$$

Hence we can conclude that

$$\dot{W}(.) < 0, \;\; \forall x(t) \in \mathcal{M} \text{ for sub-case II.a.} \tag{198}$$

Case II.b: $2x^{\mathsf{T}}PB\bar{v}(t) \geq -v_{\min}Z_B||x(t)||$

Complexities arise in the stability analysis because the rectangular saturation function

does not necessarily preserve the direction of the control inputs as they hit their limits. Therefore as defined in (103), $\bar{v}(t)$ is decomposed into $v_d(t)$ and $\tilde{v}(t)$ as

$$\bar{v}(t) = v_d(t) + \tilde{v}(t) = \frac{v(t)}{||v(t)||}||v_d(t)|| + \tilde{v}(t), \tag{199}$$

and $v_d(t)$ is chosen such that

$$||v_d(t)|| \geq \max\left[||\tilde{v}(t)||,\ v_{\min}\right], \tag{200}$$

as depicted in Figure 64. The decomposition can be constructed without loss of generality. The condition to this subcase implies that

$$2x^{\mathsf{T}}(t)PB\frac{v(t)}{||v(t)||}||v_d(t)|| + v_{\min}Z_B||x(t)|| + 2x^{\mathsf{T}}(t)PB\tilde{v}(t) \geq 0. \tag{201}$$

Multiplying $\frac{||v(t)||}{||v_d(t)||}$ in (201), we obtain

$$2x^{\mathsf{T}}(t)PBv(t) + v_{\min}Z_B||x(t)||\frac{||v(t)||}{||v_d(t)||} + 2x^{\mathsf{T}}(t)PB\tilde{v}(t)\frac{||v(t)||}{||v_d(t)||} \geq 0. \tag{202}$$

Since $v_d(t)$ in (199) is chosen such that $\frac{v_{\min}}{||v_d(t)||} < 1$ and $\frac{||\tilde{v}(t)||}{||v_d(t)||} < 1$ hold, we have

$$2x^{\mathsf{T}}(t)PBv(t) + 3Z_B||x(t)||||v(t)|| \geq 0. \tag{203}$$

Adding (194) to (203), we obtain

$$\begin{aligned}\dot{W}(.) \leq\ & -x^{\mathsf{T}}(t)Qx(t) + 2x^{\mathsf{T}}(t)PB\left(\hat{K}^{\mathsf{T}}(t) - K^{*\mathsf{T}}(t)\right)x(t) + 2x^{\mathsf{T}}(t)PB\bar{v}(t) \\ & + 2x^{\mathsf{T}}(t)PB_r r(t) + 3Z_B||x(t)||||v(t)||.\end{aligned} \tag{204}$$

Note that $||v(t)|| \leq \Theta^*_{\max}||x(t)|| \leq n\Theta_{\max}||x(t)||$, and $||\bar{v}(t)|| \leq v_0$, as a result we have

$$\dot{W}(.)\left((3n+2)Z_B\Theta_{\max} - \lambda_{\min}(Q)\right)||x(t)||^2 + Z_B\left(2v_0 + 2r_{\max}\right)||x(t)||. \tag{205}$$

From equation (184), we know $(3n+2)Z_B\Theta_{\max} - \lambda_{\min}(Q) < 0$, and then we have

$$\dot{W}(.) < 0, \quad ||x(t)|| > \frac{Z_B\left(2v_0 + 2r_{\max}\right)}{\lambda_{\min}(Q) - (3n+2)Z_B\Theta_{\max}} := x_{\min}. \tag{206}$$

From the definition of $x_{\min}$, we conclude that

$$\dot{W}(.) < 0, \quad \forall x(t) \in \mathcal{M} \text{ for sub-case II.b.} \tag{207}$$

As a direct consequence of (198) and (207), it follows that

$$\dot{W}(.) < 0, \quad \forall x(t) \in \mathcal{M}. \tag{208}$$

□

Remark 7. *Theorem 4 implies that if the initial conditions of the state and the parameter error lie within certain bounds, then the adaptive system will have bounded solutions. The local nature of the result for unstable systems is because of the saturation limits on the control input. For open-loop stable systems the results are global. The gas turbine engine model we are using for our simulations is an open-loop stable system, hence it is globally stable when we use saturated control inputs for the augmented plant.*

Remark 8. *As long as the limits of the control inputs are greater than zero (i.e., $v_{i,max} > 0$ for all i), Theorem 4 is valid. However, in practice, these control limits may not be able to be too close to zero, and there is a lower bound for each one of these control limits, in other words $v_{i,max} \geq \epsilon_i^v > 0$. For all i, the lower bounds ϵ_i^v can be found by simulation studies of the specific dynamical system of interest. In our example, where we control the turboshaft engine from idle to cruise, and vice versa, the simulation studies suggest the following approximate values for the lower bounds of the control limits: $\epsilon_1^v = 0.05$ and $\epsilon_1^v = 0.03$.*

4.3.4 Towards GS-MRAC Software Verification

Following the discussions presented in Section 3.3.3, we are considering the engine GS-MRAC case. In this case the stability of the closed-loop system (116) and (118) is analyzed using the Lyapunov function $V(e(t), \tilde{K}(t)) = e^{\mathsf{T}}(t)Pe(t) + \text{trace}\left(\tilde{K}(t)^{\mathsf{T}}\Gamma^{-1}\tilde{K}(t)\right)$, where P satisfies (71), and Γ^{-1} is a symmetric positive definite matrix. Consider $\zeta := [e^{\mathsf{T}}, (\text{vec}\tilde{K})^{\mathsf{T}}]^{\mathsf{T}}$, and $\bar{P} := \text{diag}([P,\ \Gamma^{-1}])$, where P and Γ^{-1} are block diagonal elements in matrix $\bar{P}$. Now since we are using a Γ-projection operator to update the

control gains, hence $\tilde{K}(t)$ belongs to a priori known compact set. As a result, one invariant ellipsoid which possibly can be used in the GS-MRAC software verification process is

$$\mathcal{E} = \left\{ \zeta \in \Re^{(1+m)l} | \zeta^{\mathsf{T}} \bar{P} \zeta \leq 1 \right\}. \tag{209}$$

Now considering the engine GS-MRAC case with constrained control inputs, we have to guarantee the stability of the closed-loop system (142) and (144) in addition to the boundedness of states in system (109). The boundedness of signals $(e_v(t), \tilde{K}(t), \tilde{K}_\Delta(t))$ are analyzed using the Lyapunov function $V(e_v(t), \tilde{K}(t), \tilde{K}_\Delta(t)) = e_v^{\mathsf{T}}(t) P e_v(t) + \text{trace}\left(\tilde{K}(t)^{\mathsf{T}} \Gamma^{-1} \tilde{K}(t)\right) + \text{trace}\left(\tilde{K}_\Delta(t) \Gamma_\Delta^{-1} \tilde{K}_\Delta^{\mathsf{T}}(t)\right)$, and the boundedness of $x(t)$ is guaranteed by $W(x(t)) = x^{\mathsf{T}}(t) P x(t)$, where P satisfies (71), and both Γ^{-1}, and Γ_Δ^{-1} are symmetric positive definite matrices. Now consider $\zeta_s := [x^{\mathsf{T}},\ e^{\mathsf{T}},\ (\text{vec}\tilde{K})^{\mathsf{T}},\ (\text{vec}\tilde{K}_\Delta^{\mathsf{T}})^{\mathsf{T}}]^{\mathsf{T}}$, and $\bar{P}_s := \text{diag}([P,\ P,\ \Gamma^{-1},\ \Gamma_\Delta^{-1}])$, where P, Γ^{-1} and Γ_Δ^{-1} are block diagonal elements in matrix $\bar{P}_s$. Now since we are using a Γ-projection operator to update the control gains, $\tilde{K}(t)$ belongs to a priori known compact set. As a result, one invariant ellipsoid which possibly can be used for the software verification process of GS-MRAC with constrained control inputs, can be constructed as

$$\mathcal{E}_s = \left\{ \zeta_s \in \Re^{2l(1+m)} | \zeta_s^{\mathsf{T}} \bar{P}_s \zeta_s \leq 1 \right\}. \tag{210}$$

By developing a detailed Lyapunov stability analysis for GS-MRAC and GS-MRAC with constrained control inputs, we fulfilled the fist steps towards a verifiable GS-MRAC system for gas turbine systems. Hopefully this can be used for an analytical GS-MRAC software verification process. The complete theoretical GS-MRAC software verification is beyond the scope of this dissertation and it remains a topic for future research.

Table 5: Degradation values for engine health parameters as a change from nominal values

Case	Degradation Level	High Pressure Compressor		High Pressure Turbine		Low Pressure Turbine	
		$\eta^{\dagger}$ %	Wc^{*} %	η %	Wc %	η %	Wc %
Nominal Engine (NomEng)	None	0	0	0	0	0	0
Aged Engine Case-1 (AgedEng-C1)	Moderate	-1.47	-1.955	-1.315	0.88	-0.269	0.1294
Aged Engine Case-2 (AgedEng-C2)	Harsh	-2.94	-3.91	-2.63	1.76	-0.538	0.2588

† η= Efficiency $^{*}Wc$= Flow Capacity

4.4 Turboshaft Engine Example

The effect of engine degradation due to aging is modeled in the nonlinear simulation by modifying the efficiencies and flow capacities of key engine components such as: high pressure compressor, high pressure turbine, and low pressure turbine. These efficiency and flow capacity parameters are known as engine health parameters, and the values of these parameters are used in this simulation corresponding to moderate degradation (AgedEng-C1) and harsh degradation (AgedEng-C2) of operation are shown in Table 5. The numerical values are a percentage deviation from nominal, where a nominal engine is at 100% for each of the parameters. Performance deterioration data on civil aircraft turbine engines can be found in [138, 23]. The degraded health parameter values of these two cases were introduced in the nonlinear simulation to evaluate degradation effects on engine and the adaptive controller performance.

4.4.1 Equilibrium Manifold

For a standard day at sea level condition we chose five properly separated equilibrium points on the nominal plant equilibrium manifold for linearizing the plant model at those points. The linearization matrices for these five equilibrium points and steady state values of the engine variables, the control parameters, and the scheduling parameter are given as follows:

- Equilibrium Point 1 (Full Thrust):

$u_{1e1} = 1.0$, $u_{2e1} = 16$ (deg), $x_{1e1} = 1.0$, $x_{2e1} = 0.9524$, $T_{e1} = 255.8685$ (N), $\alpha_1 = 1.3810$, and the matrices are

$$A_1^p = \begin{bmatrix} -5 & 0 \\ 3.5 & -2.3 \end{bmatrix}, \; B_1^p = \begin{bmatrix} 1.5 & 0 \\ 0.63 & -0.085 \end{bmatrix}, \\ C_1^p = I, \; , \; Ki_1 = \begin{bmatrix} -0.6 & -0.6 \\ -0.6 & -0.6 \end{bmatrix}. \tag{211}$$

- Equilibrium Point 2:

  $u_{1e2} = 0.7$, $u_{2e2} = 16$ (deg), $x_{1e2} = 0.9041$, $x_{2e2} = 0.6557$, $T_{e2} = 121.2905$ (N), $\alpha_2 = 1.1168$, and

$$A_2^p = \begin{bmatrix} -2.8 & 0.2 \\ 2 & -1.7 \end{bmatrix}, \; B_2^p = \begin{bmatrix} 1.42 & 0 \\ 0.3768 & -0.05 \end{bmatrix}, \\ C_2^p = I, \; Ki_2 = \begin{bmatrix} -0.5 & -0.5 \\ -0.5 & -0.5 \end{bmatrix}. \tag{212}$$

- Equilibrium Point 3 (Cruise):

  $u_{1e3} = 0.4685$, $u_{2e3} = 16$ (deg), $x_{1e3} = 0.7264$, $x_{2e3} = 0.5$, $T_{e3} = 70.5125$ (N), $\alpha_3 = 0.8818$, and

$$A_3^p = \begin{bmatrix} -1.7 & 0.1 \\ 0.6 & -1.1 \end{bmatrix}, \; B_3^p = \begin{bmatrix} 1.2 & 0 \\ 0.3 & -0.023 \end{bmatrix}, \\ C_3^p = I, \; Ki_3 = \begin{bmatrix} -0.4 & -0.4 \\ -0.4 & -0.4 \end{bmatrix}. \tag{213}$$

- Equilibrium Point 4:

  $u_{1e4} = 0.3$, $u_{2e4} = 16$ (deg), $x_{1e4} = 0.5327$, $x_{2e4} = 0.3678$, $T_{e4} = 38.155$ (N), $\alpha_4 =$

0.6473, and

$$A_4^p = \begin{bmatrix} -0.85 & 0.032 \\ 0.32 & -0.64 \end{bmatrix},\ B_4^p = \begin{bmatrix} 1.0 & 0 \\ 0.17 & -0.011 \end{bmatrix},$$
$$C_4^p = I,\ Ki_4 = \begin{bmatrix} -0.3 & -0.3 \\ -0.3 & -0.3 \end{bmatrix}. \tag{214}$$

- Equilibrium Point 5 (Idle):

  $u_{1e5} = 0.145,\ u_{2e5} = 16\ (\text{deg}),\ x_{1e5} = 0.295,\ x_{2e5} = 0.161,\ T_{e5} = 7.317\ (\text{N}),\ \alpha_5 = 0.3361$, and the matrices are

$$A_5^p = \begin{bmatrix} -0.38 & -0.0008 \\ 0.26 & -0.34 \end{bmatrix},\ B_5^p = \begin{bmatrix} 0.7 & 0 \\ 0.1 & -0.0024 \end{bmatrix},$$
$$C_5^p = I,\ Ki_5 = \begin{bmatrix} -0.2 & -0.2 \\ -0.2 & -0.2 \end{bmatrix}. \tag{215}$$

Other controller parameters are $\epsilon_c = 1,\ \eta_c = 3$. The elements of control matrix $K_i(\alpha(t))$ have been shown as functions of scheduling parameter $\alpha(t)$ in Figure 68. Piecewise linear interpolation has been used to interpolate $K_i(\alpha(t))$ using the predesigned indexed linear controllers, which are given in equations (211) to (215).

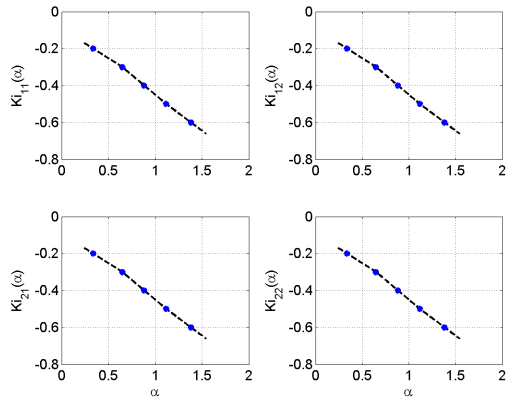

Figure 68: $K_i(\alpha(t))$ components as functions of scheduling parameter $\alpha(t)$.

To show the stability of the closed loop reference system, 40 different (30 equilibrium, and 10 non-equilibrium) linearizations have been used, to solve inequality (68)

in Matlab with the aid of YALMIP [86] and SeDuMi [164] packages. The numerical value for the common matrix P is

$$P = \begin{bmatrix} 0.4911 & 0.0794 & 0.1019 & -0.0039 & -0.0720 & -0.0390 \\ 0.0794 & 0.4465 & 0.0535 & 0.0066 & -0.0968 & -0.0130 \\ 0.1019 & 0.0535 & 0.1814 & -0.0411 & -0.0282 & -0.0219 \\ -0.0039 & 0.0066 & -0.0411 & 0.1299 & 0.0232 & 0.0126 \\ -0.0720 & -0.0968 & -0.0282 & 0.0232 & 0.3215 & 0.0447 \\ -0.0390 & -0.0130 & -0.0219 & 0.0126 & 0.0447 & 0.3318 \end{bmatrix}, \quad (216)$$

where its condition number is $\kappa(P) = 6.6303$ and $Q = 0.1 \times I_6$. Figure 69 shows the JetCat SPT5 turboshaft engine compressor map. In this map the approximate stall line and also the operating line for this simulation have been shown. The engine operates in a safe region with a big stall margin during its acceleration from idle to cruise and again during its deceleration back to the idle condition. The 40 points which are used for linearization and stability analysis of the closed-loop system also have been shown in this figure. Thirty of these points are related to the equilibrium linearizations which are situated on the steady-state operating line of the engine, and the other 10 points are related to the non-equilibrium linearizations which are situated near the steady-state operating line of the engine. This P matrix is slightly different than the one we computed in the previous chapter, since here we closed the loop of the the gain scheduled reference model using only an integral (I) control input, while in Chapter 3, the controller was proportional-integral (PI).

The engine operating lines for the nominal engine and two cases of degraded engine model are shown in this figure. As it is expected, as degradation increases in the engine, the stall margin decreases, the pressure ratio decreases and the turbine temperature increases.

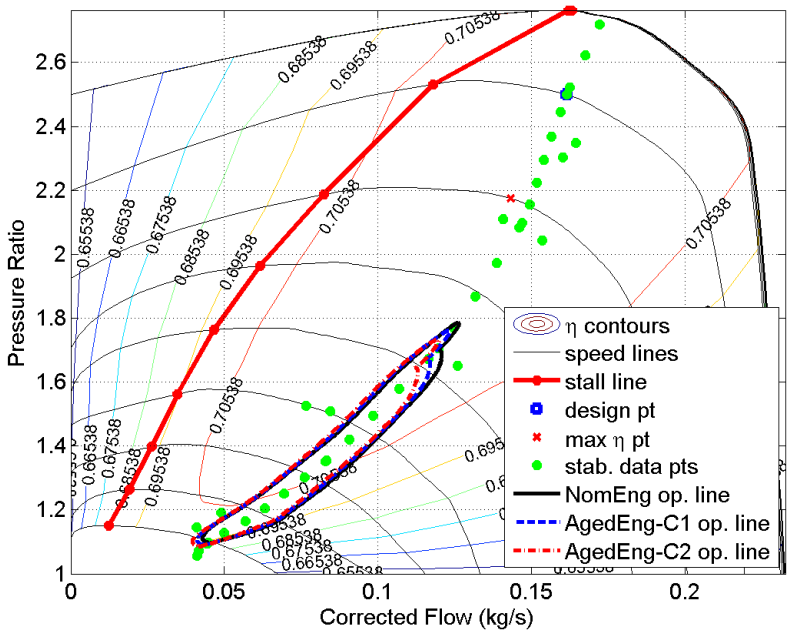

Figure 69: JetCat SPT5 engine compressor map with data points used to compute P and operating line for nominal engine, and deteriorated engine.

4.4.2 Simulation Results

The numerical values for the adaptive controller are set as follows:

$$\Gamma = \text{diag}([50,\ 50,\ 50,\ 50,\ 50,\ 50]),\quad \Gamma_\Delta = \text{diag}([30,\ 30]),$$

$$v_{1,\max} = 0.12,\ v_{2,\max} = 0.15,$$

$$\Theta_{K_i} = \begin{bmatrix} [\text{-}2, & 0] & [\text{-}2, & 0] \\ [\text{-}2, & 0] & [\text{-}2, & 0] \end{bmatrix},$$

$$\Theta_\Delta = \begin{bmatrix} \{0\} & \{0\} & [0,\ 10] & \{0\} & \{0\} & \{0\} \\ \{0\} & \{0\} & \{0\} & [0,\ 10] & \{0\} & \{0\} \end{bmatrix}^\mathsf{T}, \tag{217}$$

$$\hat{K}_i(0) = \begin{bmatrix} -0.1950 & -0.1950 \\ -0.1970 & -0.1970 \end{bmatrix},$$

$$\hat{K}_\Delta(0) = \begin{bmatrix} 0 & 0 & 2.7 & 0 & 0 & 0 \\ 0 & 0 & 0 & 2.7 & 0 & 0 \end{bmatrix}^\mathsf{T}.$$

$v_{1,\max}$ and $v_{2,\max}$ are defined in such a way so we can have $0.12 \leq u_1 \leq 0.55$, $0.12 \leq N_1 \leq 0.55$, $0.26 \leq N_2 \leq 0.78$, $-0.08 \leq \dot{N}_1 \leq 0.08$, and $-0.10 \leq \dot{N}_2 \leq 0.10$. Three different simulations are performed for 3 different cases including the control of the nominal model (NomEng) and the control of the two cases of deteriorated engines (AgedEng-C1 and AgedEng-C2). These case studies simulate the engine acceleration from the idle thrust to the cruise condition and then its deceleration back to the idle condition in a stable manner, with proper tracking performance for the standard day sea level condition. Simulation results are shown in Figures 70 to 85.

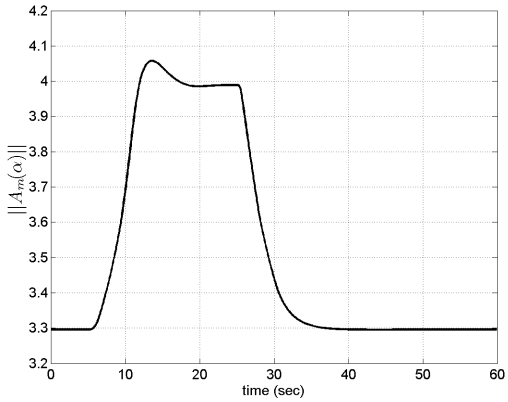

Figure 70: Norm of reference model matrix ($||A_m(\alpha(t))||$).

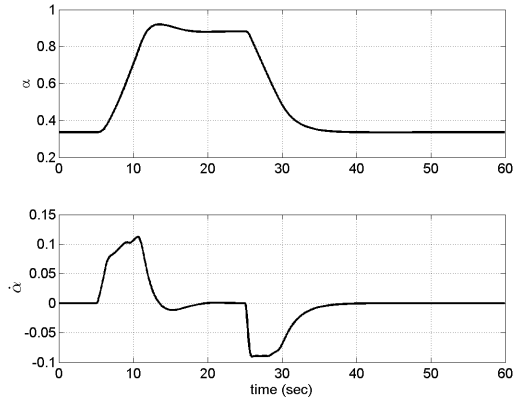

Figure 71: Scheduling parameter ($\alpha = ||x^p(t)||$) and its rate of change ($\dot{\alpha}(t)$) for the nominal engine case.

Figure 70 shows the history of the norm of the desired reference system matrix

$||A_m(\alpha(t))||$. As it can be seen, the figure shows the boundedness of these two matrices in accordance with Assumption 1, where $k_A = 4.1023$.

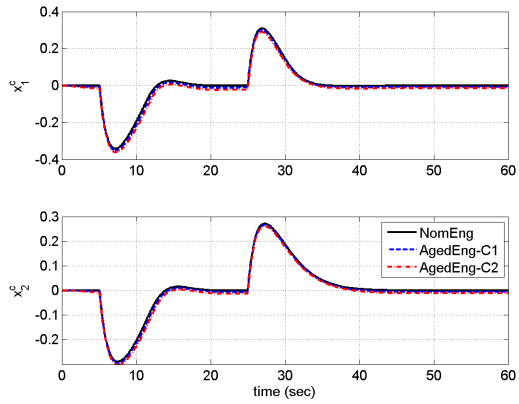

Figure 72: Controller states ($x^c(t)$).

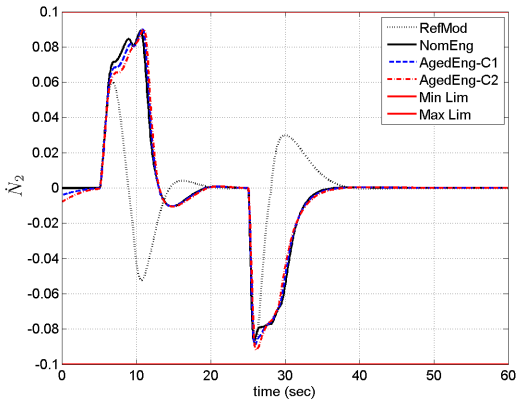

Figure 73: High pressure spool acceleration.

Figure 71 shows the history of the scheduling parameter $\alpha(t) = p(y(t)) = ||y(t)|| = ||x^p(t)||$; it is defined as the Euclidean norm of the engine spool speeds. The scheduling parameter rate $\dot{\alpha}(t) = \frac{x^{p\mathsf{T}}(t)\dot{x}^p(t)}{||x^p(t)||}$ also has been plotted. Figure 72 shows the controller states, $x^c(t)$.

Figures 73 and 74 show core and fan spool acceleration histories. Figures 77 and 78 show the outputs (i.e., core and fan spool speeds), tracking their reference signals for three cases.

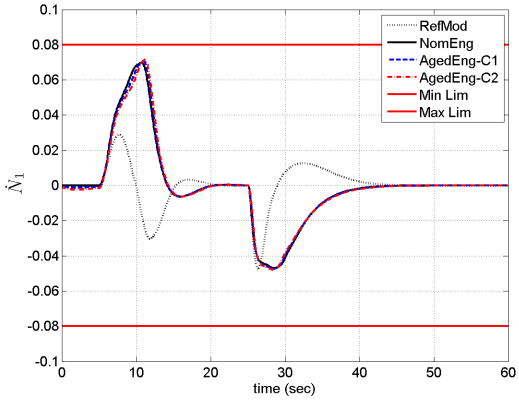

Figure 74: Low pressure spool acceleration.

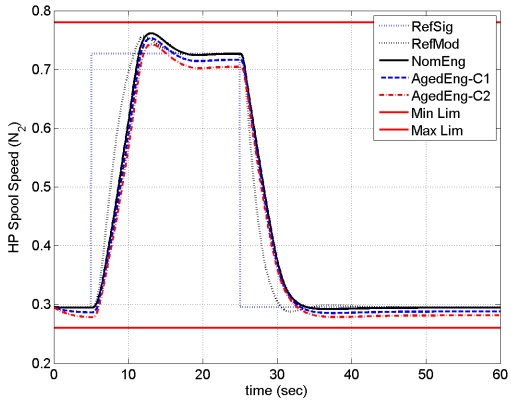

Figure 75: High pressure spool speed and its reference signal.

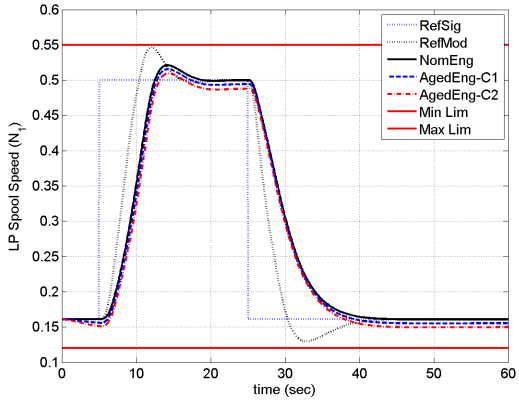

Figure 76: Low pressure spool speed and its reference signal.

Figure 77 shows the history of thrust and it is following its reference command from idle to cruise condition and then back to the idle for standard day, sea level condition.

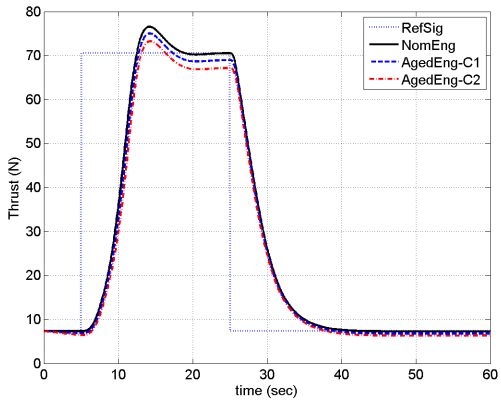

Figure 77: Thrust and its reference signal.

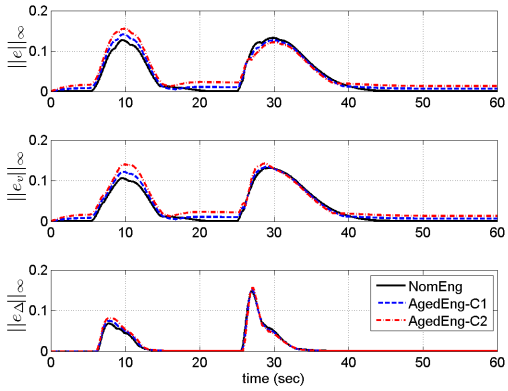

Figure 78: Norm of the error signals $||e(t)||_\infty$, $||e_v(t)||_\infty$, $||e_\Delta(t)||_\infty$.

Figure 78 shows the evolution of the infinity norm of the errors $||e(t)||_\infty$, $||e_v(t)||_\infty$, $||e_\Delta(t)||_\infty$. The steady-state errors in the aged engine (AgedEng-C1, AgedEng-C2) simulation cases are because of the effect of the aging on the engine health parameters, and this causes a change in the equilibrium manifold of the aged engine in comparison to the nominal engine (NomEng). In other words, since we are using the nominal engine equilibrium manifold to design a linear parameter dependent reference model, and the aged engine linear model has a different equilibrium manifold $x_{e,nom}(\alpha(t)) \neq x_{e,ag}(\alpha(t))$, then $\delta x_{ag}(t) = x_{ag}(t) - x^p_{e,ag}(\alpha(t)) \neq 0$, and this means $||\delta x_{ag}(t)|| > \delta x_{\min} \neq 0$ for all $t > 0$. Hence, there will be a greater than zero steady-state error values for $e_v(t)$ and $e(t)$. This issue has been explained in Remark 5.

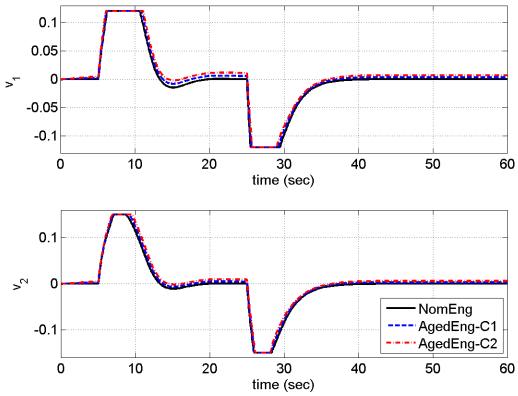

Figure 79: Control inputs to the augmented system ($v(t)$).

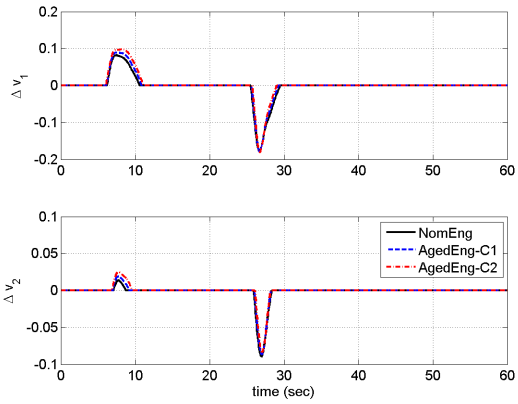

Figure 80: Deficiency of the control inputs to the augmented system ($\Delta v(t)$).

Figure 79 shows the evolution of the control inputs $v(t) = [v_1(t), v_2(t)]^T$, which are inputs to the augmented system; each element is corresponding to one of the control inputs to the original system. Figure 80 shows the evolution of the control deficiencies ($\Delta v(t)$) in presence of the saturation. For better performance and also to keep the engine in the safe range of operation, hard limits have been defined for both augmented control inputs, $|v_i| \leq v_{i,\max}$ for $i = 1, 2$. These limits will keep the fuel control input non-negative and also bounds the time rate of the control inputs, i.e. the rate of change of fuel control input $\dot{u}_1(t)$, and prop pitch angle $\dot{u}_2(t)$.

Figure 81 shows time rates of fuel and prop pitch angle inputs. Figure 82 shows the histories of fuel flow and propeller pitch angle as the control inputs to the plant.

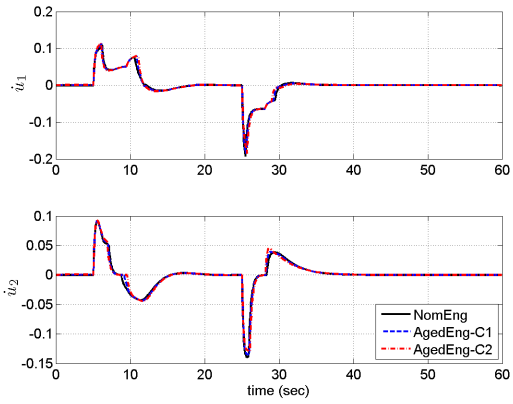

Figure 81: Rate of change for fuel and prop pitch angle control inputs ($\dot{u}(t)$).

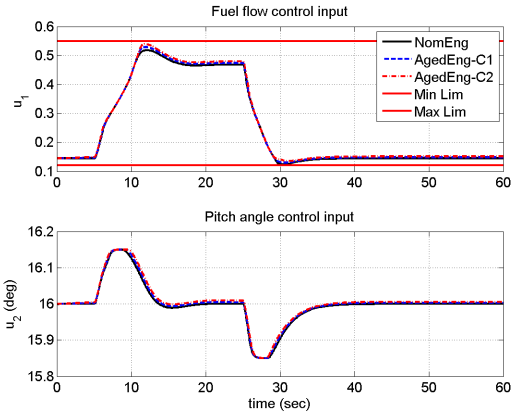

Figure 82: Fuel and prop pitch angle control inputs ($u(t)$).

Figure 83 shows the evolution of the gain scheduled controller integral gain matrix ($K_i(\alpha(t))$) and also adaptive controller gain matrix ($\hat{K}_i(t)$).

$K_i(\alpha)$ elements have been obtained by interpolation using the predesigned indexed family of fixed-gain controllers, and each controller corresponds to one equilibrium point of the engine. The numerical values of these gains are given in (213) to (215), which represent the controller gains for idle and cruise condition and one more equilibrium point in between these two operating points. $\hat{K}_i(t)$ is generated using an adaptive law. Figure 84 shows the evolution of the nonzero elements of the augmented adaptive parameter for the saturated system ($\hat{K}_\Delta(t)$). Figure 85 shows the histories of turbine temperature, thrust specific fuel consumption (TSFC), compressor

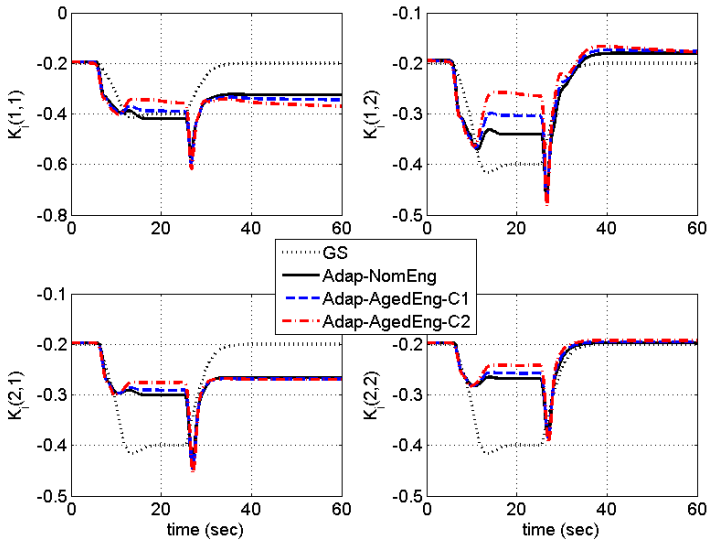

Figure 83: Integral gain matrix elements for the gain scheduled controller ($K_i(\alpha(t))$), and for the adaptive controller ($\hat{K}_i(t)$).

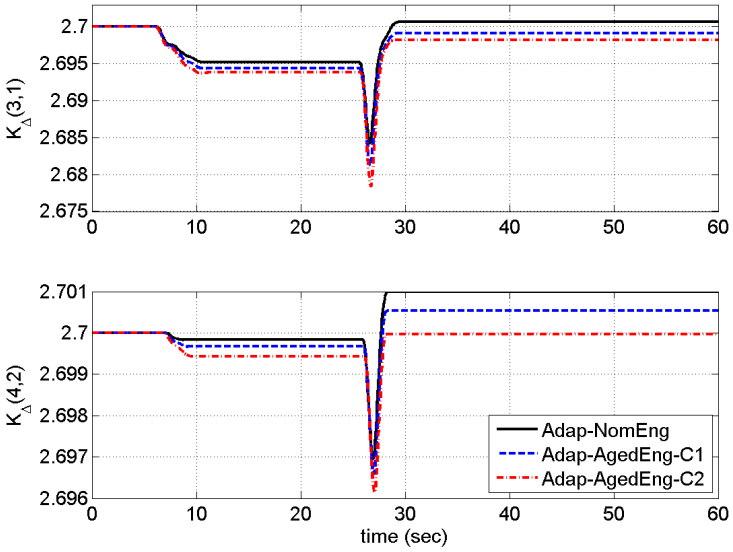

Figure 84: Nonzero elements of the augmented adaptive parameter for the saturated system ($\hat{K}_\Delta(t)$).

pressure ratio, and corrected air flow rate.

These simulations show the successful control of a MIMO turboshaft engine model for large thrust commands, with constraints on the magnitudes of the control inputs using GS-MRAC. These case studies simulate the engine acceleration from idle thrust

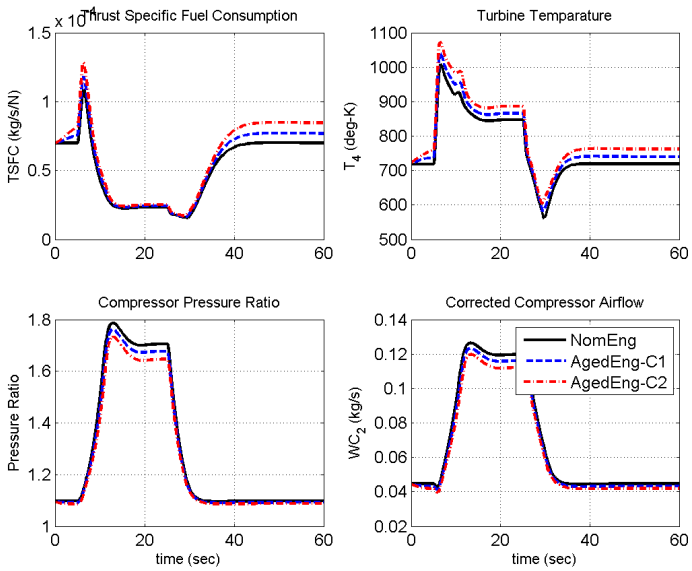

Figure 85: Turbine temperature, TSFC, compressor overall pressure ratio, and air flow rate histories.

to the cruise condition and then its deceleration back to the idle condition in the standard day, sea level condition for the nominal engine model and two different aged (deteriorated) engine model. As it can be observed all the signals are bounded. Clearly a degraded engine won't be able to match the performance of a new engine, but using adaptive control we can maintain critical parameters at acceptable levels for as much degradation as possible.

4.4.3 Engine Limit Control Discussion

Other than imposing hard constraints on the magnitudes of the control inputs, in order to handle the turbine engine system performance limits, the developed gain scheduled model reference adaptive control (GS-MRAC) system can be integrated with a reference governor. Reference governors have been developed previously; a good example of this approach is presented in [18]. Detailed development of the GS-MRAC system integrated with a reference governor is a topic for future research.

4.5 Summary

GS-MRAC rigorous stability analysis was done by proving the boundedness of the error signal, in addition to transient and steady-state performance guarantees. Then the results extended to the GS-MRAC system with constraints on the magnitudes of multi control inputs. Sufficient conditions for ultimate boundedness of the closed-loop system were derived. A semi-global stability result was proved with respect to the level of saturation for open-loop unstable plants, while the stability result becomes global for open-loop stable plants. Through the simulation based on a physics-based nonlinear model of a JetCat SPT5 turboshaft engine with severe degradation due to aging, it was demonstrated that even in the presence of the control magnitude saturation, the proposed adaptive controller tracks the reference model with guaranteed stability and proper tracking performance. The developed GS-MRAC is not only limited to control degraded gas turbine engines, but also can be used for other practical applications.

CHAPTER V

PLUG AND PLAY TECHNOLOGY CONCEPT FOR GAS TURBINE ENGINE CONTROL SYSTEM

5.1 Introduction

During the past twenty years there has been a growing interest in decentralized adaptive control. The problem deals with a system composed of N subsystems S_k, each of whose inputs is chosen by N controllers C_k, where $k = 1, 2, ..., N$. The parameters of the subsystems are assumed to be unknown, and the controllers have to generate their inputs adaptively, using all information available to them to achieve some desired objectives. Some of the works have been done on decentralized adaptive control can be found in [24, 40, 50, 52, 55, 101, 106, 107, 111, 153, 154, 155, 162, 175, 178].

Previous works on gas turbine engine control have not taken advantage of recent progress in adaptive control algorithms. An adaptive controller requires little or no a priori information about the unknown parameters and improves its performance as it adapts. One of the advantages of developing adaptive controllers for gas turbine systems is that adaptive control algorithm enables plug and play technology development for gas turbine engine control systems when there is a need to match different engine cores with different engine fans/props.

Here, we develop a decentralized version of gain scheduled model reference adaptive control which is applicable to the turboshaft engine deriving a variable pitch propeller. This decentralized control algorithm can be used for the entire flight envelope of the engine. With this control architecture, the two subsystems of the engine (i.e., engine core and engine fan/prop) can be controlled for large throttle commands using their own separate controllers.

To determine the feasibility of a decentralized adaptive gas turbine engine control approach, a systematic evaluation of the stability and performance characteristics is needed, instead of just individual sensors and actuators; that is, decentralized computing should be used at the local level and only coordinated by the Full Authority Digital Engine Control (FADEC). The impact of varying operating conditions on the performance at the global level of the hierarchical control system must be addressed.

Decentralized control architecture is an appealing configuration; in this structure there are local controllers with some authority but the entire engine system is still governed by a central supervisory controller. Decentralized control has many of the benefits of regular control structure but retains a central supervisor to communicate with the operator and handle some system level tasks such as engine startup. Decentralized control architecture enables a new engine development paradigm infeasible with regular control schemes.

An example of decentralized control architecture using multiple sensors and actuators for gas turbine engines is schematically represented in Figure 86. In this control architecture, three different sets of sensors are used for pressure, temperature, and speed measurements; and three types of actuators are used for fuel flow, fan/prop blade angle, and fan exit area actuation. Two control loops are used to control the engine core and the engine fan/prop. The engine core subsystem loop is closed by the high pressure spool speed measurement and the engine fan/prop subsystem loop is closed by the low pressure spool speed measurement. The reference signals are coming from a supervisory FADEC. In this decentralized control scheme, the independent controllers on the engine core and fan/prop are linked by the supervisory controller. This scheme is representative of the situation encountered in vertical takeoff and landing (VTOL) unmanned aerial vehicle (UAV) design and the design of new turboshafts/turboprops and variable pitch turbofans by the large commercial gas turbine manufacturers.

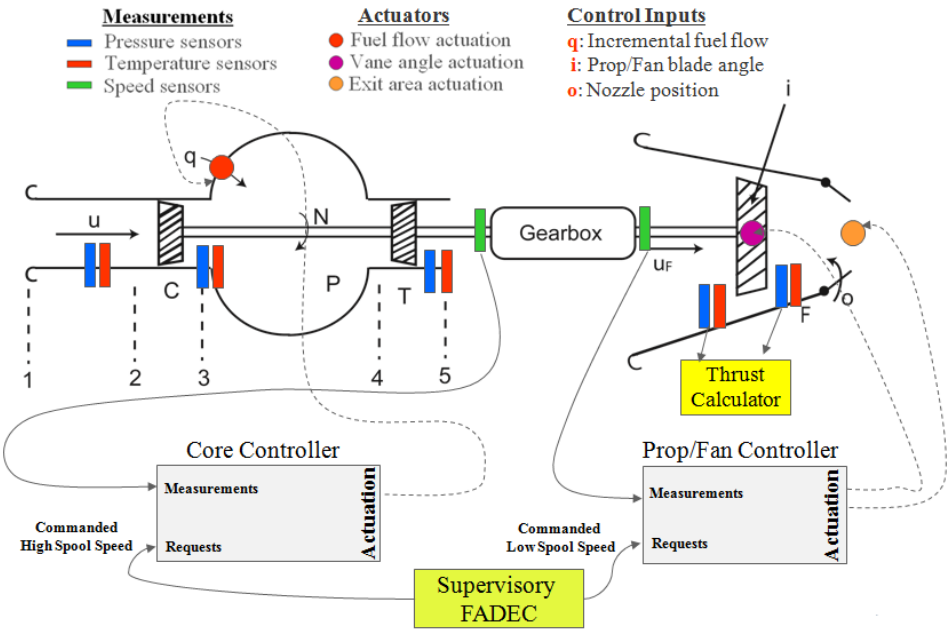

Figure 86: Example of decentralized control architecture for gas turbine engines.

In this chapter, we develop control theoretic concepts for decentralized gain scheduled model reference adaptive control (D-GS-MRAC) using the developments from Chapters 3 and 4. The results developed in Chapters 3 and 4 also can be found in [115, 116]. With this decentralized control architecture, the two subsystems of the engine (i.e., engine core and engine fan) can be controlled separately for large throttle commands. The chapter is organized as follows: First, we present the decentralized parameter dependent model for the plant. Second, we develop a decentralized gain scheduled model reference adaptive control architecture. Third, uniform ultimate boundedness of the error signals for all the subsystems of the developed decentralized system is proven. Finally, using the developed D-GS-MRAC architecture, a plug and play concept for gas turbine engine control systems is explained and tested by simulating multiple scenarios, in which various engine cores are matched with various engine props.

5.2 Decentralized Linear Parameter Dependent Modeling

Here we present a decentralized representation of the plant (40) described in Chapter 3. Each one of the subsystems is modeled to be single input, single output (SISO). Each subsystem with its filtered input can be described as

$$\begin{aligned} \begin{bmatrix} \dot{x}_k^p(t) \\ \dot{u}_k(t) \end{bmatrix} &= \begin{bmatrix} f_k^p(x^p(t), u(t)) \\ -\eta_c u_k(t) \end{bmatrix} + \begin{bmatrix} 0 \\ \eta_c \end{bmatrix} v_k(t), \\ y_k(t) &= g_k^p(x_k^p(t), u_k(t)). \end{aligned} \tag{218}$$

The controller for each subsystem has the general form

$$\begin{aligned} \dot{x}_k^c(t) &= f_k^c(x_k^c(t), y_k(t), r_k(t)), \\ v_k(t) &= g_k^c(x_k^c(t), y_k(t), r_k(t)), \end{aligned} \tag{219}$$

with the input and output signals corresponding to those of the nonlinear subsystem (218). Now, combining (218) and (219) leads to

$$\begin{aligned} \underbrace{\begin{bmatrix} \dot{x}_k^p(t) \\ \dot{u}_k(t) \\ \dot{x}_k^c(t) \end{bmatrix}}_{\dot{x}_k} &= \underbrace{\begin{bmatrix} f_k^p(x^p(t), u(t)) \\ -\eta_c u_k(t) \\ f_k^c(x_k^c(t), g_k^p(x_k^p(t), u_k(t)), r_k(t)) \end{bmatrix}}_{f_k(x_k(t), x_q(t), r_k(t))} + \underbrace{\begin{bmatrix} 0 \\ \eta_c \\ 0 \end{bmatrix}}_{b_k} v_k(t), \\ v_k(t) &= \underbrace{g_k^c(x_k^c(t), g_k^p(x_k^p(t), u_k(t)), r_k(t))}_{g_k(x_k(t), r_k(t))}, \end{aligned} \tag{220}$$

and the closed-loop nonlinear subsystem is

$$\begin{aligned} \dot{x}_k(t) &= f_k(x_k(t), x_q(t), r_k(t)) + b_k g_k(x_k(t), r_k(t)), \\ &= F_k(x_k(t), x_q(t), r_k(t)), \end{aligned} \tag{221}$$

where $x_k(t) \in D_{x_k} \subset \Re^{n_k+2}$, and $r_k(t) \in D_{r_k} \subset \Re$, and $x_q(t) \in D_{x_q}$ includes all the states from the other subsystems interconnecting with the kth subsystem.

Now, similar to controller (50), the parameter dependent controller for each subsystem is defined as

$$\begin{bmatrix} \dot{x}_k^c(t) \\ v_k(t) \end{bmatrix} = \begin{bmatrix} -\epsilon_c & 1 & -1 \\ k_{i,k}(\alpha(t)) & 0 & 0 \end{bmatrix} \begin{bmatrix} x_k^c(t) \\ \delta y_k(t) \\ \delta r_k(t) \end{bmatrix}, \quad \forall \alpha \in \Omega. \tag{222}$$

We use the *piecewise linear* interpolation method, which linearly interpolates controllers between each pair of controllers from the indexed collection of the pre-designed controllers for each subsystem.

Linearizing the nonlinear terms $f_k(.)$, $g_k(.)$, and $g_k^p(.)$ in (218) and (220) around the equilibrium manifold $(x_{e,k}(\alpha(t)), x_{e,q}(\alpha(t)), r_{e,k}(\alpha(t)))$ for all $\alpha \in \Omega$, produces the following matrices

$$\begin{aligned} A_k(\alpha(t)) &= \frac{\partial f_k(.)}{\partial x_k(t)}|_{(x_{e,k}(\alpha(t)), x_{e,q}(\alpha(t)), r_{e,k}(\alpha(t)))}, \\ A_{kq}(\alpha(t)) &= \frac{\partial f_k(.)}{\partial x_q(t)}|_{(x_{e,k}(\alpha(t)), x_{e,q}(\alpha(t)), r_{e,k}(\alpha(t)))}, \\ b_{r_k}(\alpha(t)) &= \frac{\partial f_k(.)}{\partial r_k(t)}|_{(x_{e,k}(\alpha(t)), x_{e,q}(\alpha(t)), r_{e,k}(\alpha(t)))}, \quad \forall \alpha \in \Omega, \\ C_k(\alpha(t)) &= \frac{\partial g_k^p(.)}{\partial x_k(t)}|_{x_{e,k}(\alpha(t))}, \\ K_k(\alpha(t)) &= \frac{\partial g_k(.)}{\partial x_k(t)}|_{(x_{e,k}(\alpha(t)), r_{e,k}(\alpha(t)))}, \\ k_{r_k}(\alpha(t)) &= \frac{\partial g_k(.)}{\partial r_k(t)}|_{(x_{e,k}(\alpha(t)), r_{e,k}(\alpha(t)))}. \end{aligned} \tag{223}$$

Then, the linear family of systems for the augmented subsystem (218) becomes

$$\begin{aligned} \delta \dot{x}_k(t) &= A_k(\alpha(t))\delta x_k(t) + b_k v_k(t) + b_{r_k}(\alpha(t))\delta r_k(t) \\ &\quad + \underbrace{\sum_{q=1, q\neq k}^{N} [A_{kq}(\alpha(t))\delta x_q(t)]}_{h_k(\delta x_q(t), \alpha(t))}, \quad \forall \alpha \in \Omega, \\ \delta y_k(t) &= C_k(\alpha(t))\delta x_k(t), \end{aligned} \tag{224}$$

with the state feedback controller

$$v_k(t) = K_k^{\mathsf{T}}(\alpha(t))\delta x_k(t) + k_{r_k}(\alpha(t))\delta r_k(t), \quad \forall \alpha \in \Omega, \tag{225}$$

where $\delta x_k(0) = \delta x_{0_k}$, and $\delta x_k(t) \in \Re^{n_k+2}$ is the kth subsystem state vector, $v_k(t) \in \Re$ is the kth subsystem control input, and $K_k^{\mathsf{T}}(\alpha(t)) \in \Re^{n_k+2}$ is the vector of parameter dependent control gains for subsystem k, and $\delta r_k(t) \in \Re$ is the kth subsystem reference signal. $h_k(\delta x_q(t), \alpha(t))$ is the interconnection of all other subsystems on the kth subsystem. Subscript $\mathbf{k}$ represents the kth subsystem, where $k \in \{1, ..., N\}$. In the turboshaft engine control example $k \in \{Co, Pr\}$. Note that

$$\begin{aligned} b_{r_k}(\alpha(t)) &= b_{r_k} = [0,\ 0,\ -1],^{\mathsf{T}} \\ C_k(\alpha(t)) &= C_k = [I_{n_k},\ 0, 0], \\ k_{r_k}(\alpha(t)) &= 0, \quad \forall \alpha \in \Omega. \end{aligned} \tag{226}$$

The linearized closed-loop subsystem (224) with controller (225) and simplifications from (226) becomes

$$\begin{aligned} \delta \dot{x}_k(t) = &\underbrace{\left(A_k(\alpha(t)) + b_k K_k^{\mathsf{T}}(\alpha(t))\right)}_{A_{cl,k}(\alpha(t)} \delta x_k(t) \\ &+ b_{r_k} \delta r_k(t) + h_k(\delta x_q(t), \alpha(t)), \quad \forall \alpha \in \Omega. \end{aligned} \tag{227}$$

To design a reference model for each subsystem, we ignore the effects of the interconnection terms from other subsystems and for a desired performance, we find out the specific controller $K_k^*(\alpha(t)) = [0,\ 0,\ k_{i,k}^*(\alpha)]^{\mathsf{T}}$; as a result we obtain the following closed-loop system

$$\begin{aligned} \underbrace{\begin{bmatrix} \delta \dot{x}_k^p(t) \\ \delta \dot{u}_k(t) \\ \dot{x}_k^c(t) \end{bmatrix}}_{\delta \dot{x}_{m,k}(t)} = &\underbrace{\begin{bmatrix} A_k^p(\alpha(t)) & b_k^p(\alpha(t)) & 0 \\ 0 & -\eta_c & \eta_c k_{i,k}^*(\alpha(t)) \\ 1 & 0 & -\epsilon_c \end{bmatrix}}_{A_{m,k}(\alpha(t))} \underbrace{\begin{bmatrix} \delta x_k^p(t) \\ \delta u_k(t) \\ x_k^c(t) \end{bmatrix}}_{\delta x_{m,k}(t)} \\ &+ \underbrace{\begin{bmatrix} 0 \\ 0 \\ -1 \end{bmatrix}}_{b_{r_k}} \delta r_k(t), \quad \forall \alpha \in \Omega. \end{aligned} \tag{228}$$

The stability of the reference model for each subsystem is guaranteed by Lemma 1.

5.2.1 Subsystem I: Engine Core

With the high spool speed being the output of this subsystem, $\delta y_{Co}(t) = \delta x^p_{Co}(t)$, the model which we use to control the engine high spool speed is

$$\begin{aligned}
\delta \dot{x}^p_{Co}(t) &= a^p_{Co}(\alpha(t))\delta x^p_{Co}(t) + b^p_{Co}(\alpha(t))\delta u_{Co}(t) \\
&\quad + a^p_{CoPr}(\alpha(t))\delta x^p_{Pr}(t) + b^p_{CoPr}(\alpha(t))\delta u_{Pr}(t), \\
\delta \dot{u}_{Co}(t) &= -\eta_c \delta u_{Co}(t) + \eta_c v_{Co}(t), \\
\dot{x}^c_{Co}(t) &= -\epsilon_c x^c_{Co}(t) + (\delta x^p_{Co}(t) - \delta r_{Co}(t)).
\end{aligned} \tag{229}$$

Let $\delta x_{Co}(t) = [\delta x^p_{Co}(t),\ \delta u_{Co}(t),\ x^c_{Co}(t)]^{\mathsf{T}}$, $\delta x_{Pr}(t) = [\delta x^p_{Pr}(t),\ \delta u_{Pr}(t),\ x^c_{Pr}(t)]^{\mathsf{T}}$. Engine core subsystem dynamics (229) can be written as

$$\begin{aligned}
\delta \dot{x}_{Co}(t) = &\underbrace{\begin{bmatrix} a^p_{Co}(\alpha(t)) & b^p_{Co}(\alpha(t)) & 0 \\ 0 & -\eta_c & 0 \\ 1 & 0 & -\epsilon_c \end{bmatrix}}_{\mathrm{A_{Co}(\alpha(t))}} \delta x_{Co}(t) + \underbrace{\begin{bmatrix} 0 \\ \eta_c \\ 0 \end{bmatrix}}_{\mathrm{b_{Co}}} v_{Co}(t) \\
&+ \underbrace{\begin{bmatrix} 0 \\ 0 \\ -1 \end{bmatrix}}_{b r_{Co}} \delta r_{Co}(t) + \underbrace{\underbrace{\begin{bmatrix} a^p_{CoPr}(\alpha(t)) & b^p_{CoPr}(\alpha(t)) & 0 \\ 0 & 0 & 0 \\ 0 & 0 & 0 \end{bmatrix}}_{\mathrm{A_{CoPr}(\alpha(t))}} \delta x_{Pr}(t)}_{h_{Co}(\delta x_{Pr}(t),\alpha(t))}, \quad \forall \alpha \in \Omega,
\end{aligned} \tag{230}$$

with the state feedback controller

$$v_{Co}(t) = K^{\mathsf{T}}_{Co}(\alpha(t))\delta x_{Co}(t), \quad \forall \alpha \in \Omega. \tag{231}$$

5.2.2 Subsystem II: Engine Fan/Prop

With the low spool speed being the output of this subsystem, $\delta y_{Pr}(t) = \delta x^p_{Pr}(t)$, the model which we use to control the engine thrust is

$$\begin{aligned}
\delta \dot{x}^p_{Pr}(t) &= a^p_{Pr}(\alpha(t))\delta x^p_{Pr}(t) + b^p_{Pr}(\alpha(t))\delta u_{Pr}(t) \\
&\quad + a^p_{PrCo}(\alpha(t))\delta x^p_{Co}(t) + b^p_{PrCo}(\alpha(t))\delta u_{Co}(t), \\
\delta \dot{u}_{Pr}(t) &= -\eta_c \delta u_{Pr}(t) + \eta_c v_{Pr}(t), \\
\dot{x}^c_{Pr}(t) &= -\epsilon_c x^c_{Pr}(t) + (\delta x^p_{Pr}(t) - \delta r_{Pr}(t)).
\end{aligned} \tag{232}$$

Engine fan/prop subsystem dynamics (232) can be written as

$$\begin{aligned}
\delta \dot{x}_{Pr}(t) = &\underbrace{\begin{bmatrix} a^p_{Pr}(\alpha(t)) & b^p_{Pr}(\alpha(t)) & 0 \\ 0 & -\eta_c & 0 \\ 1 & 0 & -\epsilon_c \end{bmatrix}}_{\mathrm{A_{Pr}(\alpha(t))}} \delta x_{Pr}(t) + \underbrace{\begin{bmatrix} 0 \\ \eta_c \\ 0 \end{bmatrix}}_{\mathrm{b_{Pr}}} v_{Pr}(t) \\
&+ \underbrace{\begin{bmatrix} 0 \\ 0 \\ -1 \end{bmatrix}}_{b_{r_{Pr}}} \delta r_{Pr}(t) + \underbrace{\underbrace{\begin{bmatrix} a^p_{PrCo}(\alpha(t)) & b^p_{PrCo}(\alpha(t)) & 0 \\ 0 & 0 & 0 \\ 0 & 0 & 0 \end{bmatrix}}_{\mathrm{A_{PrCo}(\alpha(t))}} \delta x_{Co}(t)}_{h_{Pr}(\delta x_{Co}(t),\alpha(t))}, \quad \forall \alpha \in \Omega,
\end{aligned} \tag{233}$$

with the state feedback controller

$$v_{Pr}(t) = K^{\mathsf{T}}_{Pr}(\alpha(t))\delta x_{Pr}(t), \quad \forall \alpha \in \Omega. \tag{234}$$

5.3 Decentralized Gain Scheduled Model Reference Adaptive Control

Here we expand the results from [115, 116] to design a decentralized gain scheduled model reference adaptive control (D-GS-MRAC) architecture. This architecture is especially suitable for turboshaft engines driving variable pitch propellers/fans.

5.3.1 Decentralized Adaptive Control Design

Consider a system S consists of N subsystems $S_1, S_2, ..., S_N$ that are interconnected. Each of the subsystems is modeled as a single input, single output (SISO) linear parameter dependent model. For convenience, we shall assume that each subsystem S_k has a controller C_k which computes the control input u_k to S_k. The subsystems S_k are described by the equations

$$\begin{aligned} S_k : \delta\dot{x}_k(t) &= A_k(\alpha(t))\delta x_k(t) + b_k v_k(t) + b_{r_k}\delta r_k(t) \\ &\quad + \underbrace{\sum_{q=1, q\neq k}^{N} [A_{kq}(\alpha(t))\delta x_q(t)]}_{h_k(\delta x_q(t), \alpha(t))}, \quad \forall \alpha \in \Omega, \\ \delta y_k(t) &= C_k \delta x_k(t), \end{aligned} \tag{235}$$

where $\delta x_k(0) = \delta x_{0_k}$, and $\delta x_k(t) \in \Re^{n_k}$ is the kth subsystem state vector, $v_k(t) \in \Re$ is the kth subsystem control input, and $\delta r_k(t) \in \Re$ is the kth subsystem reference signal. $h_k(\delta x_q(t), \alpha(t))$ is the interconnection of all other subsystems on the kth subsystem. Note that $\delta x(t) = [\delta x_1^{\mathsf{T}}(t), ..., \delta x_k^{\mathsf{T}}(t) ..., \delta x_N^{\mathsf{T}}(t)]^{\mathsf{T}}$. Subscript **k** represents the kth subsystem, where $k \in \{1, ..., N\}$.

Assumption 4. *For the interconnection term $h_k(\delta x_q(t), \alpha(t))$, there exist positive constants $c_{kq} \in \Re$, for each subsystem $q \neq k$, such that it is satisfying the following inequality*

$$\|h_k(\delta x_q(t), \alpha(t))\| \leq \sum_{q=1, q\neq k}^{N} [c_{kq} \|\delta x_q(t)\|], \quad \forall \alpha \in \Omega. \tag{236}$$

This is a result of Assumption 1, which is on the boundedness of $A_m(\alpha(t))$.

The linear parameter dependent reference model for the kth subsystem is expressed as

$$\delta\dot{x}_{m,k}(t) = A_{m,k}(\alpha(t))\delta x_{m,k}(t) + b_{r_k}\delta r_k(t), \quad \forall \alpha \in \Omega, \tag{237}$$

where $\delta r_k(t) \in \Re$ is a bounded continuous reference input signal. The parameter matrix $A_{m,k} \in \Re^{n_k \times n_k}$ is chosen with $A_{m,k}$ being Hurwitz. The boundedness of all the

reference trajectories is required in a decentralized tracking control problem, which has been showed in the previous section. Note that $\delta r_k(t) \in \Re$ is the command signal such that $||\delta r_k(t)|| \leq r_{\max,k}$.

Assumption 5. *The matrices $A_{m,k}(\alpha(t))$ for all $k = 1, ..., N$ are bounded*

$$||A_{m,k}(\alpha(t))|| \leq M_{A_k}, \quad \forall \alpha \in \Omega, \tag{238}$$

where M_{A_k} is constant for all $k = 1, ..., N$. This is a result of Assumption 1, which is on the boundedness of $A_m(\alpha(t))$.

The decentralized adaptive control of a linear parameter dependent system can be stated as follows: given N subsystems described by (235), and N reference models described by (237), and assuming that controller C_k of S_k can generate an input $v_k(t)$ such that all the signals in the system are bounded, and

$$lim_{t\to\infty} \|\delta x_k(t) - \delta x_{m,k}(t)\| = 0. \tag{239}$$

Since the effect of the interactions of subsystems on each other is bounded, we can use the following adaptive state feedback controller for each subsystem

$$C_k : \ v_k(t) = \hat{K}_k^{\mathsf{T}}(t)\delta x_k(t), \tag{240}$$

where $\hat{K}_k(t) \in \Re^{n_k}$ is the time-varying estimate of the nominal controller parameters $K_k^*(t)$.

Assumption 6. *For each subsystem S_k, there exists an ideal gain matrix $K_k^{*\mathsf{T}}(\alpha(t)) = [0, \ 0, \ k_{i,k}^{*\mathsf{T}}(\alpha(t))]$, that results in perfect matching between the reference model (237) and the plant (235) such that*

$$A_{m,k}(\alpha(t)) = A_k(\alpha(t)) + b_k K_k^{*\mathsf{T}}(\alpha(t)), \quad \forall \alpha \in \Omega, \tag{241}$$

where $A_{m,k}(\alpha)$ has the following form

$$A_{m,k}(\alpha) = \begin{bmatrix} A_k^p(\alpha(t)) & b_k^p(\alpha) & 0 \\ 0 & -\eta_c & \eta_c k_{i,k}^*(\alpha(t)) \\ 1 & 0 & -\epsilon_c \end{bmatrix}. \tag{242}$$

Assumption 7. *Let $K_k^*(t) \in \theta_k$ for all $t \geq 0$, where θ_k is a known convex compact set. We also assume that $K_k^*(t)$ is continuously differentiable, and the derivative is uniformly bounded, $||\dot{K}_k^*(t)|| \leq \bar{d}_k < \infty$ for all $t \geq 0$.*

With adaptive controller (240), the closed-loop form of subsystem S_k becomes

$$\delta\dot{x}_k(t) = A_{m,k}(\alpha(t))\delta x_k(t) + b_k\tilde{K}_k^{\mathsf{T}}(t)\delta x_k(t) + b_{r_k}\delta r_k(t) + h_k(\delta x_q(t), \alpha(t)), \tag{243}$$

where $\tilde{K}_k(t) = K_k(t) - K_k^*(t)$. The error equation in terms of state tracking error $e_k(t) = \delta x_k(t) - \delta x_{m,k}(t)$ and controller parameters is

$$\dot{e}_k(t) = A_{m,k}(\alpha(t))e_k(t) + b_k\tilde{K}_k^{\mathsf{T}}(t)\delta x_k(t) + h_k(\delta x_q(t), \alpha(t)). \tag{244}$$

Based on the error model (244), adaptive laws are presented using the Lyapunov design method. Here we consider the case that for each subsystem a single quadratic Lyapunov function exists for the error model (244). In other words, in each subsystem k, $k = \{1, ..., N\}$, for the Hurwitz matrix $A_{m,k}(\alpha(t))$ for all $\alpha \in \Omega$, there exists a positive definite matrix Q_k, and a single Lyapunov matrix $P_k = P_k^{\mathsf{T}} > 0$ such that

$$P_kA_{m,k}(\alpha(t)) + A_{m,k}^{\mathsf{T}}(\alpha(t))P_k \leq -Q_k, \quad \forall\alpha \in \Omega, \tag{245}$$

which is a result of Lemma 1. Now we use the following adaptive law:

$$\dot{\hat{K}}_k(t) = \text{Proj}_\Gamma\left(\hat{K}_k(t), -\delta x_k(t)e_k^{\mathsf{T}}(t)P_kb_k\right), \tag{246}$$

where $\Gamma_k = \Gamma_k^{\mathsf{T}}$.

A visualization of the decentralized gain scheduled model reference adaptive control architecture is given in Figure 87. In the next theorem we investigate the stability of the whole system S with N closed-loop decentralized interconnected subsystems. The stability result presented here is an extension of the results which already have been developed in [55, 40, 155] for the case where we have a gain scheduled reference model for each subsystem.

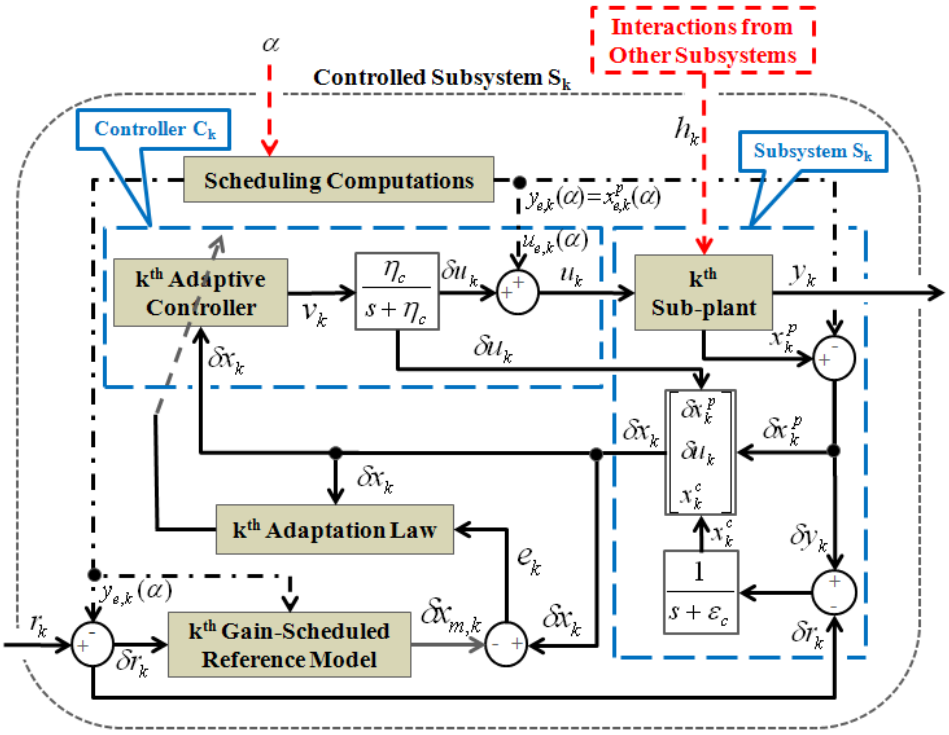

Figure 87: Decentralized gain scheduled model reference adaptive control architecture illustrated for a subsystem S_k.

Theorem 5. *Consider the system S consisting of N interconnected subsystems S_k described by (235) subject to Assumption 4, and reference model for each subsystem S_k described by (237) subject to Assumption 5 and satisfying (245). Consider, in addition for subsystems S_k, the adaptive control laws C_k defined in (240), with adaptive laws defined in (246) subject to Assumptions 6 and 7. Then the error signals $e_k(t)$ are uniformly ultimately bounded (UUB) for all $k = 1, 2, ..., N$.*

Proof. For subsystem S_k consider the Lyapunov function candidate as

$$V_k(e_k(t), \tilde{K}_k(t)) = e_k^{\mathsf{T}}(t) P_k e_k(t) + \tilde{K}_k^{\mathsf{T}}(t) \Gamma_k^{-1} \tilde{K}_k(t), \tag{247}$$

whose time derivative along (244) and (246) is

$$\begin{aligned}\dot{V}_k(.) &= \dot{e}_k^{\mathsf{T}}(t)P_k e_k(t) + e_k^{\mathsf{T}}(t)P_k\dot{e}_k(t) + \dot{\tilde{K}}_k^{\mathsf{T}}(t)\Gamma_k^{-1}\tilde{K}_k(t) + \tilde{K}_k^{\mathsf{T}}(t)\Gamma_k^{-1}\dot{\tilde{K}}_k(t)\\ &= e_k^{\mathsf{T}}(t)\left(P_k A_{m,k}(\alpha(t)) + A_{m,k}^{\mathsf{T}}(\alpha(t))P_k\right)e_k(t)\\ &+ 2e_k^{\mathsf{T}}(t)P_k b_k\tilde{K}_k^{\mathsf{T}}(t)\delta x_k(t) + 2\left(\tilde{K}_k^{\mathsf{T}}(t)\Gamma_k^{-1}\dot{\tilde{K}}^k(t)\right)\\ &+ 2e_k^{\mathsf{T}}(t)P_k h_k(\delta x_q(t),\alpha(t)).\end{aligned} \tag{248}$$

Using (245), and knowing that for scalars $a^{\mathsf{T}}b = ba^{\mathsf{T}}$, and letting $Y_{K,k}(t) = -\delta x_k(t)e_k^{\mathsf{T}}(t)P_k b_k$, and knowing $\dot{\tilde{K}}_k(t) = \dot{\hat{K}}_k(t) - \dot{K}_k^*(t)$ leads to

$$\begin{aligned}\dot{V}_k(.) &\leq -e_k^{\mathsf{T}}(t)Q_k e_k(t) + 2\left(\tilde{K}_k^{\mathsf{T}}(t)\left[\Gamma_k^{-1}\dot{\hat{K}}_k(t) - Y_{K,k}(t)\right]\right)\\ &\quad - 2\left(\tilde{K}_k^{\mathsf{T}}(t)\Gamma_k^{-1}\dot{K}_k^*(t)\right) + 2e_k^{\mathsf{T}}(t)P_k h_k(\delta x_q(t),\alpha(t))\\ &= -e_k^{\mathsf{T}}(t)Q_k e_k(t) + 2\left(\tilde{K}_k^{\mathsf{T}}(t)\left[\Gamma_k^{-1}\mathrm{Proj}_\Gamma(\hat{K}_k(t), Y_{K,k}(t)) - Y_{K,k}(t)\right]\right)\\ &\quad - 2\left(\tilde{K}_k(t)^{\mathsf{T}}\Gamma_k^{-1}\dot{K}_k^*(t)\right) + 2e_k^{\mathsf{T}}(t)P_k h_k(\delta x_q(t),\alpha(t)).\end{aligned} \tag{249}$$

Using Lemma 6

$$\dot{V}_k(.) \leq -e_k^{\mathsf{T}}(t)Q_k e(t) - 2\left(\tilde{K}_k^{\mathsf{T}}(t)\Gamma^{-1}\dot{K}_k^*(t)\right) + 2e_k^{\mathsf{T}}(t)P_k h_k(\delta x_q(t),\alpha(t)). \tag{250}$$

From Assumption 4, knowing $\delta x_q(t) = e_q(t) + \delta x_{m,q}(t)$, and letting $\bar{x}_{m,k} = sup_t(\sum_{q=1,q\neq k}^{N} c_{kq}||\delta x_{m,q}||)$, we have

$$||h_k(\delta x_q(t),\alpha(t))|| \leq \sum_{q=1,q\neq k}^{N}[c_{kq}||e_q(t)||] + \bar{x}_{m,k}. \tag{251}$$

Furthermore, using (251) in the last term of (250) results in

$$\begin{aligned}|2e_k^{\mathsf{T}}(t)P_k h_k(\delta x_q(t),\alpha(t))| &\leq 2\lambda_{\max}(P_k)||e_k(t)||||h_k(\delta x_q(t),\alpha(t))||\\ &\leq 2\lambda_{\max}(P_k)||e_k(t)||\left(\bar{x}_{m,k} + \sum_{q=1,q\neq k}^{N}[c_{kq}||e_q(t)||]\right).\end{aligned} \tag{252}$$

Notice that using Assumption 7, we obtain

$$||\tilde{K}_k^{\mathsf{T}}(t)\Gamma_k^{-1}\dot{K}_k^*(t)|| \leq ||\Gamma_k^{-1}|| \max_{K_k^*\in\theta_k}||K_k^*||\bar{d}_k, \quad \forall t \geq 0. \tag{253}$$

The following upper bound on Lyapunov function derivative for kth subsystem can be found,

$$\dot{V}_k(.) \leq -\bar{\lambda}_k||e_k(t)||^2 + \bar{\rho}_k||e_k(t)|| \sum_{q=1,q\neq k}^{N} c_{kq}||e_q(t)|| + \bar{\xi}_k||e_k(t)|| + \bar{\psi}_k, \tag{254}$$

where $\bar{\lambda}_k := (\lambda_{min}(Q_k))$, $\bar{\rho}_k := 2\lambda_{\max}(P_k)$, $\bar{\xi}_k := 2\lambda_{\max}(P_k)\bar{x}_{m,k}$, and $\bar{\psi}_k := 2||\Gamma_k^{-1}|| \max_{K_k^* \in \theta_k} ||K_k^*||\bar{d}_k$ are all positive constants. Now choosing $V(.) = \sum_{k=1}^{N} V_k(.)$ to show the stability of the whole system S, the Lyapunov function derivative for the whole system S is

$$\begin{aligned} \dot{V}(.) &= \sum_{k=1}^{N} \dot{V}_k(.) \\ &\leq \sum_{k=1}^{N} \left(-\bar{\lambda}_k||e_k(t)||^2 + \bar{\rho}_k||e_k(t)|| \sum_{q=1,q\neq k}^{N} c_{kq}||e_q(t)|| + \bar{\xi}_k||e_k(t)|| + \bar{\psi}_k \right). \end{aligned} \tag{255}$$

Letting $\psi := \sum_{k=1}^{N} \bar{\psi}_k$, and defining the following vectors and matrices

$$\bar{e}(t) := [||e_1(t)||, ..., ||e_N(t)||]^{\mathsf{T}}, \quad \xi := [\bar{\xi}_1, ..., \bar{\xi}_N]^{\mathsf{T}},$$

$$\Phi := \begin{bmatrix} 0 & \bar{\rho}_1 c_{12} & . & \bar{\rho}_1 c_{1q} & . & \bar{\rho}_1 c_{1N} \\ \bar{\rho}_2 c_{21} & 0 & . & . & . & \bar{\rho}_2 c_{2N} \\ . & . & 0 & . & . & . \\ \bar{\rho}_k c_{k1} & . & \bar{\rho}_k c_{kq} & . & . & \bar{\rho}_k c_{kN} \\ . & . & 0 & . & . & . \\ \bar{\rho}_N c_{N1} & . & \bar{\rho}_N c_{Nq} & . & \bar{\rho}_N c_{N(N_1)} & 0 \end{bmatrix}, \tag{256}$$

$$\Lambda := diag([\bar{\lambda}_1, ..., \bar{\lambda}_N]), \quad \Pi := \Lambda - \Phi,$$

the upper bound on Lyapunov function derivative becomes

$$\begin{aligned} \dot{V}(.) &\leq -\bar{e}(t)^{\mathsf{T}}\Pi\bar{e}(t) + \xi^{\mathsf{T}}\bar{e}(t) + \psi \\ &\leq -\lambda_{\min}(\Pi)||\bar{e}(t)||^2 + ||\xi||||\bar{e}(t)|| + \psi. \end{aligned} \tag{257}$$

By proper selection of Q_k for all $k = 1, ..., N$, we can make sure that $\lambda_{\min}(\Pi) > 0$. Having

$$||\bar{e}(t)|| > \frac{||\xi|| + \sqrt{||\xi||^2 + 4\lambda_{\min}(\Pi)\psi}}{2\lambda_{\min}(\Pi)}, \tag{258}$$

renders $\dot{V}(.) < 0$. Hence $e_k(t)$ is UUB for all $k = 1, ..., N$. $\square$

5.3.2 Towards D-GS-MRAC Software Verification

Following the discussions presented in Sections 3.3.3 and 4.3.4, we are now considering the engine D-GS-MRAC case. In this case the stability of the closed-loop subsystems (244) and (246) is analyzed using the Lyapunov function $V_k(e_k(t), \tilde{K}_k(t)) = e_k^{\mathsf{T}}(t)P_k e_k(t) + \tilde{K}_k^{\mathsf{T}}(t)\Gamma_k^{-1}\tilde{K}_k(t)$ for all $k = 1, ..., N$, where P_k satisfies (245), and Γ_k^{-1} is a symmetric positive definite matrix. The stability of the whole system S is then analyzed using $V = \sum_{k=1}^{N} V_k(e_k(t), \tilde{K}_k(t))$.

For each subsystem consider $\zeta_k := [e_k^{\mathsf{T}}, \tilde{K}_k^{\mathsf{T}}]^{\mathsf{T}}$, and $\bar{P}_k := \text{diag}([P_k,\ \Gamma_k^{-1}])$, where P_k and Γ_k^{-1} are block diagonal elements in the matrix $\bar{P}_k$. Since we are using Γ-projection operator to update the control gain for each subsystem, $\tilde{K}_k(t)$ belongs to a priori known compact set. For the whole system S, we define $\bar{\zeta} := [\zeta_1, ..., \zeta_N]$, $\bar{P} := \text{diag}([\bar{P}_1, ..., \bar{P}_N])$, and $\bar{n} = \sum_{k=1}^{N} 2n_k$. As a result, one invariant ellipsoid which possibly can be used in the D-GS-MRAC software verification analysis is

$$\mathcal{E} = \left\{ \bar{\zeta} \in \Re^{\bar{n}} | \bar{\zeta}^{\mathsf{T}} \bar{P} \bar{\zeta} \leq 1 \right\}. \tag{259}$$

By presenting a detailed Lyapunov stability analysis for D-GS-MRAC, we completed the fist steps towards a verifiable D-GS-MRAC system for gas turbine systems. This may help further analytical investigation of the D-GS-MRAC software verification process. The complete theoretical D-GS-MRAC software verification is beyond the scope of this dissertation, and it remains a topic for future research.

5.4 Plug and Play Technology Concept for Engine Control

When it comes to integrated propulsion systems, there is a lot of work that goes into power plant and propulsor matching on a performance level before control ever gets involved. Hence we propose the idea of core and prop/fan modules as separate elements that could be swapped around with a plug and play (PnP) technology.

Helicopters and other VTOL aircraft systems might be good candidates though, since in those cases one could consider the core power plant as a swappable module. A given helicopter with a given set of rotor blades could be made to work with a General Electric (GE) or a Rolls-Royce or a Pratt and Whitney (P&W) gas turbine engine. Furthermore, the plug and play technology can be implemented in automobile and marine propulsion systems.

Commercial manufacturers of gas turbine engines rarely design all new engine centerlines [32]; the lifespan of successful engine families is decades. Many of the new engines designed in a family are based on an existing engine core, primarily due to cost and reliability concerns. The high pressure compressor and turbine contain the highest performance, and therefore most expensive components. Engine core designs may move from military turbojets into commercial turbofans and turboshafts/turboprops [29]. A similar niche is occurring in UAV development, where small gas turbines are being used to power a variety of different lift/thrust devices. UAV development programs rarely have the resources for serious engine redevelopment and therefore must select from a limited number of commercial off the shelf (COTS) engines. In the case of small gas turbines, these COTS engines are generally designed for missile-turbojet or power generator applications, while the UAV designer may want to use the engine core in a turboprop or turbofan application. Successful development of PnP technology using decentralized adaptive control architecture for this class of engines would allow UAV designers to purchase engines with onboard controllers and mate them with their own proprietary fan/prop sections without having to design a new control system from scratch.

Decentralized adaptive control architecture developed in this chapter could enable plug and play (PnP) development of entire families of engines. In this architecture, engine cores and fans/props could be purchased with their independent controllers ready for integration into a functional propulsion system, whereas the FADEC was

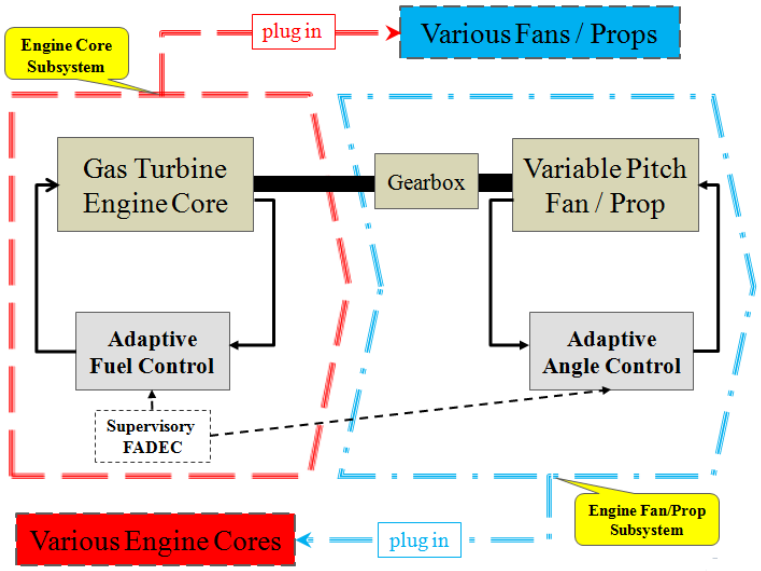

Figure 88: Schematic of plug and play control concept for gas turbine engines.

developed independently for the engine. Structuring engine control in such a de-centralized/distributed fashion would increase compatibility between different engine manufacturers and reduce development time and cost for new engines.

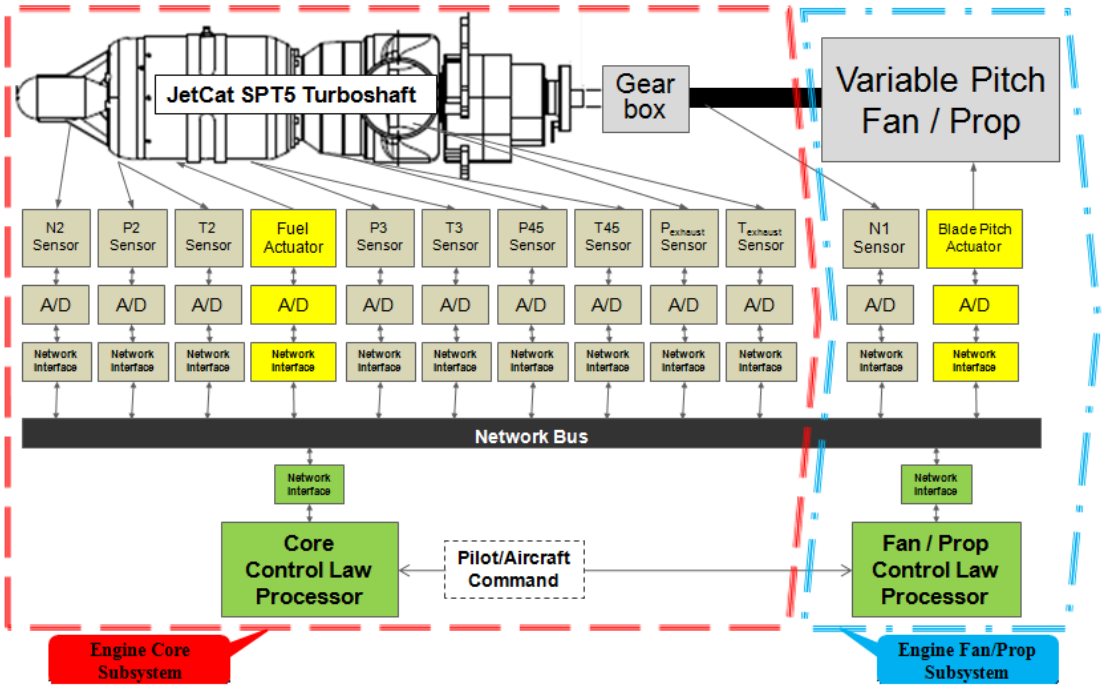

Figure 89: Plug and play technology for SPT5 turboshaft engine driving a variable pitch propeller.

For turboshaft engine PnP technology development, we use the developed decentralized adaptive control technique. Adaptive control for fuel and angle regulation in a decentralized structure is the key element of this PnP technology concept. Figure 88 shows the conceptual representation of the PnP technology. Using this technology, we can match different engine cores to different props/fans, and the whole propulsion system could work without anymore performance tuning. More detailed visualization of the PnP concept for the JetCat SPT5 turboshaft engine driving a variable pitch propeller using a distributed control architecture is shown in Figure 89. In this distributed architecture, all the elements of the control system including sensors, actuators, and control processors are connected to a databus using their network interfaces and they can communicate with each other via the databus. This distributed structure is an enabler for having new engine cores or props/fans replaced with their subordinate controllers easily, without too much performance matching by propulsion engineers. Detailed technical information about distributed modular control architecture development for the SPT5 turboshaft engine can be found in [113].

A supervisory unit in the PnP structure computes two different reference signals for core and prop spool speeds and sends each one of these reference signals to their related subsystems. These signals are computed using the thrust command we define for the supervisory unit. To compute two spool speed reference signals, we use the scheduling parameter $\alpha(t)$ and the available steady state values of the engine spool speeds and control inputs at multiple important equilibrium points including idle, cruise, and full thrust conditions. Each subsystem gets its reference signal from the supervisory unit, its spool speed measurement from a speed sensor, and computes an independent adaptive control input using its own control law processor. All of the sensor, actuator, and reference data are communicated via a databus in a distributed architecture. At this stage of the PnP technology concept, the supervisory

unit communicates a priori information about the engine to the subsystems by the reference signals, and there is no self-tuning process involved in the control architecture development. In the future, some form of online optimization (or self-tuning) capability can be integrated in the PnP structure using the peak-seeking control technique described in [137].

5.5 Turboshaft Engine Example

We apply the developed D-GS-MRAC to the physics-based model of the JetCat SPT5 turboshaft engine driving a variable pitch propeller developed in Chapter 2. Note that some of the plant states and inputs have been nondimensionalized by their design values: fuel flow input, $u_{Co}(t)$, is divided by 0.0035323 (kg/s), core spool speed, $N_{Co}(t)$, which is the plant state for core subsystem ($x^p_{Co}(t)$), and is divided by 170000 RPM, and prop spool speed, $N_{Pr}(t)$, which is the plant state for prop subsystem ($x^p_{Pr}(t)$), and is divided by 7000 RPM.

The decentralized gain scheduled model reference adaptive control (D-GS-MRAC) architecture developed for the twin spool turboshaft engine model is visualized in Figure 90. The mechanical interconnection between the engine core and engine prop is shown with a dashed line, scheduling computations are shown with dot-dashed lines, and other signals are shown with solid lines. The two subsystems are shown separately using dotted rectangles.

5.5.1 Equilibrium Manifold

For a standard day at sea level condition, we chose five properly separated equilibrium points on the nominal plant equilibrium manifold for linearizing the plant model at those points. The linearization matrices for these five equilibrium points and steady state values of the engine variables, the control parameters, and the scheduling parameter are given as follows:

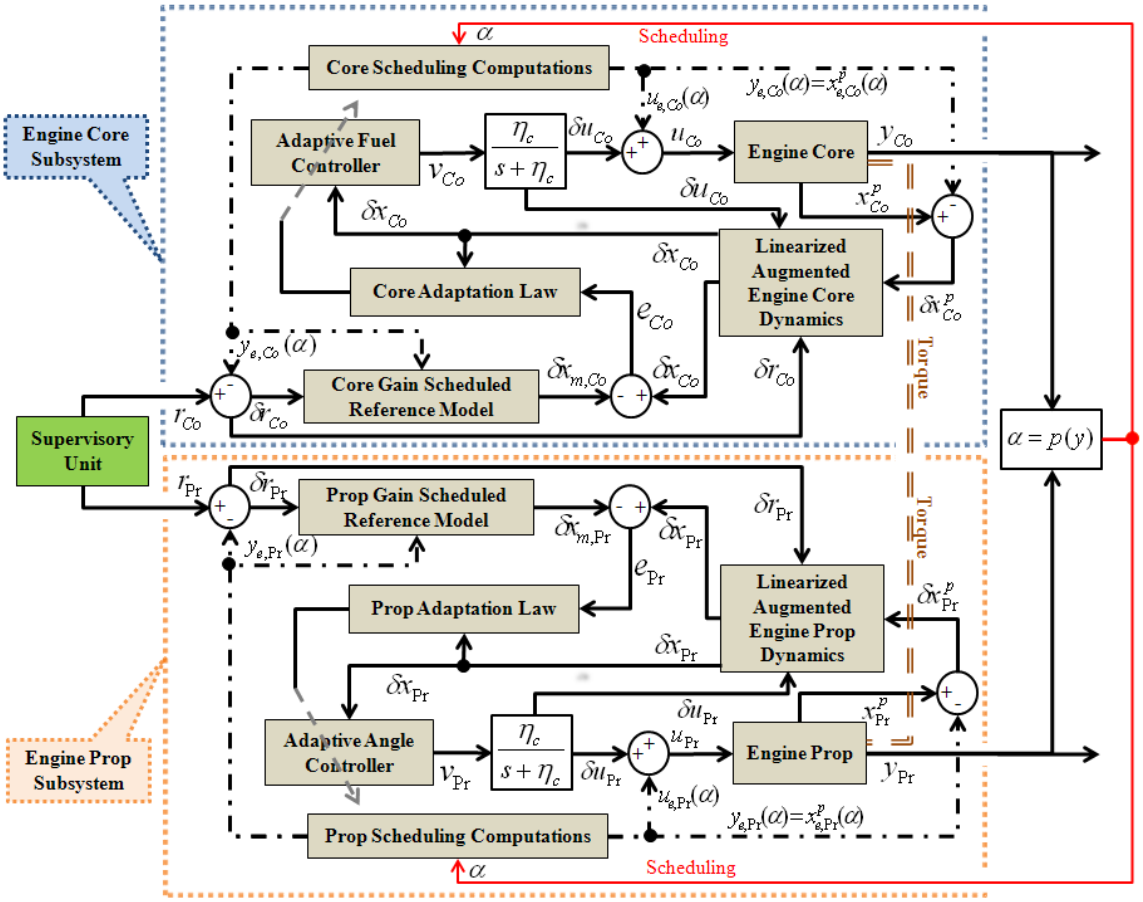

Figure 90: Decentralized gain scheduled model reference adaptive control architecture illustration for twin spool turboshaft engine driving a variable pitch propeller.

- Equilibrium Point 1 (Full Thrust): $u_{e,Co_1} = 1.0$, $u_{e,Pr_1} = 16$ (deg), $x^p_{e,Co_1} = 1.0$, $x^p_{e,Pr_1} = 0.9524$, $T_{e_1} = 255.8685$ (N), $\alpha_1 = 1.3810$, and the matrices are

$$A_{Co_1} = \begin{bmatrix} -5 & 1.5 & 0 \\ 0 & -\eta_c & 0 \\ 1 & 0 & -\epsilon_c \end{bmatrix}, \; A_{CoPr_1} = \begin{bmatrix} 0 & 0 & 0 \\ 0 & 0 & 0 \\ 0 & 0 & 0 \end{bmatrix}, \; k_{i,Co_1} = -0.9,$$
$$A_{Pr_1} = \begin{bmatrix} -2.3 & -0.085 & 0 \\ 0 & -\eta_c & 0 \\ 1 & 0 & -\epsilon_c \end{bmatrix}, \; A_{PrCo_1} = \begin{bmatrix} 3.5 & 0.63 & 0 \\ 0 & 0 & 0 \\ 0 & 0 & 0 \end{bmatrix}, \; k_{i,Pr_1} = -0.9. \tag{260}$$

- Equilibrium Point 2: $u_{e,Co_2} = 0.7,\ u_{e,Pr_2} = 16$ (deg), $x^p_{e,Co_2} = 0.9041,\ x^p_{e,Pr_2} = 0.6557,\ T_{e_2} = 121.2905$ (N), $\alpha_2 = 1.1168$, and the matrices are

$$A_{Co_2}=\begin{bmatrix} -2.80 & 1.42 & 0 \\ 0 & -\eta_c & 0 \\ 1 & 0 & -\epsilon_c \end{bmatrix},\ A_{CoPr_2}=\begin{bmatrix} 0 & 0 & 0 \\ 0 & 0 & 0 \\ 0 & 0 & 0 \end{bmatrix},\ k_{i,Co_2}=-0.8,$$
$$A_{Pr_2}=\begin{bmatrix} -1.70 & -0.050 & 0 \\ 0 & -\eta_c & 0 \\ 1 & 0 & -\epsilon_c \end{bmatrix},\ A_{PrCo_2}=\begin{bmatrix} 2 & 0.377 & 0 \\ 0 & 0 & 0 \\ 0 & 0 & 0 \end{bmatrix},\ k_{i,Pr_2}=-0.8. \tag{261}$$

- Equilibrium Point 3 (Cruise): $u_{e,Co_3} = 0.4685,\ u_{e,Pr_3} = 16$ (deg), $x^p_{e,Co_3} = 0.7264,\ x^p_{e,Pr_3} = 0.5,\ T_{e_3} = 70.5125$ (N), $\alpha_3 = 0.8818$, and the matrices are

$$A_{Co_3}=\begin{bmatrix} -1.5 & 1.2 & 0 \\ 0 & -\eta_c & 0 \\ 1 & 0 & -\epsilon_c \end{bmatrix},\ A_{CoPr_3}=\begin{bmatrix} 0.1 & 0 & 0 \\ 0 & 0 & 0 \\ 0 & 0 & 0 \end{bmatrix},\ k_{i,Co_3}=-0.7,$$
$$A_{Pr_3}=\begin{bmatrix} -1.1 & -0.023 & 0 \\ 0 & -\eta_c & 0 \\ 1 & 0 & -\epsilon_c \end{bmatrix},\ A_{PrCo_3}=\begin{bmatrix} 0.6 & 0.3 & 0 \\ 0 & 0 & 0 \\ 0 & 0 & 0 \end{bmatrix},\ k_{i,Pr_3}=-0.7. \tag{262}$$

- Equilibrium Point 4: $u_{e,Co_4} = 0.3,\ u_{e,Pr_4} = 16$ (deg), $x^p_{e,Co_4} = 0.5327,\ x^p_{e,Pr_4} =$

0.3678, $T_{e_4} = 38.155$ (N), $\alpha_4 = 0.6473$, and the matrices are

$$A_{Co_4}=\begin{bmatrix} -0.85 & 1 & 0 \\ 0 & -\eta_c & 0 \\ 1 & 0 & -\epsilon_c \end{bmatrix},\ A_{CoPr_4}=\begin{bmatrix} 0.032 & 0 & 0 \\ 0 & 0 & 0 \\ 0 & 0 & 0 \end{bmatrix},\ k_{i,Co_4}=-0.6,$$
$$A_{Pr_4}=\begin{bmatrix} -0.64 & -0.011 & 0 \\ 0 & -\eta_c & 0 \\ 1 & 0 & -\epsilon_c \end{bmatrix},\ A_{PrCo_4}=\begin{bmatrix} 0.32 & 0.17 & 0 \\ 0 & 0 & 0 \\ 0 & 0 & 0 \end{bmatrix},\ k_{i,Pr_4}=-0.6. \tag{263}$$

- Equilibrium Point 5 (Idle): $u_{e,Co_5} = 0.145$, $u_{e,Pr_5} = 16$ (deg), $x^p_{e,Co_5} = 0.295$, $x^p_{e,Pr_5} = 0.161$, $T_{e_5} = 7.317$ (N), $\alpha_5 = 0.3361$, and the matrices are

$$A_{Co_5}=\begin{bmatrix} -0.38 & 0.7 & 0 \\ 0 & -\eta_c & 0 \\ 1 & 0 & -\epsilon_c \end{bmatrix},\ A_{CoPr_5}=\begin{bmatrix} -0.0008 & 0 & 0 \\ 0 & 0 & 0 \\ 0 & 0 & 0 \end{bmatrix},\ k_{i,Co_5}=-0.5,$$
$$A_{Pr_5}=\begin{bmatrix} -0.34 & -0.0024 & 0 \\ 0 & -\eta_c & 0 \\ 1 & 0 & -\epsilon_c \end{bmatrix},\ A_{PrCo_5}=\begin{bmatrix} 0.26 & 0.1 & 0 \\ 0 & 0 & 0 \\ 0 & 0 & 0 \end{bmatrix},\ k_{i,Pr_5}=-0.5. \tag{264}$$

Other controller parameters are $\epsilon_c = 1$, $\eta_c = 3$. The elements of the $A_{Co}(\alpha(t))$ and $A_{Pr}(\alpha(t))$ matrices have been shown as functions of scheduling parameter α in Figures 91 and 92. The elements of interconnection matrices $A_{CoPr}(\alpha(t))$ and $A_{PrCo}(\alpha(t))$ have been shown as functions of scheduling parameter α in Figures 93 and 94. In this simulation, the scheduling parameter α, is defined to be the Euclidean norm of the gas turbine engine spool speeds, which are the subsystems outputs. Piecewise linear interpolation has been used to compute matrices in between the available linearization matrices of each pair of adjacent equilibrium points.

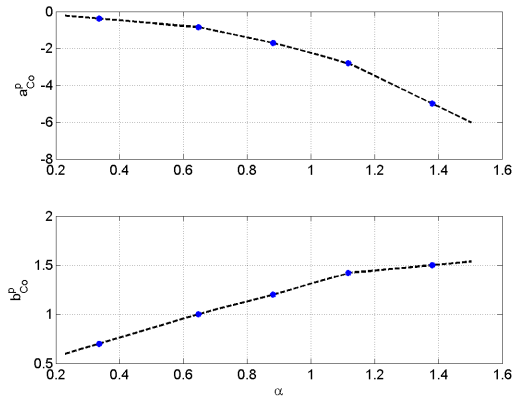

Figure 91: $A_{Co}(\alpha(t))$ components as functions of scheduling parameter $\alpha(t)$.

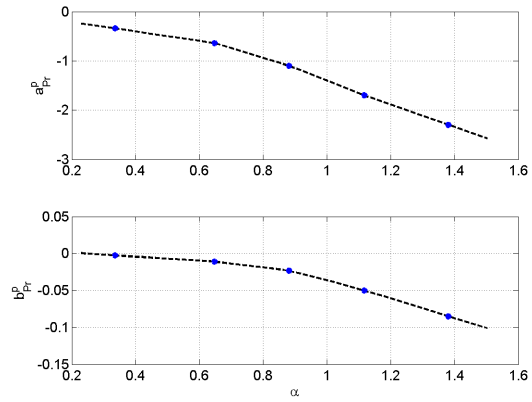

Figure 92: $A_{Pr}(\alpha(t))$ components as functions of scheduling parameter $\alpha(t)$.

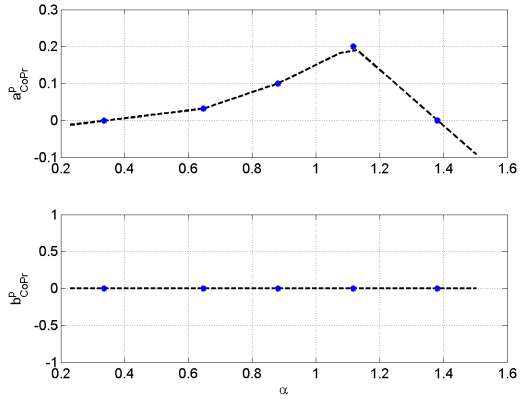

Figure 93: $A_{CoPr}(\alpha(t))$ components as functions of scheduling parameter $\alpha(t)$.

The equilibrium values of the states and control inputs for each subsystem S_k are shown in Figures 95 and 96 as functions of scheduling parameter $\alpha(t)$. Piecewise

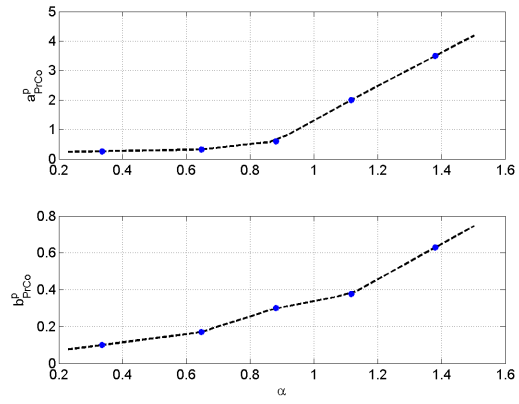

Figure 94: $A_{PrCo}(\alpha(t))$ components as functions of scheduling parameter $\alpha(t)$.

linear interpolation has been used to compute equilibrium values in between each pair of adjacent equilibrium points. The equilibrium manifolds in a 3D space of two spool speeds and control input C_k for each subsystem S_k are shown in figure Figures 97 and 98.

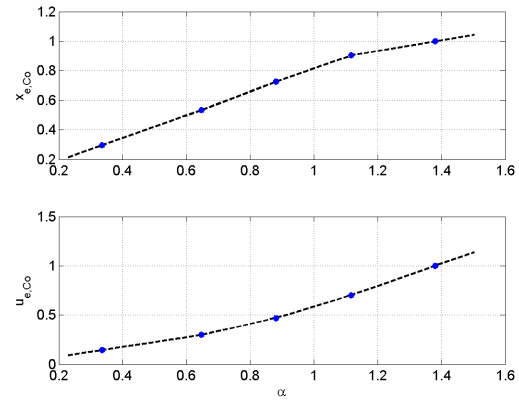

Figure 95: $x_{e,Co}(\alpha(t))$ and $u_{e,Co}(\alpha(t))$ as functions of scheduling parameter $\alpha(t)$.

The integral control gain for engine core $k_{i,Co}(\alpha(t))$ and engine prop $k_{i,Pr}(\alpha(t))$ subsystems have been shown as functions of scheduling parameter α in Figures 99 and 100. Piecewise linear interpolation has been used to interpolate $k_{i,k}(\alpha)$ using the predesigned indexed linear controllers, which are given in equations (260) to (264).

To show the stability of the closed-loop reference model for each subsystem, 40 different (30 equilibrium, and 10 non-equilibrium) linearizations have been used to

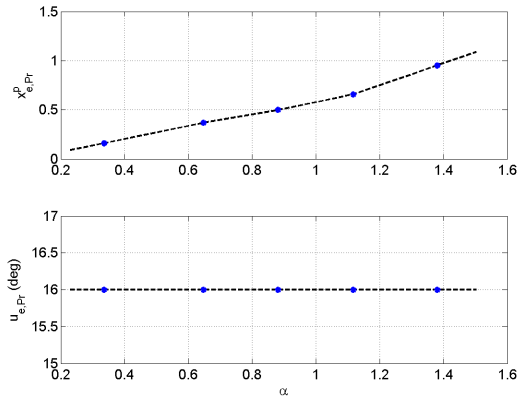

Figure 96: $x_{e,Pr}(\alpha(t))$ and $u_{e,Pr}(\alpha(t))$ as functions of scheduling parameter $\alpha(t)$.

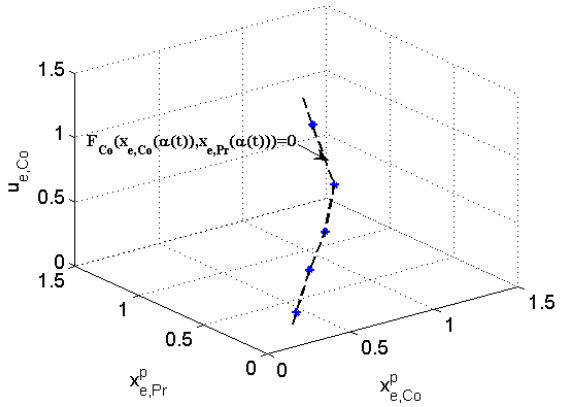

Figure 97: Engine core subsystem equilibrium manifold in 3D space of spool speeds and fuel control input.

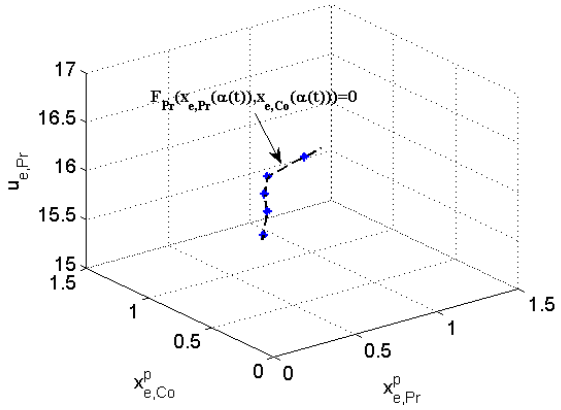

Figure 98: Engine prop subsystem equilibrium manifold in 3D space of spool speeds and pitch angle control input.

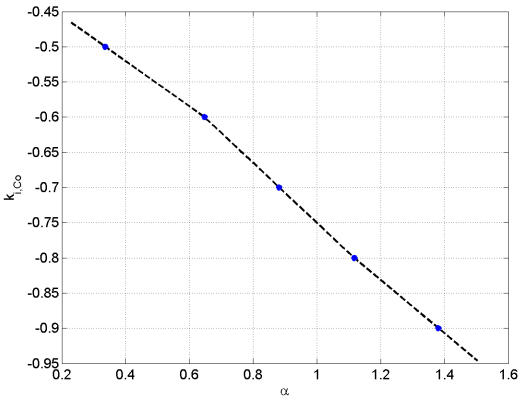

Figure 99: $k_{i,Co}(\alpha(t))$ as a function of scheduling parameter $\alpha(t)$.

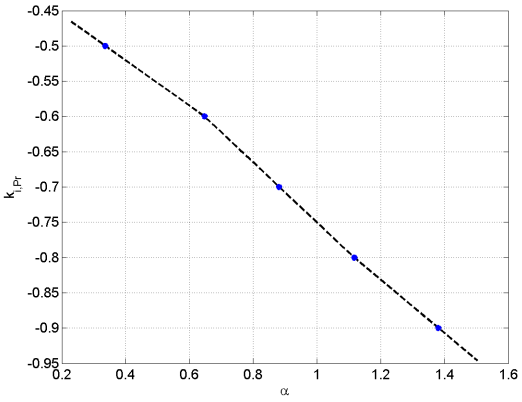

Figure 100: $k_{i,Pr}(\alpha(t))$ as a function of scheduling parameter $\alpha(t)$.

solve inequality (68) in Matlab with the aid of YALMIP [86] and SeDuMi [164] packages. The numerical value for Q_{Co}, and the common matrix P_{Co} for the engine core subsystem is

$$P_{Co} = \begin{bmatrix} 4.9034 & 0.9895 & -0.6234 \\ 0.9895 & 1.7716 & -0.1078 \\ -0.6234 & -0.1078 & 3.4583 \end{bmatrix}, \quad Q_{Co} = 0.1 \times I_3, \tag{265}$$

where the condition number for P_{Co} is $\kappa(P_{Co}) = 3.6384$. The numerical value for Q_{Pr} and the common matrix P_{Pr} for the engine prop subsystem is

$$P_{Pr} = \begin{bmatrix} 1.9015 & 0.0513 & 0.1912 \\ 0.0513 & 0.3882 & -0.0553 \\ 0.1912 & -0.0553 & 1.0811 \end{bmatrix}, \quad Q_{Pr} = 0.1 \times I_3, \tag{266}$$

where its condition number is $\kappa(P_{Pr}) = 5.1066$.

5.5.2 Simulation Results

To show the feasibility of the PnP technology concept for gas turbine engine control systems, three test scenarios are developed. These simulations of D-GS-MRAC architecture include the control of the nominal model (NomEng), the control of the engine with a new propeller (NewProp), and also control of the engine with a new core (NewCore). These decentralized adaptive control case studies simulate the engine acceleration from the idle thrust to the cruise condition and then its deceleration back to the idle condition in a stable manner, with proper tracking performance, for the standard day at sea level condition. To simulate new engine cores and propellers, the low and high pressure spool inertias are changed. The nominal values for the spool inertias and also the changed values for the new engine core and prop subsystems are shown in Table 6.

Table 6: Values for engine PnP test scenarios

Case	**HP Spool Inertia (I_{hps})**	**LP Spool Inertia (I_{lps})**
Nominal Engine (NomEng)	4×10^{-5} $(kg.m^2)$	0.0216 $(kg.m^2)$
Nominal Core with a New Prop (NewProp)	4×10^{-5} $(kg.m^2)$	$0.0216\times$ 2 $(kg.m^2)$
Nominal Prop with a New Core (NewCore)	$4\times10^{-5}\times$ 2 $(kg.m^2)$	0.0216 $(kg.m^2)$

The developed decentralized control structure for the gas turbine engine has two control loops, one for the engine prop subsystem and one for the engine core subsystem. Fuel flow is the main control input for the engine core subsystem and prop pitch angle is the main control input for the engine prop subsystem. The main goals for core and

prop control loops are to force the core and prop spool speeds to track their desired trajectories. In these simulations $r_{Pr}(t)$ is the reference signal for the engine prop subsystem output, and $r_{Co}(t)$ is the reference signal for the core subsystem output; and they change from idle to cruise condition.

The initial conditions for each subsystems and the numerical values for the corresponding adaptive controllers are set as follows

$$\begin{gathered} x_{Co}(0) = x_{m,Co}(0) = [0.295,\ 0.145,\ 0]^{\mathsf{T}}, \\ x_{Pr}(0) = x_{m,Pr}(0) = [0.161,\ 16,\ 0]^{\mathsf{T}}, \\ \hat{K}_{Co}(0) = [0,\ 0,\ -0.49]^{\mathsf{T}}, \quad \hat{K}_{Pr}(0) = [0,\ 0,\ -0.49]^{\mathsf{T}}, \\ \Gamma_{Co} = \mathrm{diag}([10,\ 10,\ 10]), \quad \Gamma_{Pr} = \mathrm{diag}([10,\ 10,\ 10]), \\ K^*_{Co} \in \theta_{k_{Co}} = [[-2,\ 0], [-2,\ 0], [-2,\ 0]]^{\mathsf{T}}, \\ K^*_{Pr} \in \theta_{k_{Pr}} = [[-2,\ 0], [-2,\ 0], [-2,\ 0]]^{\mathsf{T}}. \end{gathered} \tag{267}$$

5.5.2.1 NewProp Scenario: Matching Nominal Engine Core with a New Prop

In this scenario, we match a new engine propeller with the nominal engine core. To simulate a new engine prop, we assumed the low pressure spool inertia is $I_{lps,new} = 2I_{lps,nom}$. Simulation results for this scenario are shown in Figures 101 to 120.

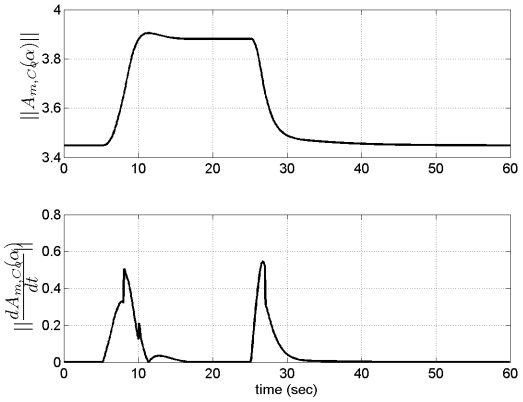

Figure 101: Norm of reference model matrix for engine core subsystem ($||A_{m,Co}(t)||$).

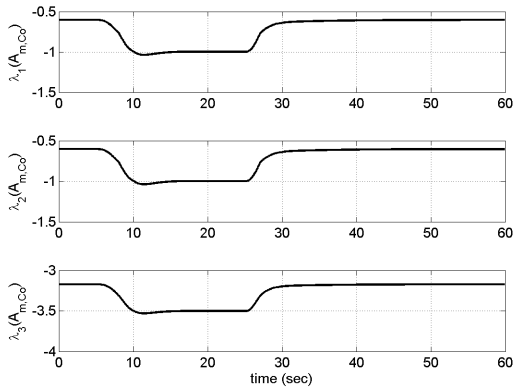

Figure 102: Engine core subsystem reference model eigenvalues ($\lambda[A_{m,Co}(\alpha(t))]$).

Figure 101 shows the history of the norm of the desired reference system matrix $||A_{m,Co}(t)||$ for the engine core subsystem. As it can be seen, the figure shows the boundedness of these two matrices, in accordance with Assumption 5, where $M_{A_{Co}} = 3.8986$. Figure 102 shows the history of the desired reference system matrix eigenvalues $\lambda[A_{m,Co}(\alpha(t))]$ for the core subsystem. As it is apparent, all three eigenvalues remain negative with the time change of the scheduling parameter α.

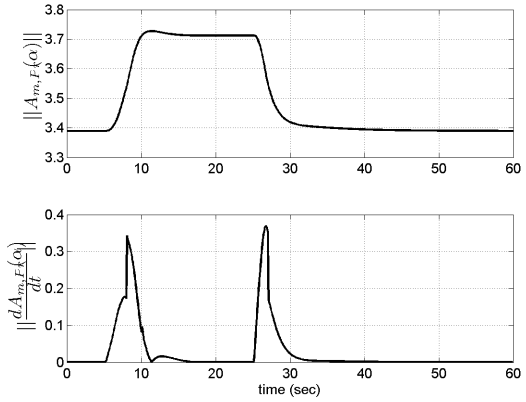

Figure 103: Norm of reference model matrix for engine prop subsystem ($||A_{m,Pr}(t)||$).

Figure 103 shows the history of the norm of the desired reference system matrix $||A_{m,Pr}(t)||$ for the engine prop subsystem. As it can be seen, the figure shows the boundedness of these two matrices, in accordance with Assumption 5, where

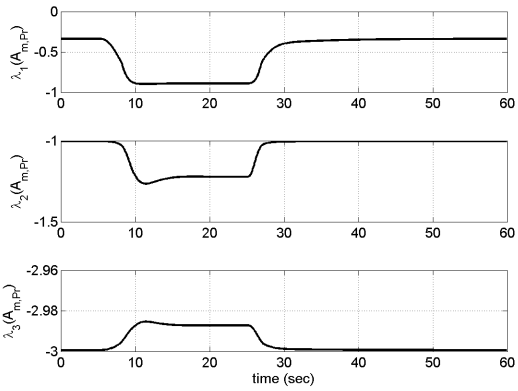

Figure 104: Engine prop subsystem reference model eigenvalues ($\lambda[A_{m,Pr}(\alpha(t))]$).

$M_{A_{Pr}} = 3.7237$. Figure 104 shows the history of the desired reference system matrix eigenvalues $\lambda[A_{m,Pr}(\alpha(t))]$ for the core subsystem. As it is apparent, all three eigenvalues remain negative with the time change of the scheduling parameter $\alpha(t)$.

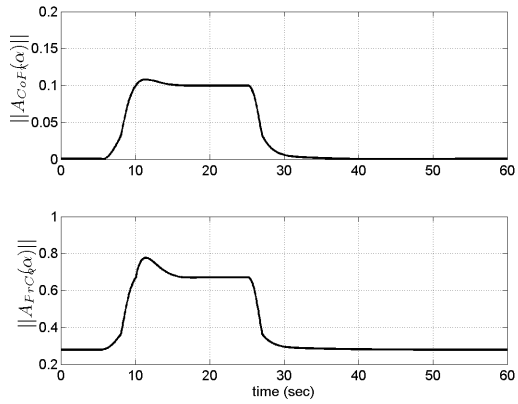

Figure 105: Norm of interference matrices for the engine core ($||A_{CoPr}(t)||$) and prop subsystems ($||A_{PrCo}(t)||$).

Figure 105 shows the history of the norm of interference matrices for the engine core ($||A_{CoPr}(t)||$) and prop subsystems ($||A_{PrCo}(t)||$). Figure 106 shows the history of the scheduling parameter $\alpha(t) = p(y(t)) = ||y(t)|| = ||x^p(t)||$; it is defined as the Euclidean norm of the engine spool speeds. The rate of the scheduling parameter, $\dot{\alpha}(t) = \frac{x^{p\mathsf{T}}(t)\dot{x}^p(t)}{||x^p(t)||}$, also has been plotted.

Figures 107 and 108 show the output of the core subsystem ($x^p_{Co}(t)$) and prop

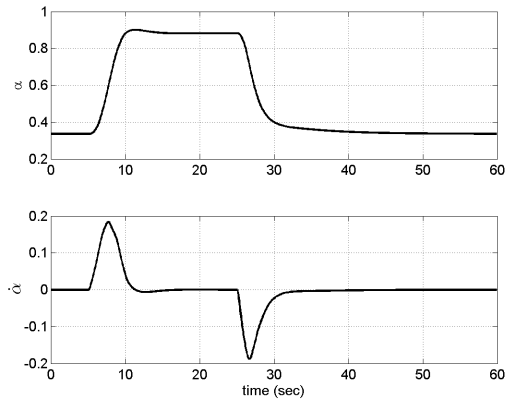

Figure 106: Scheduling Parameter ($\alpha(t) = ||x^p(t)||$) and its rate of change ($\dot{\alpha}(t)$) for the nominal engine case.

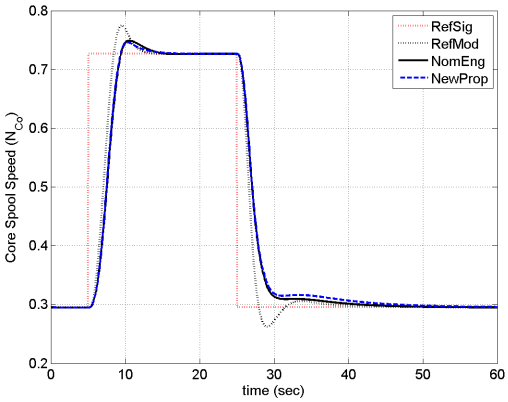

Figure 107: Core spool speed and its reference signal.

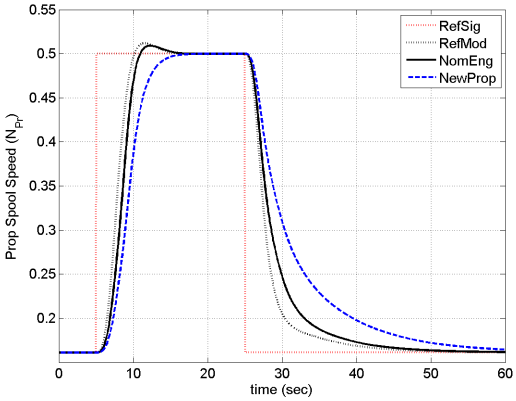

Figure 108: Prop spool speed and its reference signal.

subsystem ($x^p_{Pr}(t)$), tracking their reference signals. Figures 109 and 110 show core and prop spool acceleration histories.

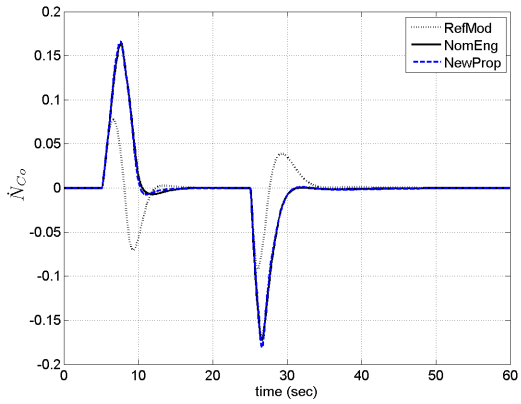

Figure 109: Core spool acceleration.

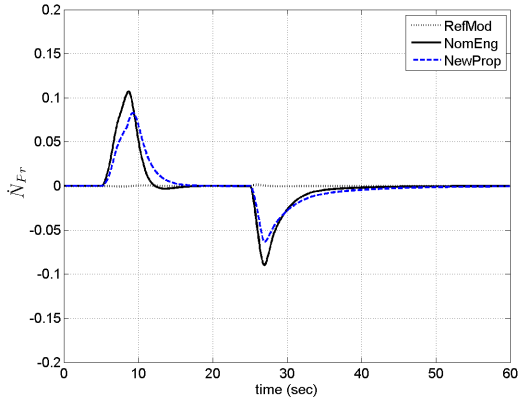

Figure 110: Prop spool acceleration.

Figure 111 shows the controller states for engine core ($x^c_{Co}(t)$) and prop ($x^c_{Pr}(t)$) subsystems. Figure 112 shows the evolution of the control inputs to the augmented engine core ($v_{Co}(t)$) and prop ($v_{Pr}(t)$) subsystems; each element is corresponding to one of the control inputs to the original subsystem.

Figure 113 shows time rates of fuel ($\dot{u}_{Co}(t)$) and prop pitch angle ($\dot{u}_{Pr}(t)$) inputs. Figure 114 shows the histories of fuel flow ($u_{Co}(t)$) and propeller pitch angle ($u_{Pr}(t)$) as the control inputs to each subsystem. Figures 115 shows gain scheduled and adaptive

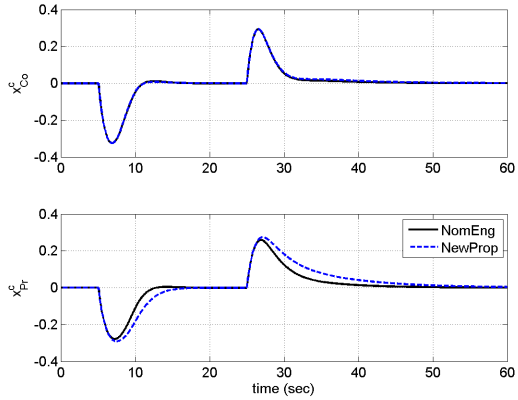

Figure 111: Controller states for engine core ($x^c_{Co}(t)$) and prop ($x^c_{Pr}(t)$) subsystems.

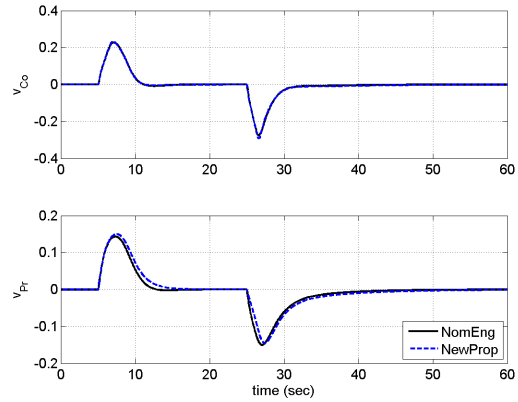

Figure 112: Control inputs to the augmented engine core ($v_{Co}(t)$) and prop ($v_{Pr}(t)$) subsystems.

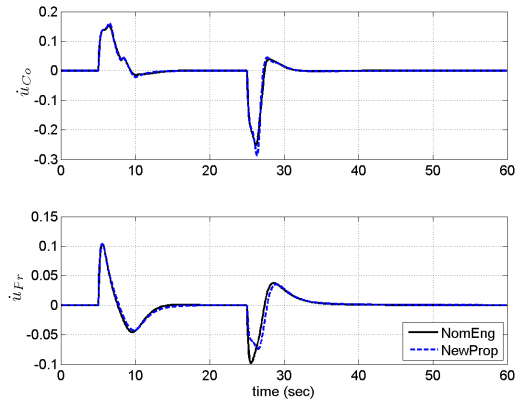

Figure 113: Rate of change for fuel ($\dot{u}_{Co}(t)$) and prop pitch angle ($\dot{u}_{Pr}(t)$) control inputs.

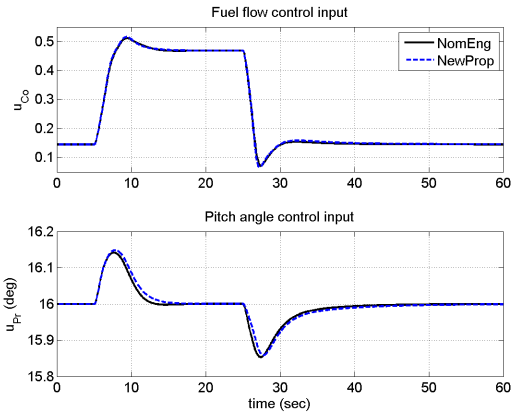

Figure 114: Fuel ($u_{Co}(t)$) and prop pitch angle ($u_{Pr}(t)$) control inputs.

integral gain for the engine core ($k_{i,Co}(\alpha(t))$, $\hat{k}_{i,Co}(t)$) and prop ($k_{i,Pr}(\alpha(t))$, $\hat{k}_{i,Pr}(t)$) subsystems. The gain scheduled control gains have been obtained by interpolation using the predesigned indexed family of fixed-gain controllers, and each controller corresponds to one equilibrium point of the engine. The numerical values of these gains are given in (262) to (264), which represent the controller gains for idle and cruise condition and one more equilibrium point in between these two operating points. $\hat{k}_{i,Co}(t)$ and $\hat{k}_{i,Pr}(t)$ are generated using adaptive laws designed for each subsystem.

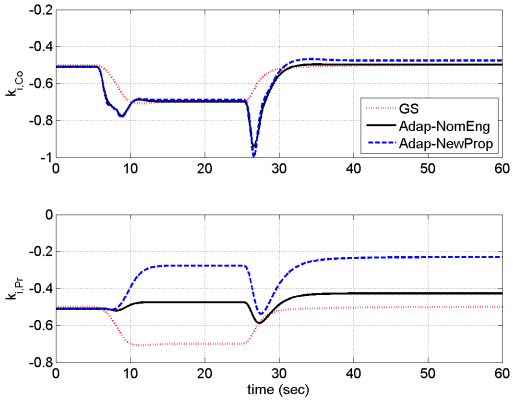

Figure 115: Gain scheduled and adaptive integral gain for the engine core ($k_{i,Co}(\alpha(t))$, $\hat{k}_{i,Co}(t)$), and prop ($k_{i,Pr}(\alpha(t))$, $\hat{k}_{i,Pr}(t)$) subsystems.

Figure 116 shows the history of thrust; as it is apparent thrust follows its reference command from idle to cruise condition and then back to the idle for standard day,

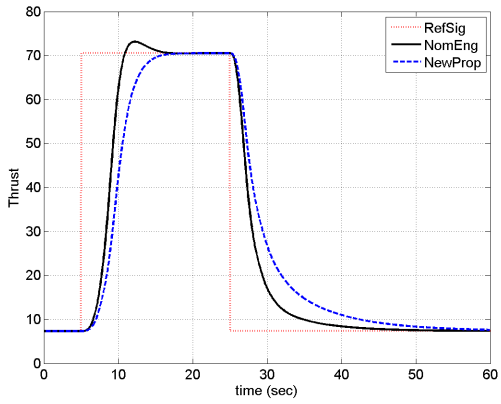

Figure 116: Thrust and its reference signal for NomEng and NewProp cases.

sea level condition. Figure 117 shows the evolution of the infinity norm of the errors $||e_{Co}(t)||$ and $||e_{Pr}(t)||$. Figure 118 shows norm of the interconnection terms for the engine core $||h_{Co}(t)||$, and prop $||h_{Pr}(t)||$ subsystems.

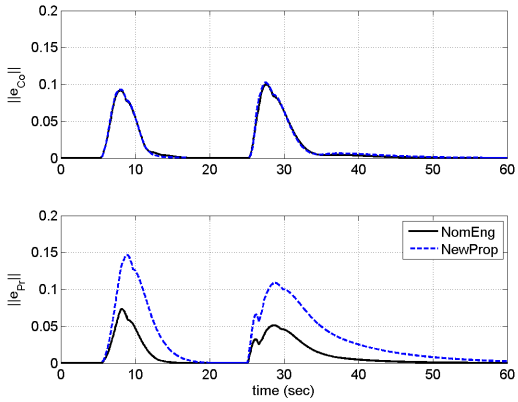

Figure 117: Norm of the error signals for the engine core $||e_{Co}(t)||$ and prop $||e_{Pr}(t)||$ subsystems.

Figure 119 shows the histories of turbine temperature, thrust specific fuel consumption (TSFC), compressor pressure ratio, and corrected air flow rate. Figure 120 shows the JetCat SPT5 turboshaft engine compressor map. In this map the approximate stall line and also the operating line for this simulation have been shown. The engine operates in a safe region with a big stall margin during its acceleration from idle to cruise and again during its deceleration back to the idle condition. The engine

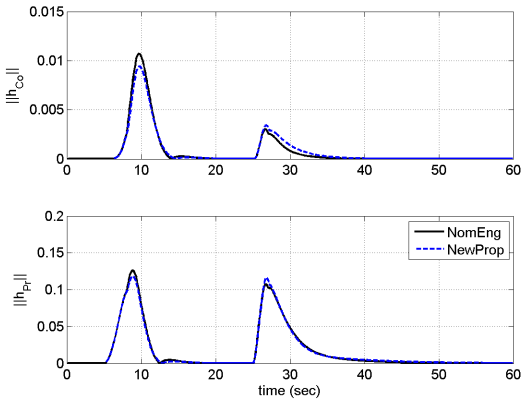

Figure 118: Norm of the interconnection terms for the engine core $||h_{Co}(t)||$, and prop $||h_{Pr}(t)||$ subsystems.

operating lines for the nominal engine and the new engine prop simulation scenarios are shown in this figure.

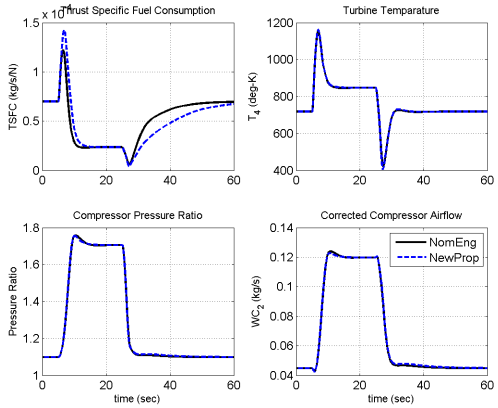

Figure 119: Turbine temperature, TSFC, compressor overall pressure ratio, and air flow rate histories.

5.5.2.2 NewCore Scenario: Matching a New Engine Core with the Nominal Prop

In this scenario, we match a new engine core with the nominal engine propeller. To simulate a new engine core, we assumed the high pressure spool inertia is $I_{hps,new} = 2I_{hps,nom}$. Simulation results for this scenario are shown in Figures 121 to 134.

Figures 121 and 122 show the output of the core subsystem $(x^p_{Co}(t))$ and prop subsystem $(x^p_{Pr}(t))$ tracking their reference signals. Figures 123 and 124 show core

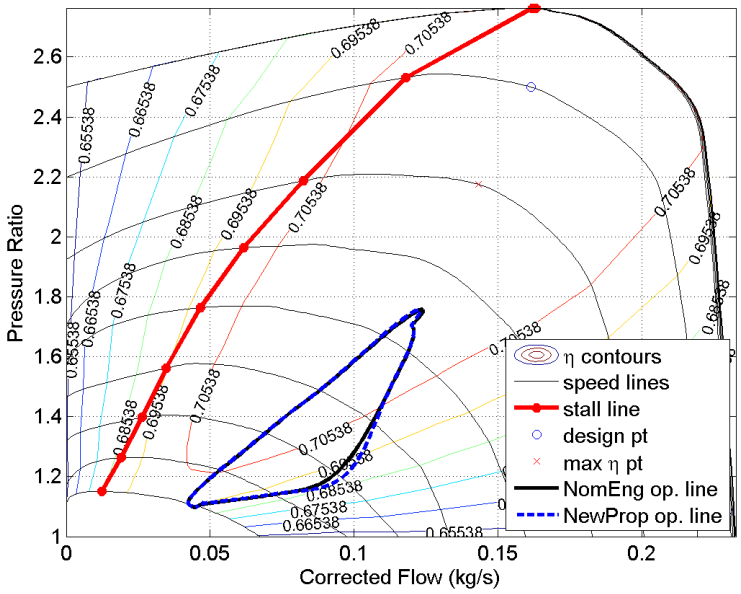

Figure 120: JetCat SPT5 engine compressor map with the operating lines for for NomEng and NewProp cases.

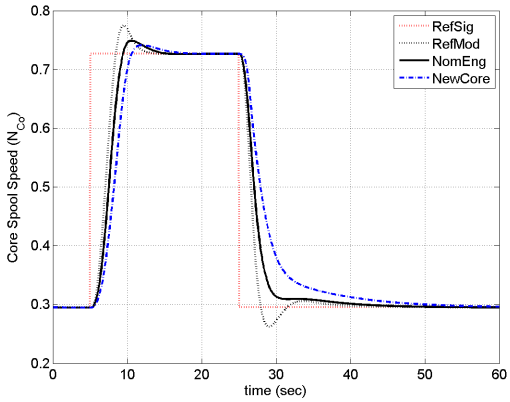

Figure 121: Core spool speed and its reference signal.

and prop spool acceleration histories.

Figure 125 shows the controller states for engine core ($x^c_{Co}(t)$) and prop ($x^c_{Pr}(t)$) subsystems. Figure 126 shows the evolution of the control inputs to the augmented engine core ($v_{Co}(t)$) and prop ($v_{Pr}(t)$) subsystems; each element is corresponding to one of the control inputs to the original subsystem.

Figure 127 shows time rates of fuel ($\dot{u}_{Co}(t)$) and prop pitch angle ($\dot{u}_{Pr}(t)$) inputs.

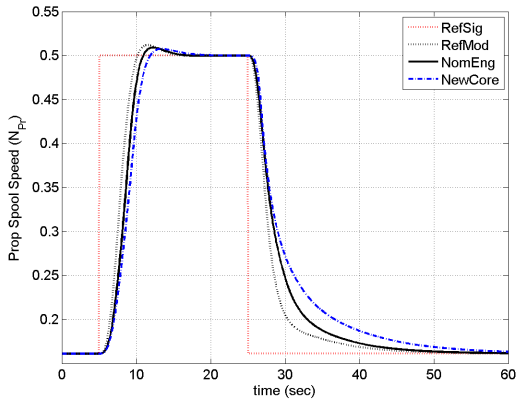

Figure 122: Prop spool speed and its reference signal.

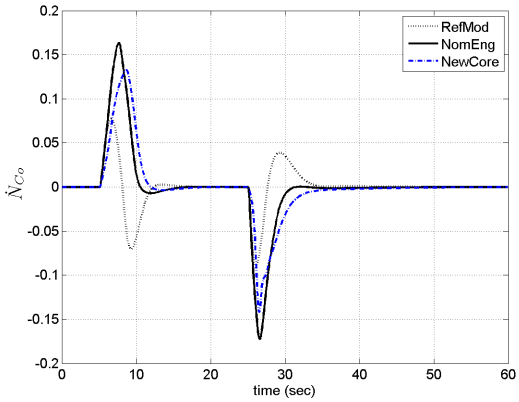

Figure 123: Core spool acceleration.

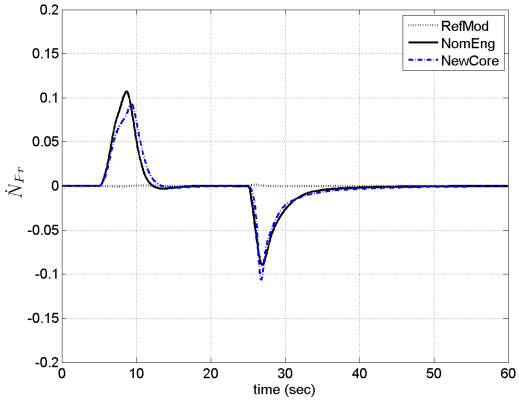

Figure 124: Prop spool acceleration.

Figure 128, shows the histories of fuel flow ($u_{Co}(t)$) and propeller pitch angle ($u_{Pr}(t)$) as the control inputs to each subsystem. Figures 129 shows gain scheduled and

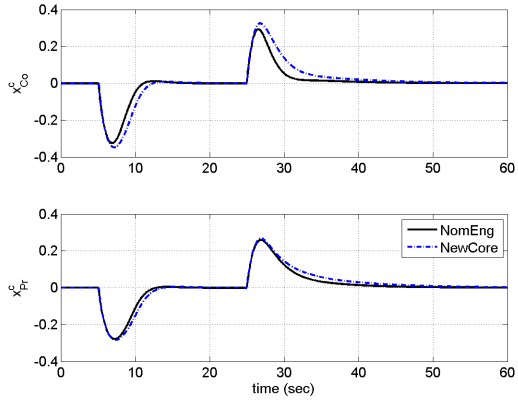

Figure 125: Controller states for engine core ($x^c_{Co}(t)$) and prop ($x^c_{Pr}(t)$) subsystems.

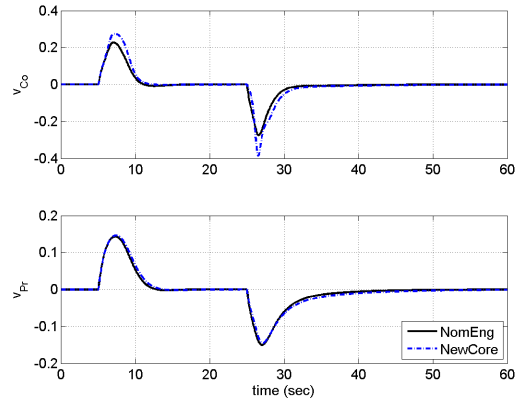

Figure 126: Control inputs to the augmented engine core ($v_{Co}(t)$) and prop ($v_{Pr}(t)$) subsystems.

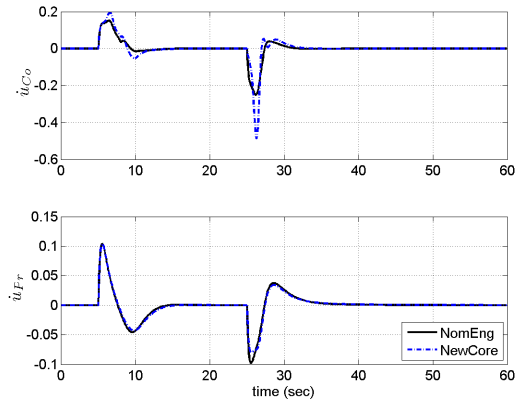

Figure 127: Rate of change for fuel ($\dot{u}_{Co}(t)$) and prop pitch angle ($\dot{u}_{Pr}(t)$) control inputs.

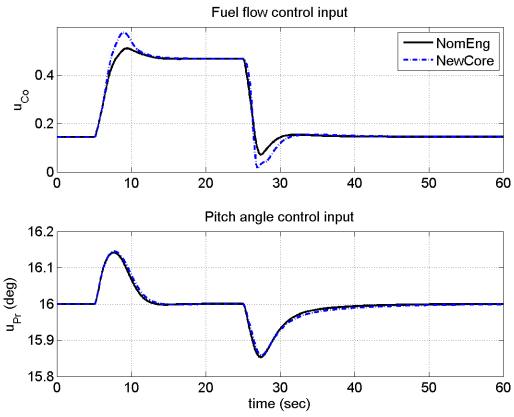

Figure 128: Fuel ($u_{Co}(t)$) and prop pitch angle ($u_{Pr}(t)$) control inputs.

adaptive integral gain for the engine core ($k_{i,Co}(\alpha(t))$, $\hat{k}_{i,Co}(t)$) and prop ($k_{i,Pr}(\alpha(t))$, $\hat{k}_{i,Pr}(t)$) subsystems. The gain scheduled control gains have been obtained by interpolation using the predesigned indexed family of fixed-gain controllers, and each controller corresponds to one equilibrium point of the engine. The numerical values of these gains are given in (262) to (264), which represent the controller gains for idle and cruise condition and one more equilibrium point in between these two operating points. $\hat{k}_{i,Co}(t)$ and $\hat{k}_{i,Pr}(t)$ are generated using adaptive laws designed for each subsystem.

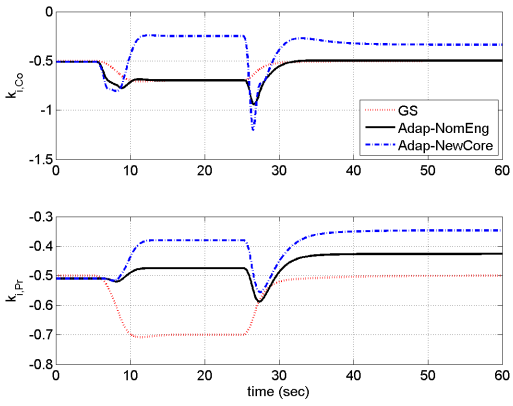

Figure 129: Gain scheduled and adaptive integral gain for the engine core ($k_{i,Co}(\alpha(t))$, $\hat{k}_{i,Co}(t)$), and prop ($k_{i,Pr}(\alpha(t))$, $\hat{k}_{i,Pr}(t)$.) subsystems

Figure 130 shows the history of thrust; and it can be seen thrust is following

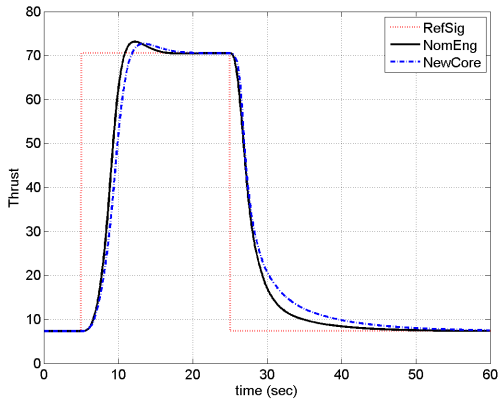

Figure 130: Thrust and its reference signal for NomEng and NewCore cases.

its reference command from idle to cruise condition and then back to the idle for standard day, sea level condition. Figure 131 shows the evolution of the infinity norm of the errors $||e_{Co}(t)||$ and $||e_{Pr}(t)||$. Figure 132 shows norm of the interconnection terms for the engine core $||h_{Co}(t)||$ and prop $||h_{Pr}(t)||$ subsystems.

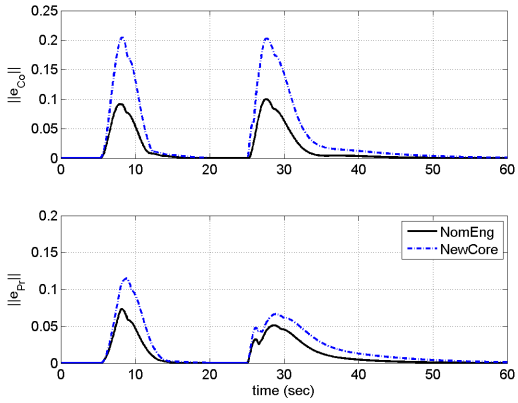

Figure 131: Norm of the error signals for the engine core $||e_{Co}(t)||$, and prop $||e_{Pr}(t)||$ subsystems.

Figure 133 shows the histories of turbine temperature, thrust specific fuel consumption (TSFC), compressor pressure ratio, and corrected air flow rate. Figure 134 shows the JetCat SPT5 turboshaft engine compressor map. In this map the approximate stall line and also the operating line for this simulation have been shown. The engine operates in a safe region with a big stall margin during its acceleration from

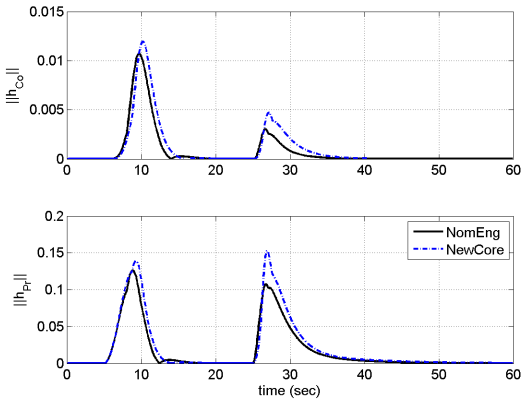

Figure 132: Norm of the interconnection terms for the engine core $||h_{Co}(t)||$, and prop $||h_{Pr}(t)||$ subsystems.

idle to cruise and again during its deceleration back to the idle condition. The engine operating lines for the nominal engine and the new engine prop simulation scenarios are shown in this figure.

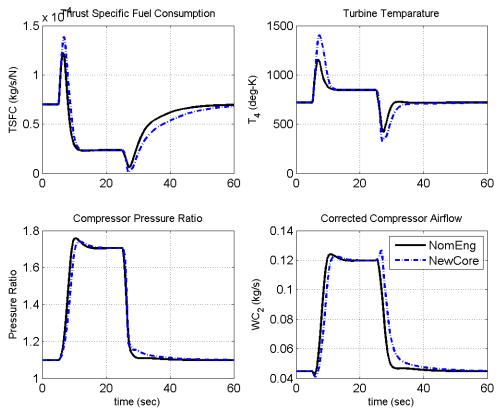

Figure 133: Turbine temperature, TSFC, compressor overall pressure ratio, and air flow rate histories.

These simulations show the successful control of a turboshaft engine model in a decentralized structure for large thrust commands using D-GS-MRAC architecture. These decentralized control case studies simulate acceleration of the engine subsystems from idle thrust to the cruise condition and then their deceleration back to the idle condition in the standard day at sea level condition for nominal engine and two

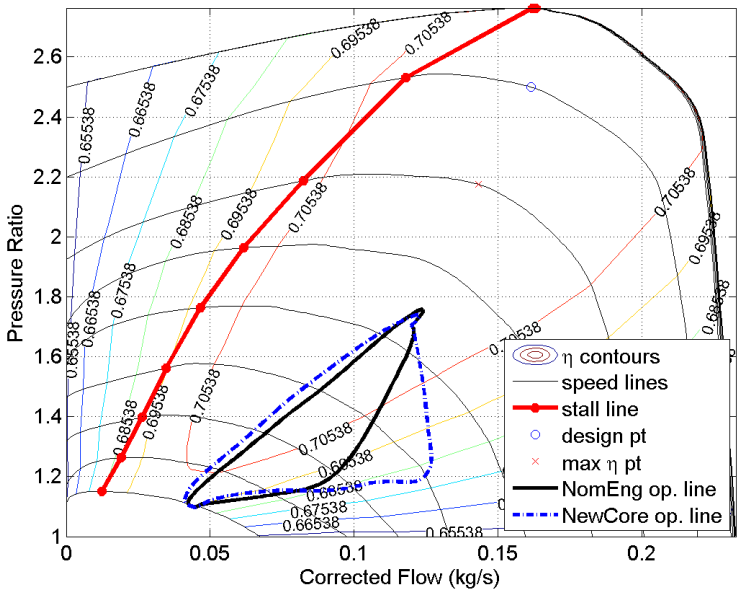

Figure 134: JetCat SPT5 engine compressor map with the operating lines for NomEng and NewCore cases.

other scenarios. These scenarios are defined to test the PnP concept development for engine control including matching various engine cores with various engine props; as it can be observed, all the signals for all the subsystems are bounded. Using the developed decentralized gain scheduled model reference adaptive control algorithm we can match different engine core and prop subsystems in various conditions.

5.5.3 Engine Limit Control Discussion

In order to handle the turbine engine system performance limits for the decentralized architecture, the developed decentralized gain scheduled model reference adaptive control (D-GS-MRAC) system can be integrated with a reference governor. Reference governors have been developed previously; one good option is developed in [18]. However, other approaches are also available to overcome the engine performance limit issue. Detailed development of the D-GS-MRAC system combined with a reference governor is a topic for future research.

5.6 Summary

D-GS-MRAC rigorous stability analysis was done by proving the uniform ultimate boundedness of the error signals for all the subsystems. Sufficient conditions for uniform ultimate boundedness of the entire system were derived. The decentralized engine model has two subsystems including the engine core with fuel flow as its control input, and the engine propeller with prop pitch angle as its control input; the control inputs are computed independently for each subsystem. Through the simulation based on a physics-based nonlinear model of the JetCat SPT5 turboshaft engine with a new engine core or prop, it was demonstrated that the proposed decentralized adaptive controllers are capable of regulating the outputs in each subsystem for the entire flight envelope of the engine. The developed D-GS-MRAC can be used to design PnP technology for the control systems of turboshaft engines with guaranteed stability and proper tracking performance.

CHAPTER VI

CONCLUDING REMARKS AND FUTURE RESEARCH

6.1 Concluding Remarks

In Chapter 2, a nonlinear physics-based model was developed for a twin spool JetCat SPT5 turboshaft engine which drives a variable pitch propeller. The model was then implemented using Matlab. Two spool speeds were used as the two main states, and fuel flow rate and propeller pitch angle were used as two control inputs of the state-space model. The model was verified with experimental data obtained from engine static tests. Performance maps for the propeller, compressor, and turbines were also constructed based on the gathered experimental data. As a result of the experimental tests, the propeller pitch angle of 16 deg. was found to be the optimal steady state angle setting. Open-loop simulation results of the engine model were also presented. This physics-based model of the JetCat SPT5 turboshaft engine was developed for nonlinear control research applicable to gas turbine engines.

In Chapter 3, first a MIMO parameter dependent linear model of the nonlinear gas turbine engine system was developed. Then, a gain scheduled controller with stability guarantees for this system was designed. Piecewise linear interpolation technique was used for interpolating the parameter varying gain scheduled controller in between the predesigned indexed family of fixed-gain controllers. The scheduling variable in the design process is defined to be the Euclidean norm of the gas turbine engine spool speeds. Using the global linearization method, guaranteed stability of the closed-loop gas turbine engine system with a gain scheduled controller was shown. With the aid of convex optimization tools, a single quadratic Lyapunov function was computed, which guaranteed the stability of the gain scheduled gas turbine engine system. To verify the

stability of the closed-loop system, an optimization problem was proposed, which was solved with sufficiently small optimization error history, using convex optimization tools. Simulation results were presented to show the applicability of the proposed controller to the nonlinear physics-based JetCat SPT5 turboshaft engine model for large thrust commands from idle to cruise condition, and vice versa. Many other simulations were performed to fully verify system performance and stability.

In Chapter 4, complete GS-MRAC stability analysis was fulfilled by proving the boundedness of the error signal, in addition to transient and steady-state performance guarantees. Then the results extended to the GS-MRAC system with constraints on the magnitudes of multi control inputs. Sufficient conditions for ultimate boundedness of the closed-loop system were derived. A semi-global stability result was proved with respect to the level of saturation for open-loop unstable plants while the stability result becomes global for open-loop stable plants. Through the simulation studies on the physics-based nonlinear model of the JetCat SPT5 turboshaft engine with degradation due to aging, it was demonstrated even in the presence of the control magnitude saturation the proposed adaptive controller tracks the reference model with guaranteed stability and proper tracking performance. The developed GS-MRAC is not only useful to control degraded gas turbine engines, but also can be used for other practical applications.

In Chapter 5, complete D-GS-MRAC stability analysis was done by proving the uniform ultimate boundedness of the error signals for all the subsystems. Sufficient conditions for uniform ultimate boundedness of the entire system were derived. Through simulation studies on the physics-based nonlinear model of the JetCat SPT5 turboshaft engine with swapped engine core and prop, it was demonstrated that the proposed decentralized and separate adaptive controllers are successful to regulate the outputs of the subsystems to track their reference models for the entire flight envelope of the engine. The developed D-GS-MRAC can be used to design PnP technology for

the control systems of the turboshaft engines with guaranteed stability and proper tracking performance. In the developed PnP concept, each subsystem of the engine (i.e. engine core and engine prop) has its own independent controller.

6.2 Recommended Future Research

We recommend the following future research topics:

(*i*) Developing complete software verification analysis for GS control of the gas turbine systems using the Lyapunov stability approach. Since we showed that the gain scheduled engine system is stable by computing a single quadratic Lyapunov equation, the engine control software verification process can be done using the Lyapunov stability method combined with temporal logic, and Floyd-Hoare framework [33, 124].

(*ii*) Analyzing the integration of the developed GS, GS-MRAC, and D-GS-MRAC architectures with a reference governor [18] which helps handling the engine performance limits.

(*iii*) Since the problem of adaptive control of systems with unmatched uncertainties and unmodelled dynamics is not an entirely solved problem in the adaptive control literature [49], theoretical stability analysis for this problem in the context of GS-MRAC can be a topic of future research. One of the interesting examples of such a situation can be observed in the systems with equilibrium shift (e.g. deteriorated or damaged gas turbine engines).

(*iv*) Developing stability proofs for D-GS-MRAC with constrained control inputs, which is useful for constructing better PnP architectures for gas turbine engine control systems.

(*v*) In the current PnP engine architecture, the two subsystems of the D-GS-MRAC use the same scheduling parameter $\alpha(t) = ||[x^p_{Co}, x^p_{Pr}]^\mathsf{T}||$. One interesting problem to follow is to investigate the stability of the D-GS-MRAC architecture in

which each subsystem has its own independent scheduling parameters, i.e., define $\alpha_k(t) = |x_k^p|$ for the kth subsystem.

(*vi*) Since there is no self-tuning process involved in the control architecture of the developed PnP concept for engine control, one possible improvement could be the integration of some form of online optimization (or self-tuning) capability in the distributed control architecture using the peak-seeking control technique described in [137].

(*vii*) Developing a complete setup of the JetCat SPT5 distributed control hardware for experimental implementation of the developed GS, GS-MRAC, and D-GS-MRAC architectures.

REFERENCES

[1] "JetCat SPT5 Turboshaft Engine Manual," JetCat USA, 2009.

[2] "Aurora Flight Sciences Inc.," 2012. URL: `http://www.aurora.aero`.

[3] "JetCat SPT5 Turboshaft Engine," 2012. URL: `http://www.jetcatusa.com/spt5.html`.

[4] "MIT Gas Turbine Lab (GTL)," 2012. URL: `http://web.mit.edu/aeroastro/labs/gtl/index.html`.

[5] Ajami, A., Hovakimyan, N., and Lavretsky, E., "Design Examples: Adaptive Tracking Control in the Presence of Input Constraints for a Fighter Aircraft and a Generic Missile," in *Proceedings of the AIAA Guidance, Navigation and Control Conference*, (San Francisco, CA), 2005.

[6] Akhtar, S. and Bernstein, D. S., "Lyapunov-Stable Discrete-Time Model Reference Adaptive Control," in *Proceedings of the 2005 American Control Conference*, vol. 5, pp. 3174–3179, 2005.

[7] Akhtar, S. and Bernstein, D. S., "Lyapunov-Stable Discrete-Time Model Reference Adaptive Control," *International Journal of Adaptive Control and Signal Processing*, vol. 19, no. 10, pp. 745–767, 2005.

[8] Akhtar, S., Bernstein, D., and Venugopal, R., "Discrete-Time Direct Adaptive Stabilization," in *Proceedings of the 2003 American Control Conference*, vol. 1, pp. 214–219, 2003.

[9] Annaswamy, A. M., Jang, J., and Lavretsky, E., "Adaptive Gain-Scheduled Controller in the Presence of Actuator Anomalies," in *Proceedings of the AIAA Guidance, Navigation and Control Conaerence*, (Honolulu, Hawaii), 2008.

[10] Aouf, N., Bates, D. G., Postlethwaite, I., and Boulet, B., "Scheduling Schemes for an Integrated Flight and Propulsion Control System," *Control Engineering Practice*, vol. 10, no. 7, pp. 685–696, 2002.

[11] Ariffin, A. E. and Munro, N., "Robust Control Analysis of a Gas-Turbine Aeroengine," *IEEE Transactions on Control Systems Technology*, vol. 5, no. 2, pp. 178–188, 1997.

[12] Astrom, K. J. and Wittenmark, B., *Adaptive Control*. Prentice-Hall, Englewood Cliffs, NJ, 1994.

[13] Athans, M., Kapasouris, P., Kappos, E., and Spang III, H. A., "Linear-Quadratic Gaussian with Loop-Transfer Recovery Methodology for the F-100 Engine," *International Journal of Robust and Nonlinear Control*, vol. 9, no. 1, pp. 45–52, 1986.

[14] Aurora Flight Sciences, "Excalibur UAV," 2012. URL: `http://www.aurora.aero/ TacticalSystems/Excalibur.aspx`.

[15] Aurora Flight Sciences, "Golden Eye 80 UAV," 2012. URL: `http://www.aurora.aero/TacticalSystems/GoldenEye80.aspx`.

[16] Balas, G., "Linear Parameter-Varying Control and Its Application to a Turbofan Engine," *International Journal of Robust and Nonlinear Control*, vol. 12, no. 9, pp. 763–796, 2002.

[17] Behbahani, A., and Culley, D., and Smith, B. J., and Darouse, C., and Millar, R., and Wood, B., and Krodel, J., and Carpenter, S., and Mailander, B., and Mahoney, T., and Quinn, R., and Bluish, C., and Hegwood, B., and Battestin, G., and Roney, W., and Rhoden, W., and Storey, B., "Status Vision and Challenges of an Intelligent Distributed Engine Control Architecture," in *Proceedings of SAE AeroTech Congress and Exhibition*, (Los Angeles, CA), SAE, 2007.

[18] Bemporad, A., "Reference Governor for Constrained Nonlinear Systems," *IEEE Transactions on Automatic Control*, vol. 43, no. 3, pp. 415–419, 1998.

[19] Boyce, M. P., *Gas Turbine Engineering Handbook*. Elsevier, Burlington, MA, third ed., 2006.

[20] Boyd, S., El Ghaoui, L., Feron, E., and Balakrishnan, V., *Linear Matrix Inequalities in System and Control Theory*. Philadelphia: SIAM, 1994.

[21] Bruzelius, F., Breitholtz, C., and Pettersson, S., "LPV-Based Gain Scheduling Technique Applied to a Turbofan Engine Model," in *Proceedings of the 2002 International Conference on Control Applications*, pp. 713–718, 2002.

[22] Butchart, R. L. and Shackcloth, B., "Synthesis of Model Reference Adaptive Control Systems by Lyapunovs Second Method," in *Proc. IFAC Symp. on Adaptive Control*, (Teddington, UK), 1965.

[23] Chatterjee, S. and Litt, J. S., "Online Model Parameter Estimation of Jet Engine Degradation for Autonomous Propulsion Control," NASA Technical Report 212608, 2003.

[24] Chen, Y. H., Leitmann, G., and Xiong, Z. K., "Robust Control Design for Interconnected Systems with Time-Varying Uncertainties," *International Journal of Control*, vol. 54, no. 5, pp. 1119–1124, 1991.

[25] Cohen, H., Rogers, G. F. C., and Saravanamuttoo, H. I. H., *Gas Turbine Theory*. Prentice Hall, Harlow, England, 5th ed., 2001.

[26] Corbett, M. W., Lamm, P. T., Miller, K. L., Wolff, J. M., and Walters, E. A., "Transient Analysis of an Aircraft/Propulsion System with Hardware-in-the-Loop Power Extraction," in *Proceedings of the 43th AIAA/ASME/SAE/ASEE Joint Propulsion Conference*, (Cincinnati, OH), 2007.

[27] Corbett, M. W., Lamm, P. T., Owen, P. R., Phillips, S. D., Blackwelder, M. J., Alt, J. T., McNichols, J. M., Boyd, M. A., and Wolff, J. M., "Transient Turbine Engine Modeling with Hardware-in-the-Loop Power Extraction," in *Proceedings of the 6th International Energy Conversion Engineering Conference*, (Cleveland, OH), 2008.

[28] Culley, D. and Saus, T. R., "Concepts for Distributed Engine Control," in *Proceedings of the 43rd AIAA/ASME/SAE/ASEE Joint Propulsion Conference*, (Cincinnati, OH), 2007.

[29] Cumpsty, N., *Jet Propulsion: A Simple Guide to the Aerodynamic and Thermodynamic Design and Performance of Jet Engines*. Cambridge University Press, Cambridge, UK, 2nd ed., 2003.

[30] CVX Research, Inc., "CVX: Matlab Software for Disciplined Convex Programming, version 2.0 beta," 2012. URL: `http://cvxr.com/cvx`.

[31] DeCastro, J. A., Litt, J. S., and Frederick, D. K., "A Modular Aero-Propulsion System simulation of a Large Commercial Aircraft Engine," in *Proceedings of the 44th AIAA/ASME/SAE/ASEE Joint Propulsion Conference*, (Hartford, CT), AIAA-2008-4579, 2008.

[32] Epstein, A., "Aircraft Turbine Engines Course Notes: An Engineering History of Gas Turbines (Lecture 1)." MIT, 2007.

[33] Feron, E., "From Control Systems to Control Software," *IEEE Control Systems Magazine*, vol. 30, pp. 50–71, Dec. 2010.

[34] Feron E., and Roozbehani, M., "Certifying Controls and Systems Software." arXiv:cs/0701132v2 [cs.SE] 23 Jan 2007.

[35] Flack, R. D., *Fundamentals of Jet Propulsion with Applications*. Cambridge University Press, New York, NY, 2005.

[36] Frederick, D., DeCastro, J., and Litt, J., "User's Guide for the Commercial Modular Aero-Propulsion System Simulation (*C-MAPSS*)," NASA Technical Report 215026, 2007.

[37] Frederick, D. K., Garg, S., and Adibhatla, S., "Turbofan Engine Control Design using Robust Multivariable Control Technologies," *IEEE Transactions on Control Systems Technology*, vol. 8, no. 6, pp. 961–970, 2000.

[38] Garg, S., "Turbofan Engine Control System Design Using the LQG/LTR Methodology," in *Proceedings of the American Control Conference*, (Pittsburgh, PA), 1989.

[39] Garg, S., "A Simplified Scheme for Scheduling Multivariable Controllers," *IEEE Control Systems Magazine*, vol. 17, no. 4, pp. 24–30, 1997.

[40] Gavel, D. T. and Siljak, D. D., "Decentralized Adaptive Control: Structural Conditions for Stability," *IEEE Trans. on Automatic Control*, vol. 34, no. 4, pp. 413–426, 1989.

[41] Gilbert, W., Henrion, D., Bernussou, J., and Boyer, D., "Polynomial LPV Synthesis Applied to Turbofan Engines," *Control Engineering Practice*, vol. 18, no. 9, pp. 1077–1083, 2010.

[42] Goodwin, G. C. and Sin, K. S., *Adaptive Filtering, Prediction, and Control* . Prentice-Hall, Englewood Cliffs, NJ, 1984.

[43] Grant, M. and Boyd, S., "Graph Implementations for Nonsmooth Convex Programs," in *Recent Advances in Learning and Control* (Blondel, V., Boyd, S., and Kimura, H., eds.), Lecture Notes in Control and Information Sciences, pp. 95–110, Springer-Verlag Limited, 2008. URL: `http://stanford.edu/~boyd/graph_dcp.html`.

[44] Grunberg, D. B., *A Methodology for Designing Robust Multivariable Nonlinear Control Systems*. PhD thesis, MIT, 1986.

[45] Haddad, W. M., Hayakawa, T., and Leonessa, A., "Direct Adaptive Control for Discrete-Time Nonlinear Uncertain Dynamical Systems," in *Proceedings of the 2002 American Control Conference*, vol. 3, pp. 1773–1778, 2002.

[46] Han, Z. and Narendra, K. S., "New Concepts in Adaptive Control using Multiple Models," *IEEE Transactions on Automatic Control*, vol. 57, pp. 78–89, Jan. 2012.

[47] Hayakawa, T., Haddad, W. M., and Leonessa, A., "A Lyapunov-Based Adaptive Control Framework for Discrete-Time Non-Linear Systems with Exogenous Disturbances," *INT. J. CONTROL*, vol. 77, no. 3, pp. 250–263, 2004.

[48] Heck, B. S., Wills, L. M., and Vachtsevanos, G. J., "Software Technology for Implementing Reusable, Distributed Control Systems," *IEEE Control Systems Magazine*, vol. 23, pp. 21–35, Feb. 2003.

[49] Hovakimyan, N. and Cao, C., L_1 *Adaptive Control Theory: Guaranteed Robustness with Fast Adaptation*. SIAM, Philadelphia, 2010.

[50] Hovakimyan, N., Lavretsky, E., Yang, B. J., and Calise, A. J., "Coordinated Decentralized Adaptive Output Feedback Control of Interconnected Systems," *IEEE Trans. on Neural Net.*, vol. 16, no. 1, pp. 185–194, 2005.

[51] Hovakimyan, N., "Robust Adaptive Control Course Notes." University of Illinois at Urbana Champaign (UIUC), 2009.

[52] Huang, S., N., Tan, K. K., and Lee, T. H., "Decentralized Control of a Class of Large-Scale Nonlinear Systems using Neural Networks," *Automatica*, vol. 41, no. 9, pp. 1645–1649, 2005.

[53] Hurt, J. M., "New Difference Equation Technique for Solving Nonlinear Differential Equations," in *Proceeding of the Spring Joint Computer Conference*, vol. 25, pp. 169–179, 1964.

[54] Ioannou, P. and Fidan, B., *Adaptive Control Tutorial* . Society for Industrial and Applied Mathematics, Philadelphia, PA, 2006.

[55] Ioannou, P. A., "Decentralized Adaptive Control of Interconnected Systems," *IEEE Trans. on Automatic Control*, vol. AC-31, no. 4, pp. 291–298, 1986.

[56] Ioannou, P. A. and Sun, J., *Robust Adaptive Control*. Prentice Hall, Englewood Cliffs, NJ, 1996.

[57] Jang, J., *Adaptive Control Design with Guaranteed Margins for Nonlinear Plants*. PhD thesis, MIT, 2009.

[58] Jang, J., Annaswamy, A. M., and Lavretsky, E., "Adaptive Control of Time-Varying Systems with Gain-Scheduling," in *Proceedings of the 2008 American Control Conference*, (Seattle, Washington), pp. 3416–3421, 2008.

[59] Jaw, L. C. and Mattingly, J. D., *Aircraft Engine Controls*. American Institute of Aeronautics and Astronautics, Reston, VA, 2009.

[60] Jobredeaux, R., Herencia-Zapana, H., Neogi, N., and Feron, E., "Developing Proof Carrying Code to Formally Assure Termination in Fault Tolerant Distributed Controls Systems," in *IEEE 51st Annual Conference on Decision and Control (CDC)*, (Maui, Hawaii), pp. 1816–1821, Dec. 2012.

[61] Jobredeaux, R., Wang, T., and Feron, E., "Autocoding Control Software with Proofs I: Annotation Translation," in *Proceedings of the IEEE/AIAA 30th Digital Avionics Systems Conference (DASC)*, Oct. 2011.

[62] Johansson, O., Linden, T., and Ornberg, G., "Dynamic Simulation - A Control System Development Tool," Volvo Technology Report, pp. 54-67, 1990.

[63] Johnson, E. N. and Calise, A. J., "Limited Authority Adaptive Flight Control for Reusable Launch Vehicles," *Journal of Guidance, Control, and Dynamics*, vol. 26, pp. 906–913, Mar.-Apr. 2003.

[64] Kanellakopoulos, I., "A Discrete-Time Adaptive Nonlinear System," *IEEE Transactions on Automatic Control*, vol. 39, no. 11, pp. 2362–2365, 1994.

[65] Kapasouris, P., Athans, M., and Spang III, H. A., "Gain-Scheduled Multivariable Control for the GE-21 Turbofan Engine using the LQG/LTR Methodology," in *Proceedings of the American Control Conference*, (Boston, MA), pp. 109–118, 1985.

[66] Karason, S. P. and Annaswamy, A. M., "Adaptive Control in the Presence of Input Constraints," *IEEE Transactions on Automatic Control*, vol. 39, pp. 2325–2330, Nov. 1994.

[67] Kaufman, H., Barkana, I., and Sobel, K., *Direct Adaptive Control Algorithms: Theory and Applications*. Springer-Verlag, London, 1993.

[68] Kelemen, M., "A Stability Property," *IEEE Transactions on Automatic Control*, vol. 31, no. 8, pp. 766–768, 1986.

[69] Kerrebrock, J. L., *Aircraft Engines and Gas Turbines*. The MIT Press, Cambridge, MA, 1996.

[70] Khalil, H. K., *Nonlinear Systems*. third ed., 2002.

[71] Khalil, H. K. and Kokotovic, P. V., "On Stability Properties of Nonlinear Systems with Slowly Varying Inputs," *IEEE Transactions on Automatic Control*, vol. 36, no. 2, p. 229, 1991.

[72] Krstic, M., Kanellakopoulos, I., and Kokotovic, P., *Nonlinear and Adaptive Control Design*. John Wiley and Sons, New York, NY, 1995.

[73] Kulikov, G. G. and Thompson, H. A., *Dynamic Modelling of Gas Turbines: Identification, Simulation, Condition Monitoring and Optimal Control*. Springer-Verlag, London, 2004.

[74] Kurzhanski A., and Valyi, I., *Ellipsoidal Calculus for Estimation and Control*. Birkhauser, Boston, MA, 1997.

[75] Lambiris, B., Mathioudakis, K., Stamatis, A., and Papailiou, K., "Adaptive Modeling of Jet Engine Performance With Application of Condition Monitoring," *Journal of Propulsion and Power*, vol. 10, no. 6, pp. 890–896, 1994.

[76] Lavretsky, E. and Hovakimyan, N., "Positive μ-Modification for Stable Adaptation in the Presence of Input Constraints," in *Proceedings of the American Control Conference*, pp. 2545–2550, July 2004.

[77] Lavretsky, E. and Hovakimyan, N., "Stable Adaptation in the Presence of Actuator Constraints with Flight Control Applications," *Journal of Guidance, Control, and Dynamics*, vol. 30, pp. 337–345, Mar.-Apr. 2007.

[78] Lavretsky, E., "Adaptive Control Course Notes." California Institute of Technology, 2010.

[79] Lavretsky, E., and Gibson, T. E., and Annaswamy, A. M., "Projection Operator in Adaptive Systems." arXiv:1112.4232v6 [nlin.AO], 16 Oct. 2012.

[80] Lawrence, D. A. and Rugh, W. J., "On a Stability Theorem for Nonlinear Systems with Slowly Varying Inputs," *IEEE Transactions on Automatic Control*, vol. 35, no. 7, pp. 860–864, 1990.

[81] Leith, D. J. and Leithead, W. E., "Survey of Gain-Scheduling Analysis and Design," *International Journal of Control*, vol. 73, no. 11, pp. 1001–1025, 2000.

[82] Leonessa, A., Haddad, W., and Hayakawa, T., "Adaptive Tracking for Nonlinear Systems with Input Constraints," in *Proceedings of the American Control Conference*, (Arlington, VA), pp. 1292–1297, June 2001.

[83] Lichtsinder, M. and Levy, Y., "Jet Engine Model for Control and Real-Time Simulations," *Journal of Engineering for Gas Turbines and Power*, vol. 128, pp. 745–753, Oct. 2006.

[84] Liu, R., Saeks, R., and Leake, R. J., "On Global Linearization," *SIAM-AMS proceedings*, pp. 93–102, 1969.

[85] Liu, R. W., "Convergent Systems," *IEEE Transactions on Automatic Control*, vol. AC-13, no. 4, pp. 384–391, 1968.

[86] Löfberg, J., "YALMIP: A Toolbox for Modeling and Optimization in MATLAB," in *Proceedings of the CACSD Conference*, (Taipei, Taiwan), 2004. URL: `http://users.isy.liu.se/johanl/yalmip`.

[87] Lohmiller, W., *Contraction Analysis of Nonlinear Systems*. PhD thesis, MIT, 1999.

[88] Lohmiller, W. and Slotine, J. J. E., "On Contraction Analysis for Nonlinear Systems," *Automatica*, vol. 34, no. 6, pp. 683–695, 1998.

[89] Lur'e, A. I., *Some Nonlinear Problems in the Theory of Automatic Control*. London: Her Majesty's Stationery Office, 1957. A Translation from the Russian Text Published in 1951.

[90] Lur'e, A. I. and Postnikov, V. N., "On the Theory of Stability of Control Systems," *Applied mathematics and mechanics*, vol. 8, no. 3, pp. 246–248, 1944. In Russian.

[91] Lyapunov, A. M., *The General Problem of the Stability of Motion*. Kharkov Mathematical Society, Kharkov, Russia, 1892.

[92] Lyapunov, A. M., *General Problem on Stability of Motion*. Grostechizdat, Moscow, Russia, 1935.

[93] Mattingly, J. D., Heiser, W. H., and Pratt, D. T., *Aircraft Engine Design*. American Institute of Aeronautics and Astronautics, Reston, VA, 2nd ed., 2002.

[94] Mattingly, J. D. and von Ohain, H., *Elements of Propulsion: Gas Turbines and Rockets*. American Institute of Aeronautics and Astronautics, Reston, VA, second ed., 2006.

[95] May, R. D., Csnak, J., Lavelle, T. M., Litt, J. S., and Guo, T.-H., "A High-Fidelity Simulation of a Generic Commercial Aircraft Engine and Controller," in *Proceedings of the 46th AIAA/ASME/SAE/ASEE Joint Propulsion Conference*, (Hartford, CT), AIAA-2010-6630, 2010.

[96] McNichols, J. M., Barnes, C., Wolff, J. M., Baudendistel, T., Corbett, M. W., and Lamm, P. T., "Hardware-in-the-Loop Power Extraction using Different Real-Time Platforms," in *Proceedings of the 6th International Energy Conversion Engineering Conference*, (Cleveland, OH), 2008.

[97] Mink, G. and Behbahani, A., "The AFRL ICF Generic Gas Turbine Engine Model," in *Proceedings of the 41st AIAA/ASME/SAE/ASEE Joint Propulsion Conference*, (Tucson, Arizona), 2005.

[98] Miotto, P., *Fixed Structure Methods for Flight Control Analysis and Automated Gain Scheduling*. PhD thesis, MIT, 1997.

[99] Miotto, P., Paduano, J. D., and Feron, E., "Modern Fixed Structure Control Design, Part I: Gain Adjustment to Improve Handling Qualities," in *Proceedings of the AIAA Guidance, Navigation and Control Conference*, (New Orleans, LA), 1997.

[100] Miotto, P., Paduano, J. D., and Feron, E., "Modern Fixed Structure Control Design, Part II: Automated Gain Scheduling," in *Proceedings of the AIAA Guidance, Navigation and Control Conference*, (New Orleans, LA), 1997.

[101] Mirkin, B. M., "Decentralized Adaptive Controller with Zero Tracking Errors," in *Proceedings of the IEEE Mediterranean Conference on Control and Automation*, (Haifa, Israel), pp. 388–398, 1999.

[102] Monopoli, R. V., "Adaptive Control for Systems with Hard Saturation," in *Proceedings of the IEEE Conference on Decision and Control*, (Piscataway, NJ), pp. 841–843, Dec. 1975.

[103] Narendra, K. S. and Annaswamy, A. M., *Stable Adaptive Systems*. Prentice-Hall, Englewood Cliffs, NJ, 1989.

[104] Narendra, K. S. and Balakrishnan, J., "Improving Transient Response of Adaptive Control Systems using Multiple Models and Switching," *IEEE Transactions on Automatic Control*, vol. 39, pp. 1861–1866, Sep. 1994.

[105] Narendra, K. S. and Balakrishnan, J., "Adaptive Control using Multiple Models," *IEEE Transactions on Automatic Control*, vol. 42, pp. 171–187, Feb. 1997.

[106] Narendra, K. S. and Oleng, N. O., "Exact Output Tracking in Decentralized Adaptive Control Systems," *IEEE Trans. on Automatic Control*, vol. 47, no. 2, pp. 390–395, 2002.

[107] Narendra, K. S., Oleng, N. O., and Mukhopadhyay, S., "Decentralized Adaptive Control with Partial Communication," *IEE Proc.-Control Theory Appl.*, vol. 153, pp. 546–555, Sep. 2006.

[108] Narendra, K. S. and Zhuo, H., "A New Approach to Adaptive Control using Multiple Models," *International journal of Adaptive Control and Signal Prosessing*, vol. 26, pp. 778–799, Aug. 2012.

[109] Oates, G. c., *Aircraft Propulsion Systems Technology and Design*. American Institute of Aeronautics and Astronautics, Reston, VA, 1989.

[110] Oates, G. c., *Aerothermodynamics of Gas Turbine and Rocket Propulsion*. American Institute of Aeronautics and Astronautics, Reston, VA, third ed., 1997.

[111] Ortega, R. and Herrera, A., "A Solution to the Decentralized Adaptive Stabilization Problem," *Syst. Control Lett.*, vol. 20, no. 4, pp. 299–306, 1993.

[112] Osburn, P. V., Whitaker, H. P., and Kezer, A., "New Developments in the design of Adaptive Control Systems," in *Proceedings of the 46th AIAA/ASME/SAE/ASEE Joint Propulsion Conference*, Paper No 61-39, Institute of Aeronautical Sciences, 1961.

[113] Pakmehr, M., Fitzgerald, N., Cazenave, T., Feron, E., Paduano, J. D., and Behbahani, A., "Distributed Modular Control System Development for Gas Turbine Engines," in *ISA 58th International Instrumentation Symposium*, (San Diego, CA), 2012.

[114] Pakmehr, M., Fitzgerald, N., Feron, E., Paduano, J., and Behbahani, A., "Physics-Based Dynamic Modeling of a Turboshaft Engine Driving a Variable Pitch Propeller," *to be submitted to the AIAA Journal of Aircraft*, 2013.

[115] Pakmehr, M., Fitzgerald, N., Feron, E., Shamma, J. S., and Behbahani, A., "Gain Scheduled Control of Gas Turbine Engines: Stability and Verification," *submitted to the ASME Journal of Dynamic Systems, Measurement, and Control*, 2012.

[116] Pakmehr, M., Fitzgerald, N., Feron, E., Shamma, J. S., and Behbahani, A., "Gain Scheduled Model Reference Adaptive Control of Gas Turbine Engines," *to be submitted to the AIAA Journal of Guidance, Control, and Dynamics*, 2013.

[117] Pakmehr, M., Fitzgerald, N., Kiwada, G., Paduano, J. D., Feron, E., and Behbahani, A., "Decentralized Adaptive Control of a Turbofan System with Partial Communication," in *Proceedings of the 46th AIAA/ASME/SAE/ASEE Joint Propulsion Conference*, (Nashville, TN), AIAA-2010-6835, 2010.

[118] Pakmehr, M., Fitzgerald, N., Paduano, J., Feron, E., and Behbahani, A., "Dynamic Modeling of a Turboshaft Engine Driving a Variable Pitch Propeller: a Decentralized Approach," in *Proceedings of the 47th AIAA/ASME/SAE/ASEE Joint Propulsion Conference*, (San Diego, California), 2011.

[119] Pakmehr, M., Mounier, M., Fitzgerald, N., Kiwada, G., Paduano, J. D., Feron, E., and Behbahani, A., "Distributed Control of Turbofan Engines," in *Proceedings of the 45th AIAA/ASME/SAE/ASEE Joint Propulsion Conference*, (Denver, Colorado), AIAA-2009-5532, 2009.

[120] Pakmehr, M., Paduano, J. D., Feron, E., and Behbahani, A., "Decentralized Adaptive Control of a Piecewise Linear Turboshaft Engine Model," in *Proceedings of the AIAA Guidance, Navigation, and Control Conference*, (Portland, Oregon), AIAA 2011-6285, 2011.

[121] Parker, K. and Guo, T. H., "Development of a Turbofan Engine Simulation in a Graphical Simulation Environment," NASA Technical Report 212543, 2003.

[122] Parker, K. and Melcher, K., "The Modular Aero-Propulsion System Simulation (*MAPSS*) User's Guide," NASA Technical Report 212968, 2004.

[123] Parks, P. C., "Lyapunov redesign of model reference adaptive control systems," *IEEE Transactions on Automatic Control*, vol. 11, pp. 362–365, 1966.

[124] Peled, D. A., *Software Reliability Methods*. Springer-Verlag, New York, 2001.

[125] Pomet, J. and Praly, L., "Adaptive Nonlinear Regulation: Estimation From the Lyapunov equation," *IEEE Transactions on Automatic Control*, vol. 37, no. 6, pp. 729–740, 1992.

[126] Popov, V. M., "Absolute Stability of Nonlinear Systems of Automatic Control," *Automation and Remote Control*, vol. 22, no. 8, pp. 857–875, 1962.

[127] Popov, V. M., "One Problem in the Theory of Absolute Stability of Controlled Systems," *Automation and Remote Control*, vol. 25, no. 9, pp. 1129–1134, 1964.

[128] Popov, V. M., *Hyperstability of Control Systems*. New York: Springer-Verlag, 1973.

[129] Pratt and Whitney, "PurePower Engine," 2012. URL: `http://www.purepowerengine.com`.

[130] Richter, H., *Advanced Control of Turbofan Engines*. Springer, New York, 2012.

[131] Roozbehani, M., *Optimization of Lyapunov Invariants in Analysis and Implementation of Safety-Critical Software Systems*. PhD thesis, MIT, 2008.

[132] Roozbehani, M., Megretski, A., and Feron, E., "Optimization of Lyapunov Invariants in Verification of Software Systems," *IEEE Transactions on Automatic Control*, vol. 58, pp. 696–711, Mar. 2013.

[133] RTCA/DO-178B, *Software Considerations in Airborne Systems and Equipment Certification*. RTCA Inc., Washington, DC, 1992.

[134] RTCA/DO-178C, *Software Considerations in Airborne Systems and Equipment Certification*. RTCA Inc., Washington, DC, 2011.

[135] RTCA/DO-333, *Formal Methods Supplement to DO-178C and DO-278A*. RTCA Inc., Washington, DC, 2011.

[136] Rugh, W. J. and Shamma, J. S., "Research on Gain Scheduling," *Automatica*, vol. 36, no. 10, pp. 1401–1425, 2000.

[137] Ryan, J. J. and Speyer, J. L., "Peak-Seeking Control using Gradient and Hessian Estimates," in *Proceedings of the American Control Conference (ACC)*, (Baltimore, MD), pp. 611–616, 2010.

[138] Sallee, G. P., "Performance Deterioration Based on Existing (Historical) Data; JT9D Jet Engine Diagnostics Program," NASA Contractor Report 135448, 1978.

[139] Sang, Q. and Tao, G., "Adaptive Control of Piecewise Linear Systems: the State Tracking Case," in *Proceedings of the 2010 American Control Conference*, pp. 4040–4045, 2010.

[140] Sang, Q. and Tao, G., "Adaptive Control of Piecewise Linear Systems: The Output Tracking Case," in *Proceedings of the 2011 American Control Conference*, pp. 2000–2005, July 2011.

[141] Sang, Q. and Tao, G., "Adaptive Control of Piecewise Linear Systems with Applications to NASA GTM," in *Proceedings of the 2011 American Control Conference*, pp. 1157–1162, July 2011.

[142] Sang, Q. and Tao, G., "Adaptive Control of Piecewise Linear Systems: the State Tracking Case," *IEEE Transactions on Automatic Control*, vol. 57, pp. 522–528, Feb. 2012.

[143] Sang, Q. and Tao, G., "Multivariable Adaptive Piecewise Linear Control Design for NASA Generic Transport Model," *Journal of Guidance, Control, and Dynamics*, vol. 35, pp. 1559–1567, Sep.-Oct. 2012.

[144] Sanghi, V., Lakshmanan, B. K., and Sundararajan, V., "Survey of Advancement in Jet-Engine Thermodynamic Simulation," *Journal of Propulsion and Power*, vol. 16, pp. 797–807, Sep.-Oct. 2000.

[145] Sastry, S. and Bodson, M., *Adaptive Control: Stability, Convergence, and Robustness*. Prentice-Hall, Englewood Cliffs, NJ, 1989.

[146] Schwager, M., "Towards Verifiable Adaptive Control for Safety Critical Applications," Master's thesis, MIT, 2005.

[147] Schwager, M., Annaswamy, A. M., and Lavretsky, E., "Adaptation-Based Reconfiguration in the Presence of Actuator Failures and Saturation," in *Proceedings of the 2005 American Control Conference*, pp. 2640–2645, June 2005.

[148] Schwager, M. and Annaswamy, A., "Direct Adaptive Control of Multi-Input Plants with Magnitude Saturation Constraints," in *Proceedings of the 44th IEEE Conference on Decision and Control, and 2005 European Control Conference*, pp. 783–788, Dec. 2005.

[149] Shamma, J. S., *Analysis and Design of Gain Scheduled Control Systems*. PhD thesis, MIT, 1988.

[150] Shamma, J. S., "Gain Scheduling," in *DISC Summer School on Identification of Linear Parameter-Varying Systems*, (Koningshof, Veldhoven, The Netherlands), pp. 6988–6993, 2006.

[151] Shamma, J. S., "Overview of LPV Systems," in *Control of Linear Parameter Varying Systems with Applications* (Mohammadpour, J. and Scherer, C. W., eds.), Chapter 1, pp. 3–26, New York, NY: Springer, 2012.

[152] Shamma, J. S. and Athans, M., "Analysis of Gain Scheduled Control for Nonlinear Plants," *IEEE Transactions on Automatic Control*, vol. 35, no. 8, pp. 898–907, 1990.

[153] Shi, L. and Singh, S. K., "Decentralized Adaptive Controller Design of Large-Scale Systems with Higher Order Interconnections," *IEEE Trans. on Automatic Control*, vol. 37, pp. 1106–1118, Aug. 1992.

[154] Siljak, D., "Decentralized Control and Computations: Status and Prospects," *Annual Reviews in Control*, vol. 20, pp. 131–141, 1996.

[155] Siljak, D. D., *Decentralized Control of Complex Systems*. Academic Press, Boston, MA, 1990.

[156] Slotine, J. J. E. and Li, W., *Applied Nonlinear Control*. Prentice-Hall, Englewood Cliffs, NJ, 1991.

[157] Soares, C., *Gas Turbines: a Handbook of Air, Land and Sea Applications*. Butterworth-Heinemann-Elsevier, Burlington, MA, 2008.

[158] Sobey, A. J. and Suggs, A. M., *Control of Aircraft and Missile Powerplants*. John Wiley and Sons, Inc., New York, 1963.

[159] Society of Automotive Engineers (SAE), "Real-Time Modeling Methods for Gas Turbine Engine Performance," SAE Aerospace Information Report (AIR) 4548, Warrendale, PA, 1995.

[160] Spang III, H. A. and Brown, H., "Control of Jet Engines," *Control Engineering Practice*, vol. 7, pp. 1043–1059, 1999.

[161] Spooner, J., Maggiore, M., Ordonez, R., and Passino, K., *Stable Adaptive Control and Estimation for Nonlinear Systems: Neural and Fuzzy Approximator Techniques*. John Wiley and Sons, New York, NY, 2002.

[162] Spooner, J. and Passino, K., "Decentralized Adaptive Control of Nonlinear Systems using Radial Basis Neural Networks," *IEEE Trans. on Automatic Control*, vol. 44, no. 11, pp. 2050–2057, 1999.

[163] Stilwell, D. J. and Rugh, W. J., "Stability Preserving Interpolation Methods for the Synthesis of Gain Scheduled Controllers," *Automatica*, vol. 36, no. 5, pp. 665–671, 2000.

[164] Sturm, J. F., Romanko, O., and Plik, I., "SeDuMi (Self-Dual-Minimization): A MATLAB Toolbox for Optimization over Symmetric Cones," 2001. URL: `http://sedumi.ie.lehigh.edu`.

[165] Tao, G., *Adaptive Control Design and Analysis* . John Wiley and Sons, New York, NY, 2003.

[166] Tsakalis, K. S. and Ioannou, P. A., "Adaptive Control of Linear Time-Varying Plants," *Automatica*, vol. 23, pp. 459–468, July 1987.

[167] Tsakalis, K. S. and Ioannou, P. A., "Adaptive Control of Linear Time-Varying Plants: A New Model Reference Controller Structure," *IEEE Transactions on Automatic Control*, vol. AC-34, pp. 1038–1046, Oct. 1989.

[168] Tsakalis, K. S. and Ioannou, P. A., *Linear Time-Varying Systems: Control and Application*. Prentice-Hall, Englewood Cliffs, NJ, 1993.

[169] Venugopal, R., Rao, V. G., and Bernstein, D. S., "Lyapunov-Based Backward-Horizon Adaptive Stabilization," *International Journal of Adaptive Control and Signal Processing*, vol. 17, no. 1, pp. 67–84, 2003.

[170] Visser, W. P. J., Kogenhop, O., and Oostveen, M., "A Generic Approach for Gas Turbine Adaptive Modeling," *Journal of Engineering for Gas Turbines and Power*, vol. 128, pp. 13–19, Jan. 2006.

[171] von Mises, R., *Theory of Flight*. McGraw Hill, New York, NY, 1945.

[172] Walsh, P. P. and Fletcher, P., *Gas Turbine Performance*. Blackwell Science Ltd, Oxford, UK, 2nd ed., 2004.

[173] Wang, J., Hovakimyan, N., and Cao, C., "L_1 Adaptive Augmentation of Gain-Scheduled Controller for Racetrack Maneuver in Aerial Refueling," in *Proceedings of the AIAA Guidance, Navigation and Control Conference*, (Chicago, Illinois), AIAA, 2009.

[174] Wang, T., and Jobredeaux, R., and Feron, E., "A Graphical Environment to Express the Semantics of Control Systems." arXiv:1108.4048v1 [cs.SY], 19 Aug 2011.

[175] Wen, C. and Soh, Y., "Decentralized Model Reference Adaptive Control without Restriction on Subsystem Relative Degree," *IEEE Trans. on Automatic Control*, vol. 44, no. 7, pp. 1464–1469, 1999.

[176] Yu, D., Zhao, H., X. Z., Sui, Y., and Liu, J., "An Approximate Non-linear Model for Aeroengine Control," *Proceedings of the Institution of Mechanical Engineers, Part G: Journal of Aerospace Engineering*, vol. 255, no. 12, pp. 1366–1381, 2011.

[177] Yucelen, T. and Haddad, W. M., "A Robust Adaptive Control Architecture for Disturbance rejection and Uncertainty Suppression with L_∞ Transient and Steady-State Performance Guarantees," *International Journal of Adaptive Control and Signal Processing*, vol. 26, pp. 1024–1055, 2012.

[178] Yucelen, T., Yang, B., and Calise, A., "Derivative-Free Decentralized Adaptive Control of Large-Scale Interconnected Uncertain Systems," *Journal of the Astronautical Sciences*, 2012.

[179] Zhao, H., Liu, J., and Yu, D., "Approximate Nonlinear Modeling and Feedback Linearization Control of Aeroengines," *Journal of Engineering for Gas Turbines and Power*, vol. 133, no. 11, pp. 111601–1–111601–10, 2011.

VITA

Mr. Pakmehr received his B.Sc. degree in Aerospace Engineering from Sharif University of Technology, Tehran, Iran, and his M.Sc. degree in Mechanical Engineering from Concordia University, Montreal, Canada. He also has two M.Sc. degrees in Aerospace Engineering and Mathematics, both from the Georgia Institute of Technology, Atlanta, GA. Since 2007 he has been with the the School of Aerospace Engineering, Georgia Institute of Technology, where he is currently working toward his Ph.D. degree in Aerospace Engineering.

His research interests include control theory, flight dynamics and control, distributed control of propulsion systems, and control software verification. He has publications on modeling and control of gas turbine propulsion systems, modeling and control of delta wing systems, and intelligent control of autolanding systems for commercial jet transports.